AD-A095 252 PURDUE UNIV LAFAYETTE IN PROJECT SQUID HEADQUARTERS F/G 20/4
MEASUREMENTS OF A SEPARATING TURBULENT BOUNDARY LAYER.(U)
APR 80 R L SIMPSON, Y CHEW, B G SHIVAPRASAD N00014-75-C-1143
UNCLASSIFIED SQUID-SMU-4-PU NL

1 OF 3

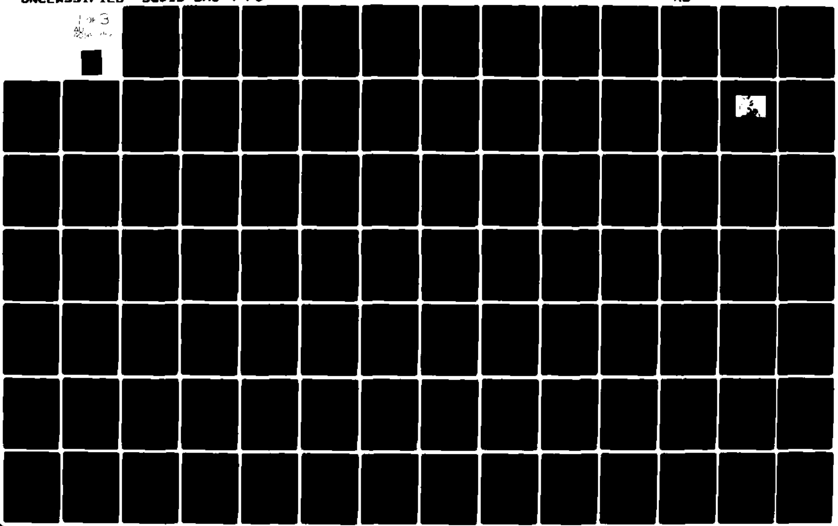

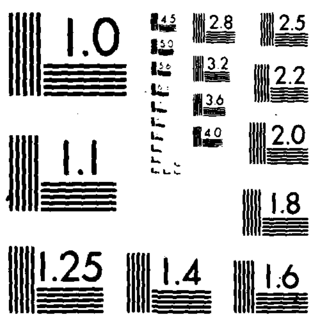

MICROCOPY RESOLUTION TEST CHART
NATIONAL BUREAU OF STANDARDS-1963-A

Unclassified

SECURITY CLASSIFICATION OF THIS PAGE (When Data Entered)

REPORT DOCUMENTATION PAGE

READ INSTRUCTIONS BEFORE COMPLETING FORM

1. REPORT NUMBER: SMU-4-PU	2. GOVT ACCESSION NO.: AD-A095 252
3. RECIPIENT'S CATALOG NUMBER	
4. TITLE (and Subtitle): Measurements of a Separating Turbulent Boundary Layer	5. TYPE OF REPORT & PERIOD COVERED: Technical October 1976-February 1979
	6. PERFORMING ORG. REPORT NUMBER
7. AUTHOR(s): Roger L. Simpson, Y.-T. Chew, and B. G. Shivaprasad	8. CONTRACT OR GRANT NUMBER(s): N00014-75-C-1143 NR-098-038
9. PERFORMING ORGANIZATION NAME AND ADDRESS: Southern Methodist University Dallas, Texas 75275	10. PROGRAM ELEMENT, PROJECT, TASK AREA & WORK UNIT NUMBERS
11. CONTROLLING OFFICE NAME AND ADDRESS: Project SQUID Chaffee Hall Purdue University West Lafayette, Indiana 47907	12. REPORT DATE: April 1980
	13. NUMBER OF PAGES: 207
14. MONITORING AGENCY NAME & ADDRESS (if different from Controlling Office): Office of Naval Research - Power Program Code 473, Dept. of the Navy 800 N. Quincy Street Arlington, Virginia 22217	15. SECURITY CLASS. (of this report): Unclassified
	15a. DECLASSIFICATION/DOWNGRADING SCHEDULE

16. DISTRIBUTION STATEMENT (of this Report)

This document has been approved for public release and sale; its distribution is unlimited.

DISTRIBUTION STATEMENT A
Approved for public release;

LEVEL II

17. DISTRIBUTION STATEMENT (of the abstract entered in Block 20, if different from Report)

Same

DTIC ELECTE FEB 20 1981

18. SUPPLEMENTARY NOTES

19. KEY WORDS (Continue on reverse side if necessary and identify by block number)

Separation
Turbulence
Laser Anemometer
Fluid Dynamics

Original contains color plates: All DTIC reproductions will be in black and white

20. ABSTRACT (Continue on reverse side if necessary and identify by block number)

The problem of turbulent boundary layer separation due to an adverse pressure gradient is an old but still important problem in many fluid flow devices. Until recent years little quantitative experimental information was available on the flow structure downstream of separation because of the lack of proper instrumentation. The directionally-sensitive laser anemometer now provides the ability to accurately measure the instantaneous flow direction and magnitude.

DD FORM 1473, 1 JAN 73 EDITION OF 1 NOV 65 IS OBSOLETE

SECURITY CLASSIFICATION OF THIS PAGE (When Data Entered)

AD A095252

DDC FILE COPY

81 2 17 110

(20, cont.)

The experimental results described in this report are concerned with a nominally two-dimensional separating turbulent boundary layer for an airfoil-type flow in which the flow was accelerated and then decelerated until separation. Upstream of separation single and cross-wire hot-wire anemometer measurements are also presented. Measurements obtained in the separated zone with a directionally-sensitive laser anemometer system are presented for U, V, $\overline{u^2}$, $\overline{v^2}$, $-\overline{uv}$, $\overline{u^3}$, $\overline{u^4}$, $\overline{v^3}$, $\overline{v^4}$, the fraction of time that the flow moves downstream, the fraction of time that the flow moves away from the wall, and u spectra.

In addition to confirming the earlier conclusions of Simpson et al. (1977) regarding a separating airfoil-type turbulent boundary layer, much new information about the separated region has been gathered. (1) The backflow mean velocity profile scales on the maximum negative mean velocity U_N and its distance from the wall N. A U^+ vs. y^+ law-of-the-wall velocity profile is not consistent with this result. (2) The turbulent velocities are comparable with the mean velocity in the backflow, although low turbulent shearing stresses are present. (3) Mixing length and eddy viscosity models are physically meaningless in the backflow. (4) Negligible turbulence energy production occurs in the backflow.

These and other results lead to significant conclusions about the nature of the separated flow when the thickness of the backflow region is small as compared with the shear layer thickness. The backflow is controlled by the large-scale outer region flow. The small mean backflow does not come from far downstream, but appears to be supplied intermittently by large-scale structures as they pass through the separated flow. Downstream of fully-developed separation, the mean backflow appears to be divided into three layers: a viscous layer nearest the wall that is dominated by the turbulent flow unsteadiness but with little Reynolds shearing stress effects; a rather flat intermediate layer that seems to act as an overlap region between the viscous wall and outer regions; and the outer backflow region that is really part of the large-scaled outer region flow. The Reynolds shearing stress must be modeled by relating it to the turbulence structure and not to local mean velocity gradients. The mean velocities in the backflow are the results of time-averaging the large turbulent fluctuations and are not related to the source of the turbulence.

Accession For

By______

Distribution/

Availability Codes

Dist	Avail and/or Special
A	

Technical Report SMU-4-PU

PROJECT SQUID

A COOPERATIVE PROGRAM OF FUNDAMENTAL RESEARCH
AS RELATED TO JET PROPULSION
OFFICE OF NAVAL RESEARCH, DEPARTMENT OF THE NAVY

CONTRACT N00014-75-C-1143 NR-098-038

MEASUREMENTS OF A SEPARATING TURBULENT BOUNDARY LAYER

by

Roger L. Simpson, Y.-T. Chew, and B. G. Shivaprasad
SOUTHERN METHODIST UNIVERSITY

April 1980

Published for ONR by
School of Mechanical Engineering
Chaffee Hall
Purdue University
West Lafayette, Indiana 47907

MEASUREMENTS OF A SEPARATING TURBULENT BOUNDARY LAYER

by

Roger L. Simpson*, Y.-T. Chew**, and B.G. Shivaprasad***
Southern Methodist University

ABSTRACT

The problem of turbulent boundary layer separation due to an adverse pressure gradient is an old but still important problem in many fluid flow devices. Until recent years little quantitative experimental information was available on the flow structure downstream of separation because of the lack of proper instrumentation. The directionally-sensitive laser anemometer now provides the ability to accurately measure the instantaneous flow direction and magnitude.

The experimental results described in this report are concerned with a nominally two-dimensional separating turbulent boundary layer for an airfoil-type flow in which the flow was accelerated and then decelerated until separation. Upstream of separation single and cross-wire hot-wire anemometer measurements are also presented. Measurements obtained in the separated zone with a directionally-sensitive laser anemometer system are presented for U, V, $\overline{u^2}$, $\overline{v^2}$, $\overline{-uv}$, $\overline{u^3}$, $\overline{u^4}$, $\overline{v^3}$, $\overline{v^4}$, the fraction of time that the flow moves downstream, the fraction of time that the flow moves away from the wall, and u spectra.

---

*Professor of Mechanical Engineering
**Visiting Assistant Professor; currently at Department of Mechanical and Production Engineering, University of Singapore.
***Visiting Assistant Professor.

In addition to confirming the earlier conclusions of Simpson et al. (1977) regarding a separating airfoil-type turbulent boundary layer, much new information about the separated region has been gathered. (1) The backflow mean velocity profile scales on the maximum negative mean velocity U_N and its distance from the wall N. A U^+ vs. y^+ law-of-the-wall velocity profile is not consistent with this result. (2) The turbulent velocities are comparable with the mean velocity in the backflow, although low turbulent shearing stresses are present. (3) Mixing length and eddy viscosity models are physically meaningless in the backflow. (4) Negligible turbulence energy production occurs in the backflow.

These and other results lead to significant conclusions about the nature of the separated flow when the thickness of the backflow region is small as compared with the shear layer thickness. The backflow is controlled by the large-scale outer region flow. The small mean backflow does not come from far downstream, but appears to be supplied intermittently by large-scale structures as they pass through the separated flow. Downstream of fully-developed separation, the mean backflow appears to be divided into three layers: a viscous layer nearest the wall that is dominated by the turbulent flow unsteadiness but with little Reynolds shearing stress effects; a rather flat intermediate layer that seems to act as an overlap region between the viscous wall and outer regions; and the outer backflow region that is really part of the large-scaled outer region flow. The Reynolds shearing stress must be modeled by relating it to the turbulence structure and not to local mean velocity gradients. The mean velocities in the backflow are the results of time-averaging the large turbulent fluctuations and are not related to the source of the turbulence.

NOMENCLATURE

a	$\equiv$	$\tau/\rho\overline{q^2}$
a_1	$\equiv$	$-\overline{uv}/(\overline{u^2} + \overline{v^2})$
a_2	$\equiv$	$aF^{4/3}$, defined in equation (36)
$B(y/\delta)$	$\equiv$	$RU_\infty/\lvert U_N\rvert$, normalized backflow function
C	$\equiv$	$\int_0^\infty f_2(\eta_2)d\eta_2$, Perry and Schofield constant
C_1		defined in equation (34)
C_2	$\equiv$	$C_1F^{1/3}$, defined in equation (35)
$C_f/2$	$\equiv$	$\tau_0/\rho U_\infty^2$, local skin-friction coefficient
C_p	$\equiv$	$2\,(P - P_i)/\rho U_{\infty\,i}^2$, pressure coefficient
e	$\equiv$	LU_τ^2/U_{MP}^2, Perry and Schofield inner layer length scale, equation (12).
F		ratio of total turbulence energy production to shear production, equation (33)
F_u, F_v		$\overline{u^4}/(\overline{u^2})^2$, $\overline{v^4}/(\overline{v^2})^2$, kurtosis or flatness factor for u and v fluctuations, respectively.
$F(n)$		$(1/\overline{u^2})(du^2/dn)$; $1 = \int_0^\infty F(n)dn$; spectrum function for u.
f_1, f_2		Perry and Schofield correlation functions, defined in equations (14) and (10), respectively.
G		Bradshaw large eddy diffusion function, defined in equation (28)
H_{12}	$\equiv$	δ_1/δ_2, velocity profile shape factor

L	distance from the wall to the maximum pseudo-shear stress
ℓ	mixing length, defined in equation (20)
M	distance from the wall to the maximum
N	number of signal bursts in equation (4); distance from wall to minimum velocity in backflow.
n_b	peak frequency of nF(n) spectral distribution
P, p	mean and fluctuation pressure
PL,PR	left and right sides of equation (8)
$P(\mathcal{U})$	velocity probability distribution, equation (5)
$\overline{q^2}$	$\overline{u^2} + \overline{v^2} + \overline{w^2}$
$R(y/\delta)$	"backflow" function defined by equation (19)
Re_{δ_2}	$\equiv U_\infty \delta_2/\nu$, momentum thickness Reynolds number
S_u, S_v	$\overline{u^3}/(\overline{u^2})^{3/2}$, $\overline{v^3}/(\overline{v^2})^{3/2}$, skewness factors for u and v fluctuations, respectively
$\mathcal{U}, \mathcal{V}, \mathcal{W}$	instantaneous velocity components in x, y, z directions, respectively
U, V, W	mean velocities in x, y, z directions, respectively
u, v, w	instantaneous fluctuations velocities in x, y, z directions
u', v', w'	rms fluctuation velocities in x, y, z directions, respectively
U_τ	$\equiv (\tau_0/\rho)^{1/2}$, shear velocity

U^+	$\equiv U/U_\tau$
U_M	$(-\overline{uv})^{1/2}_{max}$
U_{MP}	maximum pseudo-shearing stress, equation (16)
U_0	$2U(1/2) - U_\infty$ at X_0 in equation (17)
U_s	Perry and Schofield velocity scale, defined in equation (10)
V_p	entrainment velocity
x,y,z	streamwise, normal, and spanwise coordinates
X_0	streamwise distance from reference point in equation (17)
$Y_{1/2}$	perpendicular distance from reference streamwise line to where U is $U_\infty/2$ for mixing layer of Wygnanski and Fiedler.

<u>Greek Symbols</u>

γ_{pu}, γ_{pv}	fraction of time the flow moves downstream and away from the wall, respectively.
Δ	$\equiv U_\infty\delta_1/CU_s$, length scale in Perry and Schofield correlation
δ	y where $U = 0.99\ U_\infty$
$\delta_{0.995}$	y where $U = 0.995\ U_\infty$
δ_1	$\equiv \int_0^\infty (1 - U/U_\infty)\ dy$, displacement thickness
δ_2	$\equiv \int_0^\infty (U/U_\infty)(1 - U/U_\infty)\ dy$, momentum thickness

ε	rate of turbulent energy dissipation in equation (31)
η_1	$\equiv y/e$
η_2	$\equiv y/\Delta$
θ	angle of inclination of principal axis to the flow direction
ν	kinematic viscosity
ν_e	eddy viscosity, defined in equation (23)
ρ	density
σ'	mixing layer parameter in equation (17)
τ	shearing stress
$\omega(y/\delta)$	wake function in equation (18)

Subscripts

i	denotes initial value
max	denotes maximum value
min	denotes minimum value
0	denotes wall value
∞	denotes free-stream condition

ACKNOWLEDGMENTS

The authors would like to thank the graduate students who participated in remodeling and testing the wind tunnel during 1976-77: C. R. Shackleton, E. B. Bowles, K. R. Saripalli, and G. P. Kokolis. Dr. R. E. Nasburg and J. Sallas kept the data acquisition computer operational. Diana Cantu, Judy Whirley, and Yolanda Contreras put the figures, tables, and manuscript into the present form.

TABLE OF CONTENTS

I. INTRODUCTION

The problem of turbulent boundary layer separation due to an adverse pressure gradient is an important factor in the design of many devices such as jet engines, rocket nozzles, airfoils and helicopter blades, and the design of fluidic logic systems. Until the last five years little quantitative experimental information was available on the flow structure downstream of separation because of the lack of proper instrumentation.

In 1974 after several years of development, a one velocity component directionally-sensitive laser anemometer system was used to reveal some new features of a separating turbulent boundary layer (Simpson et al., 1974). The directional sensitivity of the laser anemometer system was necessary since the magnitude and direction of the flow must be known when the flow moves in different directions at different instants in time. In addition to much turbulence structure information, it was determined: (1) that the law-of-the-wall velocity profile is apparently valid up to the beginning of intermittent separation; (2) that the location of the beginning of intermittent separation or the upstreammost location where separation occurs intermittently is located close to where the freestream pressure gradient begins to rapidly decrease; (3) that the normal stress terms of the momentum and turbulent kinetic energy equations are important near separation; and (4) that the separated flowfield shows some similarity of the streamwise velocity U, of the velocity fluctuation u', and of the fraction of time that the flow moves downstream (Simpson et al., 1977).

Based upon these results, modifications (Simpson and Collins, 1978; Collins and Simpson, 1978) to the Bradshaw et al. (1967) boundary layer prediction method were made with significant improvements. However, this prediction effort pointed to the need to understand the relationship between the pressure gradient relaxation and the intermittent separation region structure. A number of other workers have tried to predict this type flow, but with questionable assumptions about the turbulence structure near the wall. In nearly all efforts, the workers have simply extended the velocity and turbulence profile correlations that apply to attached flows to the backflow region. Even though turbulent fluctuations near the wall in the backflow region are as large as or larger than mean velocities, these predictors use a turbulence model that is tied to the mean velocity gradient. Even with adjustment of turbulence model "constants" to fit one feature or another, these models do not predict simultaneously the backflow velocity profile, the steamwise pressure distribution, and the fact that length scales increase along the flow. Clearly then, a limiting factor for further improvement of the prediction of separated flows is the lack of fundamental experimental velocity and turbulence structure information with which to develop adequate models, especially for the backflow region. Such data are presented here.

The experimental results described in this report are concerned with a nominally two-dimensional separating turbulent boundary layer for an airfoil-type flow in which the flow was accelerated and then decelerated until separation. Upstream of separation single and cross-wire hot-wire anemometer measurement results are presented. Measurements obtained in the separated zone with a directionally-sensitive laser anemometer system are presented for U, V, $\overline{u^2}$, $\overline{v^2}$, $-\overline{uv}$, $\overline{u^3}$, $\overline{v^3}$, $\overline{u^4}$, $\overline{v^4}$, the fraction of time that the flow moves downstream γ_u, fraction of time that the flow moves away from the wall γ_v, and u spectra. The implications of these results to flow models are discussed.

II EXPERIMENTAL EQUIPMENT

II.1 Basic Wind Tunnel

The mainstream flow of the blown open-circuit wind tunnel is introduced into the test section after first passing through a filter, blower, a fixed-setting damper, a plenum, a section of honeycomb to remove the mean swirl of the flow, seven screens to remove much of the turbulence intensity, and finally through a two-dimensional 4:1 contraction ratio nozzle to further reduce the longitudinal turbulence intensity while accelerating the flow to test speed. These same components were in an earlier version of this wind tunnel with a shorter test section that was used in previous research (Simpson et al., 1977; Simpson and Wallace, 1975; Simpson and Shackleton, 1977).

Fig. 1 is a side view schematic of the 25 feet long, 3 feet wide test section of the wind tunnel. The upper wall is adjustable such that the free-stream velocity or pressure gradient can be adjusted. The side walls are made of plexiglass. The test wall is constructed from 3/4 inches thick fin-form plywood, reinforced every 11 inches with 3 x 1½ x ¼ inches cross section steel channel.

The active boundary layer control system, which is described in section II.2 below, is used to eliminate preferential separation of the curved top wall boundary layer. Highly two-dimensional wall jets of high velocity air are introduced at the beginning of each of the eight feet long sections. At the latter two streamwise locations the oncoming boundary layer is partially removed by a highly two-dimensional suction system. In order to accommodate the increased energy dissipation in the wind tunnel laboratory due to the boundary layer control system, a new 3 ton air conditioner was added.

The inviscid core flow is uniform within 0.05% in the spanwise direction and within 1% in the vertical direction with a turbulence intensity of 0.1% at 60 fps. The test wall boundary layer is tripped by the blunt leading edge of the

FIGURE 1. SIDEVIEW SCHEMATIC OF THE TEST SECTION. MAJOR DIVISIONS ON SCALES: 10 INCHES. NOTE BAFFLE PLATE UPSTREAM OF BLUNT LEADING EDGE ON BOTTOM TEST WALL AND SIDE AND UPPER WALL JET BOUNDARY LAYER CONTROLS.

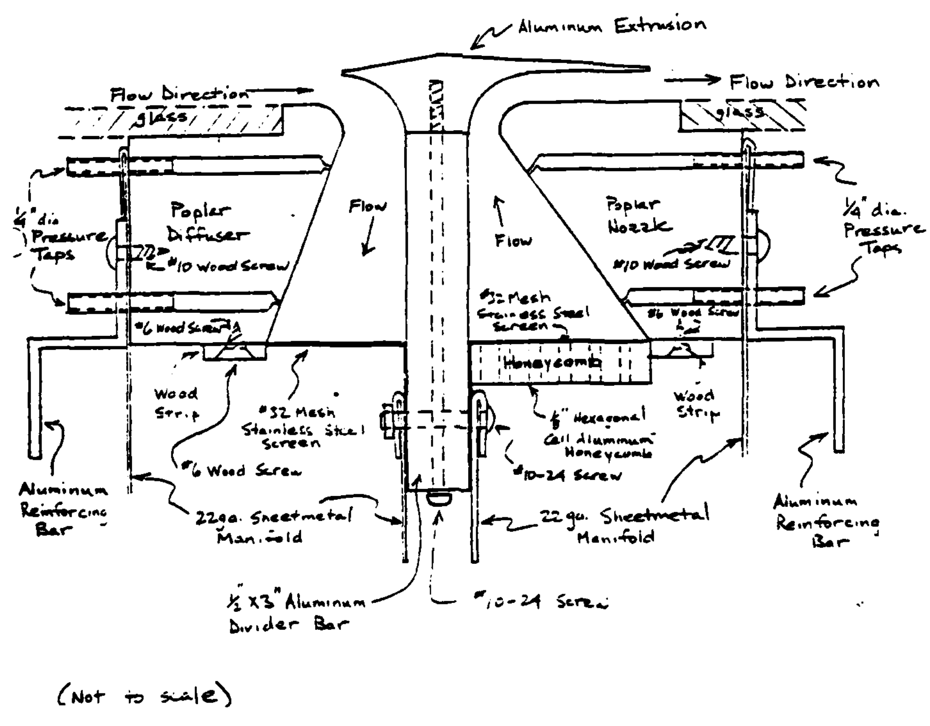

Figure 2. Cross sectional view of wall jet-wall suction assembly.

plywood floor, the height of the step from the wind tunnel contraction to the test wall being ¼ inches. Smoke can be introduced uniformly into the boundary layer just upstream of this trip for use with the laser doppler anemometer.

II.2 Boundary Layer Control System

An active boundary layer control system was installed on the nontest walls of the test section to inhibit undesirable flow three-dimensionality and to prevent separation. Because the static pressure in the test section is time varying in a series of unsteady experiments at the same mean conditions as in the case reported here (Simpson et al., 1980), no passive boundary layer control can be used that depends on a steady test section pressure higher than the pressure outside the tunnel. In previous steady freestream separated flow experiments in the old tunnel test section (Simpson et al., 1977), a perforated plate was located at the test section exit to produce static pressures in the test section that were above atmospheric pressure. In that case, the upper wall boundary layer was bled from the test section just upstream of the separation zone.

In the current case, the active boundary layer control system removes low momentum fluid by sucking off the boundary layer and supplies high momentum fluid through trangential wall jets. Its performance is less influenced by the fluctuating test section static pressure in the unsteady experiments than that of the previous passive system. Fig. 2 is a cross-sectional view of the wall suction and wall jet units located at 100 inches and 200 inches on the non-test walls. Only the wall jet portion of this unit is installed at the test section entrance. Only the essential features of this system are summarized here; other details are contained in Simpson et al. (1980) and in an unpublished report by Bowles (1977).

A fan supplies the wall jets with air sucked through the suction slots and with additional makeup air. Sheet metal ducting, flow dampers, resistance baffles, and manifolds that contain the wall suction and wall jet units are used to direct and control the air distribution. All of the wall suction and wall jet units have identical cross sections. As much care as possible was taken to make these units geometrically and aerodynamically two-dimensional. As shown in Fig. 2 the wall jet portion is a 6:1 area ratio nozzle that accelerates the fluid before it is injected along the glass tunnel sides walls or plexiglas top. The suction portion is a 1:3.6 area ratio diffuser that decelerates the removed flow. An aluminum divider plate separates the wall jet and suction flows, forming one wall of the jet nozzle and one wall of the diffuser. The specially extruded aluminum deflector directs the jet flow parallel to the tunnel wall and scoops the suction flow from the upstream tunnel flow. Shims were placed between the aluminum divider plate and the extruded aluminum deflector to make the jet flow exit gap uniform within 0.0016 inches along a given unit. The gap was nominally 0.25 inches, but was slightly different for each unit. The suction side flow entrance gap was less uniform, being within 0.01 inches of the nominal 5/16 inches.

As also shown in Fig. 2, 32 mesh stainless steel screen and 1/8 inches cell hexagonal aluminum honeycomb are located at the nozzle entrance to evenly distribute and straighten the flow from the jet manifold. After initial system testing, additional screen was mounted on top of the honeycomb opposite the manifold duct entrance from the supply duct. This eliminated preferential flow due to impringement of the incoming flow. In one case a flow deflector was required at the manifold entrance to further distribute the flow. 32 mesh screen was also placed over the diffuser exit to distribute the suction flow more evenly over the flow cross-sectional area. A small gap between the screen and each endplate was used to induce a greater flow along the endplates. This greater flow benefits the momentum deficient wind tunnel corner flows.

Two pressure taps were located in the nozzle and in the diffuser. After calibration, the measured pressure difference between these taps allowed the nozzle and the diffuser to be used as jet flow and suction flow meters, respectively. Excellent linear calibrations were found between measured dynamic pressures and the respective differential pressures.

The average dynamic pressure of the jet exit flow was measured along the length of each unit with a 0.25 inches dia. impact probe. The standard deviation of the dynamic pressure variation was less than 2.5% along each of the jet units. The dynamic pressure in the 3/4 inches nearest the end of each unit was about 2/3 of that for the midsection. The jets at the test section entrance were operated at an average velocity of 90 fps; at the 100 inches location the wall jet velocity was 120 fps for the upper wall and 72 fps for the side walls; at the 200 inches location the upper wall and side wall jet velocities were 75 fps and 57 fps.

Fig. 3 shows the mean velocity and streamwise turbulence intensity profiles in the midplane along the second streamwise upper wall jet that were obtained from a hot-wire anemometer. Note that the velocity profile is asymmetric with more high velocity flow near the freestream side of the jet. Saripalli and Simpson (1979) have shown that such an asymmetric jet is more effective in preventing boundary layer separation than a uniform jet with a greater momentum flow rate. This is due to the fact that less of the asymmetric jet momentum is wasted on increased wall drag while greater mixing occurs with the outer region flow.

The variation of the dynamic pressure of the suction flow was measured along the length of each unit. The difference between the static pressure inside the diffuser at a particular location and atmospheric pressure had a standard

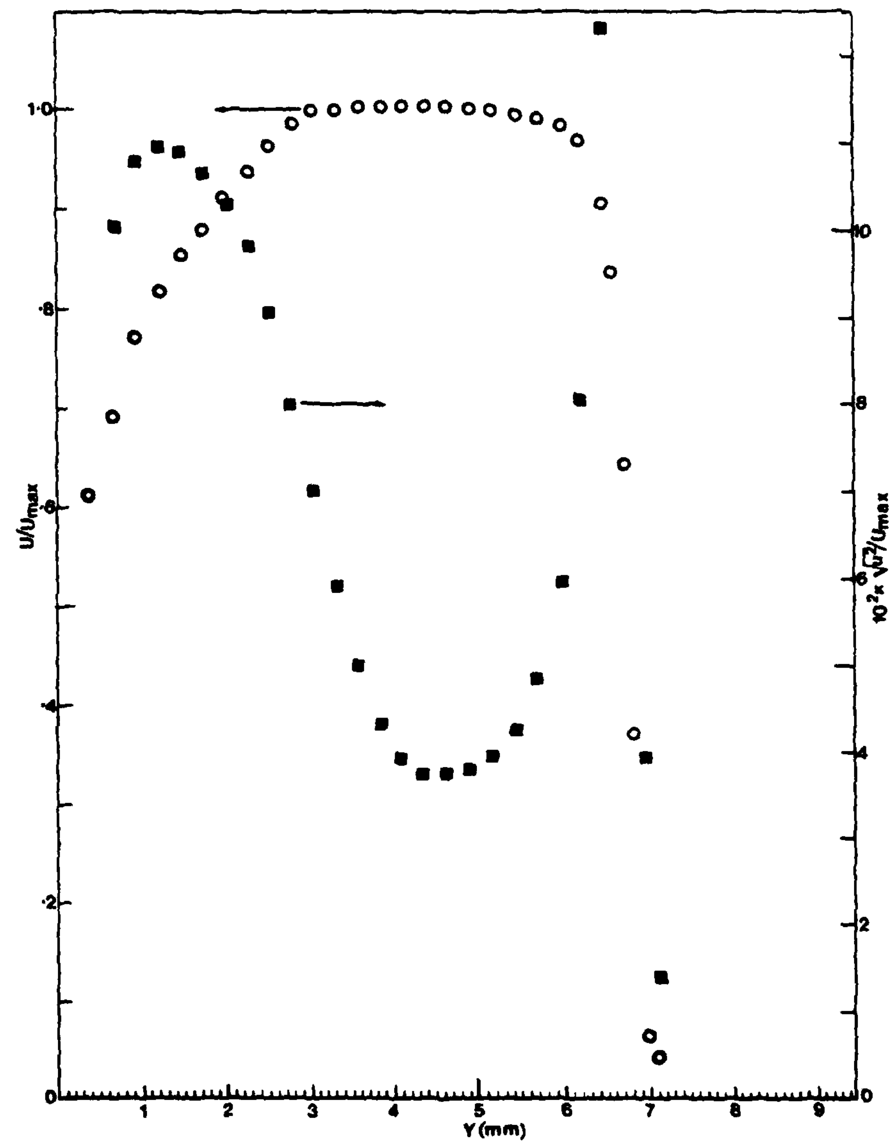

Figure 3. Wall jet mean velocity and streamwise turbulence intensity profiles, upper wall jet at 100 inches.

deviation of no more than 2% along each suction unit. Most of the departure from uniformity occurred near the ends where, fortunately, about 20% greater suction dynamic pressure occurred. Thus a greater amount of momentum deficient wind tunnel corner fluid could be removed, partly overcoming the effect of the dynamic pressure deficiency at the ends of the wall jet sections. The average suction velocity at the 100 inches location was 45 fps while for the 200 inches location it was 75 fps for the upper wall and 56 fps for the side walls.

The hot-wire anemometer mean velocity and streamwise turbulence intensity profiles in the midplane along the first streamwise upper wall suction unit were almost uniform. This indicates that some of the upstream flow is deflected toward the wall by the suction since the boundary layer velocity profile is not uniform. Immediately downstream the asymmetric velocity profile jet momentum is then rapidly mixed with the remaining upstream boundary layer flow.

It should be noted that the flows in this control system are relatively insensitive to the $\pm$ 1 cm of water static pressure oscillation in the test section in the unsteady experiments. The large volume of the control system and the 12 inches of water static pressure loss in its components act as a large low-pass-frequency filter. Dynamic pressure oscillations of the wall jet flow were of the order $\pm$ 0.016 inches of water.

II.3 Hot-wire Anemometers

Miller-type (1976) integrated circuit hot-wire anemometers and linearizers, as modified by Simpson et al. (1979) were constructed and used. A TSI Model 1050 anemometer was used with the surface hot-wire element that is described in section II.4 below. The frequency response was flat up to 7.5 kHz for an overheat ratio of 0.7. this moderately high overheat ratio was used since Wood (1975) showed that the range of flat frequency response is improved with a higher overheat ratio.

Standard TSI model 1274-TI.4 normal wire and model 1248-TI.5 cross-wire probes were used for boundary layer measurements. The closest to the wall that these probes could safely make measurements was about 0.002 inches and 0.035 inches, respectively. The sensing elements are 0.00015 inches diameter, 0.050 inches length platinum-plated tungsten wires.

The traversing mechanism used for the boundary layer velocity measurements was mounted on the supporting frame for the upper wall and provided for precise positioning of the probe sensors as described by Strickland and Simpson (1973). A cathetometer was used to accurately locate the probe sensor from the wall within an uncertainty of about ± 0.002 inches. The detailed streamwise free-stream velocity distributions were obtained using a the Model 1274-TI.5 probe mounted on the toy racing car shown in Fig. 3 of Simpson and Wallace (1975). The car was easily positioned along the flow by fishing line.

Calibrations were made in a TSI Model 1127 calibrator. There was no detectable drift of the anemometer; the function-module type linearizers had a small mount of DC drift. Each linearized calibration had a low level of dispersion from a straight line, with a product moment correlation coefficient (Bragg, 1974) in excess of 0.09999. The slope of each calibration varied no more than about 4% over the life of a given probe.

A standard TSI model 1015C correlator was used to obtain sum and difference values for u and v from cross-wire signals. Electronic multipliers (Analog Devices AD533JH) were used to produce the turbulence quantities uv, u^2v, and v^3. These were trimmed to within ± 1% fullscale nonlinearity error. True integrating voltmeters, consisting of a voltage-controlled oscillator (Tektronix FG501 Function Generator) and a digital counter (Tektronix DC503 Universal Counter), were used to obtain true time-averaged results.

II.4 Surface Hot-wire Skin Friction Gage

Because a single universal calibration is valid in both laminar and turbulent flow and is insensitive to pressure gradients (Murthy and Rose, 1978; Higuchi and Peake, 1978), a Rubesin et al. (1975) type surface hot-wire skin friction gage was constructed and used. The basic advantages of this type gage are that the surface-heating-element dimension in the streamwise direction is very small and that conduction losses to a very low thermal conductivity substrate are minimized.

A 0.001 inches diameter platinum - 10% rhodium wire was mounted between 0.052 inches diameter nickel electrodes located 0.4 inches apart whose ends were flush with the flat polystyrene surface. Conduction losses to the electrodes are small since the wire length-to-diameter ratio of 400 is large. Several drops of ethyl acetate were used to dissolve the polystyrene in the vicinity of the wire and imbed it in the surface. The ends of the wire were then soldered to the electrodes. A 0.00015 inches diameter wire was tried but was too fragile for use with simple construction techniques. The polystyrene was mounted on a thin portable plexiglas plate. The resulting surface was sanded and polished flat and smooth before the wire was mounted. This plate allows a single element to be moved to variaous measurement locations with a minimum of flow disturbance. The element is sufficiently downstream of the end of the small ramp and sufficiently upstream of the trailing edge to avoid sensing local disturbances generated by the plate. A 0.001 inches diameter platinum and platinum-10% rhodium thermocouple was mounted 3/32 inches downstream of the hot-wire element.

Rubesin et al. found that overheat temperatures of at least $80^{o}F$ were needed to make the heat loss from a wire proportional to its temperature rise, or $E^2/R\Delta T$ a constant. Peake and Higuchi found that overheats greater than $176^{o}F$ caused the wire to melt the substrate and separate from the surface. Here the cold resistance at $77^{o}F$ was 3.70 Ω and 0.5 Ω overheat resistance was used, so with a temperature coefficient of resistivity of $0.89 \times 10^{-3}\ {}^{o}F^{-1}$ then ΔT was $152^{o}F$. The wire was not observed to separate from the surface.

A simple stainless steel cone with 0.5^{o} angle between the cone and the plate surface was constructed for calibration of this gage. A brass housing held the cone in place on the plate. The hot-wire was aligned with a radial line from the cone apex. The velocity gradient at the plate surface was independent of the radial position since the cone surface velocity, ωr, and the spacing between the cone and the plate, r tan (0.5^{o}), each vary linearly with the radius. Because the maximum surface velocity gradient of interest was about 9.6×10^{4} sec, a high-speed grinder motor (Sears and Roebuck, Model 315.17440, 26000 RPM) and a Variac power control were used to produce 600 rpm $< f <$ 8000 rpm. A vinyl tubing flexible connector was used between the cone shaft and the grinder to minimize misalignment. The angular speed f was measured by reflecting a light from the hexagonal grinder chuck nut into a photomultipler tube and counting the signal pulse rate f_p on a digital counter; thus $f = f_p/6$. Heating of the calibrator flow occurred above 8000 rpm due to substantial frictional heating in the steel-brass bearing. Since the air temperature was measured with the thermocouple, corrections could be made. After calibration, a Miller-type exponential electronic linearizer was used to linearize the bridge output voltage.

II.5 Laser Anemometer and Signal Processing

The laser anemometer used in these experiments and shown in Fig. 4 is

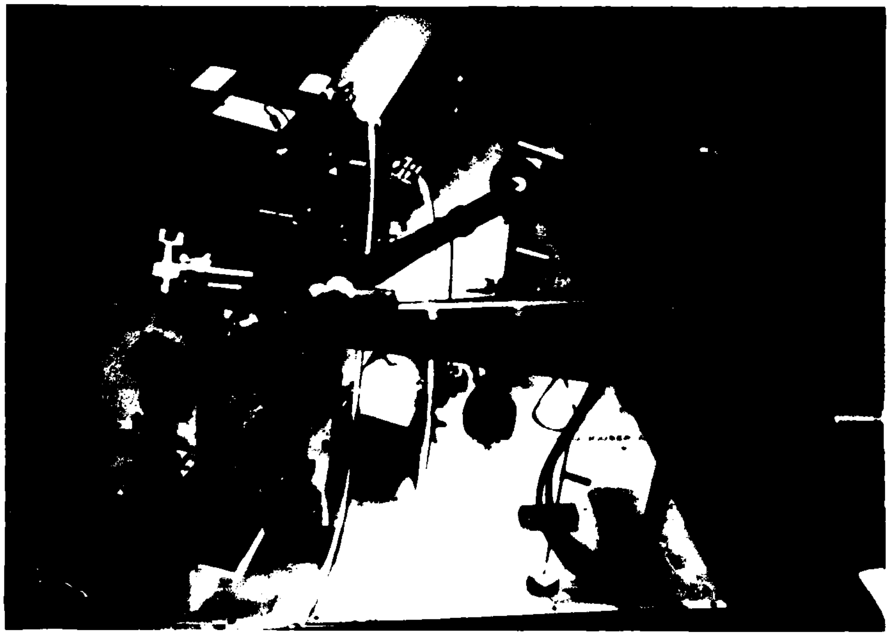

Figure 4. Photograph of current two-velocity component directionally-sensitive fringe-type laser anemometer.

described in some detail by Simpson and Chew (1979). In essence this is a two-velocity-component (U, V) directionally-sensitive fringe type system that has been used in earlier work (Simpson et al., 1977). The unshifted and 25 MHz Bragg-cell shifted beams lie in an almost horizontal plane and measure the streamwise velocity with vertical fringes. The unshifted and 15 MHz Bragg-cell shifted beams lie in a vertical plane and measure ($V \cos 4.4^\circ + W \sin 4.4^\circ$) with almost horizontal fringes. The 25 MHz and 15 MHz beams form a third fringe pattern that measures $(U - V \cos 4.4^\circ - W \sin 4.4^\circ)/\sqrt{2}$ around 10 MHz. Since $\overline{u^2}$ and $\overline{(v \cos 4.4^\circ + w \sin 4.4^\circ)^2}$ were measured independently and $\overline{uw}$ was presumed very small, the Reynolds shearing stress $-\overline{uv}$ resulted from this measurement. Signal processing was by fast-sweep-rate sampling spectrum analysis, as described by Simpson and Barr (1975).

The 1 micron dioctal phthalate particles follow the highly turbulent oscillations found in separated regions (Simpson and Chew, 1979). It should be noted that it is impossible to seed a highly turbulent flow in any prescribed manner. Highly turbulent flows are characterized by intense mixing with the flow. In this case there is also significant entrainment of freestream fluid into the turbulent motions. This would progressively dilute the particle concentration if only the shear flow has been seeded. Instead of needless worry over prescribed particle concentration, we have been concerned with proper averaging of available signals as described below, with enough particles to provide a high data rate, and with sufficiently small particles to accurately follow the flow. In fact, without any seeding we were able to obtain signals from ambient dust. However, we used minimal seeding to produce a signal data rate of about 400 per second.

Since the particle number density in a highly turbulent flow cannot be made uniform, the time between the passage of successive signal generating particles will be unequal. This effect alone presents no particular signal processing problem if the time intervals between successive signal bursts are small compared to $1/f_{max}$, the time period of the highest flow oscillation frequency f_{max} to be detected, i.e., if the signal is almost continuous. One can simply treat the signal as a continuous hot-wire anemometer signal to obtain the averages

$$U = \frac{1}{T} \int_0^T \mathcal{U}(t)dt \tag{1}$$

$$\overline{u^n} = \frac{1}{T} \int_0^T (\mathcal{U}(t) - U)^n \, dt \tag{2}$$

where n = 2, 3, 4 .... When the time intervals between successive signal bursts are long compared to $1/f_{max}$ (high signal dropout rate) and are unequal, these equations should also be used in the fashion explained below.

First, let us look at the commonly used method of particle averaging for individual particle velocity measurements. The averages are made over the number of signal bursts N obtained during the time period T:

$$U_N = \frac{\sum_{i=1}^{N} \mathcal{U}_i}{N} \tag{3}$$

$$\overline{U_N{}^n} = \frac{\sum_{i=1}^{N} (\mathcal{U}_i - U_N)^n}{N} \tag{4}$$

where n = 2, 3, 4 .... These averages are not made with respect to time and are biased unless the time intervals between signal bursts are equal. McLaughlin and Tiederman (1973) proposed a biasing correction that is based upon the idea that higher velocity flow carries more particles through the focal volume per unit time. Thus, more high velocity signal bursts will be obtained and U_N will be too high. However, high velocity particles speed less time in the focal volume so that in the case of sampling spectrum analysis signal processing, the chance of detecting a given signal burst varies as $(U^2 + V^2 + W^2)^{-1/2}$. Thus, this effect tends to cancel the above mentioned bias for particle averaging. Durão and Whitelaw (1975) showed that if the Doppler bursts are randomly sampled before particle averaging, the bias effects are reduced significantly. Even so, particle averaging is not fundamentally a time average.

Consider now time-averaging of signals according to equations (1) and (2), even though the signal dropout rate may be large. Only ergodic flows, whose averaged quantities in equations (1) and (2) become independent of time for large T, are considered. This restriction is also required for particle averaging. The last sampled signal must be held by a sample-and-hold circuit until a new signal is detected for time-averaging. With exception of the instant at which a new signal is detected, the sampled-and-held voltage does not correspond to the actual instantaneous velocity. However, the voltage value at each instant corresponds to the instantaneous velocity at some instant during a record time T for an ergodic flow. Since any averaging process removes time domain dependency, it does not matter when during the time period T that it is averaged. It is unlikely that a given signal voltage will be averaged too long (Simpson and Chew, 1979). This method of averaging eliminates the need for the high velocity flow bias correction.

The mechanics of evaluating a true time average in this research made use of a velocity probability histogram, such as shown in Figure 5. A SAICOR Model 41 Correlator and Probability Analyzer was used.

$$1 = \int_{-\infty}^{+\infty} P(\mathcal{U})dU \tag{5}$$

$$U = \int_{-\infty}^{+\infty} P(\mathcal{U})dU \tag{6}$$

$$\overline{u^n} = \int_{-\infty}^{+\infty} (\mathcal{U} - U)^n P(\mathcal{U})dU \tag{7}$$

where n = 2, 3, 4 .... The histogram $P(\mathcal{U})$ is constructed by sampling the $\mathcal{U}(t)$ sample-and-held signal at equal intervals in time Δt for the period T. Thus the histogram reflects a true time integral and the results from equations (5-7) will be equivalent to those from equations (1-2). The time interval Δt between digital samples should be no larger than the shortest time between signal bursts, otherwise some data will be lost. For example, $\Delta t = 10^{-4}$ sec for about 400 new signals per second. The averaging time T was at least a half minute, so at least 12,000 new data signals and 3×10^5 *equal time interval* samples were involved for one histogram. An added benefit of the histogram approach is that noise can be detected while $P(\mathcal{U})$ is being constructed. If one has an oscilloscope display, the noise will cause the base level of $P(\mathcal{U})$ to grow. Thus, the resulting $P(\mathcal{U})$ can be corrected for noise or the discriminator level in the signal processor can be adjusted on-line and a new $P(\mathcal{U})$ constructed. The histograms were stored on digital tape and analyzed by a digital computer.

These results are not believed to suffer strongly from bias errors. First, there is no bias in the duration of a detected signal due to the flow velocity. In other words, the time that the highest velocity particle spends in the focal volume is always large enough to produce a sufficiently large vertical voltage output from the spectrum analyzer. Minimal particle seeding was used for the

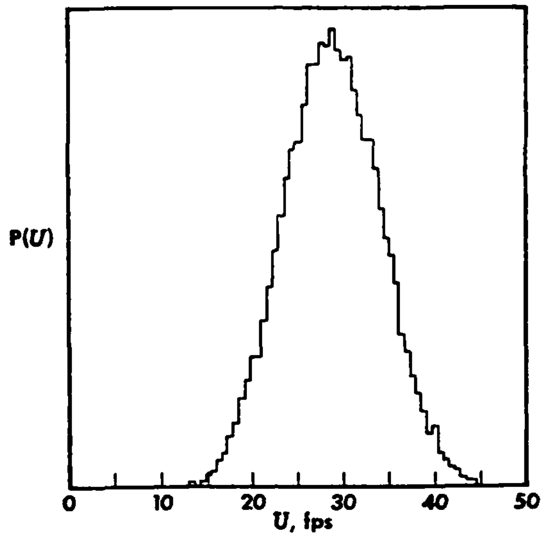

Figure 5. Typical velocity probability histogram: U = 29.1fps, $\overline{u^2}$ = 27.0(fps)^2 S_u = 0.047, F_u = 2.66. Discrete velocity bins due to probability analyzer.

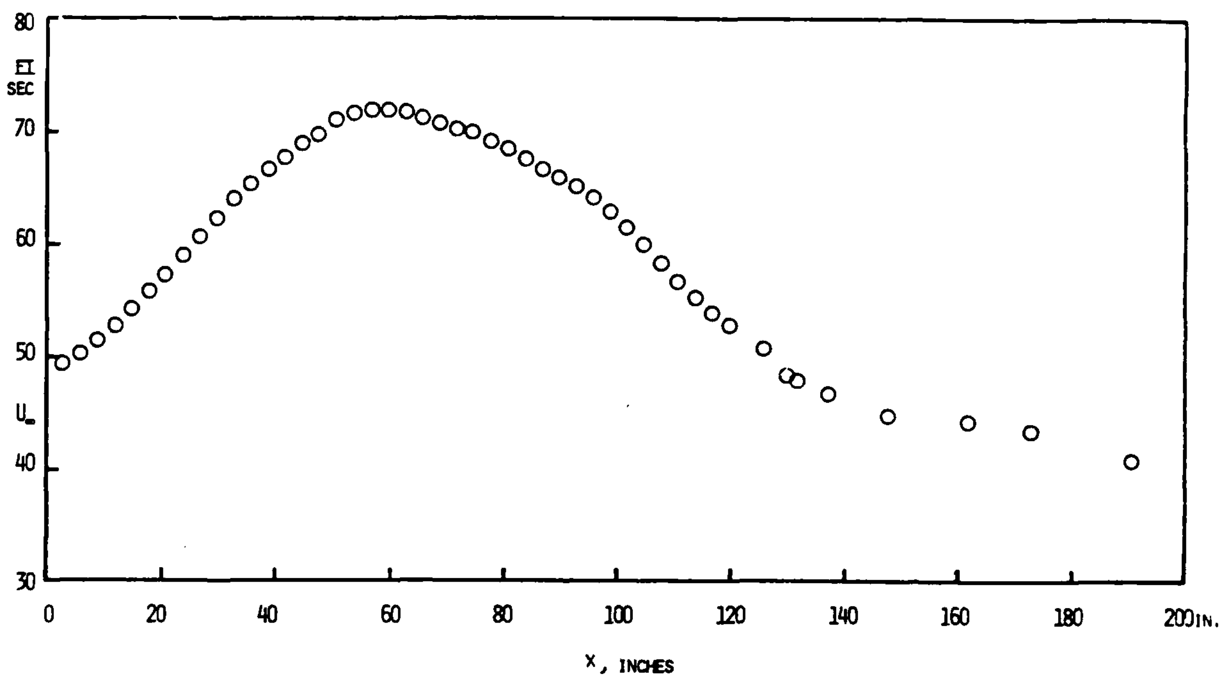

Figure 6. Freestream velocity distribution along the tunnel centerline.

best SNR and data sample rate, so significant finite transit time broadening is unlikely.

Velocity gradient broadening is not significant for any data presented here (Simpson, 1976). The focal volume diameter 0.012 inches and length 0.140 inches are small compared to the boundary layer thickness. In addition, signals from the center of the focal volume are the most likely since the scattered signals are the most intense. Large-scaled motions, which scale on the boundary layer thickness, appear to dominate the structure of highly turbulent flows, so strong instantaneous spatial velocity variations are unlikely. In any event as shown below, these results compare favorably with hot-wire anemometer data obtained in regions that do not contain significant time variation of the flow direction.

Since no spectra has previously been measured in the separated flow zone, low frequency spectra of u from the laser anemometer were measured using a Princeton Applied Research Model 4512 Fast-Fourier-Transform Spectrum Analyzer.

II. DESCRIPTION OF THE TEST FLOW

All data were obtained at atmospheric pressure and 77 $\pm$ ½°F flow conditions. Figure 6 shows the free-stream velocity distributions obtained along the tunnel centerline using the single-wire probe. This distribution was repeatable within 2.9% over the duration of these experiments, which is only a little greater than uncertainty in measuring the mean velocity with a hot-wire anemometer ($\pm$ 2.4%). Figure 7 shows the non-dimensional pressure gradient dC_p/dx along the centerline of the test wall. Here $C_p \equiv 2(P - P_i)/\rho U_{\infty i}^2 = 1 - (U_\infty/U_{\infty i})^2$, where i denotes the free-stream entrance conditions at x = 3". A five-point local least-squares curve fit of C_p data was used at each streamwise location to determine this derivative.

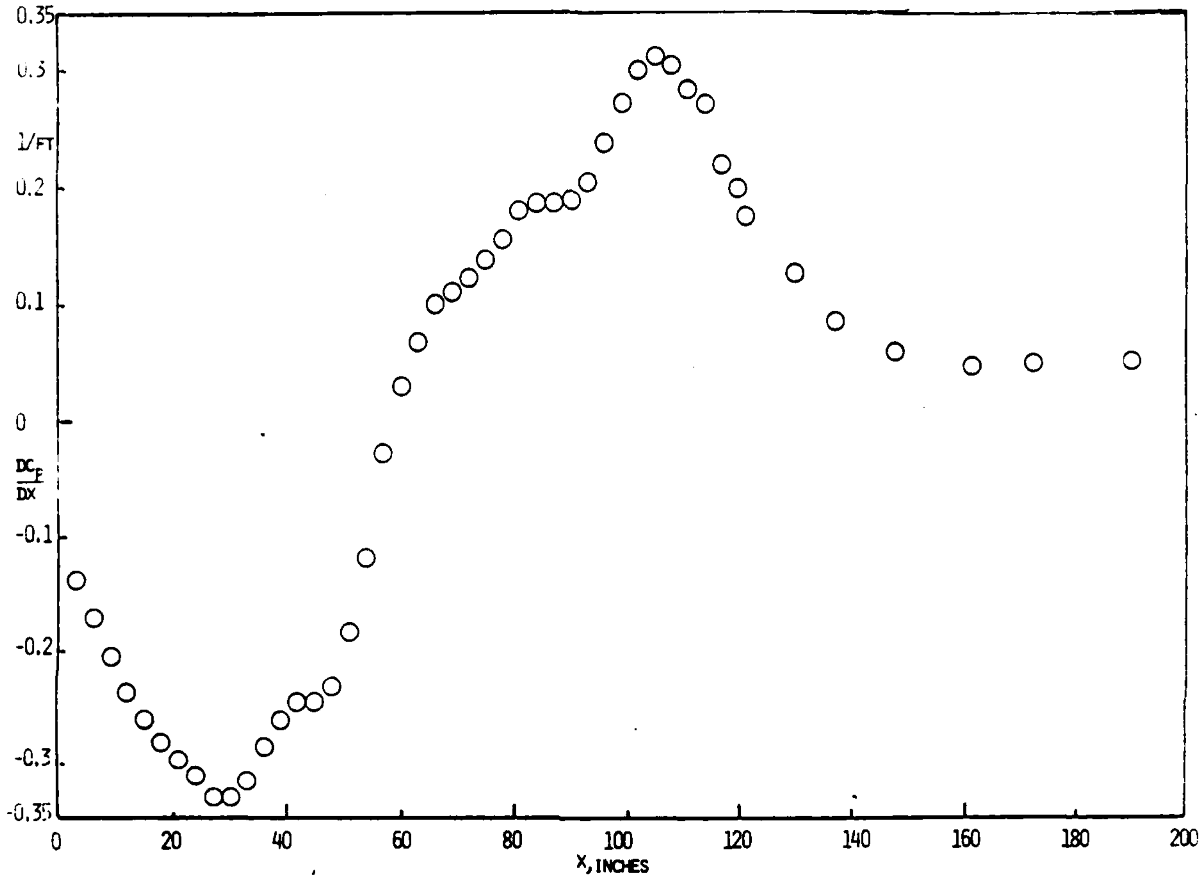

Figure 7. Non-dimensional pressure gradient along the test wall, $C_p = 2(P-P_i)/\rho U_{\infty i}^2 = 1 - (U_\infty / U_{\infty i})^2$, $U_{\infty i}$ = 49.4 fps.

Just downstream of the location of the second wall jet boundary layer control unit (100 inches), the slope of the static pressure gradient changes sign. Near 145 inches the pressure gradient drops to an approximately constant value downstream.

To examine the two-dimensionality of the mean boundary layer flow, smoke was introduced only in a spanwise portion of the test wall boundary layer at a given time. A sheet of laser light produced by a cylindrical lens was used to illuminate the smoke across the tunnel. Upstream of separation, negligible spanwise diffusion of the smoke was observed, indicating no gross flow three-dimensionality. Mean velocity profiles at several spanwise locations indicated that the mean velocity was two-dimensional within 1%. Downstream of separation greater spanwise diffusion occurred, so that downstream of 170 inches no nominally two-dimensional flow remained. On the basis of these observations, the wall jet and suction boundary layer controls were adjusted to produce a nearly two-dimensional flow pattern downstream of separation. Smoke flow patterns in the sidewall and corner flows were symmetric about the channel centerline.

After laser and hot-wire anemometer data were available, examination of the two-dimensionality was done by evaluating the terms in the two-dimensional continuity equation and the momentum integral equation. In the first method, the differential continuity equation was written as

$$R = 1 + (U_{X + \Delta X} - U_X) \Big/ \left(\frac{\partial V}{\partial y}\right) \Delta X$$

R was computed by finding the gradient of V with respect to y and also the change in U with respect to X at a constant y location. Only where LDV data were available was this method useful, because it requires good V data.

For many streamwise locations R lies between +0.5 and -0.5 in the middle region of the boundary layer, with an uncertainty of $\pm$ 0.46. Nearer the wall, ΔU becomes relatively more uncertain while $\partial V/\partial y$ is more uncertain in the outer region. As a result one can expect greater uncertainties in R in these regions. Thus, at least in the middle region of the boundary layer, the flow is two-dimensional within the uncertainty of evaluating R. This is a stringent test since it is based only on the local flow field, but it suffers from the disadvantage of needing to differentiate experimental velocity distributions.

On the other hand, the momentum integral equation provides a global test based on conservation of momentum over a large flow volume. In this method, the momentum integral equation was again integrated in the x-direction to yield

$$U_\infty^2\theta\Big]_{x_0}^{x} + \int_{x_0}^{x} (U_\infty\delta_1^*) \frac{dU_\infty}{dx}dx = \int_{x_0}^{x} \frac{C_f}{2} U_\infty^2\, dx + \int_{x_0}^{x} \left[\int_0^\infty \frac{\partial}{\partial x} (\overline{u'^2} - \overline{v'^2})\right]dx \qquad (8)$$

where the l.h.s. is PL and the r.h.s. is PR. The last term of PR is due to the normal stresses and its effect in the vicinity of separation has been shown (Simpson et al., 1977) to be significant. Using the experimental data, PL and PR of eqn. (8) were evaluated with and without the normal stress term and the ratio, $\frac{PL}{PR} - 1$, was computed for both the cases. The distributions on the ratio in the streamwise direction are shown in Fig. 8 along with estimated uncertainty bands. The ratio computed without the normal stress term is within $\pm$ 0.16 up to 122 inches, indicating that the flow is reasonably two-dimensional.

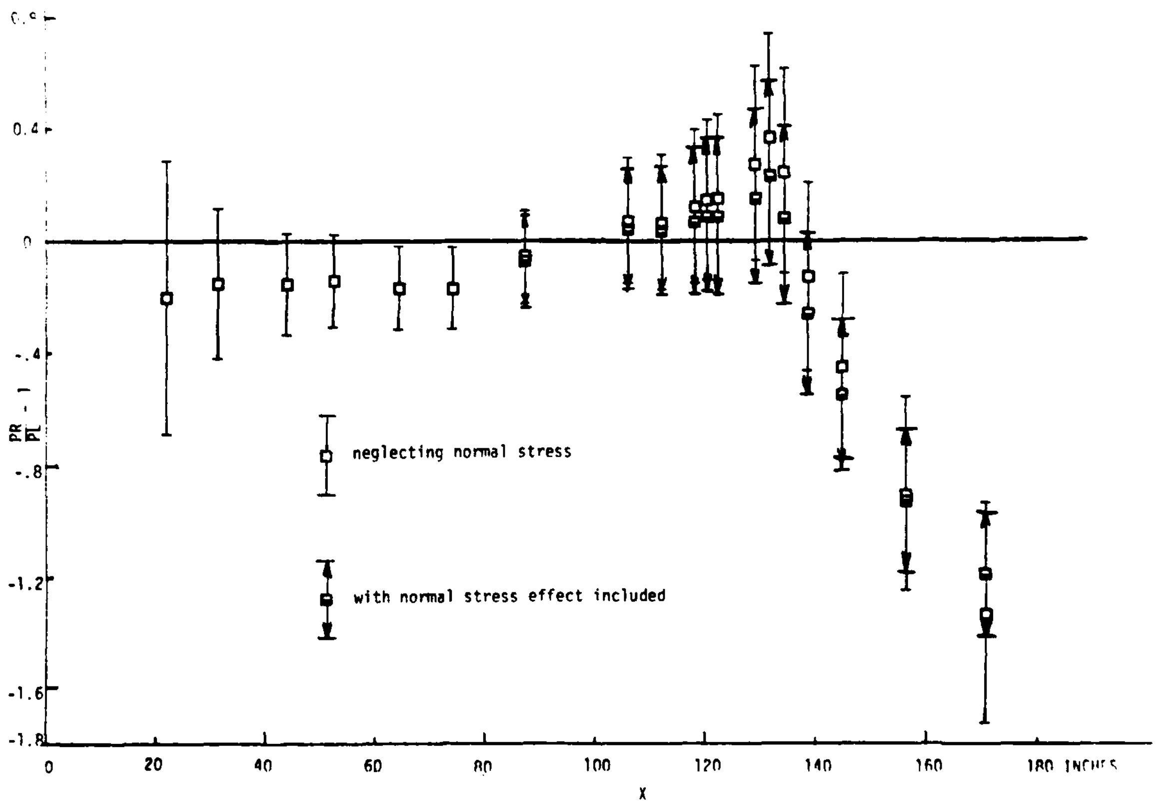

Figure 8. Fractional imbalance of the momentum integral equation, PL/PR - 1, vs. X. Associated uncertainty denoted by vertical band.

Downstream the normal stresses play an more important role, although they are not large enough to account for the imbalance far downstream of separation.

IV. EXPERIMENTAL RESULTS FOR THE MEAN FLOW

IV.1 Mean Velocity Profiles

Mean velocity profiles were obtained in the unseparated upstream boundary layer and the outer part of the separated flow using single wire and cross-wire hot-wire anemometer probes. The directionally-sensitive laser anemometer provided velocity profiles in the separated zone and the region immediately upstream.

Figures 9a and 9b show the streamwise mean velocity profiles for steady flow for a few typical stations in the near separation and the separated regions obtained using all three different techniques. There is good agreement among these measurements, with the maximum discrepancy among them being about 6 to 7%. In the separated region only the laser anemometer measurements are meaningful. Table 1 presents the experimental uncertainties for each measured quantity as determined by the method of Kline and McClintock (1953). As shown by Simpson and Chew (1979), the laser anemometer results obtained on different days at the same location indicate a high level of data repeatability.

Figures 10 and 11 show non-dimensional streamwise mean velocity profiles across the boundary layer at various streamwise stations in linear and semi-logarithmic co-ordinates. These results were obtained by smoothing a curve between the laser and valid cross-wire data. While the smoothing was a somewhat subjective procedure, one can see from Figures 9a and 9b that this procedure basically just eliminated a few scattered data points.

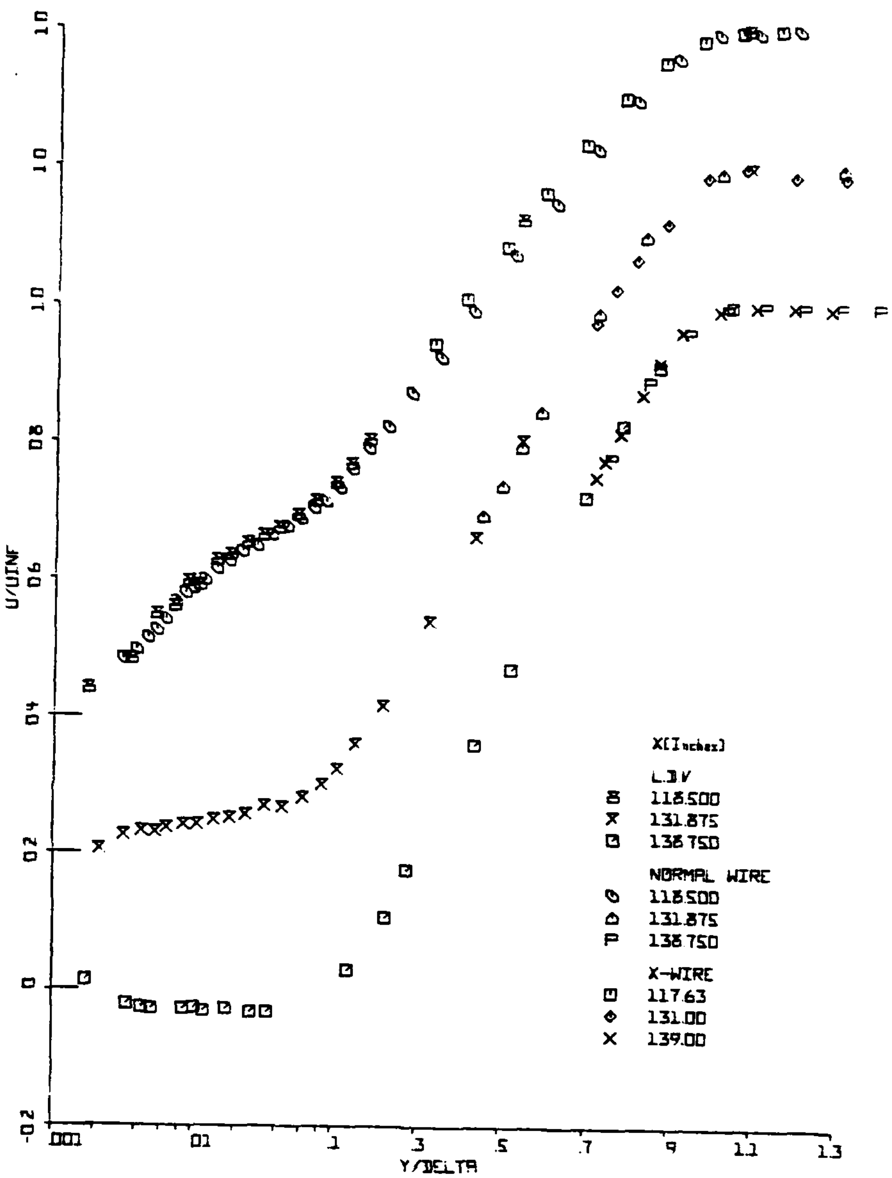

Figure 9 (a). Non-dimensional streamwise mean velocity profile data from the laser and hot-wire anemometers. Note displaced ordinates.

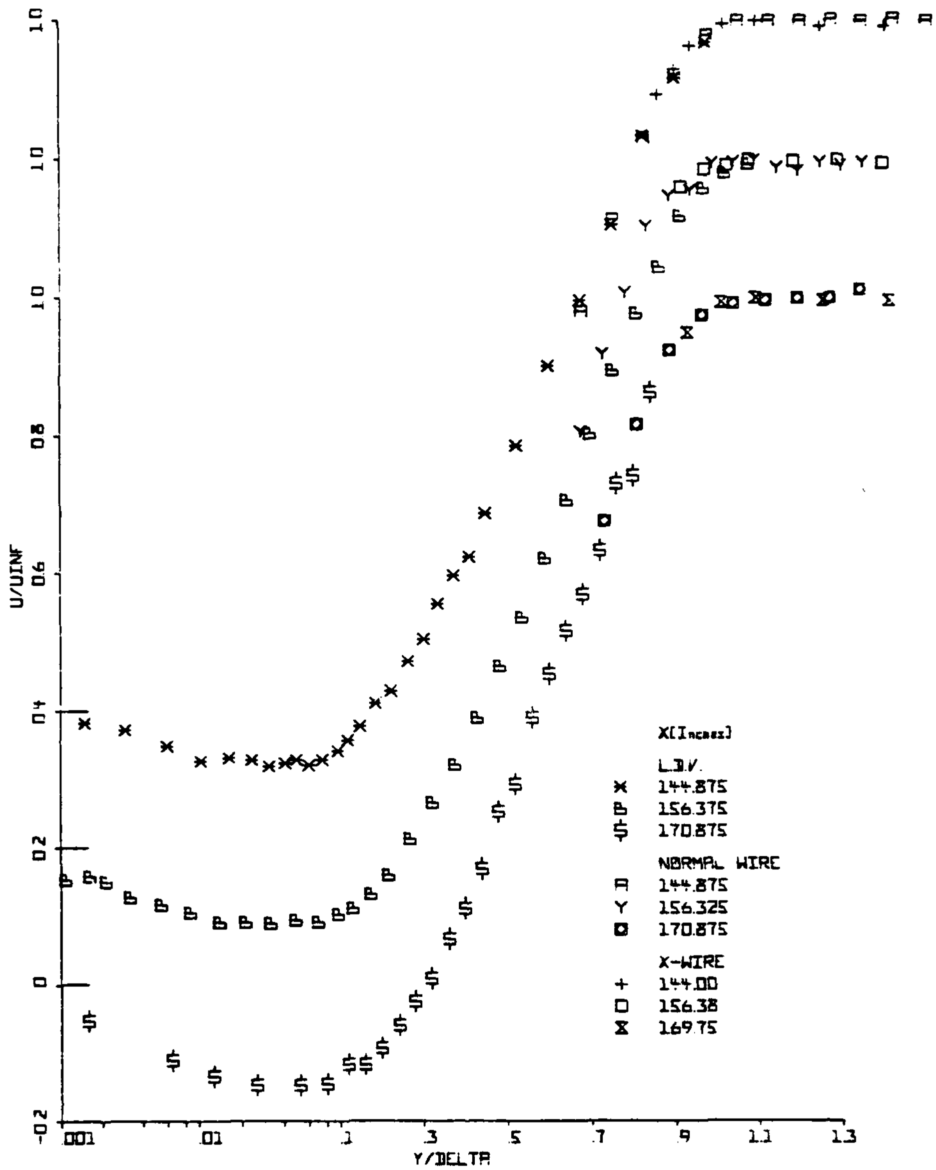

Figure 9 (b). Non-dimensional streamwise mean velocity profile data from the laser, single hot-wire, and cross hot-wire anemometers. Note displaced ordinates.

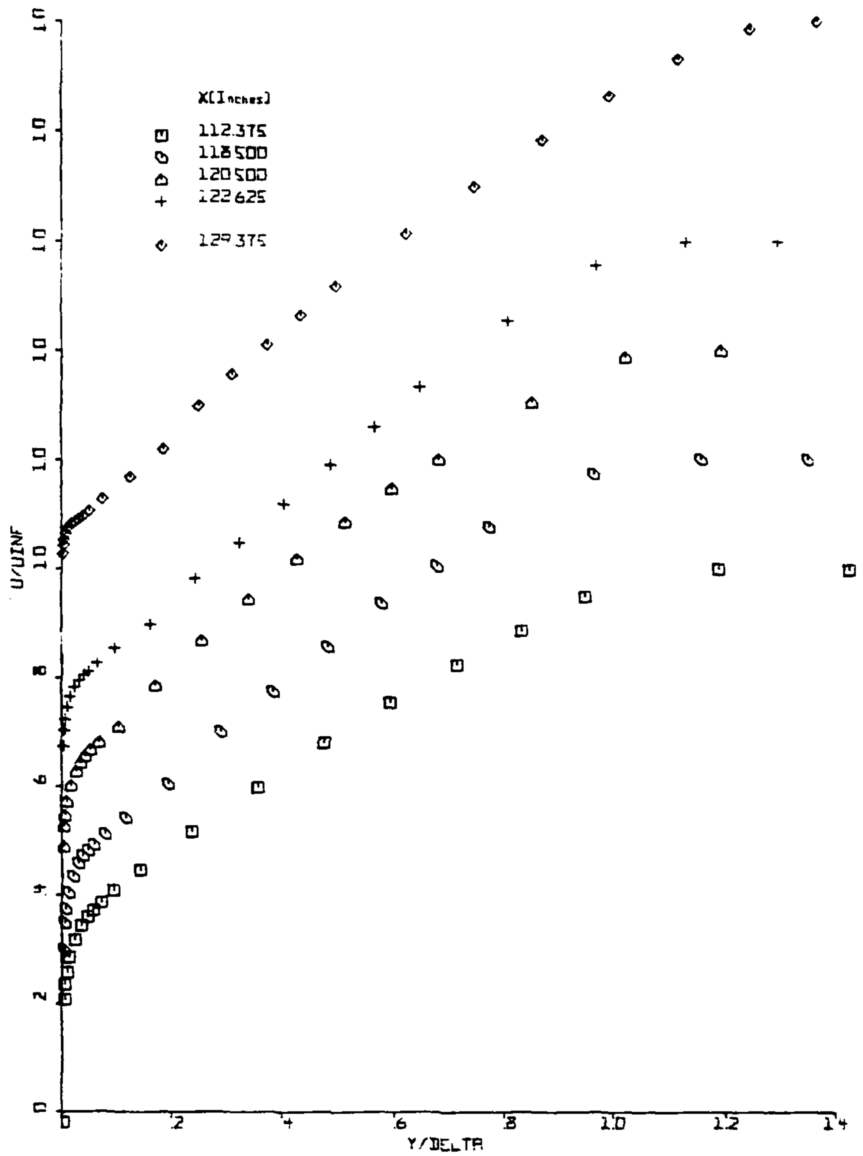

Figure 10(a). Smoothed results from laser and hot-wire anemometer data. Note displaced ordinates.

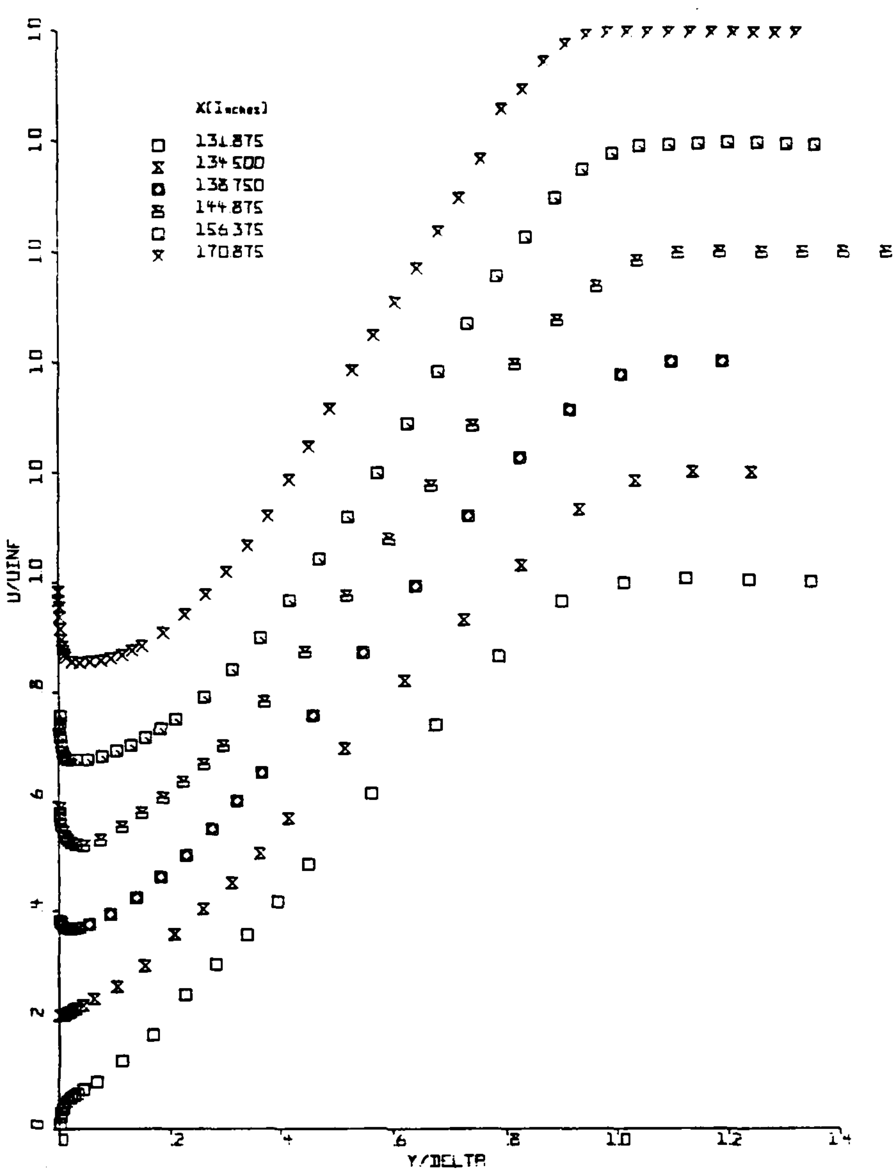

Figure 10(b). Smoothed results from laser and hot-wire anemometer data. Note displaced ordinates.

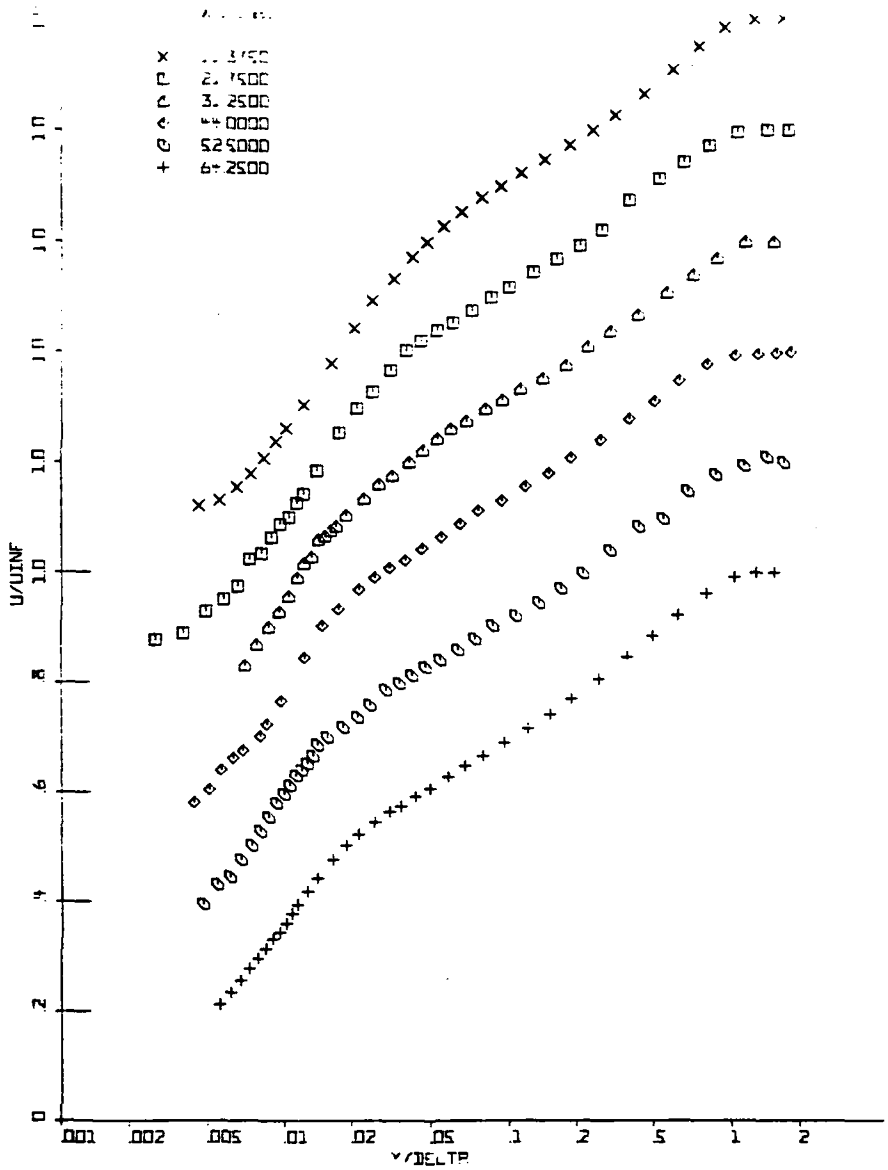

Figure 11(a). Non-dimensional streamwise mean velocity profiles: single hot-wire results.

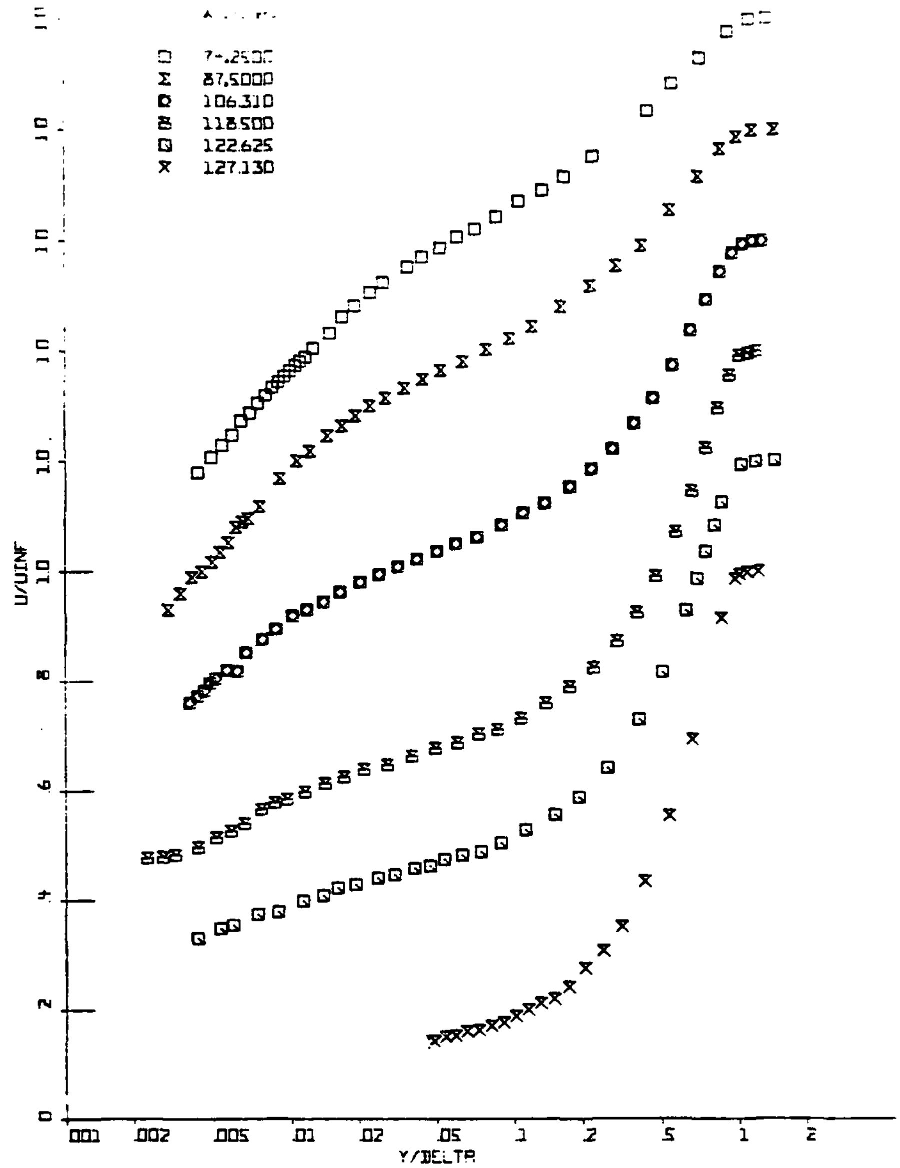

Figure 11(b). Non-dimensional streamwise mean velocity profiles: single hot-wire results.

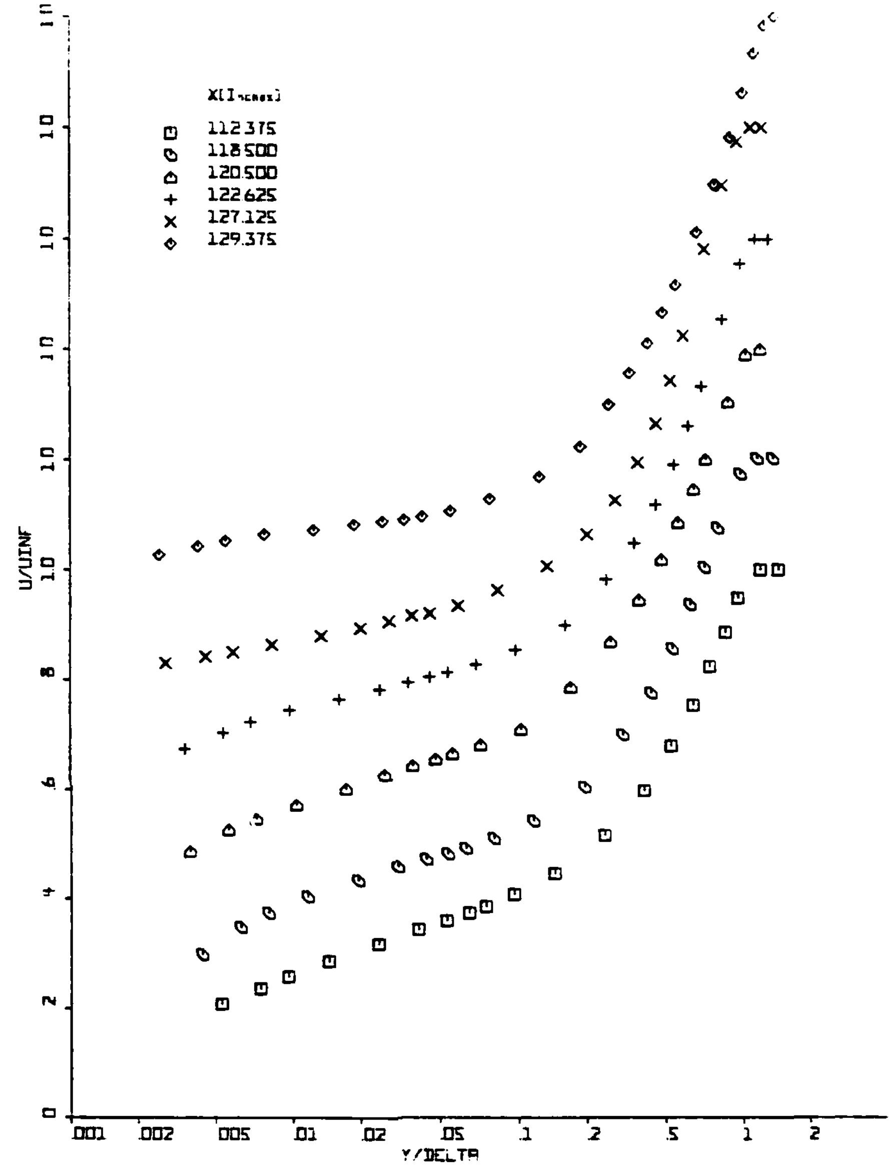

Figure 11(c). Non-dimensional streamwise mean velocity profiles: smoothed laser and valid single hot-wire anemometer results.

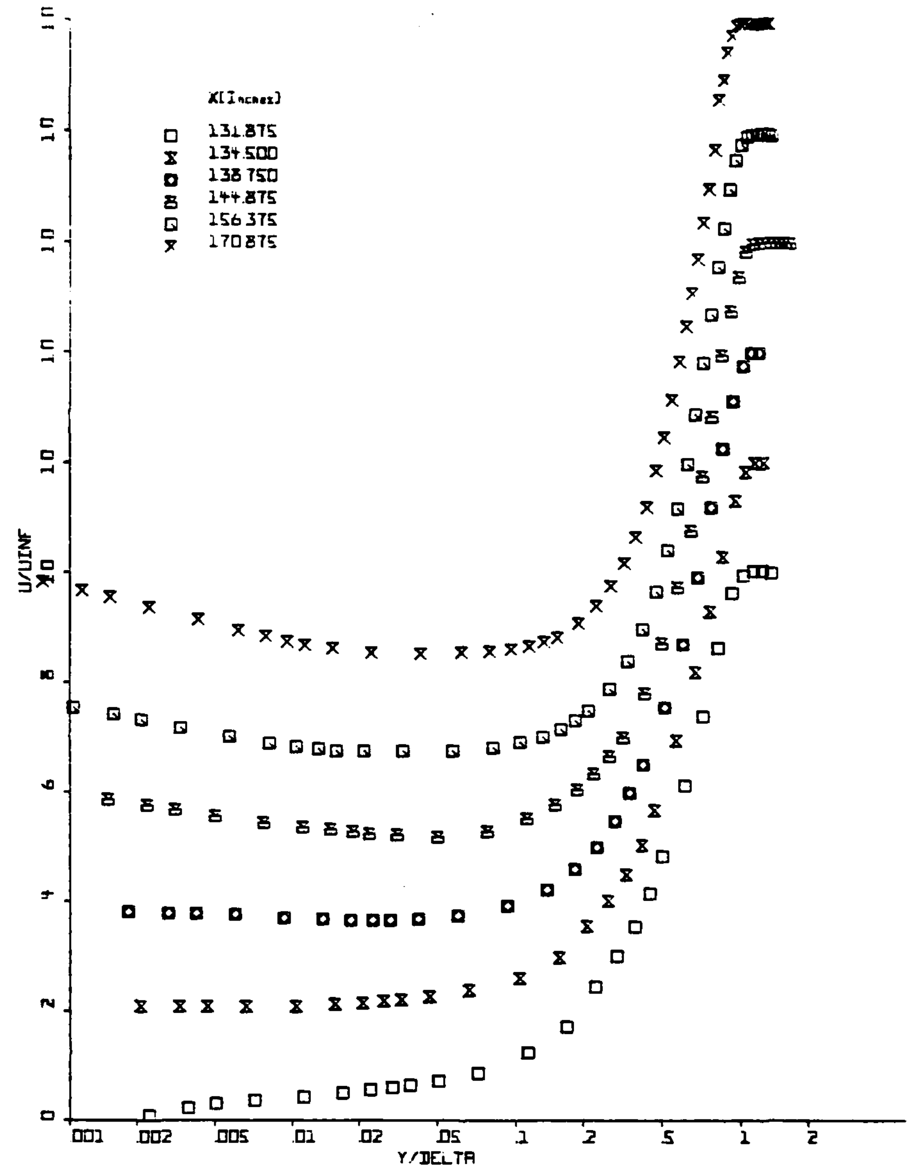

Figure 11(d). Non-dimensional streamwise mean velocity profiles: smoothed laser and valid single hot-wire anemometer results.

Figure 12 shows non-dimensional laser anemometer and cross-wire anemometer results for the normal velocity component V just upstream of separation and in the separated region. At most streamwise locations, there is good agreement. However, as shown in Table 1, there is a fairly large uncertainty in the cross-wire result, mainly because of the uncertainty of the probe orientation with respect to the test wall. Therefore, the laser anemometer results are more reliable.

IV.2 Turbulence Quantities

Figures 13, 14, and 15 show u'/U_∞, v'/U_∞, and $-\overline{uv}/U_\infty^2$ vs. y/δ, respectively. The agreement between the laser and cross-wire anemometer results is good with the apparent discrepancies being due to the experimental uncertainties shown in Table 1. The discrepancies in the $-\overline{uv}/U_\infty^2$ plots are the greatest due to the uncertainty in orientation of the cross-wire probe with respect to the test wall. Since $\overline{u^2}$ and $\overline{v^2}$ are much larger than $-\overline{uv}$, only a very small misalignment is required to produce a much different $-\overline{uv}$ result. Figures 16 (a-e) show profiles obtained by smoothing a curve between the laser anemometer and valid cross-wire data. Figure 17 shows u'/U_∞, v'/U_∞, and $-\overline{uv}/U_\infty^2$ profiles upstream of the near separation zone. Figures 18 (a) and (b) show u'/U_∞ obtained from the single wire anemometer.

IV.3 Upstream-downstream Intermittency

Only the directionally-sensitive laser anemometer results from these measurements give information on the fraction of time that the flow moves downstream or γ_{pu}. This quantity is the fraction of the area of the velocity probability histogram that has a positive velocity. The directionally-insensitive hot-wire anemometer cannot yield γ_{pu} values (Simpson, 1976).

Normal hot-wire:	$U \pm 2.4\%$, $\overline{u^2} \pm 7\%$
Cross hot-wire: (including misalignment uncertainty)	$U \pm 3.2\%$, $\overline{u^2} \pm 10\%$ $v^2 \pm 11\%$, $-\overline{uv} \pm 17\%$, $S_v \pm 0.1$
Laser anemometer:	U, $V \pm 0.2$ fps; $\overline{u^2}$ and $\overline{v^2}$ $\pm$ 4% max. profile value; $\overline{uv} \pm 6\%$ max. profile value; skewness ± 0.1; flatness ± 0.2; $\gamma_{pu} \pm 0.1 \exp(-U^2/2\overline{u^2})$; $\gamma_{pv} \pm 0.1 \exp(-V^2/2\overline{v^2})$
Position from wall:	$\pm$ 0.002 inches
Skin friction coefficient C_f:	Ludwieg-Tillman, $\pm$ 6.5%; Preston tube, $\pm$ 8.5%; Surface hot-wire, $\pm$ 12%.

Table 1. Estimated uncertainties of measured quantities.

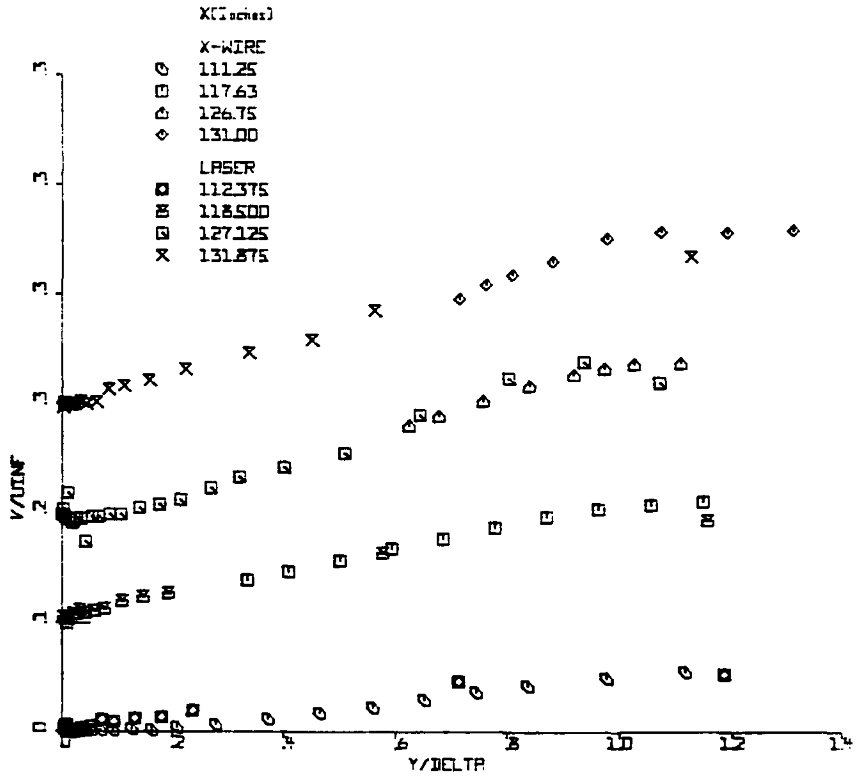

Figure 12(a). Mean velocity V/U_∞ vs. y/δ profiles, laser and cross hot-wire anemometer data.

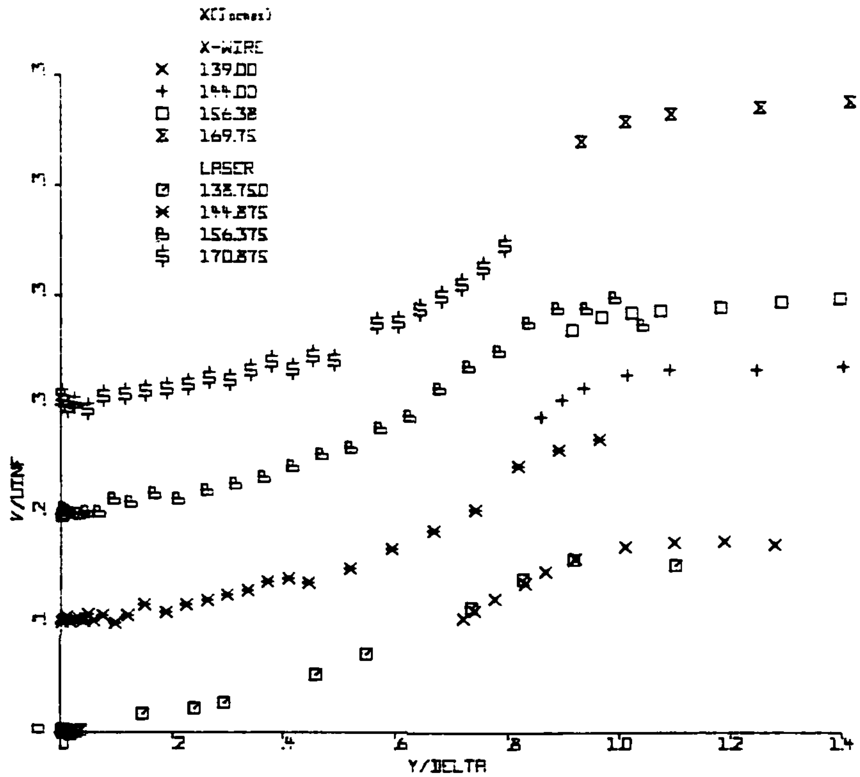

Figure 12(b). Mean velocity V/U_∞ vs. y/δ profiles, laser and cross hot-wire anemometer data.

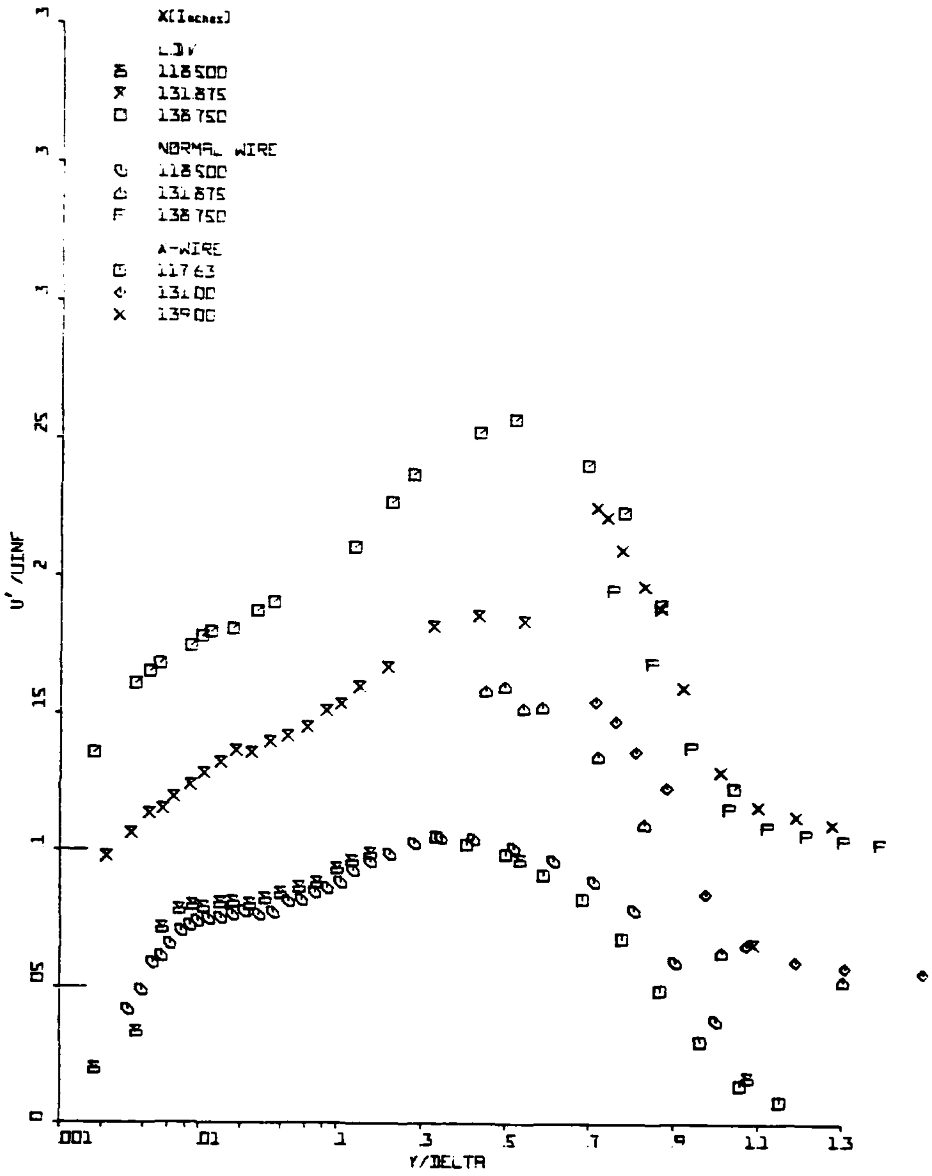

Figure 13(a). Streamwise turbulence intensity u'/U_∞ vs. y/δ profiles: laser, single hot-wire, and cross hot-wire anemometer results. Note displaced ordinates.

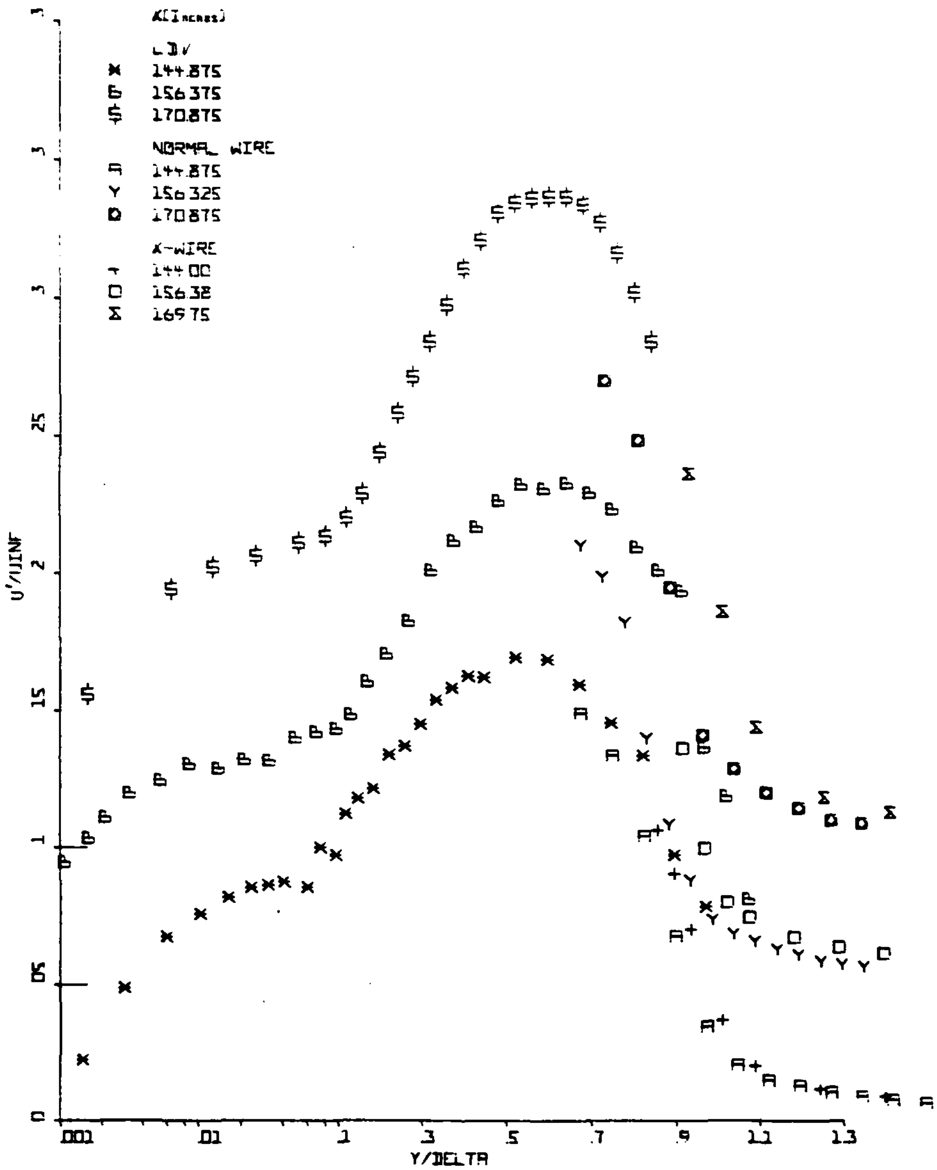

Figure 13(b). Streamwise turbulence intensity u'/U_∞ vs. y/δ profiles: laser, single hot-wire, and cross hot-wire anemometer results. Note displaced ordinates.

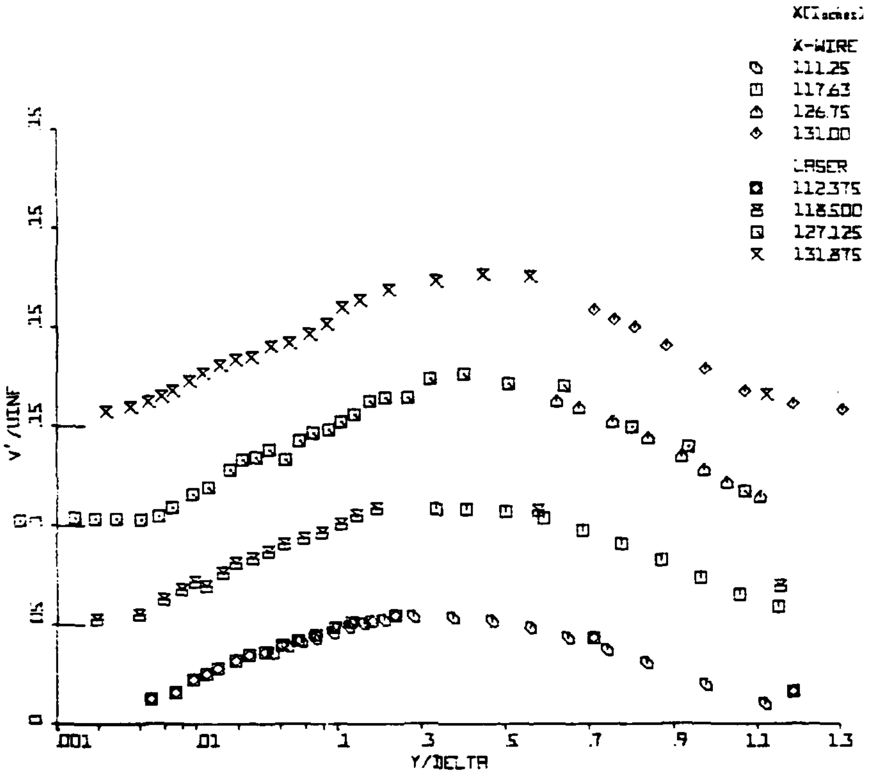

Figure 14(a). v'/U_∞ vs. y/δ profiles: laser and cross hot-wire anemometer results. Note displaced ordinates.

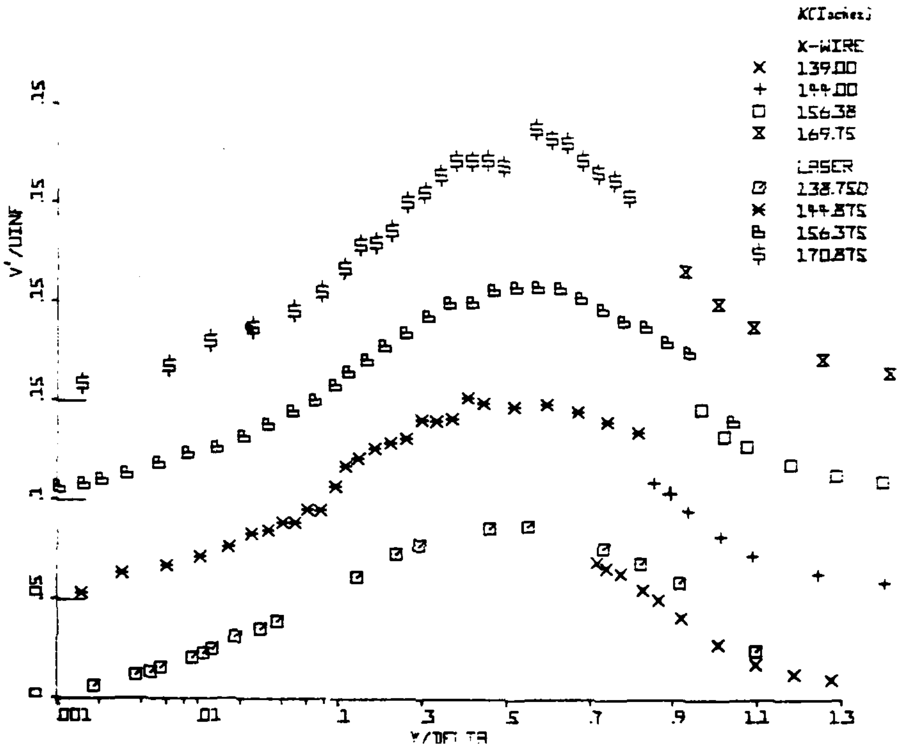

Figure 14(b). v'/U_∞ vs. y/δ profiles: laser and cross hot-wire anemometer results. Note displaced results.

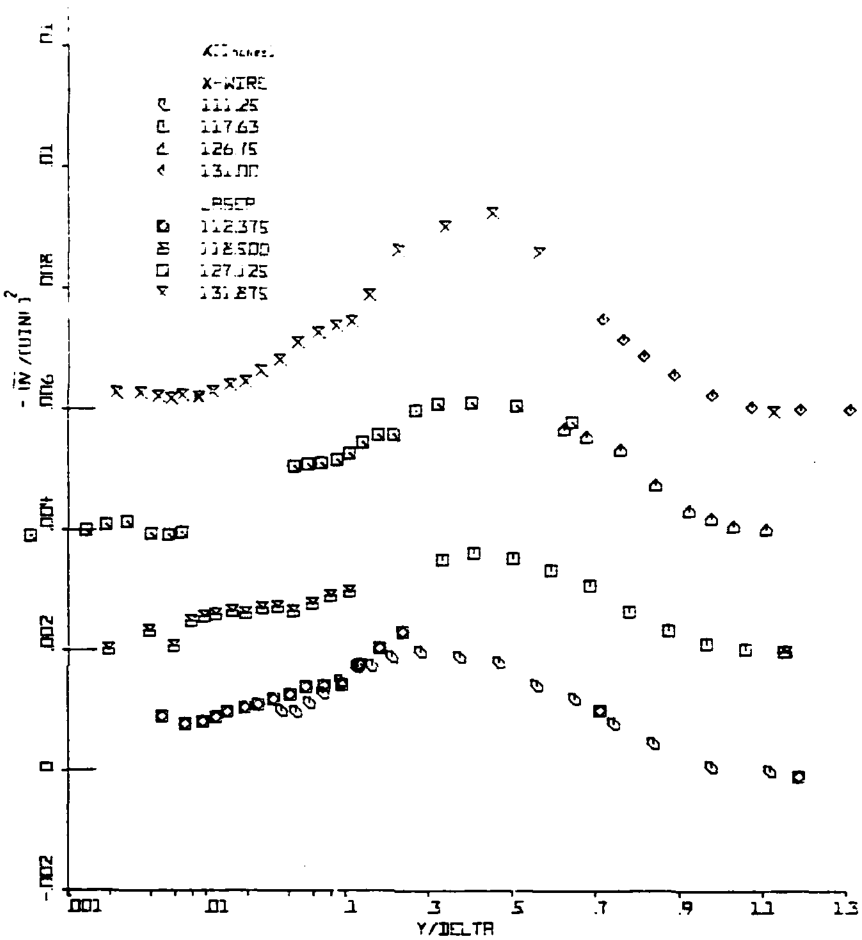

Figure 15(a). Reynolds shearing stress $-\overline{uv}/U_{\infty}^{2}$ vs. y/δ profiles: laser and cross hot-wire anemometer results. Note displaced ordinates.

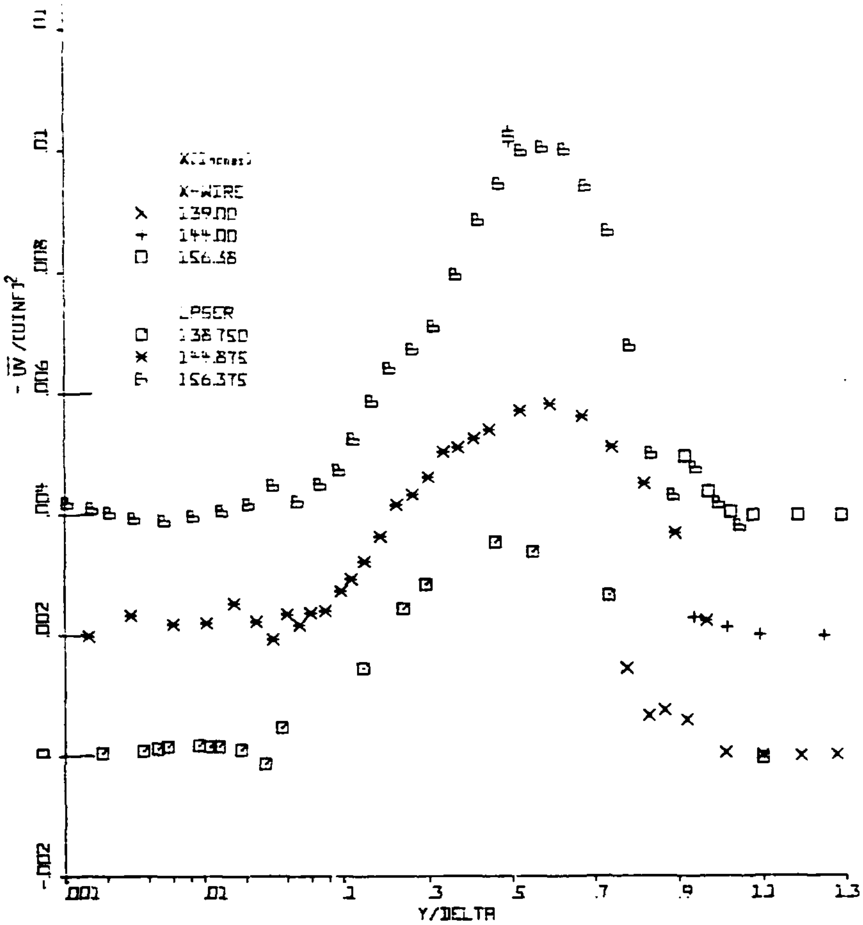

Figure 15(b). Reynolds shearing stress $-\overline{uv}/U_\infty^2$ vs. y/δ profiles: laser and cross hot-wire anemometer results. Note displaced ordinates.

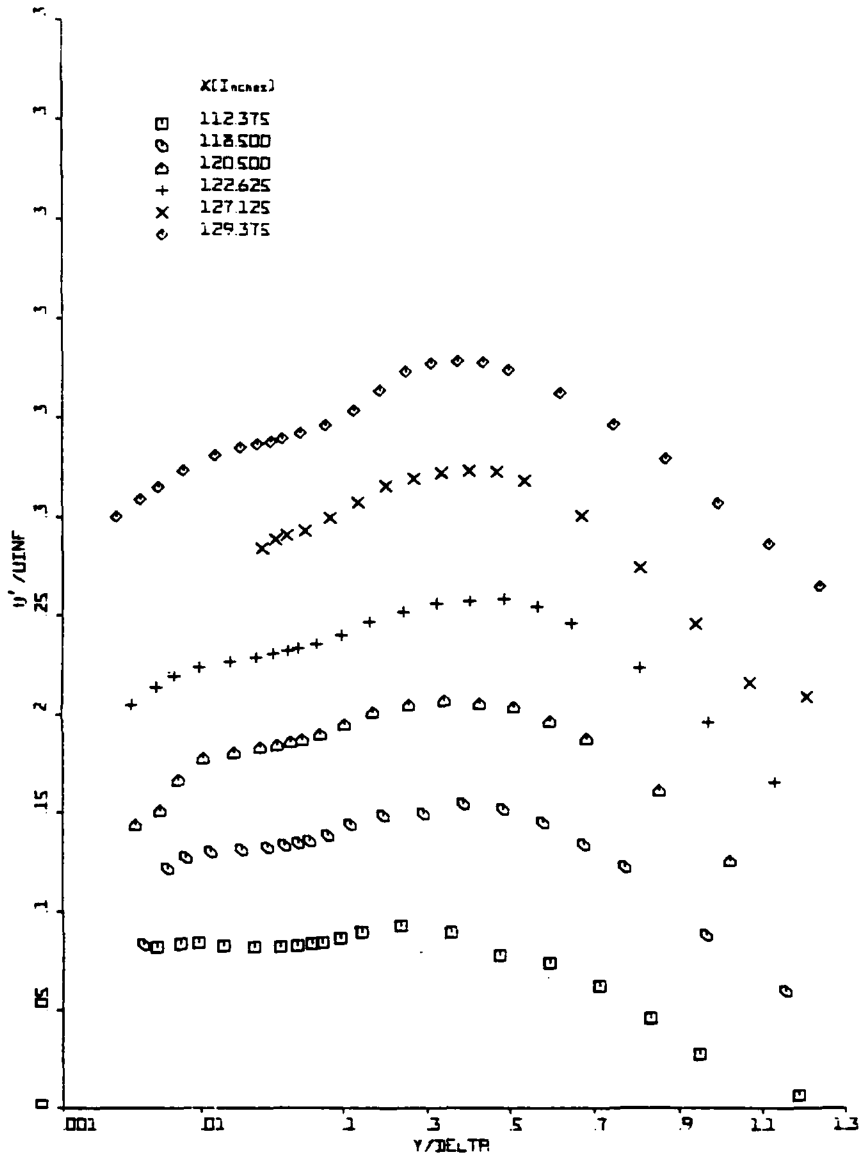

Figure 16(a). Smoothed u'/U_∞ vs. y/δ results from hot-wire and laser anemometers. Note displaced ordinates.

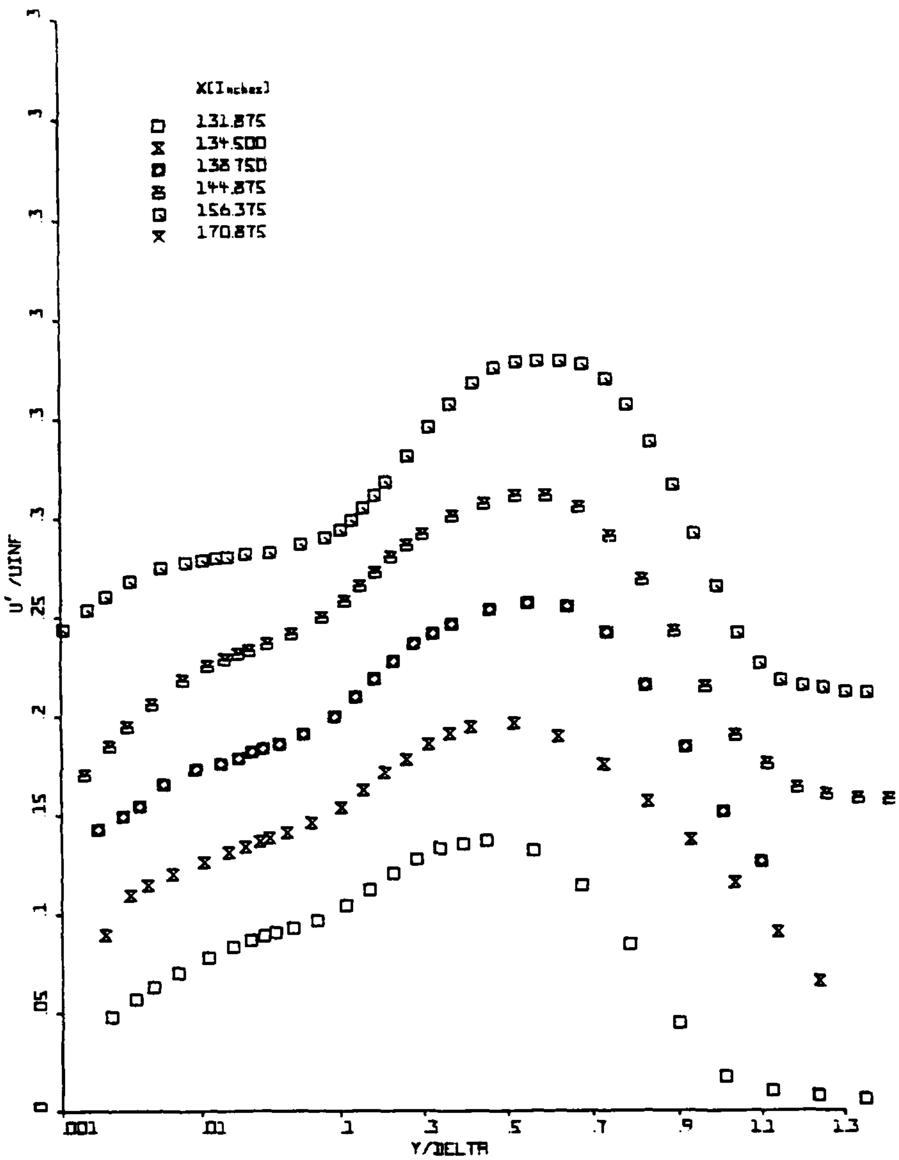

Figure 16(b). Smoothed u'/U_∞ vs. y/δ results from hot-wire and laser anemometers. Note displaced ordinates.

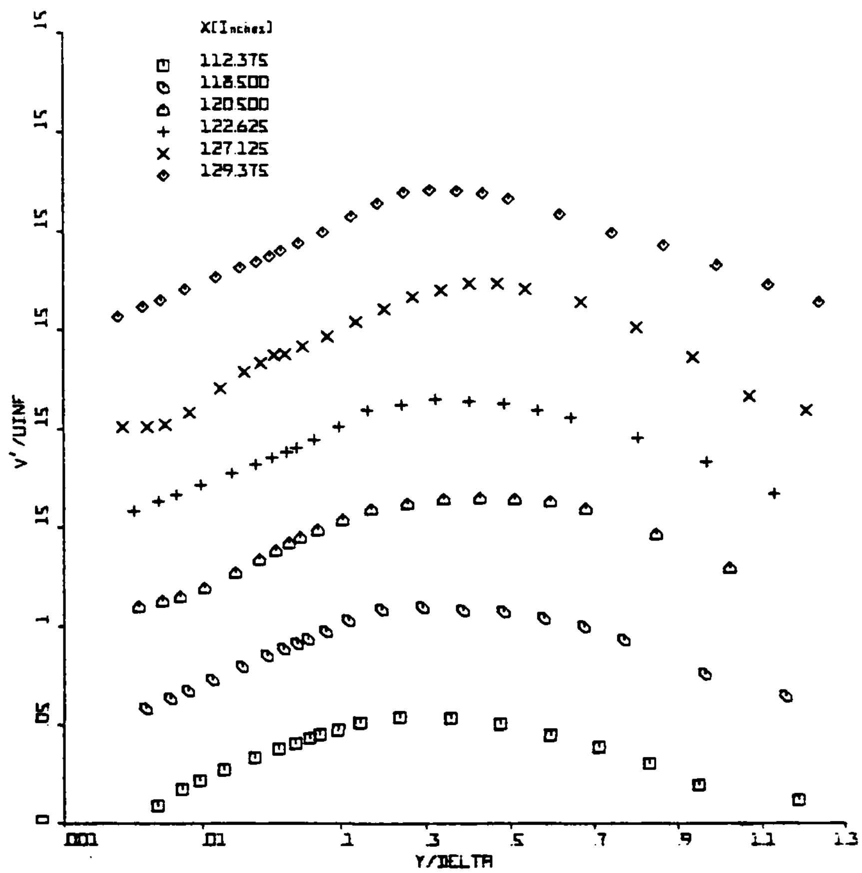

Figure 16(c). Smoothed v'/U_∞ vs. y/δ results from hot-wire and laser anemometers. Note displaced ordinates.

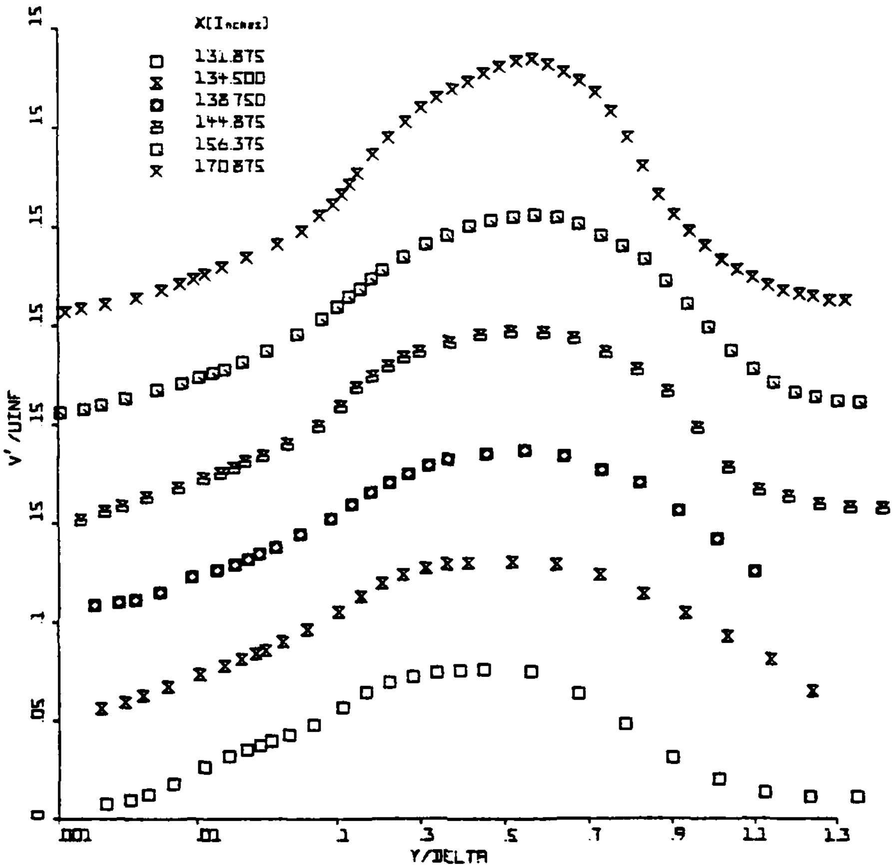

Figure 16(d). Smoothed v'/U_∞ vs. y/δ results from hot-wire and laser anemometers. Note displaced ordinates.

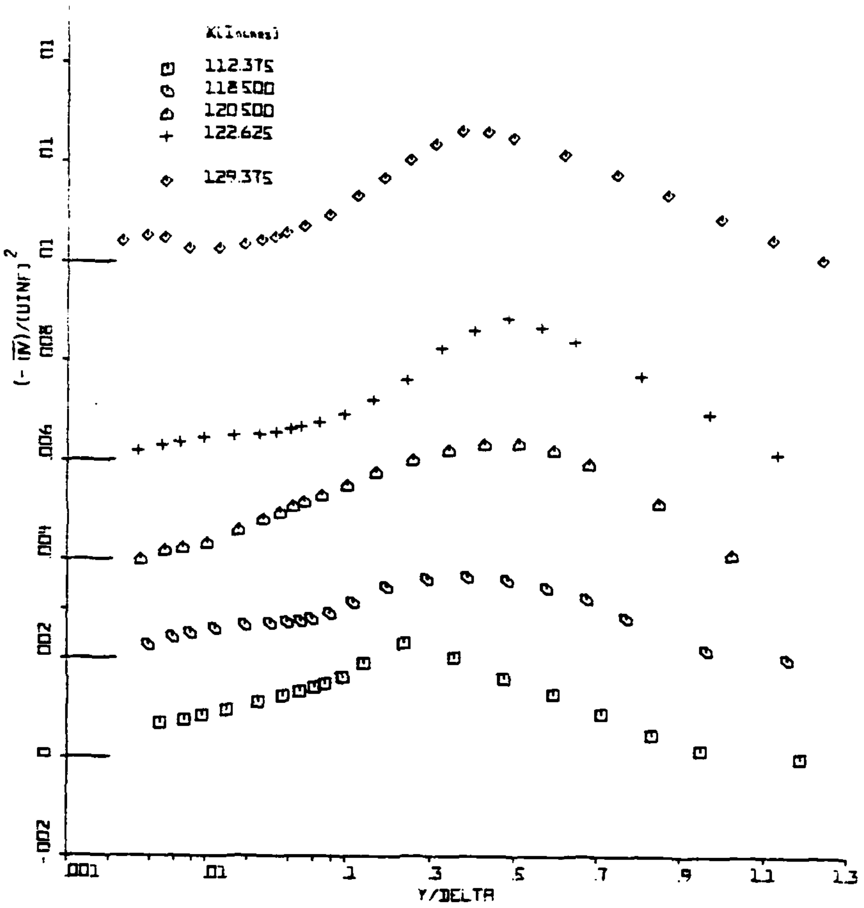

Figure 16(e). Smoothed Reynolds shearing stress $-\overline{uv}/U_\infty^2$ vs. y/δ results from laser and hot-wire anemometers. Note displaced ordinates.

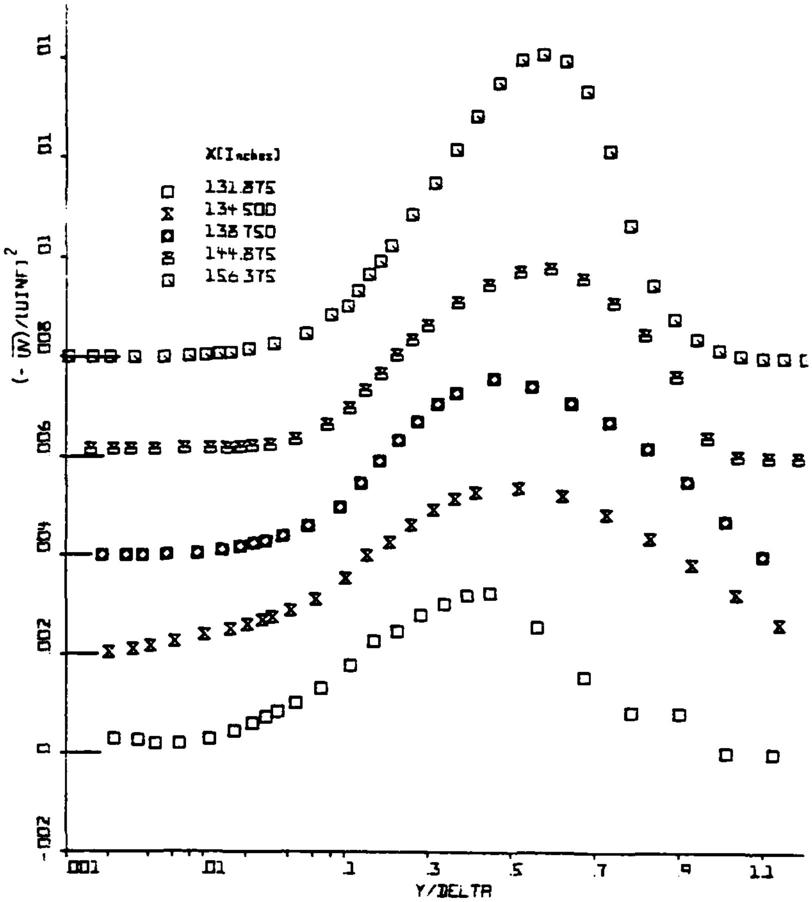

Figure 16(f). Smoothed Reynolds shearing stress $-\overline{uv}/U_\infty^2$ vs. y/δ results from laser and hot-wire anemometers. Note displaced ordinates.

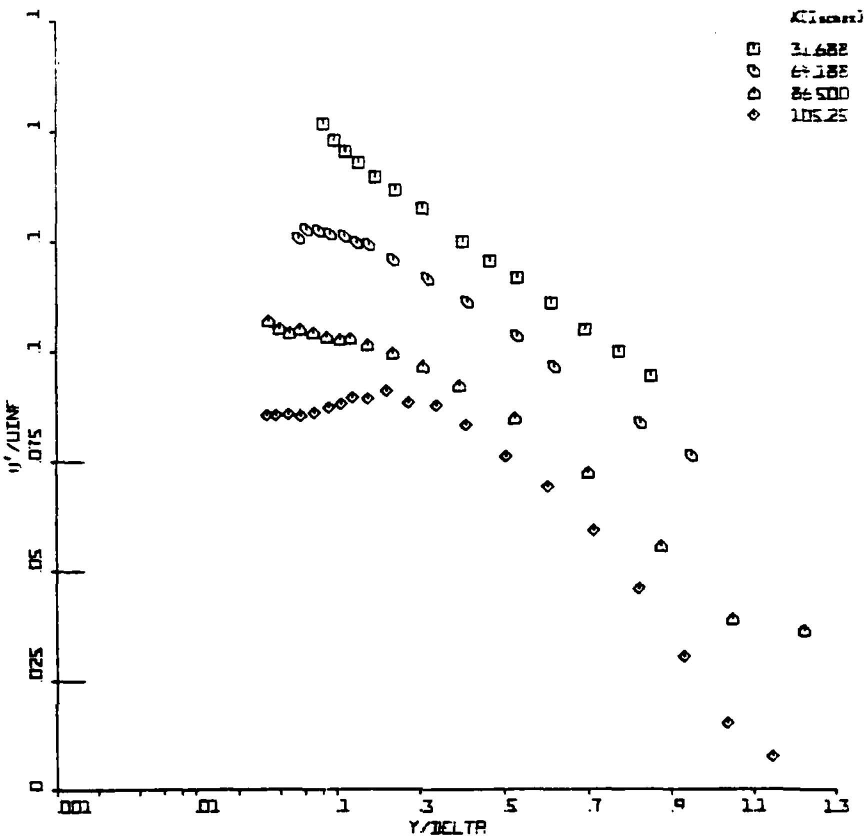

Figure 17(a). Cross hot-wire anemometer results well upstream of separation: u'/U_∞.

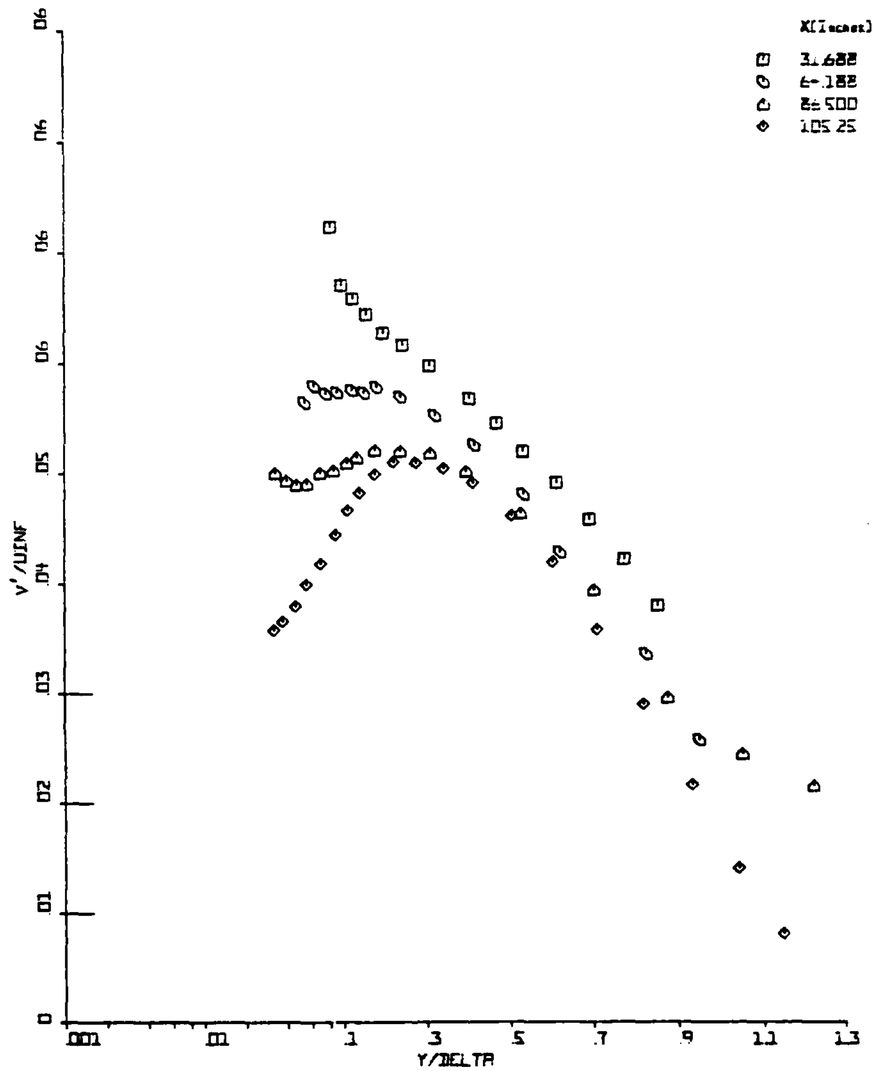

Figure 17(b). Cross hot-wire anemometer results well upstream of separation: v'/U_∞.

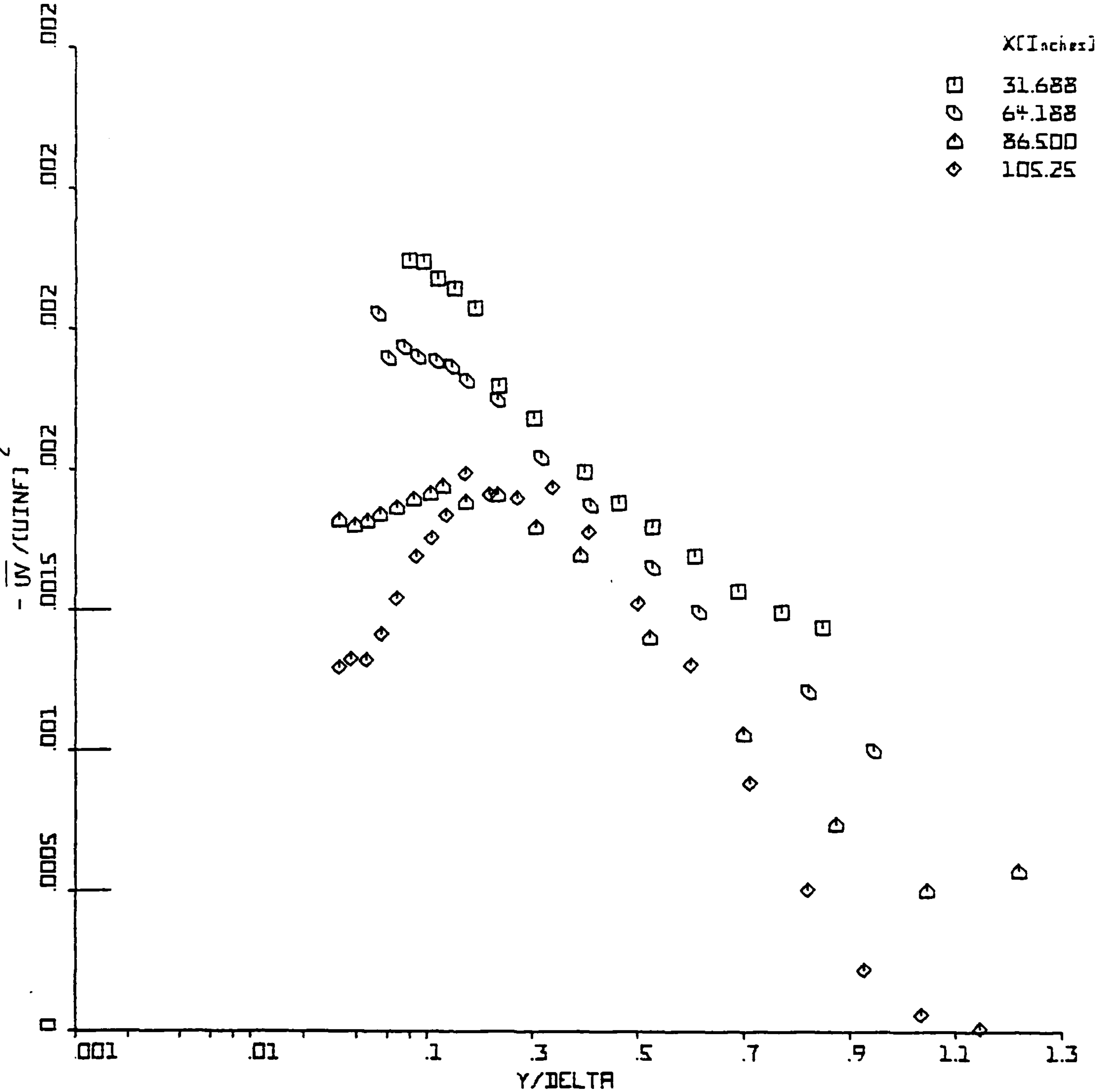

FIGURE 17(c). CROSS HOT-WIRE ANEMOMETER RESULTS WELL UPSTREAM OF SEPARATION: $\overline{-uv}/U_\infty^2$.

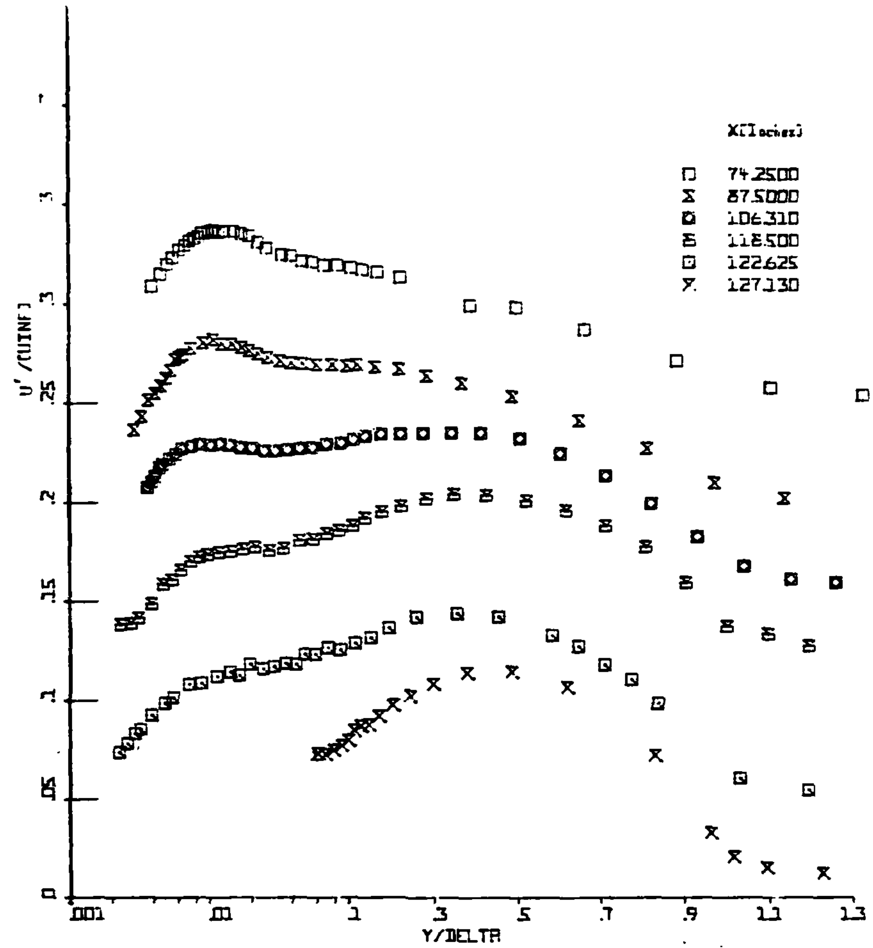

Figure 18(a). u'/U_∞ vs. y/δ, single hot-wire anemometer results.

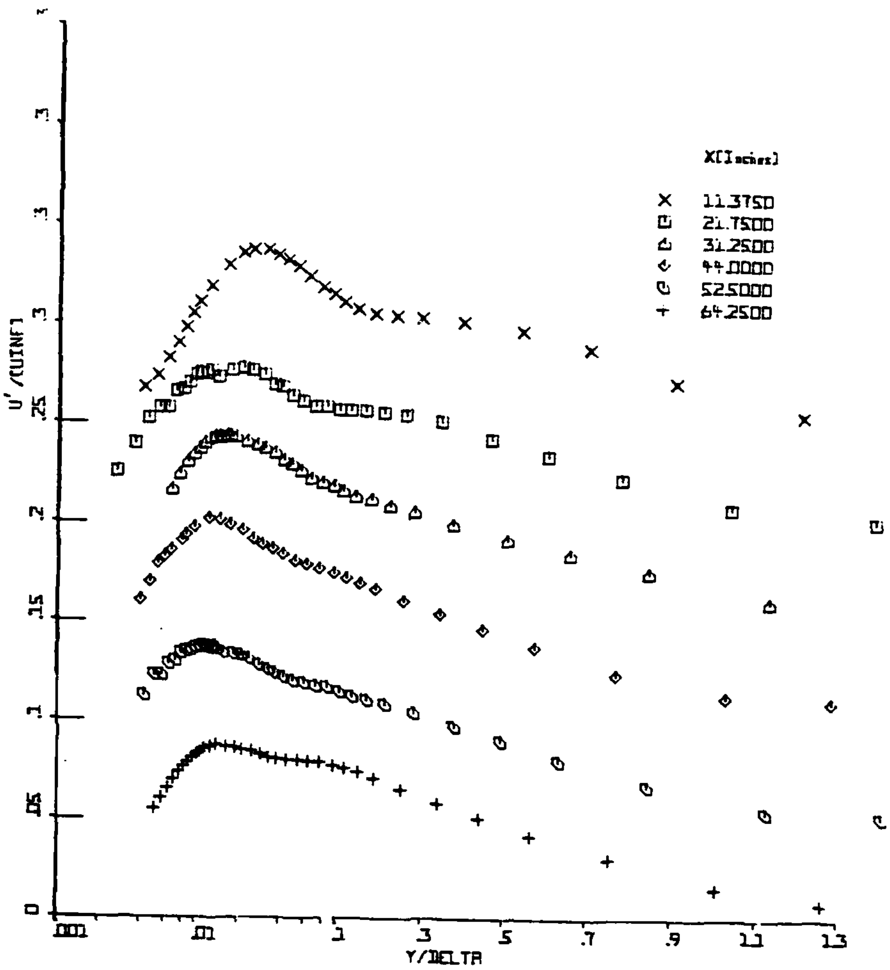

Figure 18(b). u'/U$_\infty$ vs. y/δ single hot-wire anemometer results.

Figure 19 shows the distributions of the intermittency across the boundary layer for the region approaching separation and downstream of it. The reverse flow first starts appearing at 122.6 inches but becomes clearly observable beyond 127 inches. Further downstream, the backflow intensifies and also spreads outwards from the wall. γ_{pu} reaches the lowest value of approximately 0.05 at the last station of measurement in the separated region, where backflow extends up to about 60% of the boundary layer thickness. The distributions in the separated region are trough-shaped near the wall showing that the maximum amount of reverse flow occurs slightly away from the wall. This is consistent with the velocity profile shape that shows that the highest velocity for the backflow is reached at a point slightly away from the wall. However, as shown in Table 1, the uncertainty in γ_{pu} becomes large as the mean velocity approaches zero, so one cannot place too much emphasis on this coincidence. Figure 20 shows the decay of γ_{pu} near the wall, γ_{puo}, as a function of the streamwise co-ordinate. As mentioned earlier the reverse flow is first measured at 122.6 inches and thereafter its persistence increases continuously, until it reaches a level where it exists 90% of the time after which its rate of increase diminishes.

IV. 4 Higher-order Turbulence Correlations

To investigate the effect of separation on higher order structure functions, the third and fourth moments given by equation (7) were calculated from the *U* and *V* LDV histograms. Simpson and Chew (1979) showed that the skewness factors, $S_u = (\overline{u^3})/(\overline{u^2})^{3/2}$ and $S_v = (\overline{v^3})/(\overline{v^2})^{3/2}$, and flatness factors, $F_u = (\overline{u^4})/(\overline{u^2})^2$ and $F_v = (\overline{u^4})/(\overline{v^2})^2$, were about $\pm$ 0.1 and $\pm$ 0.2 uncertain. Data obtained on different days were in close agreement, with the

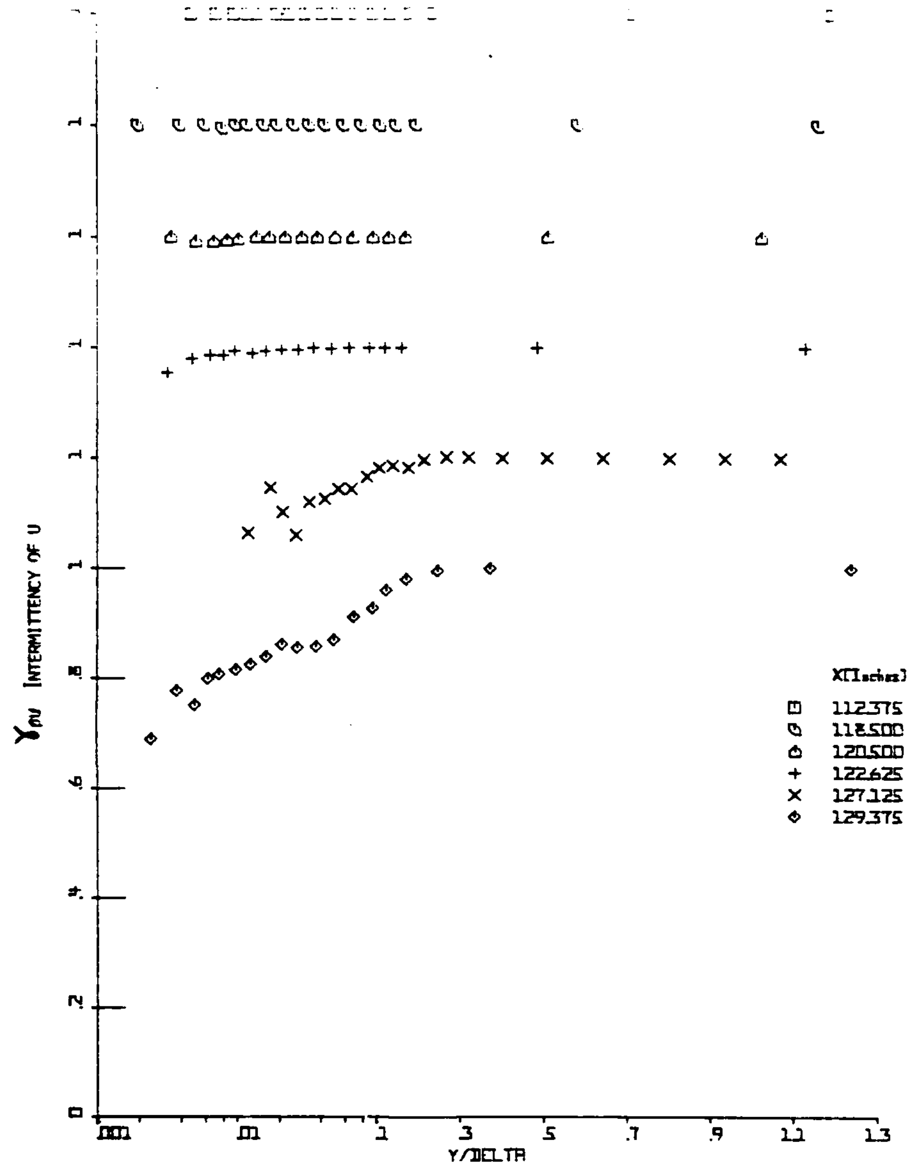

Figure 19(a). Streamwise fraction of time flow moves downstream, γ_{pu} vs. y/δ.

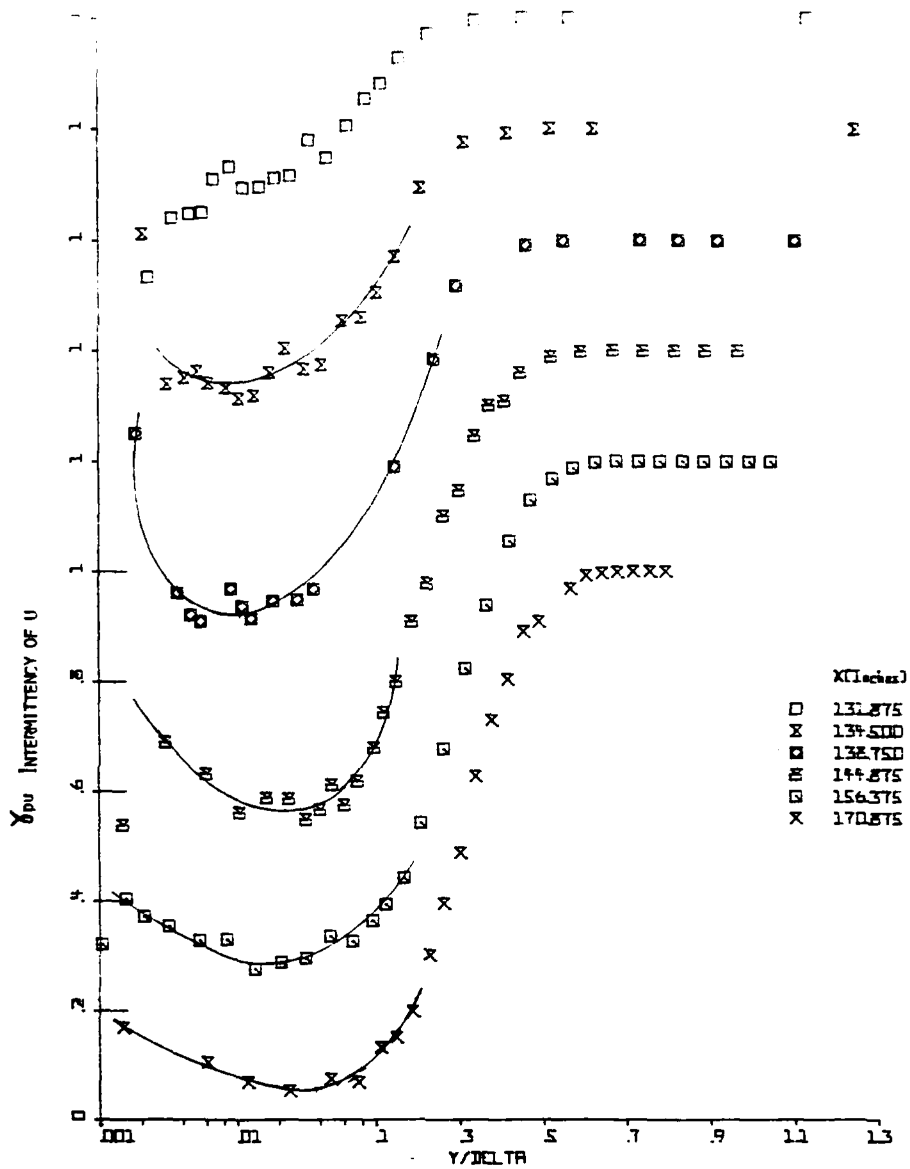

Figure 19(b). Streamwise fraction of time flow moves downstream, γ_{pu} vs. y/δ.

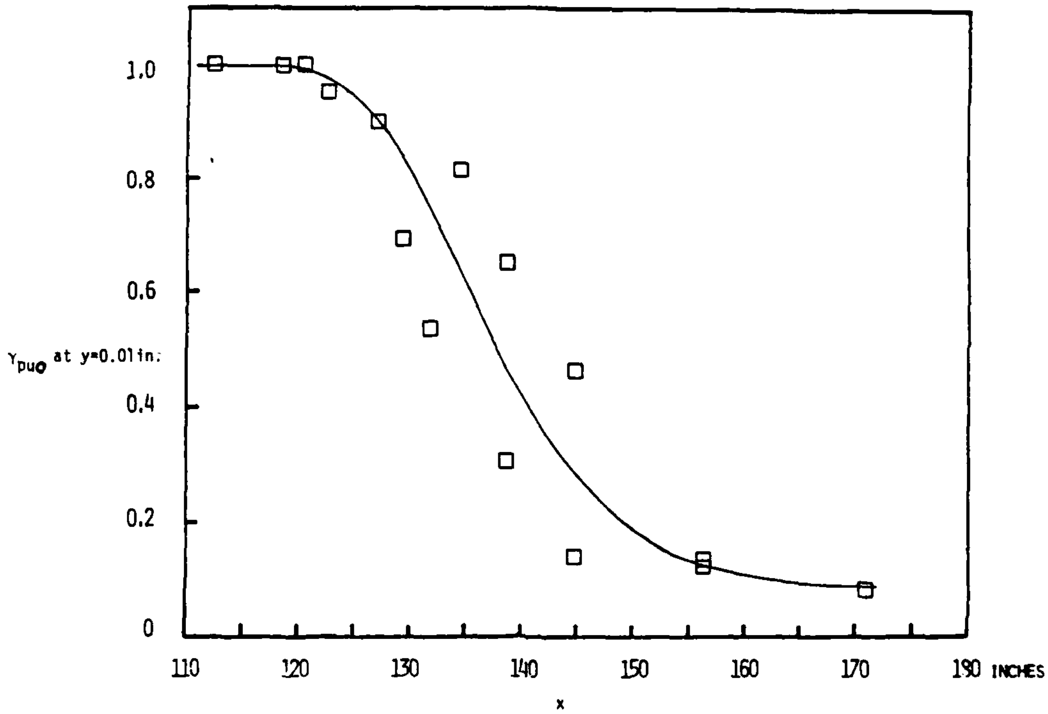

Figure 20. γ_{pu} at 0.01 inches from wall vs. X: □, experimental data; solid line for visual aid only.

scatter being within these uncertainty levels.

For purposes of comparison and for additional information, $\overline{u^2v}$ and $\overline{v^3}$ triple correlation data were obtained from the cross-wire anemometer. The main source of uncertainty in these measurements is the drift of the mean voltage level in the multipliers. This was kept to a minimum by adjusting the offset voltage before, several times during, and after taking a set of data, so that a zero voltage input produced a zero voltage output. During data reduction a correction was applied for the offset voltage. Table 2 gives the maximum uncertainties for each streamwise location that data are presented. All data which were greater 25% uncertain are not presented here. This arbitrary uncertainty limit is not really very high, considering that third-order correlations are expected to have high uncertainties.

Figure 21 shows the skewness factor S_v results obtained by laser and cross-wire anemometers for several streamwise locations. The agreement between the two types of experimental results away from the wall at a given location is generally within the estimated uncertainties. In the separated zone the hot-wire measurements were confined to the outer region where the instantaneous flow direction differed less than 45^o from the mean flow direction.

IV.5 Skin-friction Results

Three different ways of deducing the near wall shearly-stress distribution were used: the Ludwieg-Tillman skin-friction correlation, a Preston tube, and the surface hot-wire gage described in section II.4 above. Figure 22 shows the results from these three methods, which are in agreement within the uncertainties given in Table 1. Table 3 gives the Ludwieg-Tillman results.

Table 2: Uncertainties for the diffusion results, y/δ positions given in parentheses.

x	value at the location where the uncertainty was computed		Maximum absolute value		Maximum value of the absolute uncertainty		
Inches	$\overline{u^2v}$ (ft/sec)^3	$\overline{v^3}$ (ft/sec)^3	$\overline{u^2v}$ (ft/sec)^3	$\overline{v^3}$ (ft/sec)^3	$\overline{u^2v}$ (ft/sec)^3	$\overline{v^3}$ (ft/sec)^3	U_∞ (ft/sec)
31.688	0.58 (0.401)	3.93 (0.465)	4.78	6.43	0.2	0.15	62.36
86.5	1.07 (1.221)	1.03 (1.396)	14.53	10.09	0.91	1.0	66.73
117.625	3.09 (0.27)	3.02 (0.407)	11.49	3.5	1.7	0.25	51.86
126.75	12.72 (0.623)	4.83 (0.837)	16.6	8.59	1.02	0.33	48.94
131.0	13.38 (0.714)	3.44 (0.88)	13.86	4.69	1.37	0.5	47.97
144.0	9.67 (0.895)	4.13 (0.933)	11.24	6.2	1.03	0.39	47.06
156.375	6.97 (0.966)	1.53 (1.073)	14.27	9.74	1.57	0.88	45.33

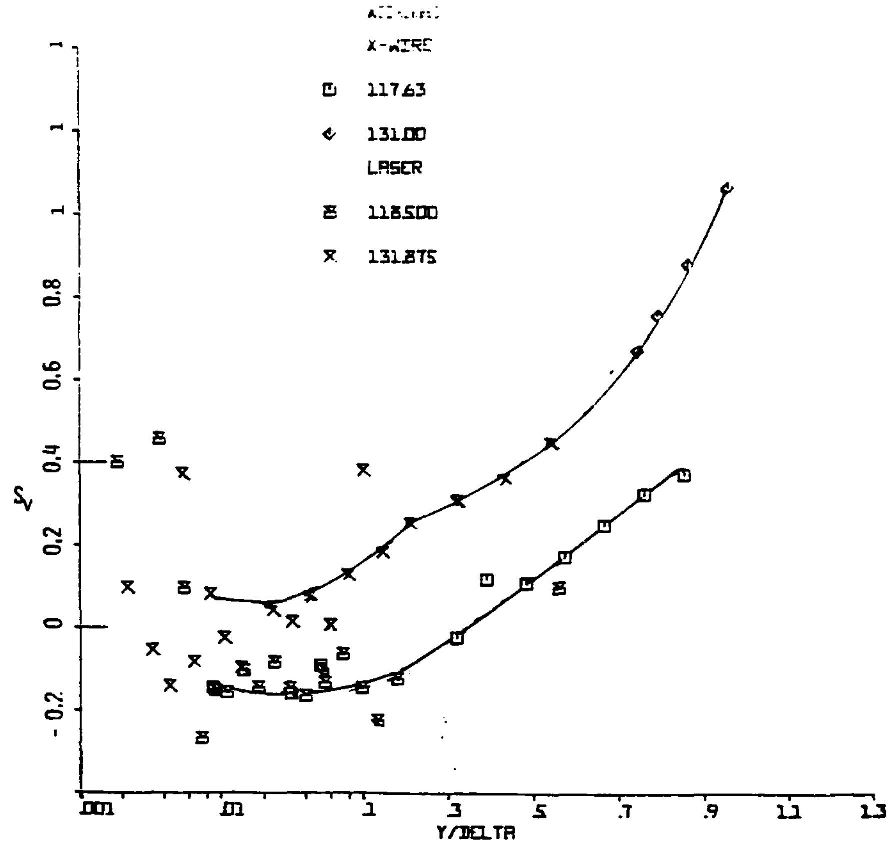

Figure 21. Comparison of skewness factor S_v for v from laser and hot-wire anemometers. Solid lines for visual aid only. Note displaced ordinates.

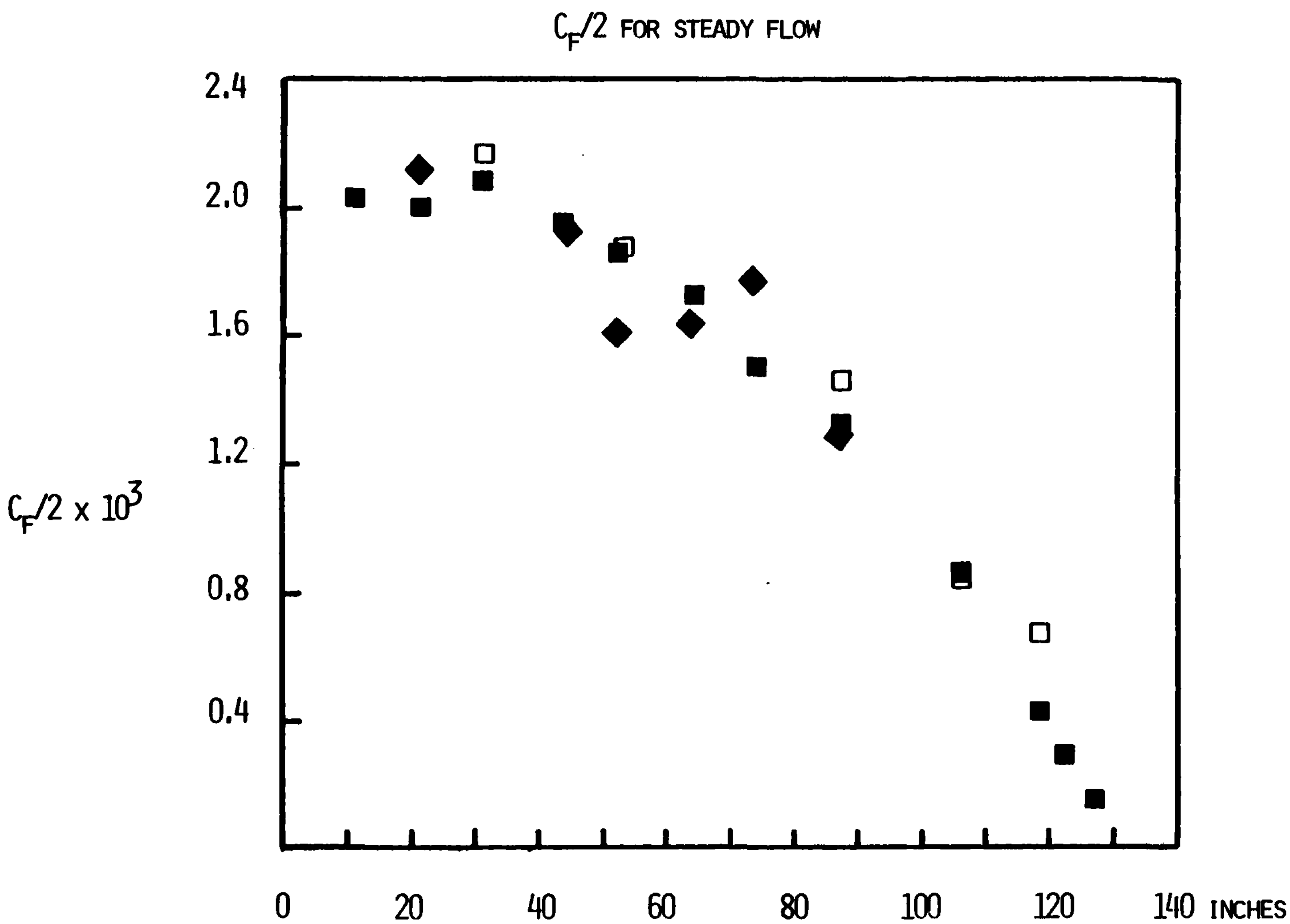

FIGURE 22. FRICTION FACTOR $C_F/2$ VS. X FROM THE SEVERAL EXPERIMENTAL METHODS: ■, LUDWIG -TILLMAN LAW; □, SURFACE HOT-WIRE GAGE; ◆, PRESTON TUBE.

X (INS.)	UINF (FT./SEC.)	DUINF/DX (1/SEC.)	δ_{99} (INS.)	δ_{995} (INS.)	δ_1 (INS.)	R_{δ_2}	H_{12}	$10^3 \times C_f/2$
11.375	52.600	5.38	.492	.517	.0699	1381.2	1.378	2.0350
21.750	57.800	6.48	.574	.615	.0728	1570.2	1.367	2.0010
31.250	63.200	6.30	.531	.563	.0707	1677.0	1.339	2.0810
44.000	68.700	4.38	.776	.907	.0898	2345.9	1.323	1.9530
52.500	71.500	2.40	.712	.761	.0901	2490.9	1.343	1.8620
64.250	71.600	-1.32	.792	.842	.1103	2900.6	1.357	1.7240
74.250	70.000	-2.36	.909	.959	.1481	3669.3	1.413	1.5030
87.500	66.800	-3.54	1.235	1.290	.2182	5201.9	1.418	1.3300
106.310	59.300	-6.31	1.828	1.891	.4612	8616.7	1.625	.8590
112.375	55.900	-5.68	2.338	2.388	.6302	9888.3	1.733	.6982
118.500	53.100	-4.72	2.799	2.842	.9122	11754.7	1.989	.4469
120.500	52.150	-4.45	2.946	2.973	1.0392	12924.8	2.010	.4219
122.625	51.300	-4.11	3.280	3.322	1.2101	13684.7	2.212	.3030
127.125	49.500	-3.49	3.804	3.844	1.6444	14747.9	2.686	.1418
129.375	48.750	-3.16	4.878	4.922	2.0658	19088.9	2.533	.1680
131.875	48.100	-2.86	4.610	4.676	2.0649	16138.2	2.973	.0884
134.500	47.400	-2.55	5.829	5.895	2.6497	19736.1	3.139	.0646
138.750	46.450	-2.05	5.779	5.834	3.1099	17185.9	4.118	.0145
144.875	45.500	-1.64	6.708	6.768	4.0101	16297.7	5.404	.0020
156.375	44.600	-1.28	9.346	10.066	6.2550	18024.4	7.689	.0001
170.875	43.700	-1.21	12.518	12.841	8.3127	18664.8	9.453	.0000

Table 3: Parameters of the mean flow development

The Preston tube and Ludwieg-Tillman methods require the existence of a universal logarithmic law-of-the-wall velocity profile. The data obtained using the surface hot-wire gage are not dependent on the requirement of a logarithmic wall region. This suggests that the law of the wall is valid until the location where γ_{pu} is first less than one near the wall. These results are in agreement with results of Simpson et al., (1977).

IV.6. Data Tabulation

These data are tabulated in Table 3 and in the Appendix. These data are recorded on magnetic tape in the format required for the 1980-81 AFOSR-HTTM-Stanford Conferences on Complex Turbulent Flows, a copy of which is on file in the Thermosciences Division of the Stanford University Department of Mechanical Engineering.

V. DISCUSSION

V.1 Mean Velocity Distribution

Figure 23 shows the mean streamline pattern for the flow in the vicinity of separation. Note that in the backflow region the turbulence level is very high compared to the mean flow, so these mean streamlines do not represent the average pathlines for elements of fluid. As discussed in section VI below, it appears that the fluid in the backflow does not come from far downstream as the streamlines may suggest, but is supplied fairly locally.

Figures 24 (a) and (b) show that the U^+ vs. y^+ law-of-the-wall velocity profile holds all along the flow channel when the Ludwieg-Tillman skin friction values are used. Although no wall proximity corrections to the hot-wire data were applied in the viscous sublayer, the $U^+ = y^+$ relationship is obeyed rather well. Oka and Kostić (1972) noted that hot-wire measurements are only influenced by flow interference and conduction to the test wall for $y^+ < 4$, which

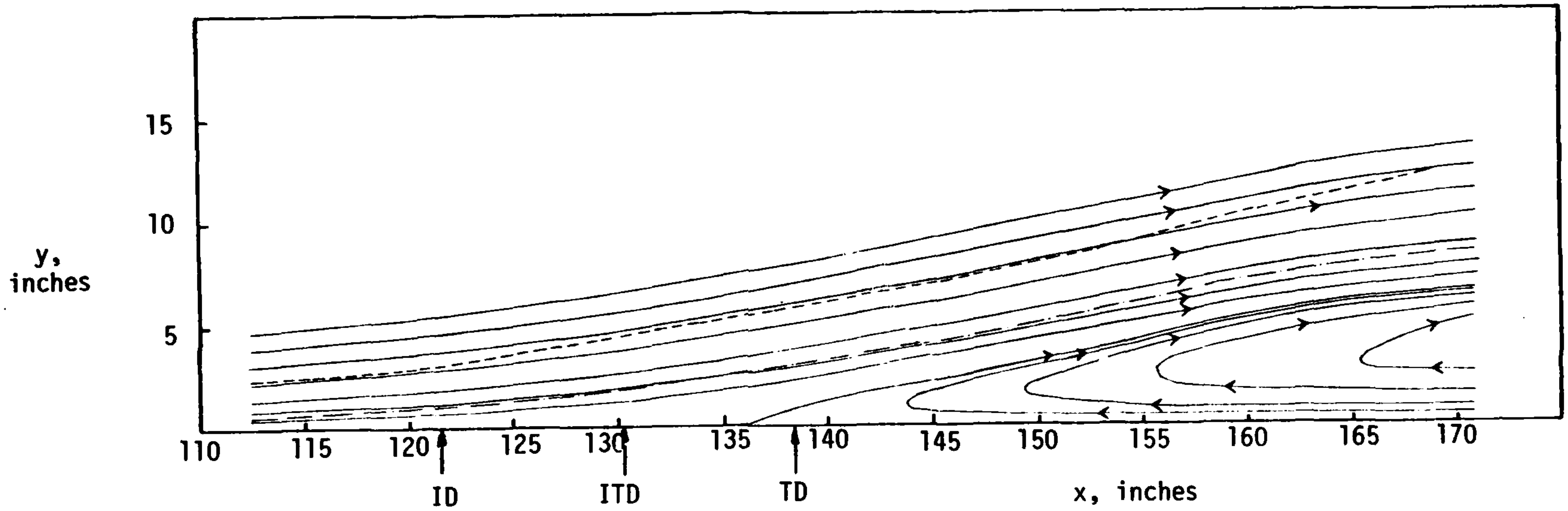

Figure 23. Mean streamline flow pattern in the vicinity of separation. —— streamlines, – – – – boundary layer edge, — ● — displacement thickness distribution.

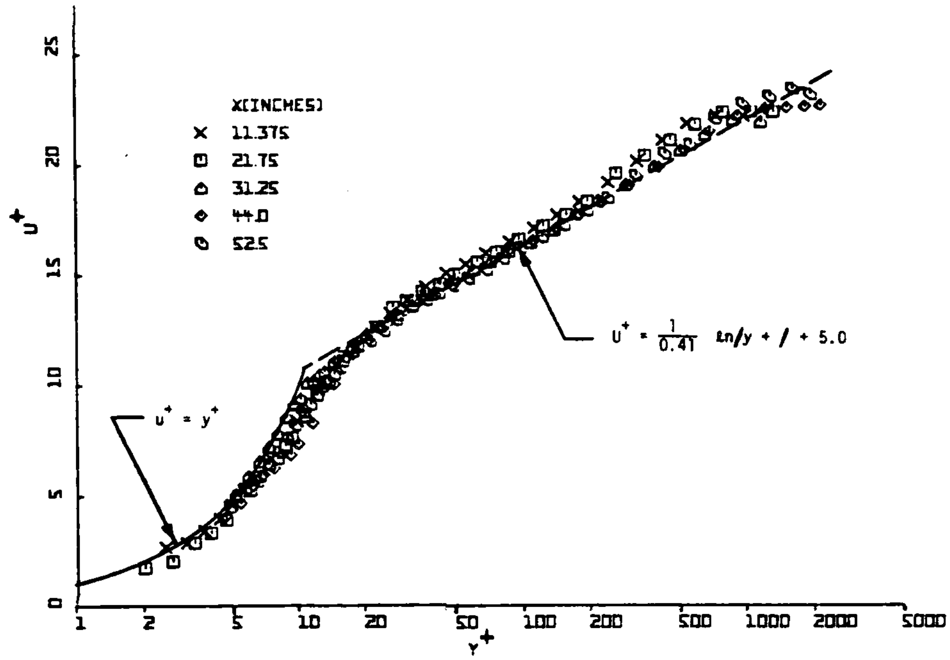

Figure 24(a). Law-of-the-wall velocity profiles, U^+ vs. y^+, upstream of separation.

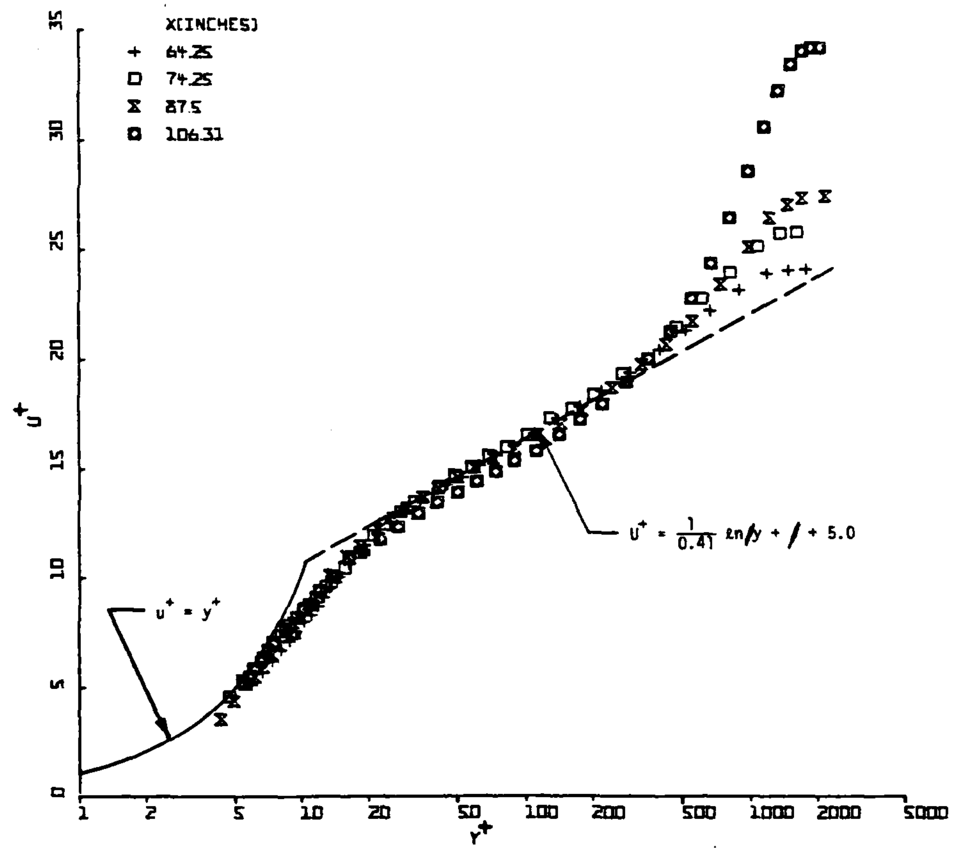

Figure 24(b). Law-of-the-wall velocity profiles, U^+ vs. y^+, upstream of separation.

explains why the present data for $y^+ > 4$ obey the viscous sublayer equation so well. Upstream of the vicinity of separation, the usual logarithmic form for $y^+ > 30$ holds

$$U^+ = \frac{1}{0.41} \ln\left|y^+\right| + 5.0 \qquad (9)$$

as shown in Figures 24.

Perry and Schofield (1973) proposed universal empirical correlations for the inner and outer regions of adverse pressure gradient boundary layers near separation. Their correlations apply to all types of adverse pressure gradient boundary layers irrespective of whether they are in equilibrium or not, but with the restriction that the ratio $(-\overline{uv})_{max}/U_\tau^2$ must exceed 1.5. They proposed the defect law for the outer flow as

$$\frac{U_\infty - U}{U_s} = f_2(\eta_2), \text{ where } \eta_2 = y/\Delta \qquad (10)$$

and

$$\Delta = \frac{U_\infty}{U_s} \frac{\delta_1}{C} \qquad (11)$$

C is a universal constant given by $C = \int_0^\infty f_2(\eta_2)\, d\eta_2$ and found empirically to be equal to 2.86. The inner law was defined as

$$\frac{U}{U_\tau} - h = f_1(\eta_1), \quad \eta_1 = \frac{y}{e}, \; e = \frac{Lu_\tau^2}{U_{MP}^2} \qquad (12)$$

where h is a constant and U_{MP}^2 and L are described later.

The condition for the overlap between the inner and the outer region lead to the following relations

$$\frac{U}{U_\infty} = 0.47\left(\frac{U_s}{U_\infty}\right)^{3/2}\left(\frac{y}{\delta_1}\right)^{1/2} - \left(\frac{U_s}{U_\infty}\right) + 1 \qquad (13)$$

$$f_1(\eta_1) = 6.4\ \eta_1^{1/2} \tag{14}$$

and

$$\frac{U_s}{U_{MP}} = 8\left(\frac{\Delta}{L}\right)^{1/2} \tag{15}$$

Equation (13) was used to obtain the values of the velocity scale factor U_s by drawing a Clauser-type chart for $\frac{U}{U_\infty}$ and $\left(\frac{Y}{\delta_1}\right)^{1/2}$ with U_s as the parameter. All the parameters obtained for Perry's correlations are given in Table 4.

The condition $(-\overline{uv})_{max}/U_\tau^2 > 1.5$ was satisfied by the data for the region downstream of x = 105 inches. Hence, Perry and Schofield's correlations were tried for the locations downstream of 105 inches where the profiles of mean velocity as well as those of normal and shear stresses were available. The data for the normal stresses are also required since Perry and Schofield neglected the normal stresses term in the momentum equation while computing the shear stress profiles from the mean velocity profiles. It was shown later by Simpson (1975) that the normal stresses term plays a significant part in both the momentum and the turbulence energy equations for flows approaching separation. The normal stresses effects have been considered in a way as discussed by Simpson et al. (1977) and in accordance the pseudo-shear stress U_{MP}^2 is defined as

$$U_{MP}^2 = \left[-\overline{uv} + \int_y^\infty \frac{\partial(\overline{u^2} - \overline{v^2})\ dy}{\partial x} \right]_{max} \tag{16}$$

and L is defined as the distance from the wall to the maximum in the pseudo-shear stress profile.

Figures 25 and 26 show the velocity profiles plotted in the inner and outer layer co-ordinates. The inner law correlation given by eqns. (12) and (14)

Table 4. Experimental values for the parameters used in the Perry and Schofield correlation.

x in inches	U_s/U_∞	U_s/U_M	U_s/U_{Mp}	y_c/Δ	$\Delta/\delta_{.99}$	$L/\delta_{.99}$
106.31	0.67	15.86	15.89	0.0889	1.077	0.340
111.125	0.78	16.80	16.64	0.0421	1.103	0.284
118.5	0.86	21.33	18.21	0.0392	1.183	0.423
126.75	1.02	22.47	18.66	0.0151	1.212	0.617

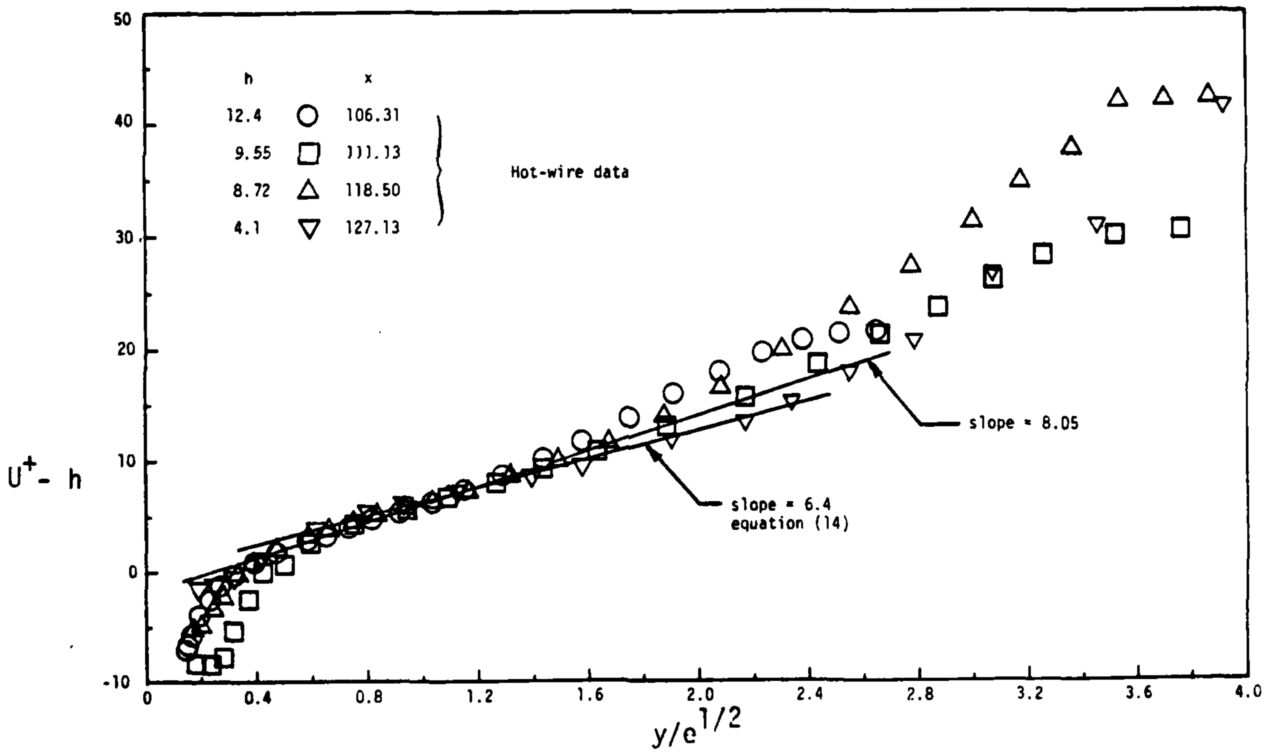

Figure 25. Perry and Schofield inner region correlation for the present data near separation, $U^+ - h$ vs. $(y/e)^{1/2}$, equations (12) and (14) given by solid lines for 6.4 and 8.05 slopes.

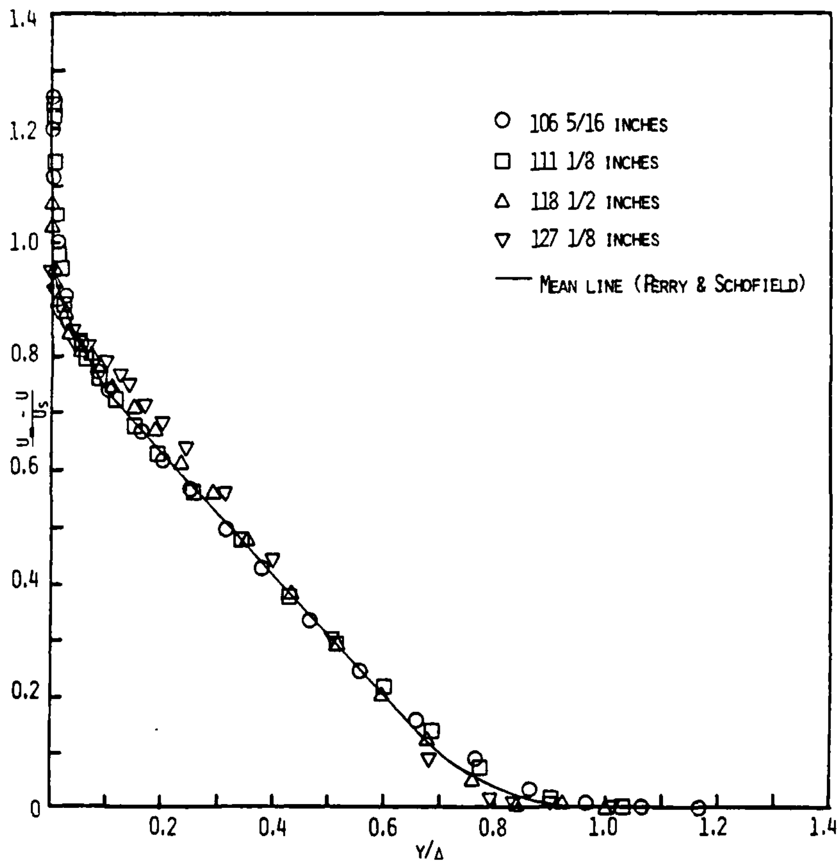

Figure 26. Perry and Schofield outer region correlation for the present data near separation, $(U_\infty - U)/U_s$ vs. y/Δ, eqn.(10); solid line is mean line from Perry and Schofield (1973).

seem to be satisfied reasonably well, although the higher slope of 8.05 satisfies the upstream most profiles better (Simpson et al., 1977). In the region near the wall, eqn. (12) takes the usual logarithmic form of eqn. (9). By matching the logarithmic and the half power regions, Perry and Schofield obtained the expression for the point of tangency as $y_c = 0.58e$. As shown in Table 4 the predicted point of tangency moves toward the wall as one proceeds downstream, indicating that the extent of the logarithmic region gradually decreases, which can also be seen in Figure 11c. The present data satisfy the other matching condition given by eqn. (15) to a reasonable extent. The present data upstream of intermittent backflow lie within the band represented by the scatter in the data plotted by Perry and Schofield.

Following Strickland and Simpson (1973), the velocity profiles in the separated region were normalized to see whether the profiles in the outer region show any resemblance to those observed in mixing layers. For this purpose $\frac{U-U_0}{U_\infty-U_0}$ was plotted as a function of $\frac{\sigma' y'}{x_0}$ as shown in Figure 27 for a few stations downstream of 127 inches. In the case of the mixing layer, y' represents the distance from the center of the mixing layer and here the location where the Reynolds Shear Stress $-\overline{uv}$ reaches a maximum was considered as the center of the shear layer. x_0 is the streamwise distance from a reference point and in the present studies x = 88" was taken as the reference point. U_0 is equal to twice the velocity at the center of the shear layer minus the free-stream velocity and σ' is a constant. Also shown is the curve obtained by Halleen (1964) for a mixing layer. An error function type of distribution represented by

$$\frac{U - U_0}{U_\infty - U_0} = \frac{1}{2}\left\{1 + \mathrm{erf}\left(\frac{\sigma' y'}{x_0}\right)\right\} \tag{17}$$

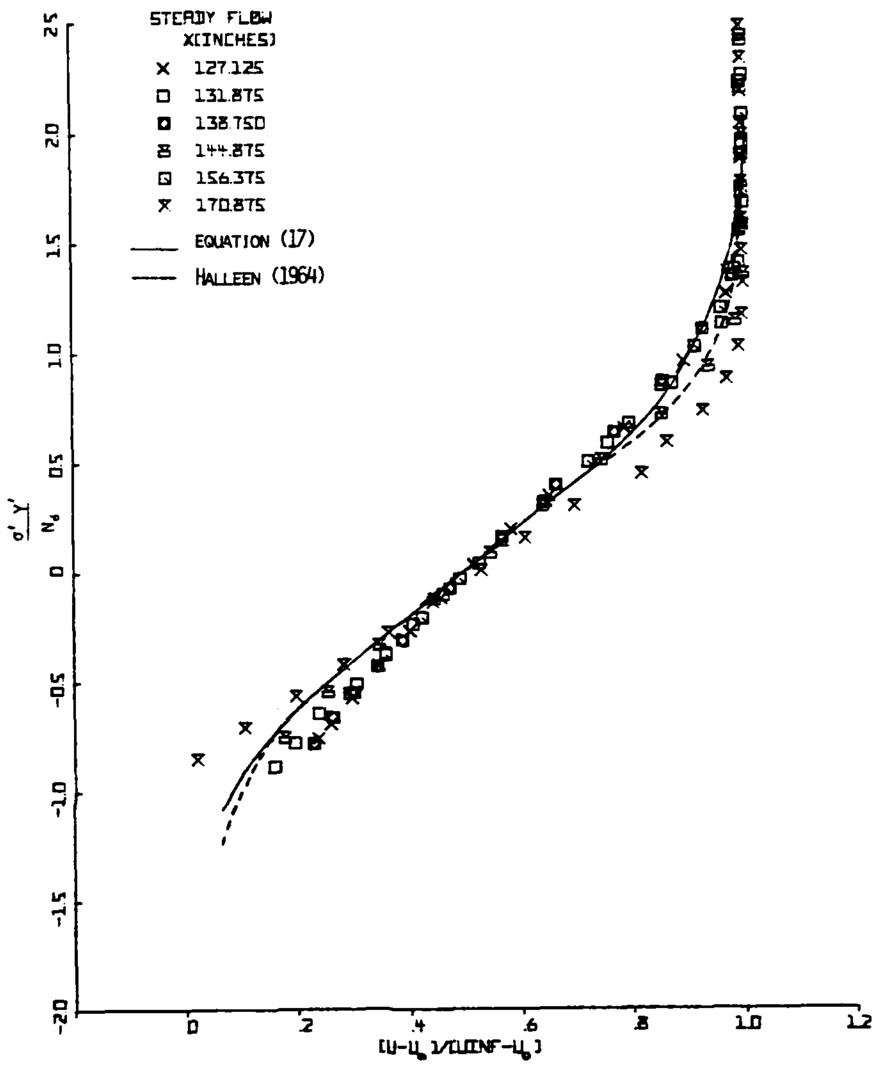

Figure 27. Present data in mixing-layer-type co-ordinates; solid line, eqn.(17) with $\sigma' = 24$ and $X_0 = 88"$; dashed line, Halleen's (1964) mixing layer correlation.

is also plotted for comparison. There is good agreement of the data with these distributions, confirming the analogy with mixing layers. However, σ' is about 24 while Halleen obtained a value of about 17.5.

As one can see in Figure 11d, there is some profile shape similarity for the backflow mean velocity downstream of 138 inches. Figure 28 shows a good correlation when normalized on the maximum negative mean velocity U_N and its distance from the wall N. A slightly poorer correlation results when δ is used instead of N. The U^+ vs. y^+ law-of-the-wall velocity profile is not consistent with this correlation since both U_N and N increase with streamwise distance, while the law-of-the-wall length scale ν/U_τ varies inversely with its velocity scale U_τ. The data of Simpson et al. (1977) for the one available location are also shown to be in fair agreement with this correlation.

An attempt was made to see if the mean velocity profiles downstream of separation could be composed of the "law-of-the-wake" (Coles and Hirst, 1969)

$$\omega(y/\delta) = 2 \sin^2\left(\frac{\pi y}{2\delta}\right) \tag{18}$$

and a similarity distribution for the remaining wall flow. Figure 29, which is a plot of $U/U_\infty - \sin^2 (\pi y/2\delta)$ vs. y/δ, shows the remainder for the wall flow. There is no significant profile similarity.

Another attempt was made to scale the wake function by using the maximum backflow velocity and the free-stream velocity before subtracting it from the velocity profile. This was done as follows:

$$\frac{U}{U_\infty} = \left[\frac{U_\infty + |U_N|}{U_\infty}\right]\frac{1}{2}\ \omega(y/\delta) - \frac{|U_N|}{U_\infty} + R(y/\delta) \tag{19}$$

where $R(y/\delta)$ can be called a "backflow" function. Furthermore, another function

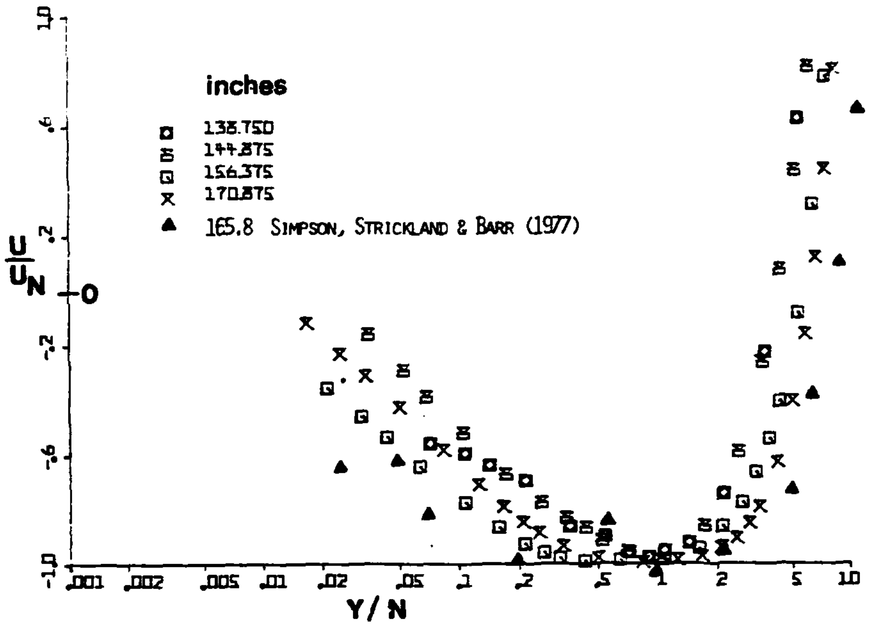

Figure 28. Normalized mean backflow velocity profiles: U_N and N, maximum mean backflow velocity and its distance from the wall, respectively.

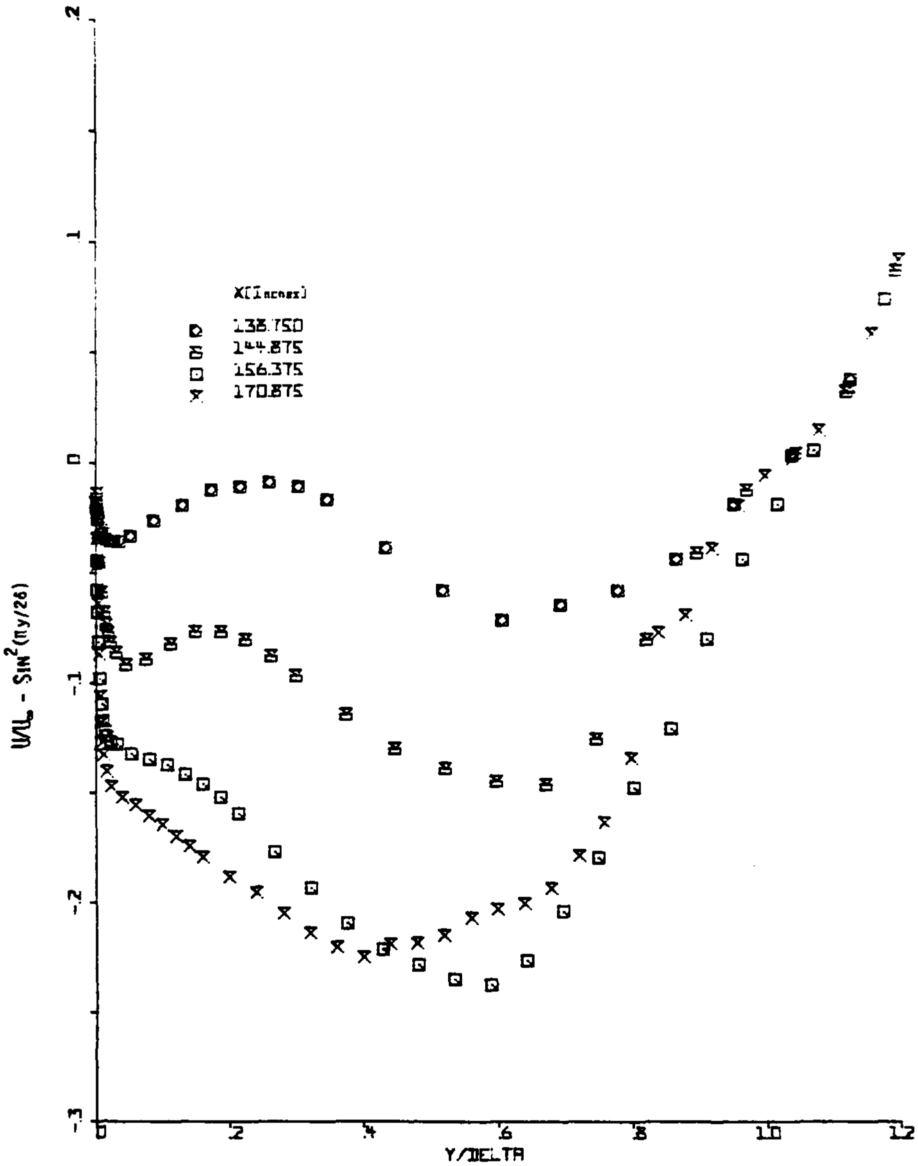

Figure 29. Difference between present mean velocity data and Coles' wake velocity profile vs. y/δ.

$B(y/\delta) = R(y/\delta) \frac{U_\infty}{|U_N|}$ was formed so that $B(y/\delta)$ has definite limits of 1 and 0 at $y/\delta = 0$ and 1, respectively. The plots of these function $R(y/\delta)$ and $B(y/\delta)$ are shown in Figures 30 and 31. They neither show any similarity nor small values in the outer region. This leads one to conclude that it is not possible to describe the velocity profile in the outer region for a separated flow by the universal wake function. No universal backflow function appears to exist.

V.2 Flow Detachment and Upstream-Downstream Intermittency

It is well established that separation of a turbulent boundary layer does not occur at a single streamwise location but is spread over a streamwise region and involves a spectrum of states. Sandborn and Kline (1961) and Sandborn and Liu (1968) defined the limiting points of the region as the "intermittent" and the "fully-developed" separation points. The former indicates the onset of separation by the appearance of intermittent backflow and the latter signifies the vanishing of the mean wall shear stress.

Sandborn and Liu (1968) gave correlations between H_{12} and $\delta_1/\delta_{.995}$ to demarcate the regions of intermittent and fully-developed separation. Figure 32 gives their correlations and the present experimental data points. According to their correlations, the present data show intermittent separation to occur at 130 inches. The value of γ_{puo} at that point is 0.81 which very nearly coincides with the value obtained by Simpson *et al*. (1977) and is also in reasonable agreement with the value obtained by Sandborn and Liu. By interpolation the fully-developed separation point occurred at 140 inches.

At the recent Project SQUID Colloquium on Flow Separation (Simpson, 1979), it was pointed out that the term "separation" must mean the entire process of

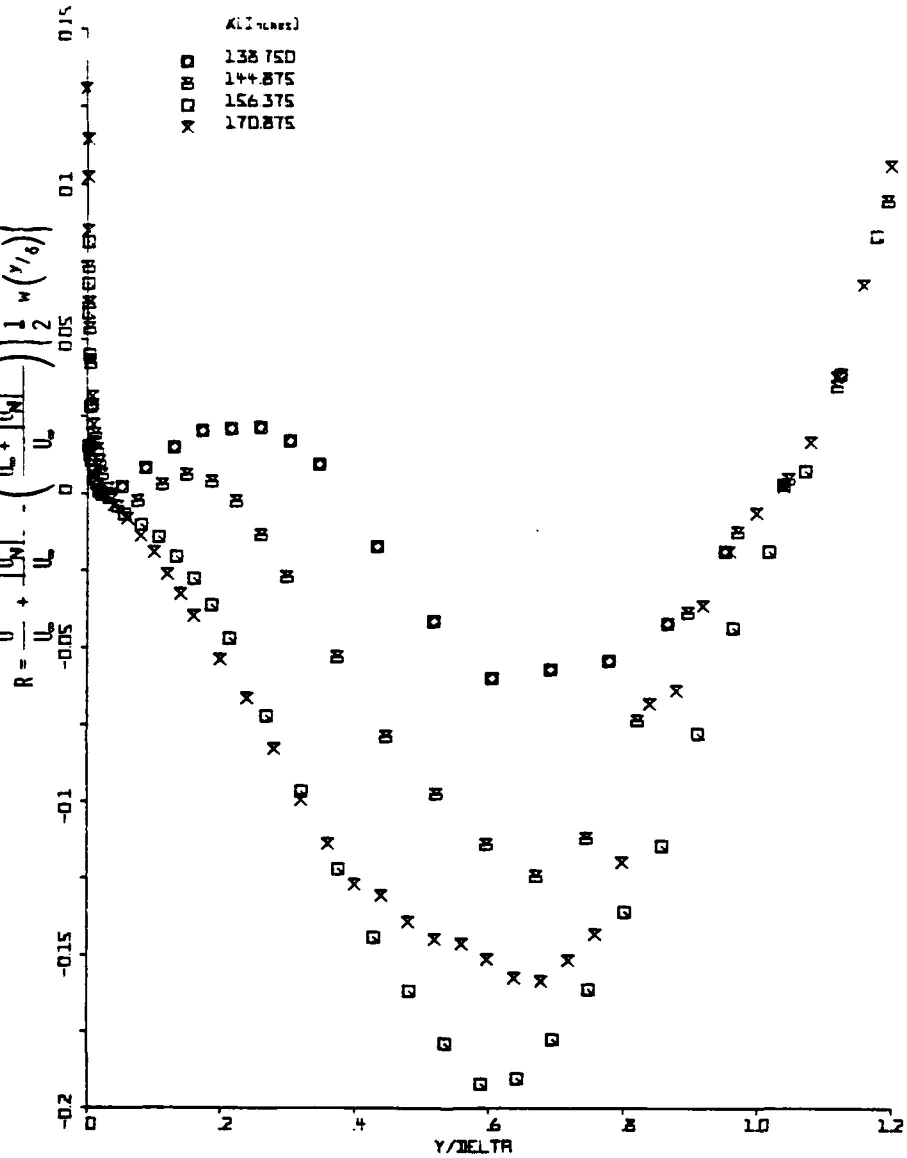

Figure 30. "Backflow" function defined in eqn.(19).

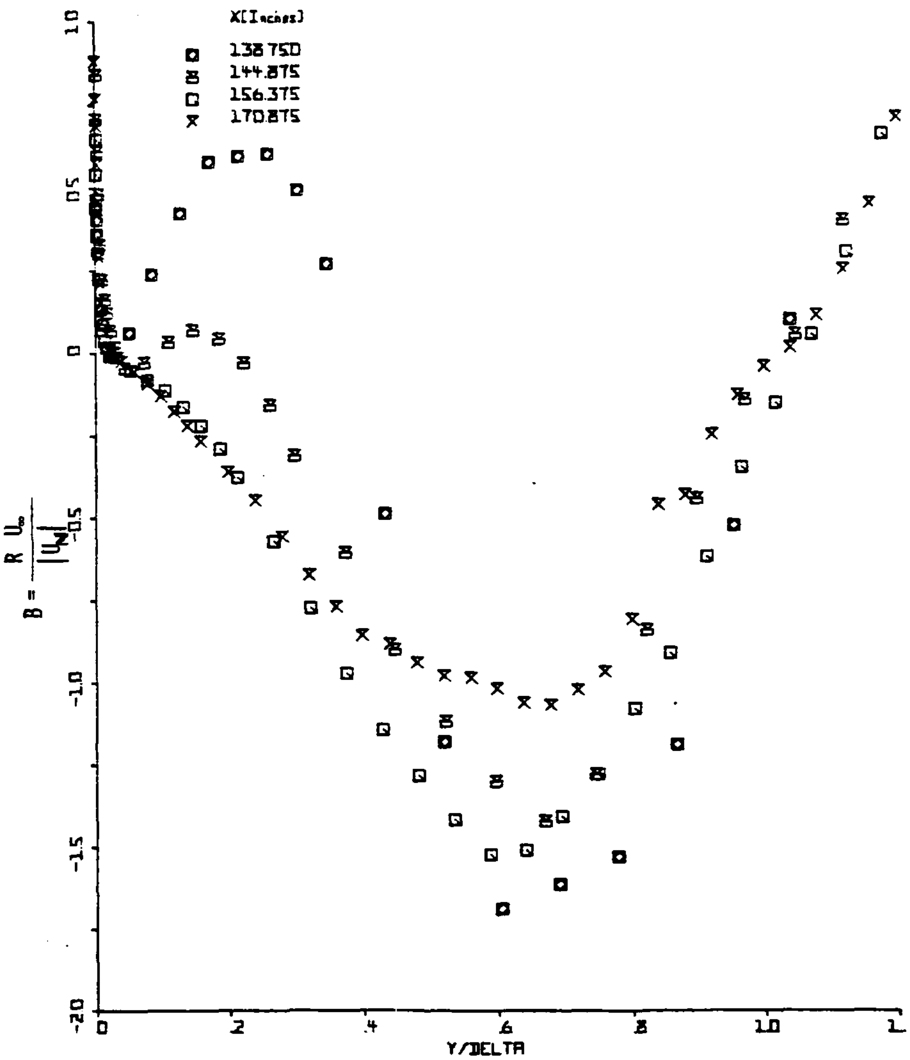

Figure 31. Normalized "backflow" function.

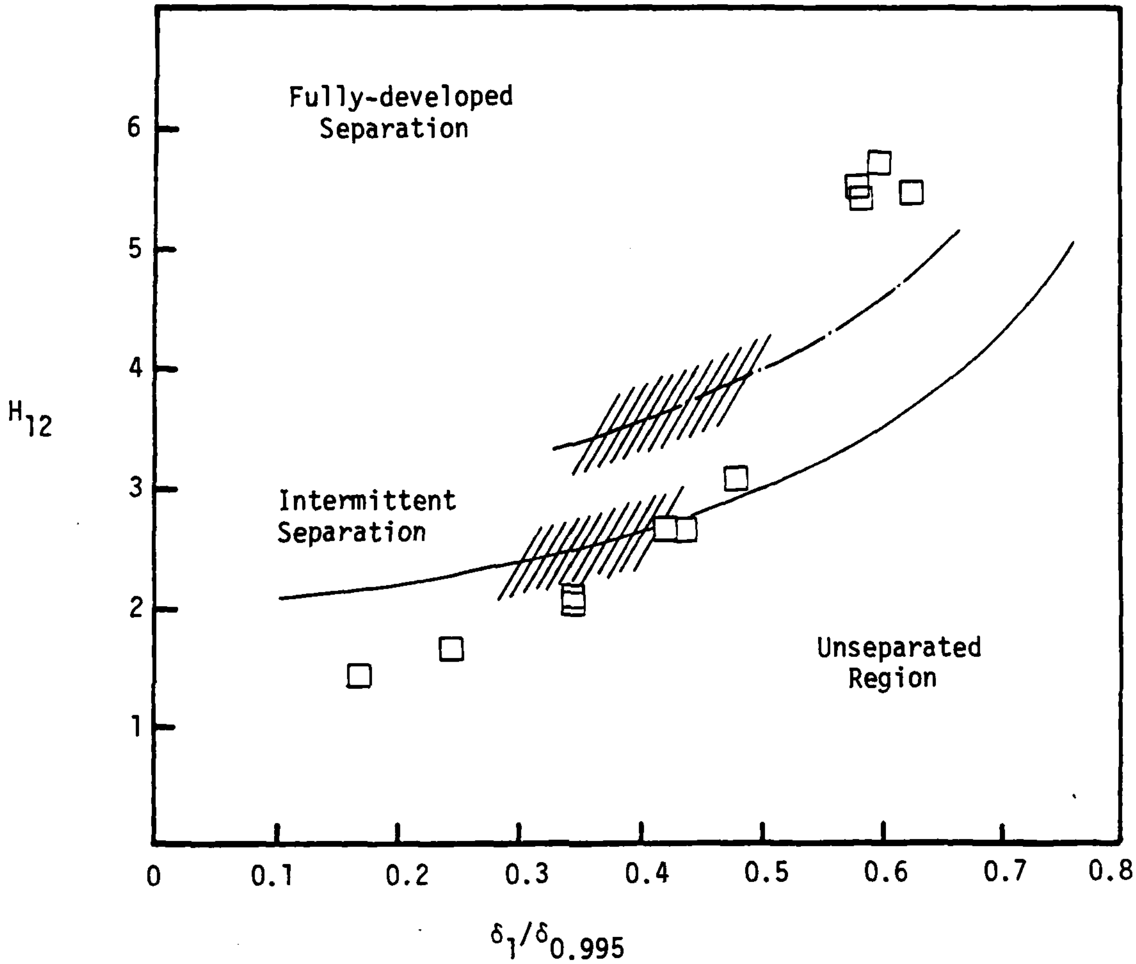

Figure 32. Sandborn's H_{12} vs. $\delta_1/\delta_{0.995}$ separation correlation: symbols, present data; solid line, intermittent separation; broken line, fully-developed separation.

"departure" or "breakaway" or the breakdown of boundary-layer flow. An abrupt thickening of the rotational flow region next to a wall and significant values of the normal-to-wall velocity component must accompany breakaway, else this region will not have any significant interaction with the freestream flow. A set of quantitative definitions were proposed and are shown on Figure 33 along with old definitions. Figure 23 shows the locations of incipient detachment, intermittent transitory detachment, and transitory detachment for the present flow obtained from Figure 20. In describing a quantitative amount of backflow, the word "detachment" was preferred over "separation" since the latter term refers to the entire phenomenon. Here we will continue to use the time-honored terminology, but mention the new terminology for the sake of completeness.

Downstream of intermittent separation, Simpson et al. (1977) showed the existence of similarity in γ_{pu} distributions by normalizing and plotting $\frac{(\gamma_{pu} - \gamma_{pu_o})}{(1 - \gamma_{pu_o})}$ vs. y/M where γ_{pu_o} was taken as the value near the wall as obtained from a figure similar to Figure 20 and M was the distance of the peak in the u' distribution from the wall. The present data also exhibit similarity, particularly in the region $0.1 \leq y/M \leq 1.0$, with it improving as one moves downstream. In fact the last two stations at 156.4 inches and 170.9 inches show the similarity to exist all across the boundary layer, including the backflow region. The similarity in the backflow region improves when the minimum value of γ_{pu} is used instead of γ_{pu_o} as shown in Figure 34. This is due to the relatively large uncertainty in γ_{pu_o}. Simpson et al. (1977) curve-fitted their data and gave an

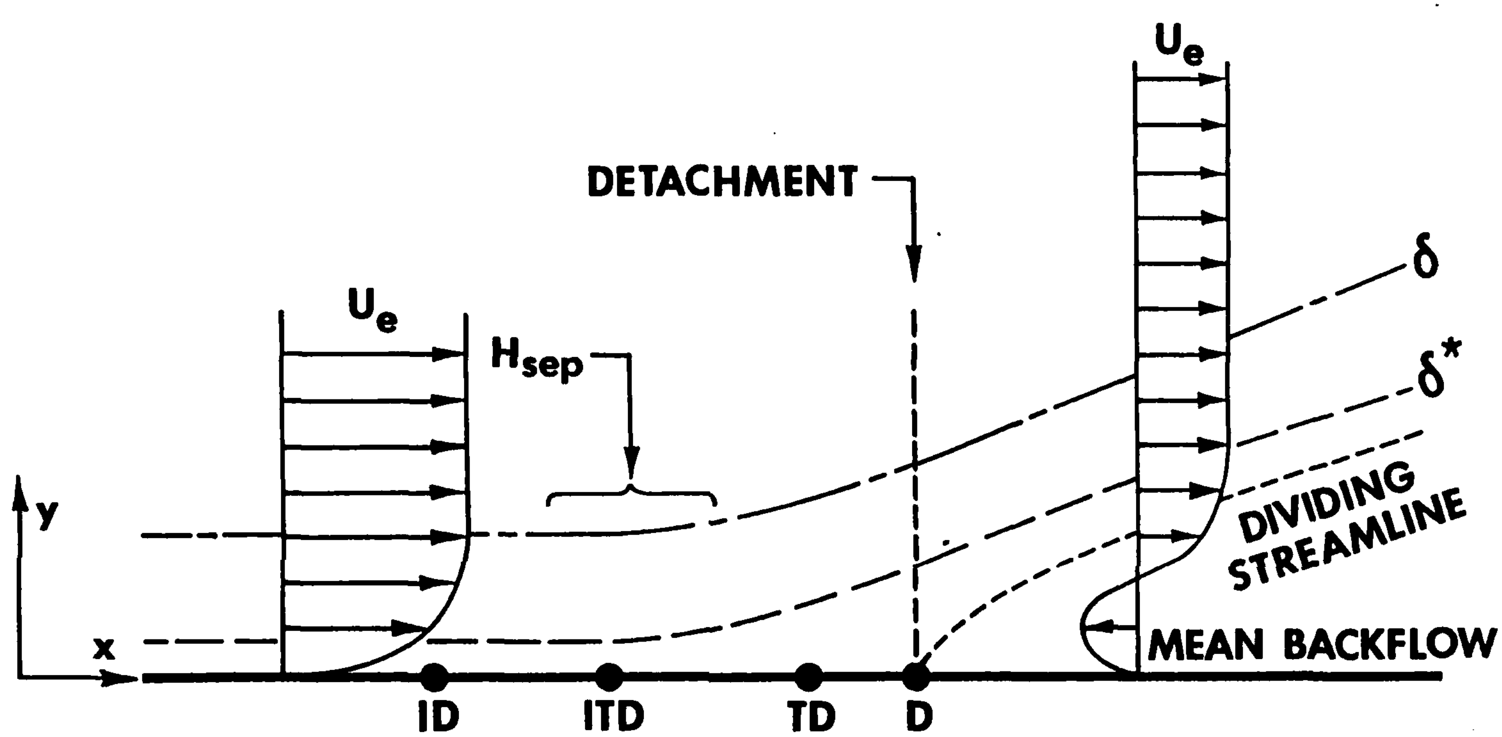

Figure 33. Definitions of two-dimensional turbulent detachment states. Distances not to scale. "% Instantaneous Backflow" means along a spanwise line at a given time, or percent of time at a point.

OLD TERM	SYMBOL	NEW TERM	CONDITION
none	ID	Incipient Detachment	1% Instantaneous Backflow
Intermittent Separation (Sandborn and Kline, 1961)	ITD	Intermittent Transitory Detachment	20% Instantaneous Backflow
none	TD	Transitory Detachment	50% Instantaneous Backflow
Steady or Fully-Developed Separation (Sandborn and Kline, 1961)	D	Detachment	$\overline{\tau}_w = 0$

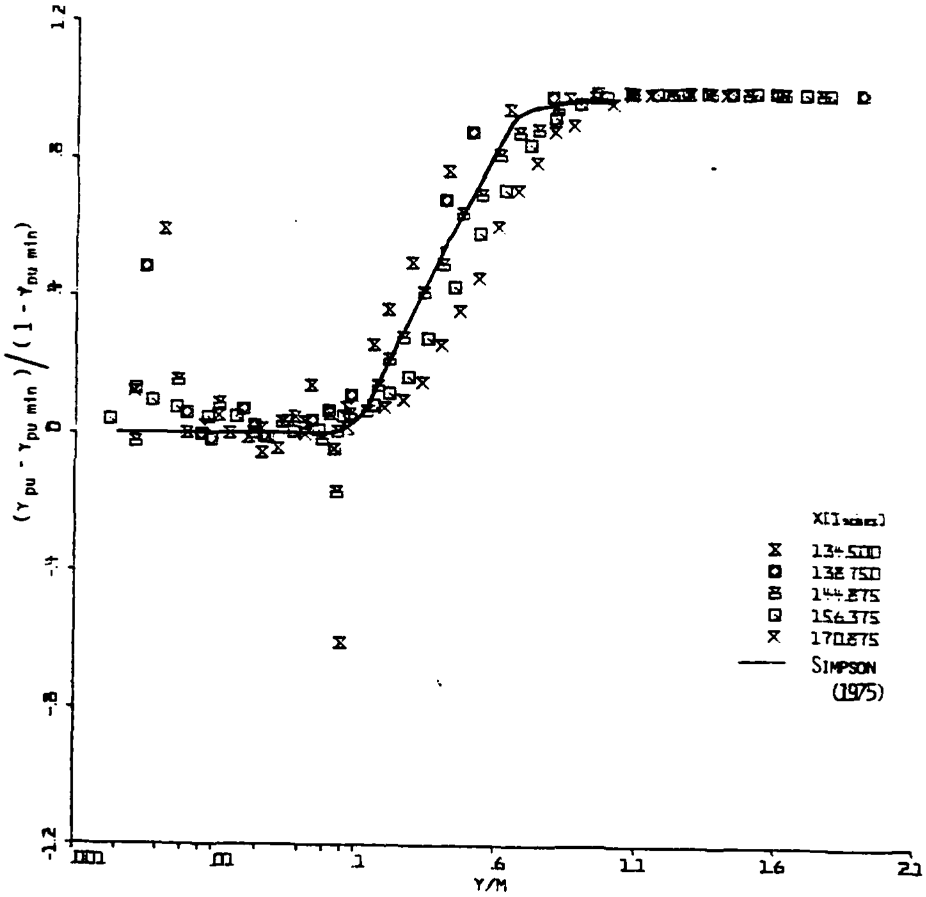

Figure 34. $(\gamma_{pu} - \gamma_{pu_{min}})/(1 - \gamma_{pu_{min}})$ vs. y/M; $\gamma_{pu_{min}}$ obtained from Figure 19; M is distance from wall to u'_{max}; solid line, distribution from data of Simpson et al. (1977).

equation for the distribution in the region $0.1 \leq y/M \leq 1.0$. Figure 34 shows that the present data approximately satisfy the equation. Similar plots drawn with M being taken as the distance from the wall to the location where peaks were observed in the v' and $-\overline{uv}$ distributions show as good or better similarity, such as in Figure 35.

Figures 36 (a) and (b) show results for γ_{pv} or the fraction of time that the flow is away from the wall. Because the uncertainties in γ_{pv} are relatively large near the wall, $\gamma_{pv_{min}}$ was used in the normalized results shown in Figure 37 for the region downstream of intermittent separation. Near the outer edge of the boundary layer the intermittency is everywhere approximately equal to one, indicating that the flow is always directed outwards. Near the wall, the intermittency γ_{pv} obtained in the region downstream of intermittent separation is higher than the values attained upstream of it, which can be attributed to the flow leaving the wall as a consequence of intermittent separation. As in the case of γ_{pu}, the distributions near the wall are trough-shaped in the region downstream of intermittent separation and show some similarity.

V.3 Turbulence Correlations

A. Reynolds Stresses Correlations

Figures 38 show distributions of the shear stress correlation coefficient $-\overline{uv}/u'v'$, which is a measure of the extent of correlation between u and v fluctuations. Table 5 gives typical uncertainty values for the correlation coefficients presented here for the central portion of the boundary layer. Near the outer edge the values are larger since $-\overline{uv}$, u' and v' approach zero. Figure 38 (a) also shows distributions for the Schubauer and Klebanoff (1951)

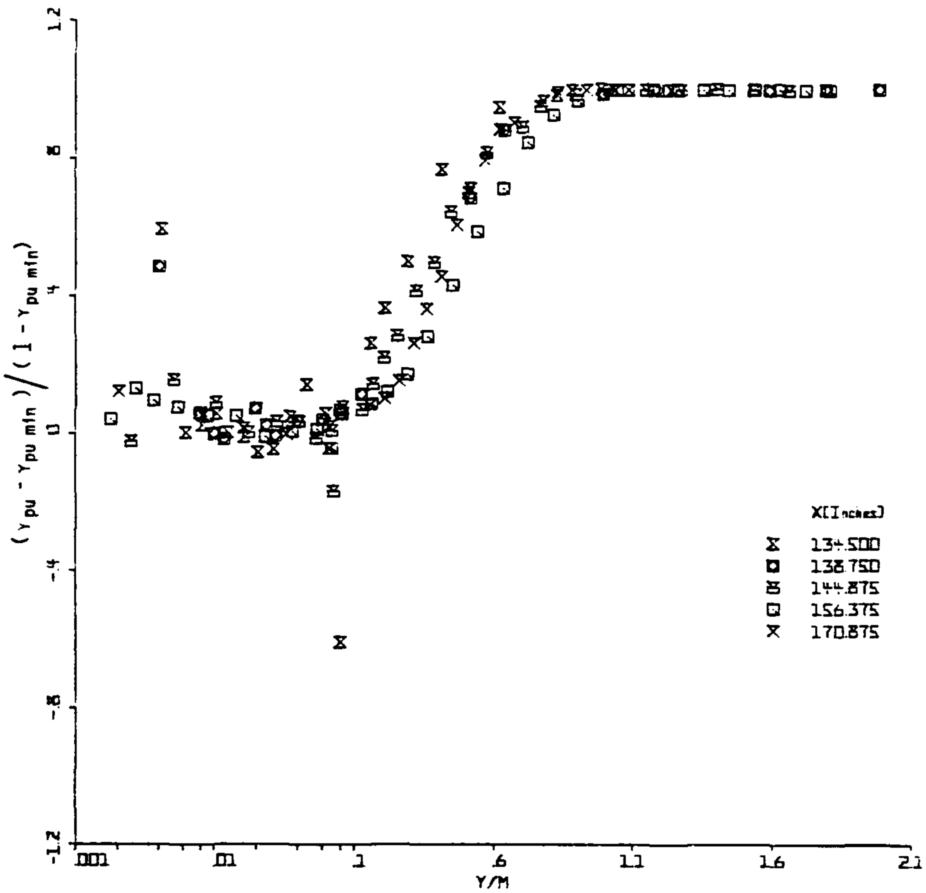

Figure 35. $(\gamma_{pu} - \gamma_{pu_{min}})/(1 - \gamma_{pu_{min}})$ vs. y/M; $\gamma_{pu_{min}}$ obtained from Figure 19; M is distance from wall to $-\overline{uv}_{max}$.

AD-A095 252 PURDUE UNIV LAFAYETTE IN PROJECT SQUID HEADQUARTERS F/G 20/4

MEASUREMENTS OF A SEPARATING TURBULENT BOUNDARY LAYER.(U)

APR 80 R L SIMPSON, Y CHEW, B G SHIVAPRASAD N00014-75-C-1143

UNCLASSIFIED SQUID-SMU-4-PU NL

2 of 3

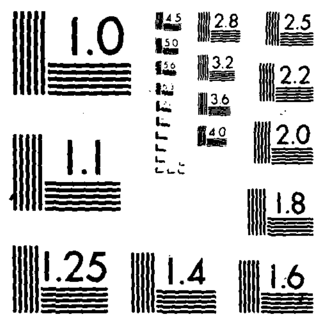

MICROCOPY RESOLUTION TEST CHART
NATIONAL BUREAU OF STANDARDS-1963-A

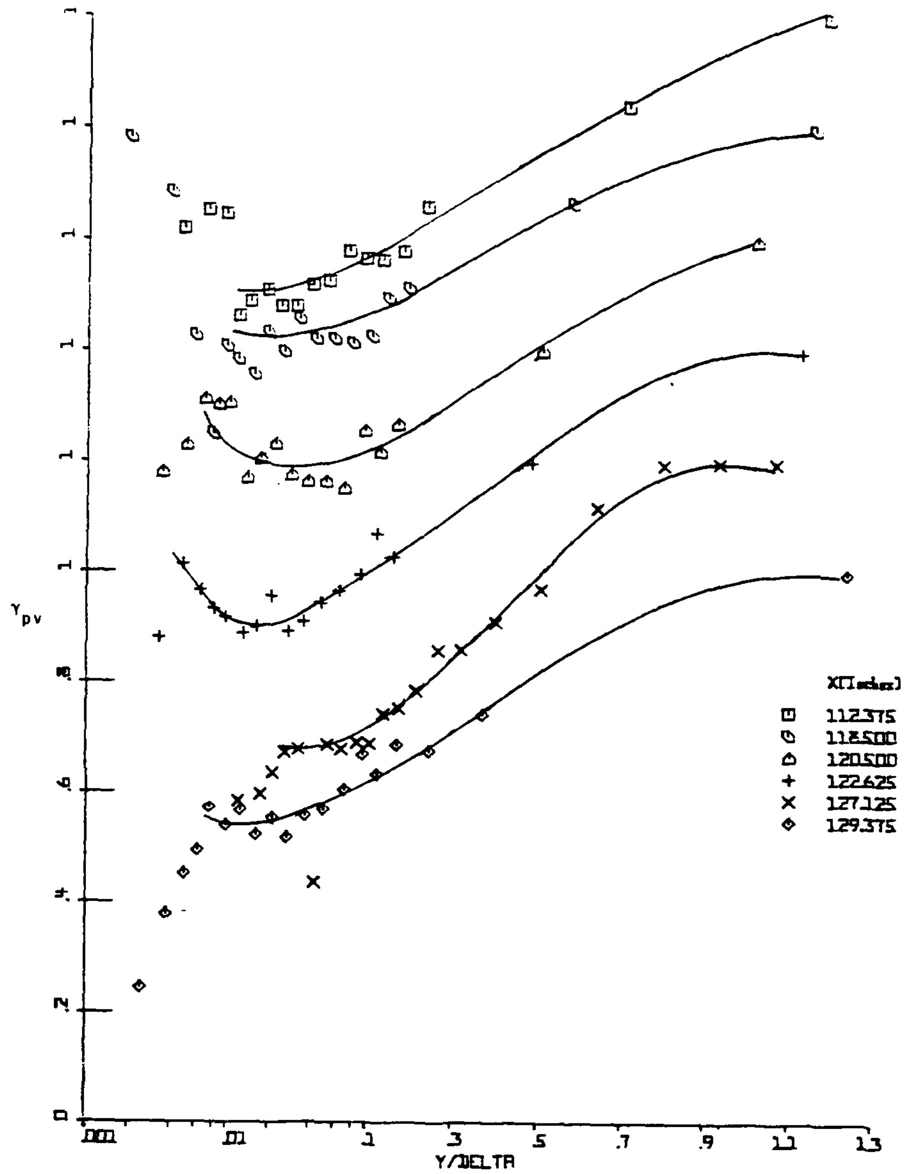

Figure 36(a). Fraction of time that the flow moves away from the wall, γ_{pv} vs. y/δ. Lines for visual aid only. Note displaced ordinates.

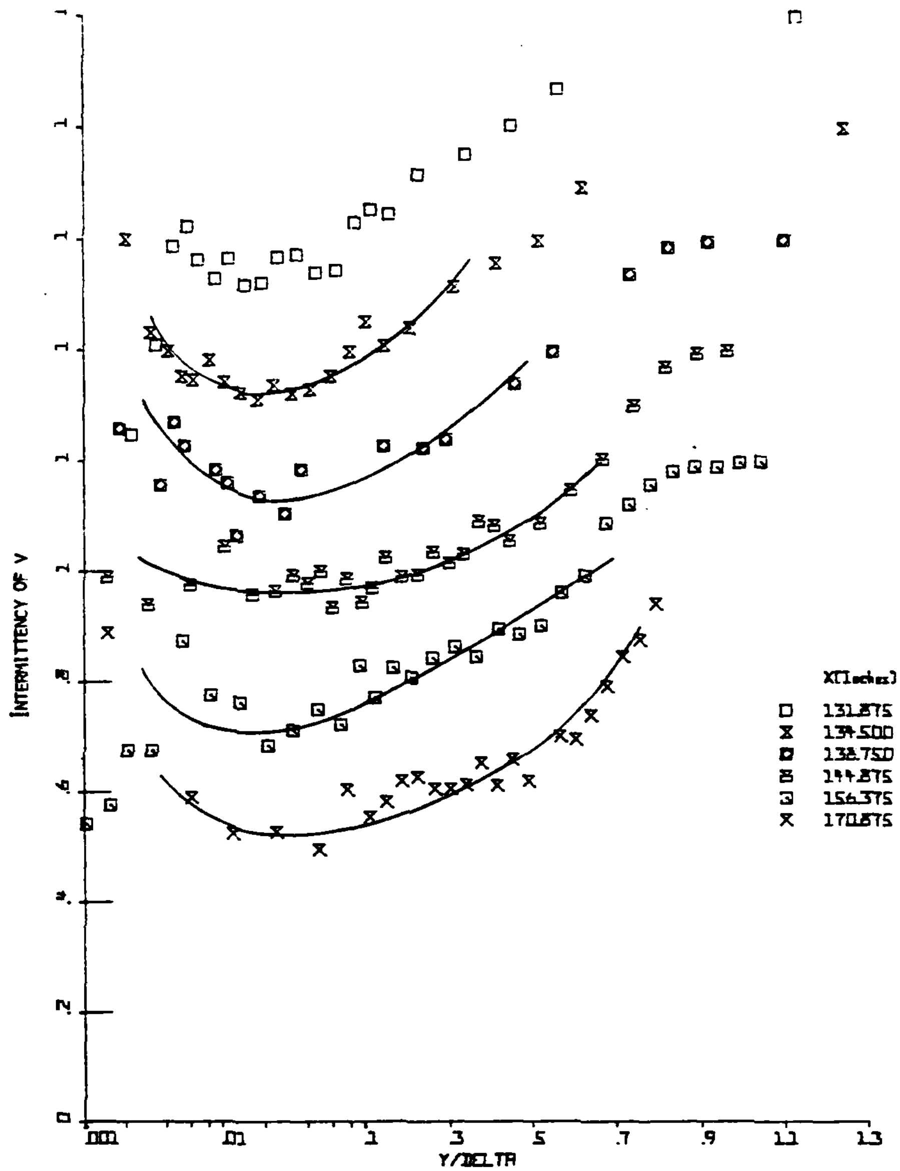

Figure 36(b). Fraction of time that the flow moves away from the wall, γ_{pv} vs. y/δ. Lines for visual aid only. Note displaced ordinates.

$$\ell = 0.4\, y\left(1 - \exp(-y/A)\right), \quad A = \frac{26\nu}{U_\tau N}, \quad N = (1 - 11.8\, p^+)^{\frac{1}{2}},$$
$$p^+ = \frac{\nu U_\infty}{U_\tau^3}\frac{dU_\infty}{dx} \tag{22}$$

for the 86.5 inches location. As recommended by Cebeci and Bradshaw (1977), a constant value of 0.08 is used for ℓ/δ in the outer region. The present data at 86.5 inches are in reasonable agreement with these results.

Although the downstream stations exhibit similarity in the inner layer, they show a continuously decreasing mixing length in the outer layer as one moves downstream. Further downstream in the intermittent separation region, the inner layer similarity gradually disappears and the mixing length in the outer layer continues to decrease with no region of constant mixing length. In the separated region, Prandtl's mixing length cannot be defined in the backflow region where $\frac{\partial U}{\partial y}$ is negative. The distributions for the forward flow region are shown in Figure 41 (d). They indicate large values of the mixing length closest to the wall where it can be defined, decreasing continuously as one moves farther away from the wall. There is also some indication of the profiles achieving similarity.

Figure 42 show the eddy viscosity profiles in the various regions. As in the case of the mixing length, a few sets of data from earlier investigations are also plotted for comparison. In general, the same comments made about the mixing length profiles are applicable to these profiles also. The present data in Figure 42 (a) show good agreement with Klebanoff's (1955) data in the zero pressure gradient region. The data in Figure 42 (b) show good agreement with Bradshaw's data in the adverse pressure gradient region in the inner layer. A prediction using Cebeci and Smith's model in the relation

$$\nu_e = \ell^2 \frac{\partial U}{\partial y} \tag{23}$$

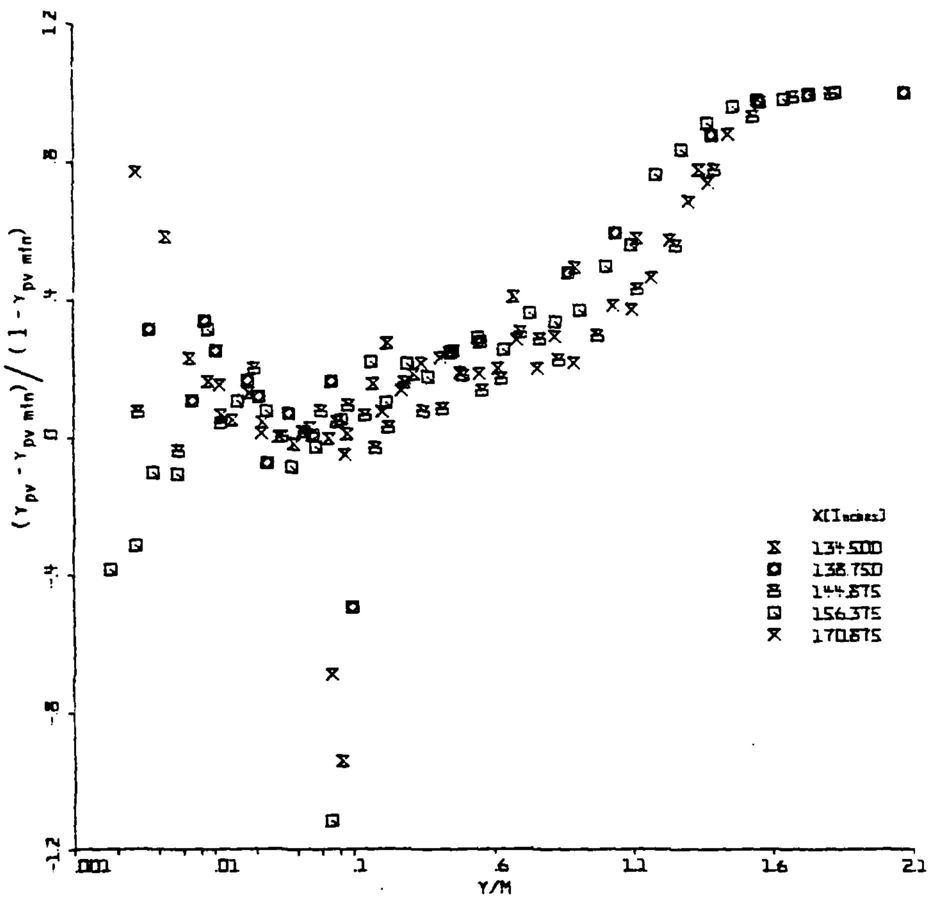

Figure 37. $(\gamma_{pv} - \gamma_{pv_{min}})/(1 - \gamma_{pv_{min}})$ vs. y/M; $\gamma_{pv_{min}}$ obtained from smoothed γ_{pv} data in Figure 36; $M = y$ at v'_{max}.

TABLE 6: Typical Uncertainties for turbulence correlations

Location X inches	Location Y inches	Quantity	Type of Data	Absolute Value	Absolute Value of the uncertainty at the particular x-y location	Estimate of percentage uncertainty for the complete data set
112.375	0.5	$\frac{-\overline{uv}}{u'v'}$	L.D.V.	0.462	0.031	6.6
111.25	0.6		x-wire	0.399	0.076	19
112.375	0.5	$\frac{-\overline{uv}}{(u'^2+v'^2)}$	L.D.V.	0.204	0.014	6.8
111.25	0.6		x-wire	0.174	0.034	19.5
112.375	0.5	$\tan^{-1}\left(\frac{-2\overline{uv}}{u'^2-v'^2}\right)$	L.D.V.	40.9°	1.8°	4.4
111.25	0.6		x-wire	35.4°	6.5°	18.4
131.875	1.0	$\frac{-(u'^2-v'^2)\frac{\partial U}{\partial x}}{-\overline{uv}\frac{\partial U}{\partial y}}$	Smoothed X-wire & L.D.V.	0.389	0.132	35
118.5	2.0	$\frac{\frac{\partial}{\partial x}(u'^2-v'^2)}{\frac{\partial}{\partial y}(-\overline{uv})}$	Smoothed x-wire & L.D.V.	-0.411	0.314	Varies widely
131.875	2.5			-0.742	0.041	
131.875	1.5	$\frac{\ell_m}{\delta}$	L.D.V.	0.052	0.0056	12
86.5	0.354		x-wire	0.064	0.013	20
131.875	1.5	$\frac{\nu_t}{U_\infty \delta_1}$	L.D.V.	0.006184	0.00074	15
86.5	0.354		x-wire	0.0133	0.0027	20

Table 6: Flow conditions for the present and previous investigations.

Parameter	streamwise location (in inches) for the present data			Data of other investigators: streamwise location (in ft) for Klebanoff's data		Bradshaw		East & Sawyer, flow 4	East & Sawyer, flow 1
	86.5	105	117.6	17.5	22.5	a=-0.15	a=-0.255		
θ (Inches)	0.153	0.284	0.458					0.338	0.129
R_θ	5205	8617	11988	18750	41850	22900	38800	-	
H_{12}	1.418	1.625	2.024	1.35	1.6	1.4	1.54	1.344	1.31
$C_{f/2} \times 10^3$	1.33	0.859	0.422	1.73	0.935			1.1	0.0014
$E_D = -\left(\frac{H_{12}}{H_{12}-1}\right)^2\left(\frac{\delta_1}{U_\infty}\frac{dU_\infty}{dx}\right)$	0.0109	0.0269	0.0271					0.0804	-0.0064
$\beta = \frac{\delta_1}{\tau_w}\frac{dP_\infty}{dx}$	-0.71	-4.64	-16.45	0	-4.57	-0.9	-5.57		

strong adverse gradient boundary layer. These two sets of measurements compare reasonably well, considering the fact that the adverse pressure gradient distributions are different. Table 6 shows a comparison of some parameters for the two flows.

Figure 38 (b) shows distributions in the vicinity of the beginning of intermittent backflow. Unlike the distributions far upstream shown in Figure 38 (a) or those observed in zero pressure gradient boundary layers, the distributions in this region do not exhibit a constant value over a large part of the outer layer. However, the distributions for some of the stations do indicate a small region with a nearly constant value as low as 0.2 to 0.3. As one moves downstream, the peaks for the distributions seem to gradually move towards the outer edge of the boundary layer. Similar features such as correlation coefficients as low as 0.3 with the peaks occuring near the outer edge of the boundary layer were observed by Spangenberg et al. (1967) in their experiments on an adverse pressure gradient flow approaching separation. Not much significance can be attached to the dips in the distributions observed near the wall except to hint that they might be a consequence of the peaks in the production curves occurring near the wall. Figure 38 (c) indicates that the profiles for the separated region seem to exhibit some similarity. These distributions compare fairly well in the outer region with the results of Wygnanski and Fielder (1970) for a mixing layer. Figure 39 gives the distributions of another type of correlation coefficient, $a_1 = -\overline{uv}/(u'^2 + v'^2)$, similar to the one used by Bradshaw et al. (1967) for converting the turbulent kinetic energy equation into an equation for shear stress. Using $w'^2 = \frac{1}{2}(u'^2 + v'^2)$, it is possible to relate a_1 to the more commonly used Bradshaw's constant 'a' defined as $a = -\overline{uv} \big/ (u'^2 + v'^2 + w'^2)$ by the relation $a = 2/3a_1$.

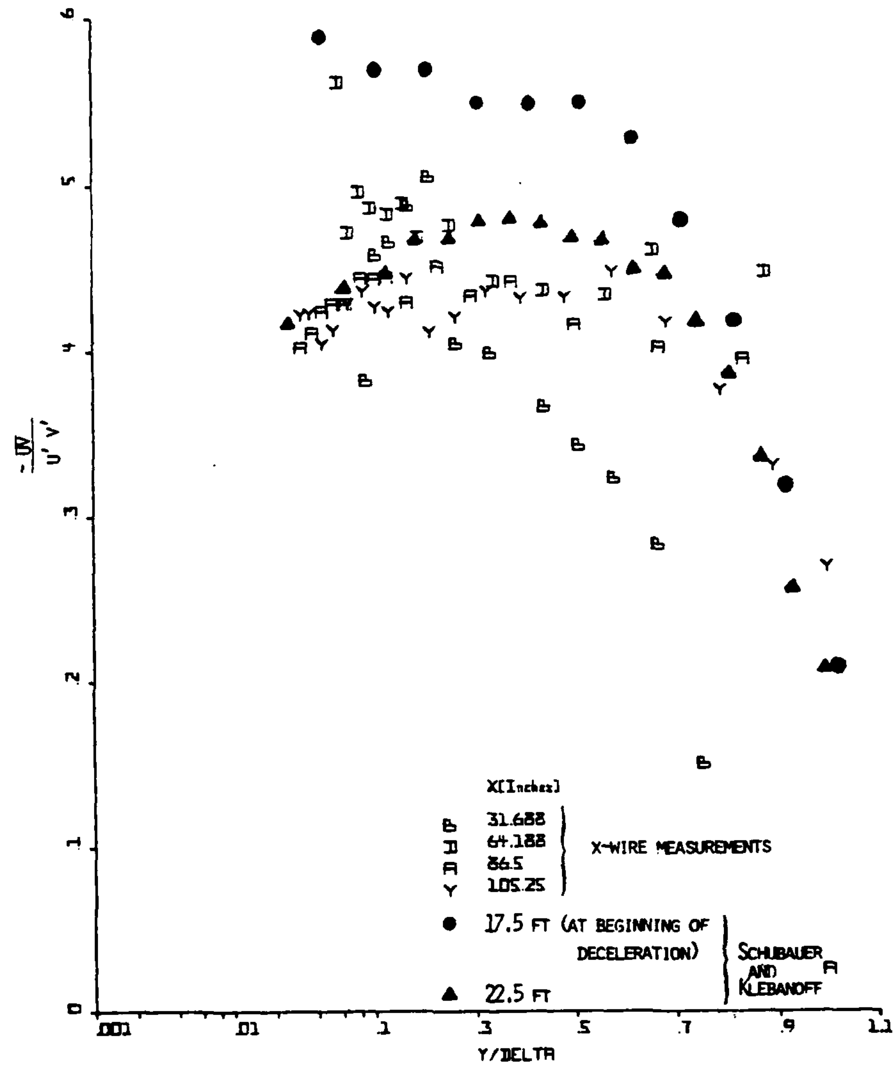

Figure 38(a). Shear stress correlation coefficient profiles from smoothed laser and hot-wire data, Figures 16, $-\overline{uv}/u'v'$ vs. y/δ : upstream of separation.

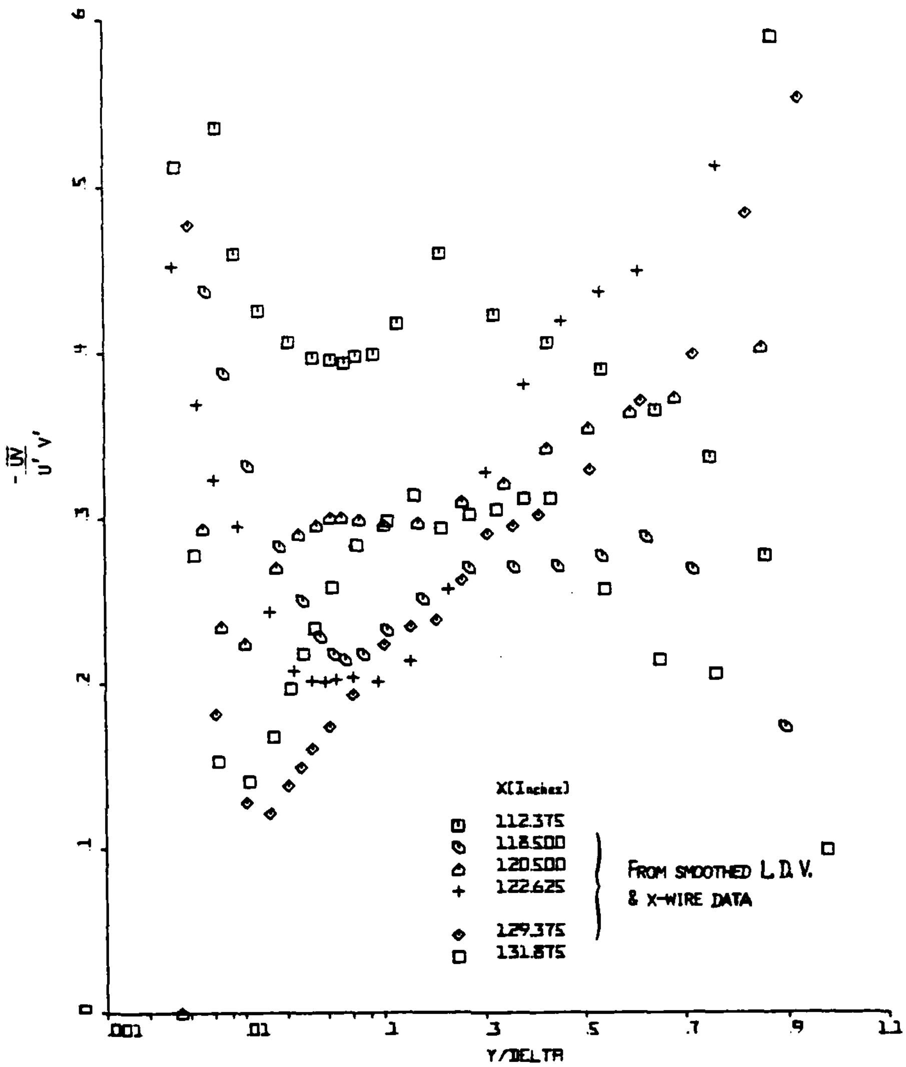

Figure 38(b). Shear stress correlation coefficient profiles from smoothed laser and hot-wire data, Figures 16, $-\overline{uv}/u'v'$ vs. y/δ: in the vicinity of the beginning of intermittent backflow.

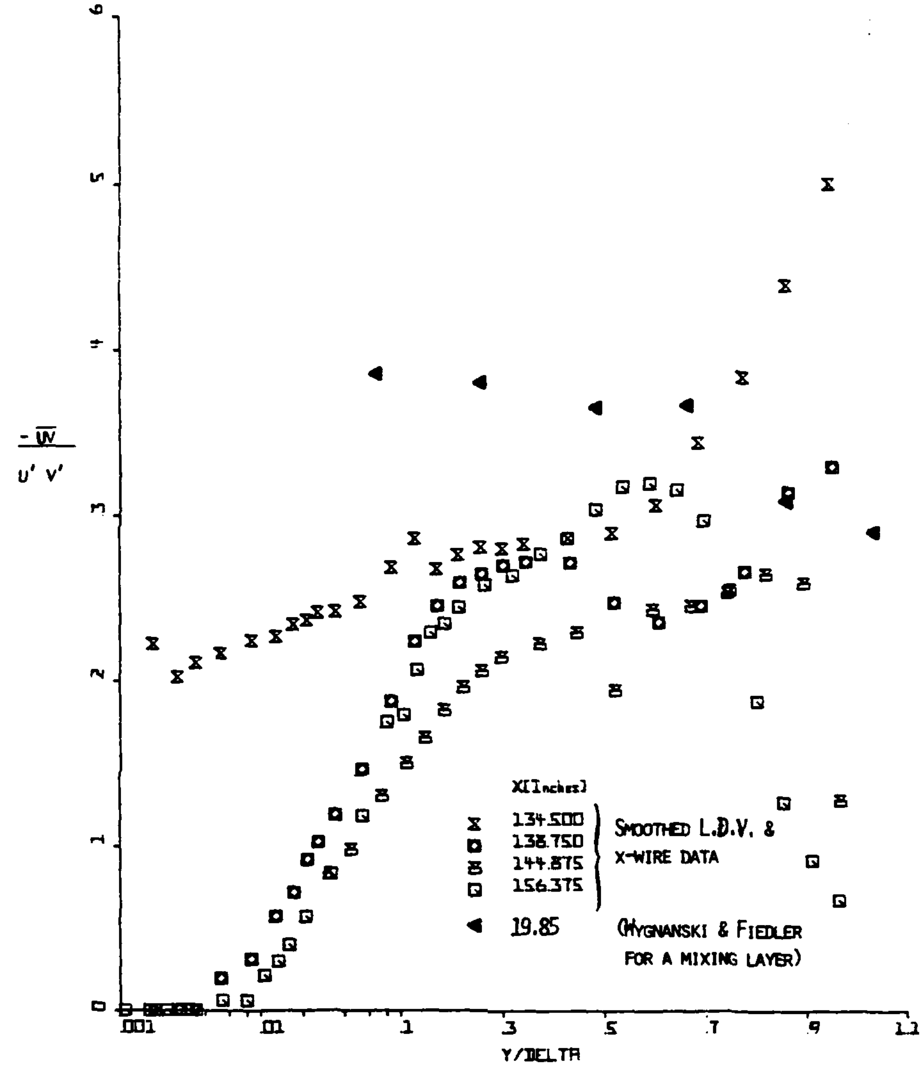

Figure 38(c). Shear stress correlation coefficient profiles from smoothed laser and hot-wire data, Figures 16, $-\overline{uv}/u'v'$ vs. y/δ: separated region.

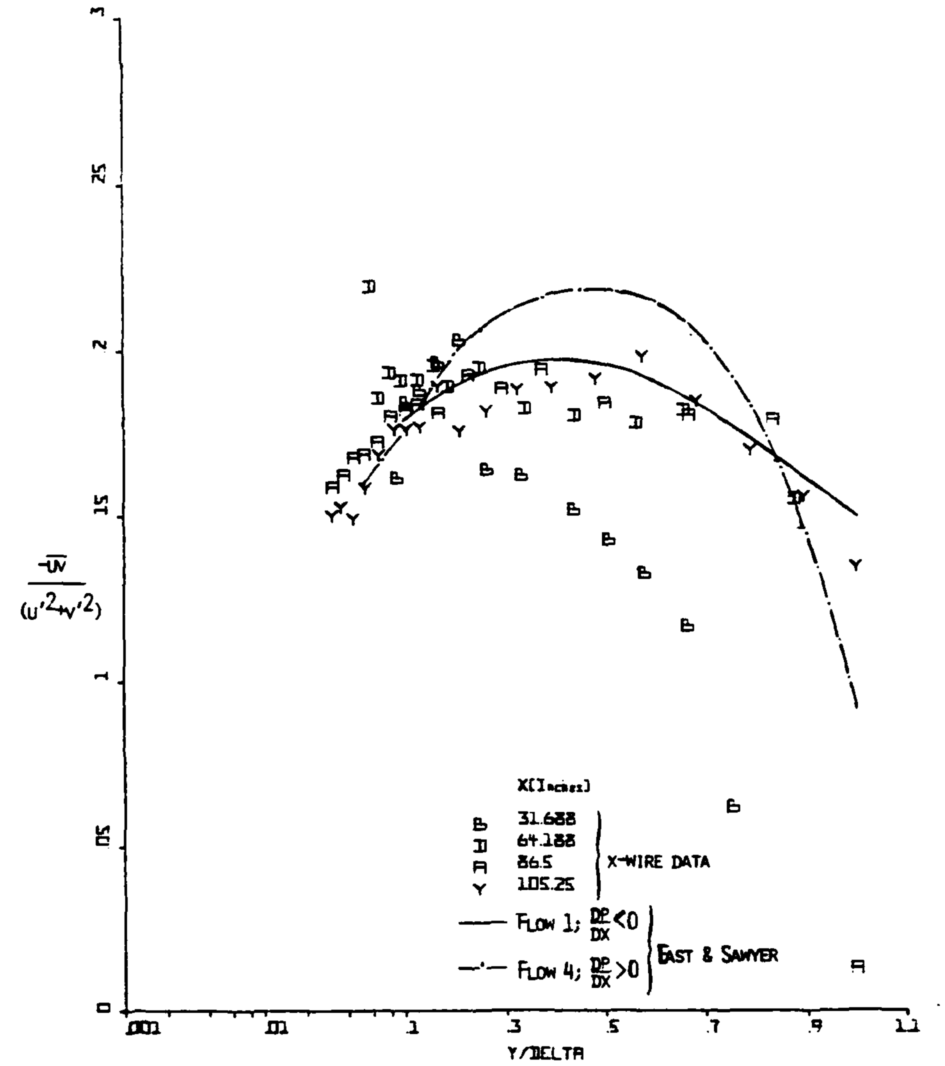

Figure 39(a). Shear stress correlation coefficient profiles from smoothed laser and hot-wire data, Figures 16, $-\overline{uv}/(u'^2 + v'^2)$ vs. y/δ: upstream of separation.

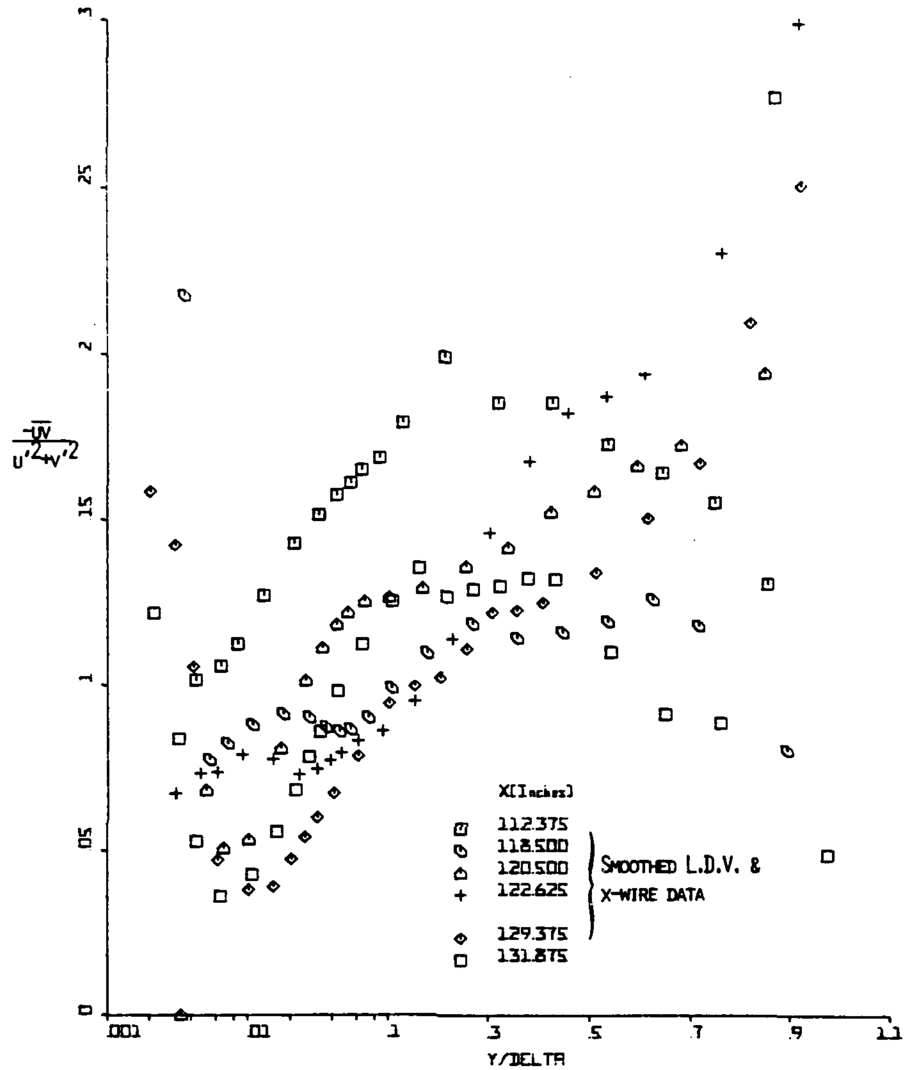

Figure 39(b). Shear stress correlation coefficient profiles from smoothed laser and hot-wire data, Figures 16, $-\overline{uv}/(u'^2 + v'^2)$ vs. y/δ: in the vicinity of the beginning of intermittent backflow.

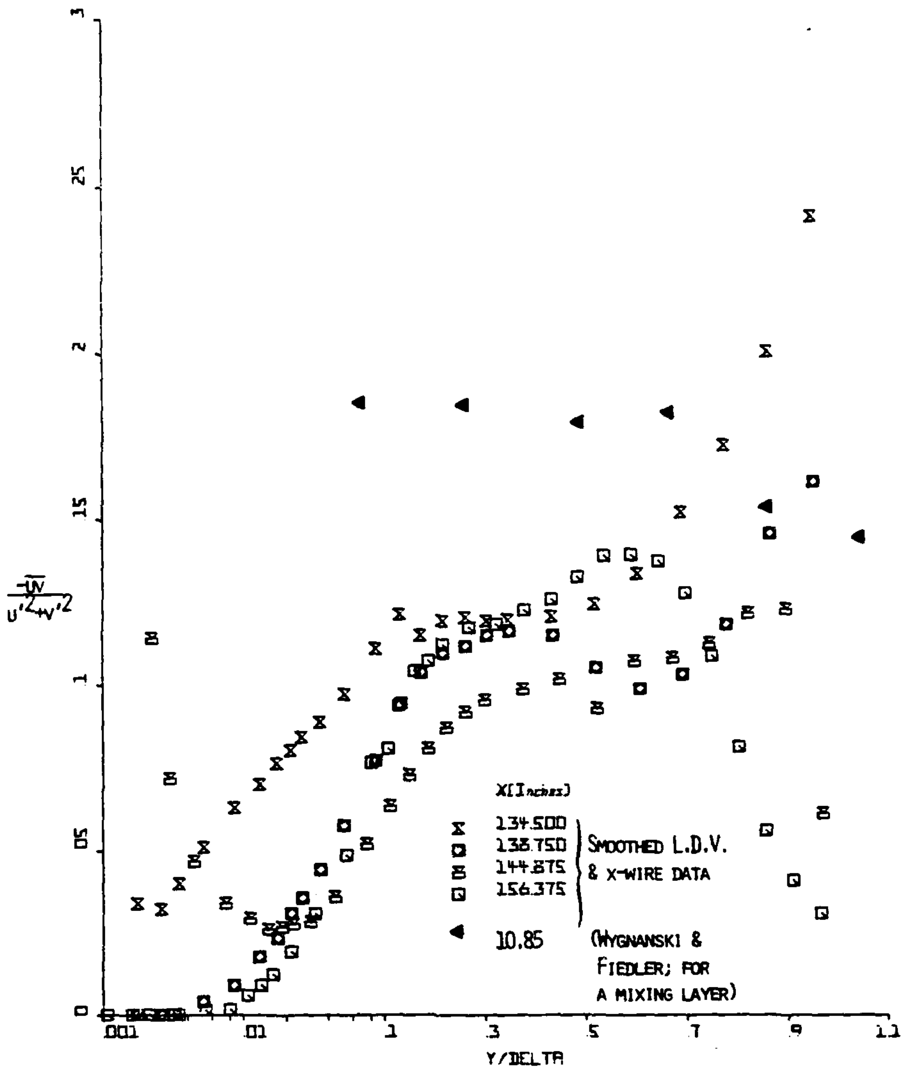

Figures 39(c). Shear stress correlation coefficient profiles from smoothed laser and hot-wire data, Figures 16, $-\overline{uv}/(u'^2 + v'^2)$ vs. y/δ: separated region.

Figure 39 (a) also contains the data of East and Sawyer (1979) for favorable and adverse pressure gradient flows. The flow conditions for those cases are given in Table 6. Considering the wide variations in the flow conditions and the uncertainties in the measurements, the agreement seems to be reasonable, particularly for the adverse pressure gradient case. The variation in the behavior of the distributions as one moves downstream is similar to that for the shear correlation coefficient $-\overline{uv}/u'v'$, with an increasingly reduced flat region and a reduction in the value of a_1 to as low as 0.1 for the separated region.

Another quantity which can be derived from u', v' and $-\overline{uv}$ is $\theta = \frac{1}{2}\tan^{-1}\left\{\frac{-2\overline{uv}}{u'^2-v'^2}\right\}$, which gives the angle of inclination of the principal axis to the flow direction. This has been plotted in Figures 40. Sandborn and Slogar (1955) observed that θ remains almost independent of x and y except for a small part of the inner layer. They also noticed that in the inner layer the angle θ decreases rapidly as the wall is approached, thus tending to align the axis of the principal stress with the flow direction. Considering the uncertainties in θ, particularly near the outer edge where all the quantities u', v' and $-\overline{uv} \rightarrow 0$, the present data seem to indicate those same trends, at least for the stations downstream of 86.5 inches and up to the beginning of the intermittent separation. In the intermittent separation region, only some of the stations indicate a weak dependence with respect to y in the outer layer. In the fully-separated region there is an indication of the profiles tending to become similar. The angle in the flat region decreases from approximately 18° at 86.5 inches to 12° in the separated region.

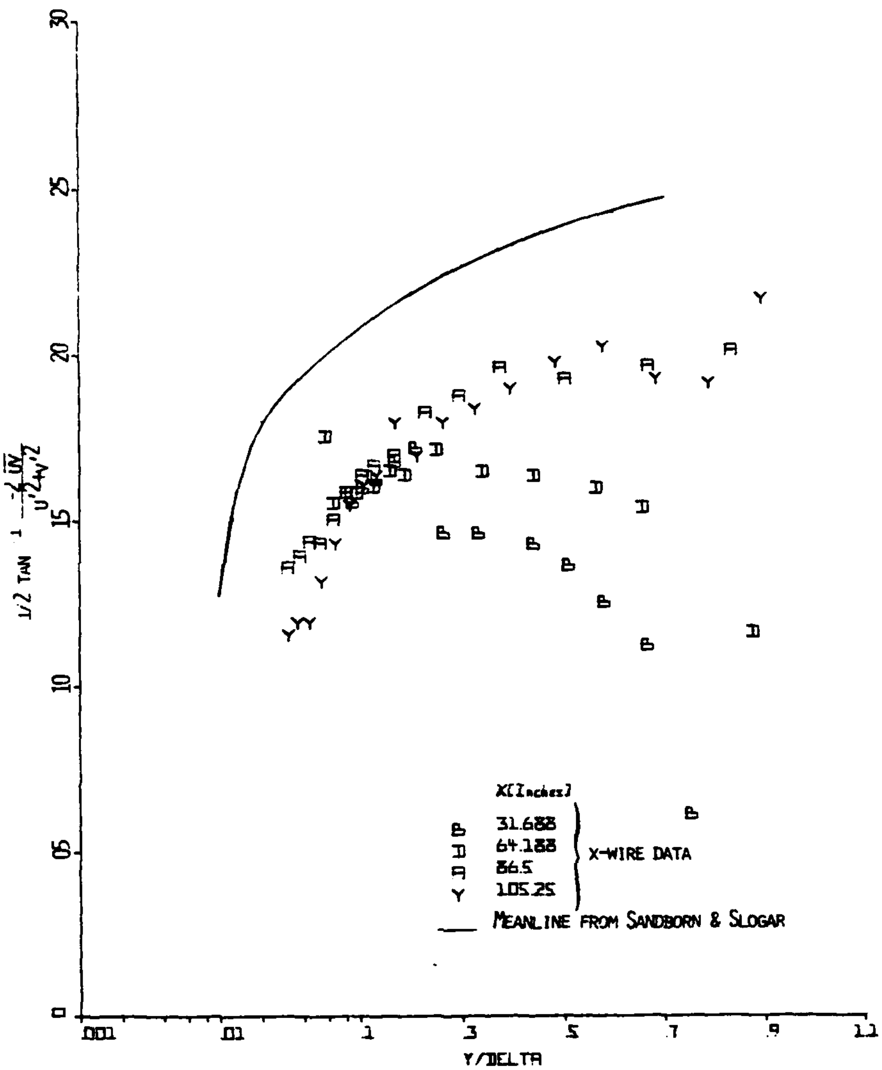

Figure 40(a). Angle of principal axis of stress to the flow direction, $\Theta = 1/2\ \tan(-2\overline{uv}/(u'^2 - v'^2))$ vs. y/δ. Solid line is mean line from Sandborn and Slogar (1955).

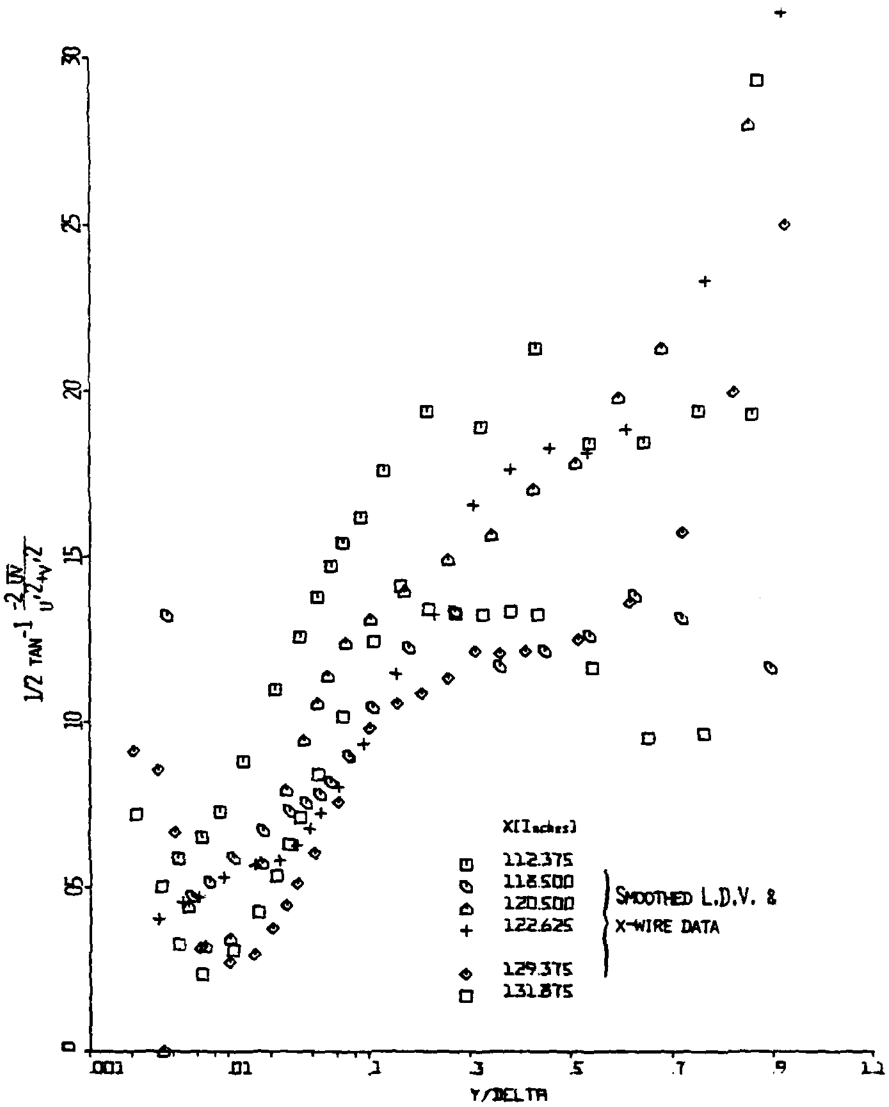

Figure 40(b). Angle of principal axis of stress to the flow direction, $\Theta = 1/2 \tan(-2\overline{uv}/u'^2 - v'^2))$ vs. y/δ. Solid line is mean line from Sandborn and Slogar (1955).

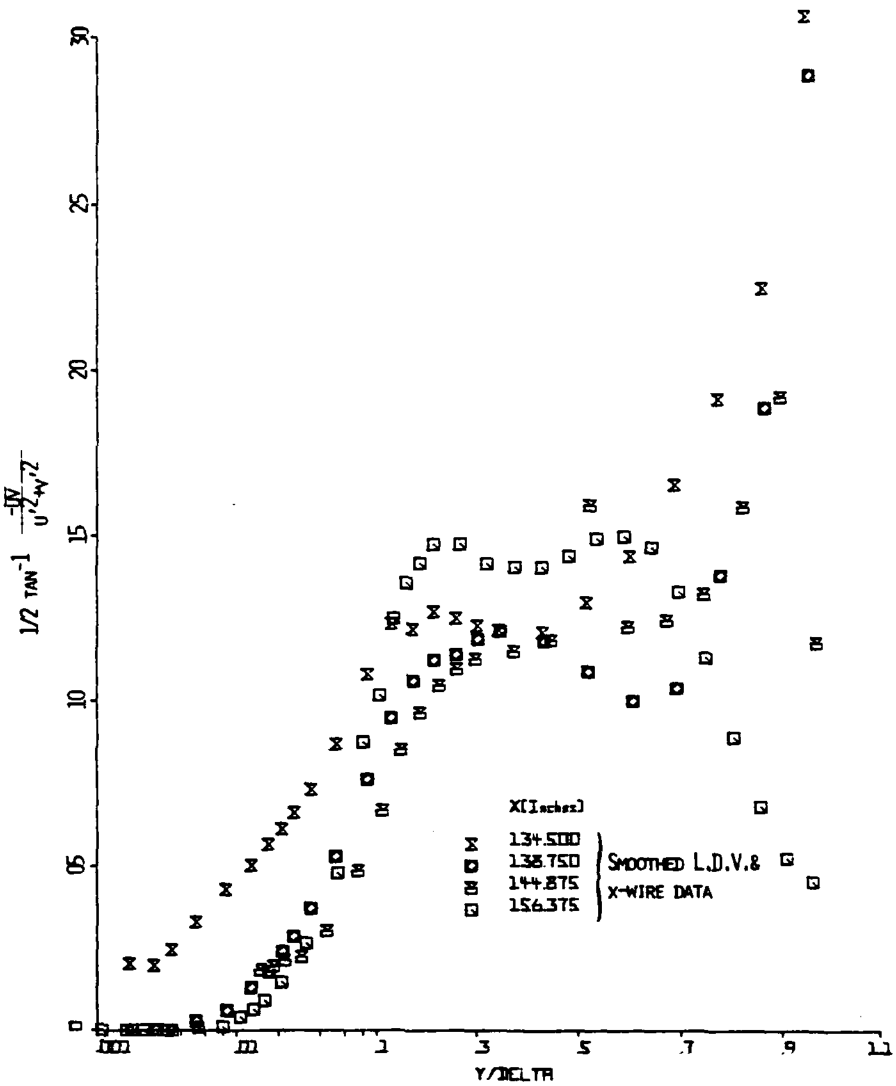

Figure 40(c). Angle of principal axis to the flow direction, $\Theta = 1/2 \tan(-2\overline{uv}/(u'^2 - v'^2))$ vs. y/δ. Solid line is mean line from Sandborn and Slogar (1955).

B. Eddy viscosity and Prandtl mixing length distributions

The Prandtl mixing length

$$\frac{\ell}{\delta} = \frac{-\overline{uv}}{\delta} \left|\frac{\partial U}{\partial y}\right|^{-1} \left(\frac{\partial U}{\partial y}\right)^{-1} \tag{20}$$

and the eddy viscosity

$$\frac{\nu_e}{U_\infty \delta_1} = \frac{-\overline{uv}}{U_\infty \delta_1 \ \partial U/\partial y} \tag{21}$$

were calculated from measured Reynolds shearing stress and calculated velocity gradient distributions. Figure 41 (a) shows the mixing length results for the region up to the throat of the test section where the pressure gradient is either favorable or approximately zero. The data of Klebanoff (1955) for a zero pr ssure gradient boundary layer and that of East and Sawyer (1979) for zero and favorable pressure gradient boundary layers are also presented for comparison. The present data at 64.2 inches show good agreement within the limits of uncertainty with the zero pressure gradient data of the earlier investigators. The data at 31.25 inches show agreement only in the inner layer with the favorable pressure gradient data of East and Sawyer. One possible reason for this might be the close proximity of that station to the entrance region of the test section.

Figure 41 (b) covers the adverse pressure gradient region of the flow up to the start of the intermittent separation. The data of Bradshaw (1967) for adverse pressure gradient equilibrium boundary layers and East and Sawyer (1979) are presented for comparison. Also shown in Cebeci and Smith's (1974) extension of van Driest's mixing length model for the inner layer

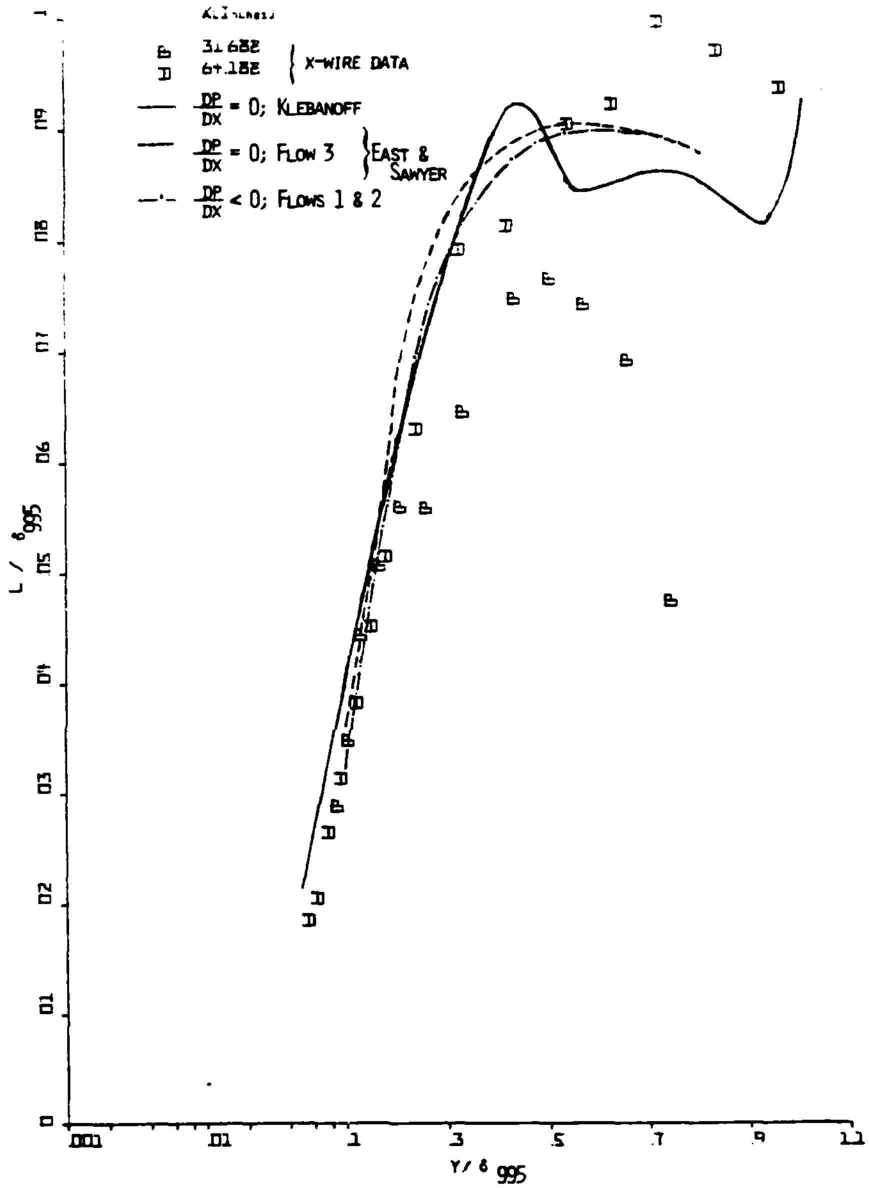

Figure 41(a). Mixing length distributions, ℓ/δ vs. y/δ: well upstream of separation.

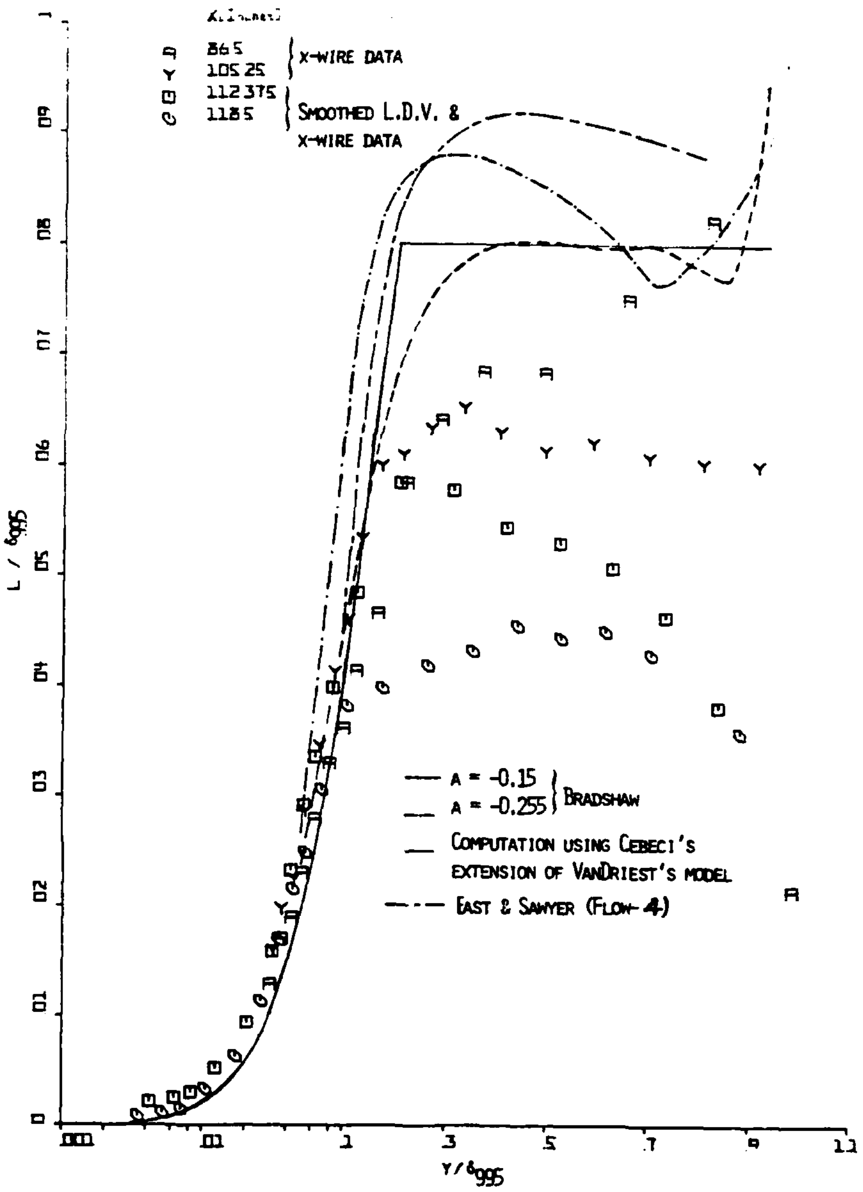

Figure 41(b). Mixing length distributions, ℓ/δ vs. y/δ: well upstream of separation.

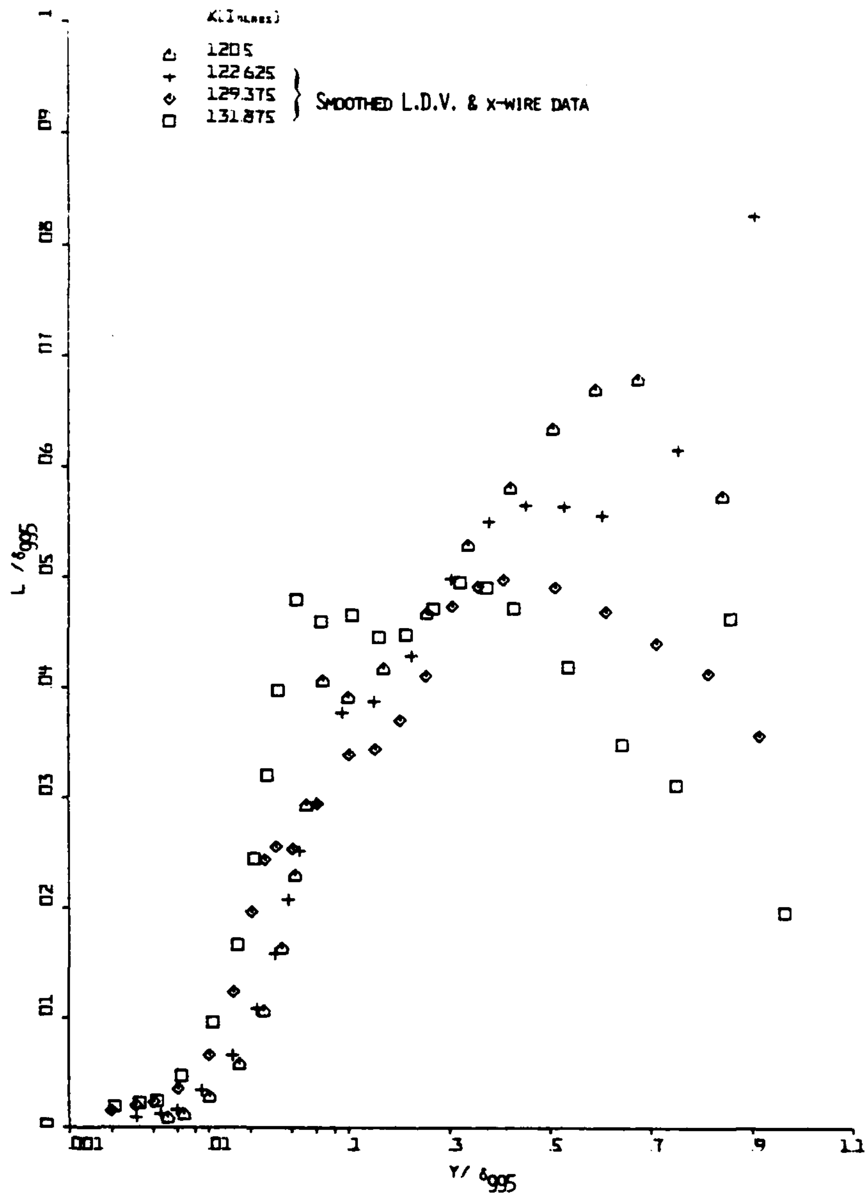

Figure 41(c). Mixing length distributions, ℓ/δ vs. y/δ: in the vicinity of separation.

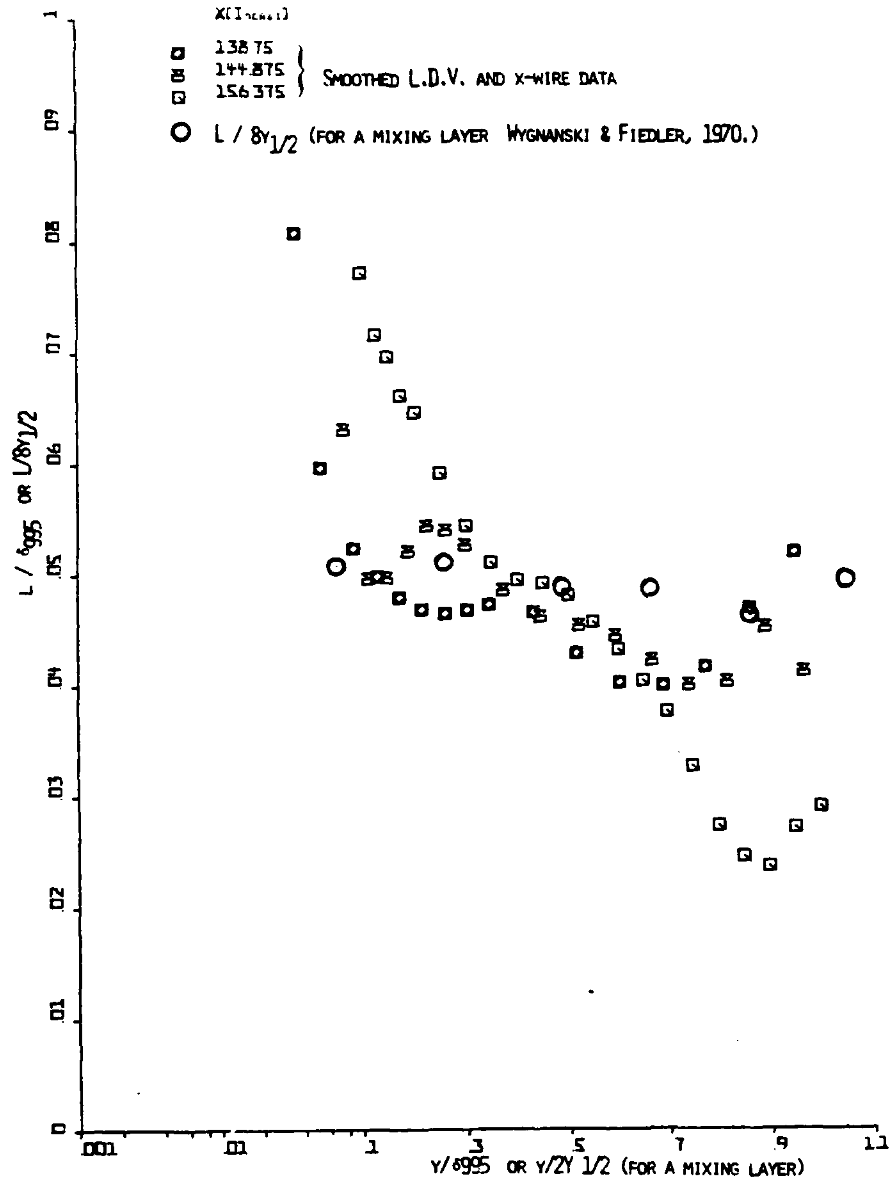

Figure 41(d). Mixing length distributions, ℓ/δ vs. y/δ: downstream of separation.

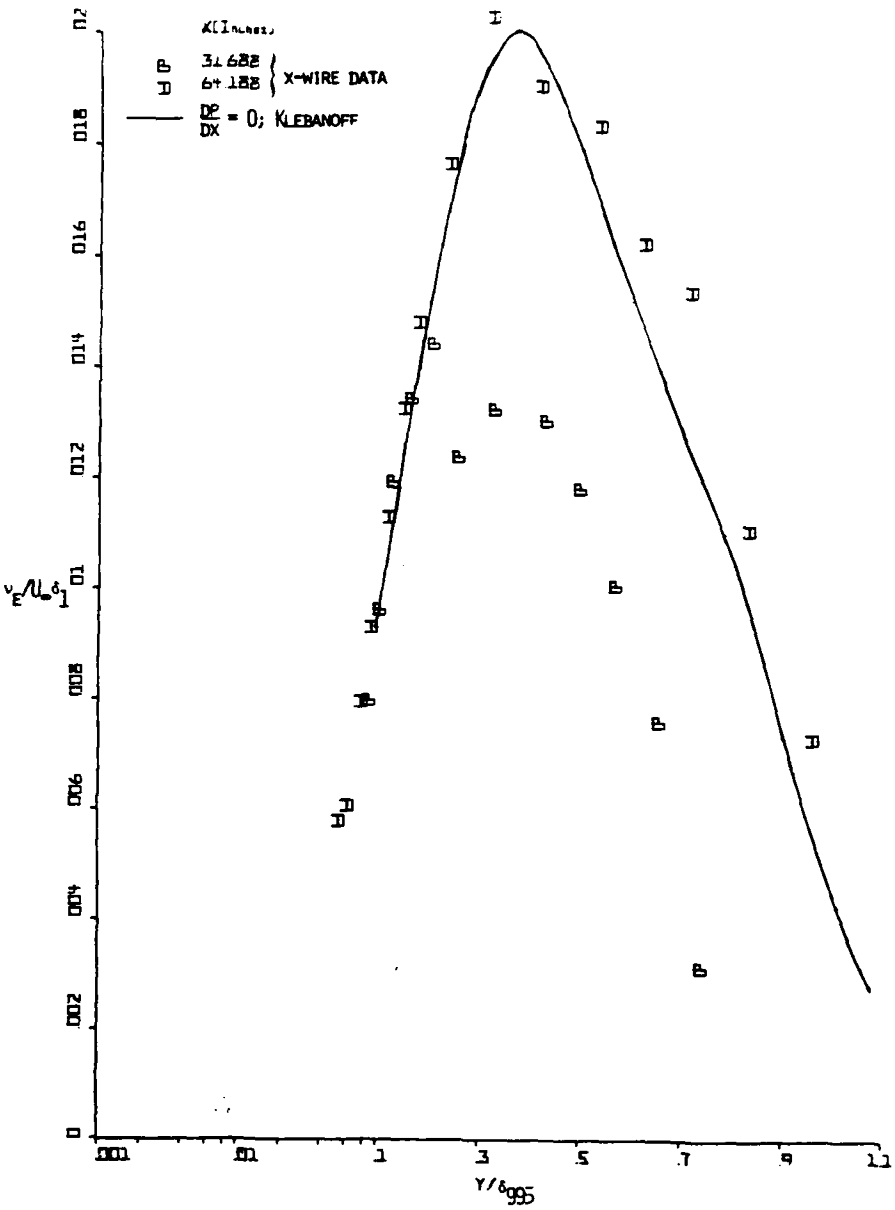

Figure 42(a). Eddy viscosity distributions, $\nu_e/U_\infty\delta_1$ vs. y/δ: well upstream of separation.

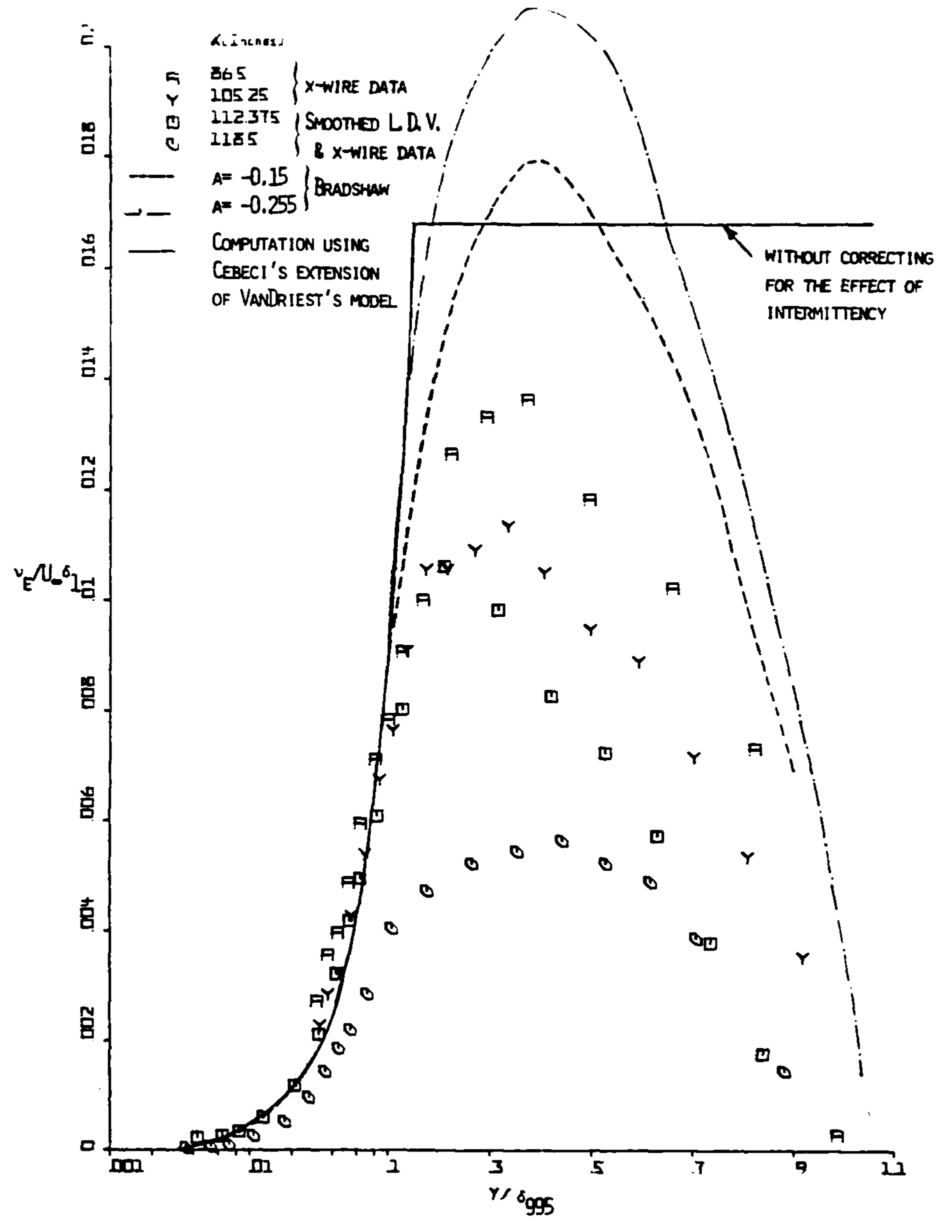

Figure 42(b). Eddy viscosity distributions, $\nu_e/U_\infty\delta_1$: well upstream of separation.

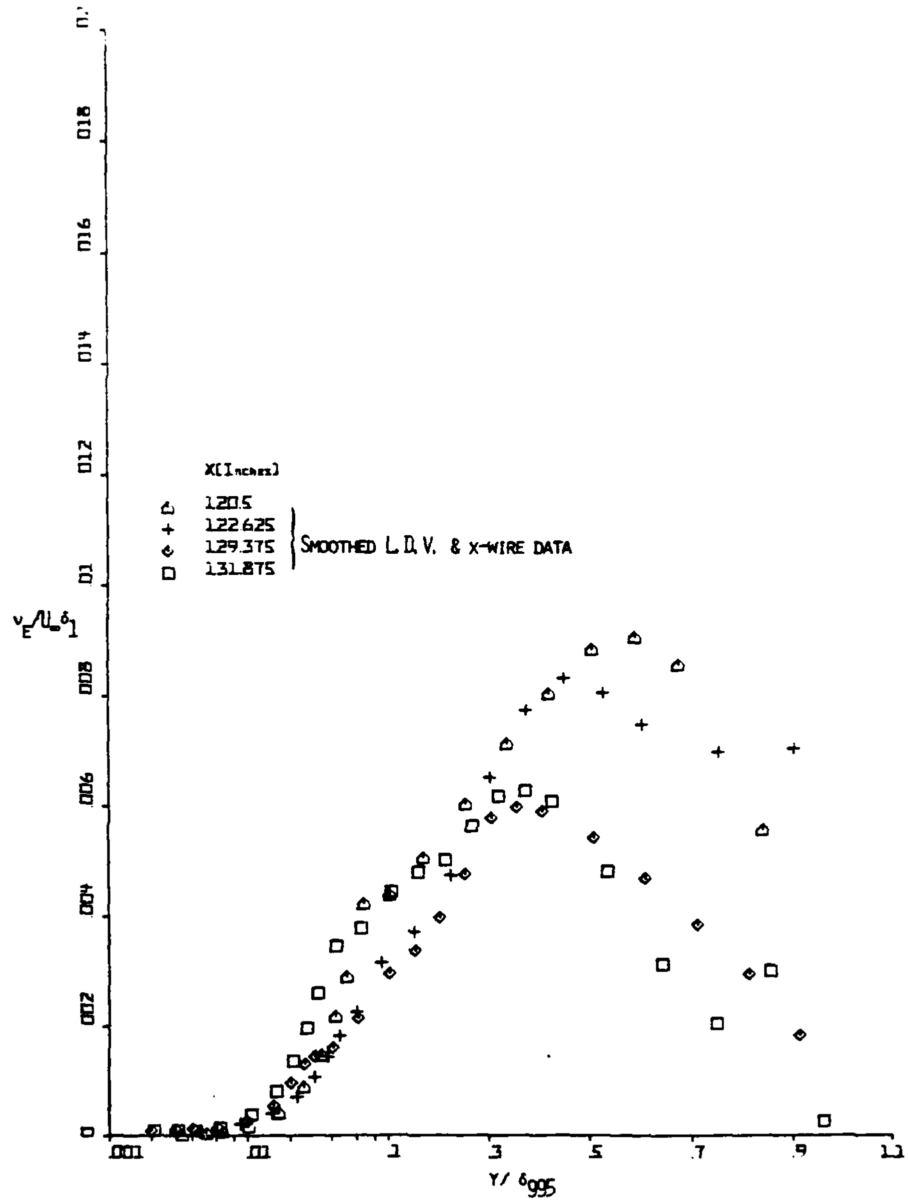

Figure 42(c). Eddy viscosity distributions, $\nu_e/U_\infty\delta_1$ vs. y/δ: in the vicinity of separation.

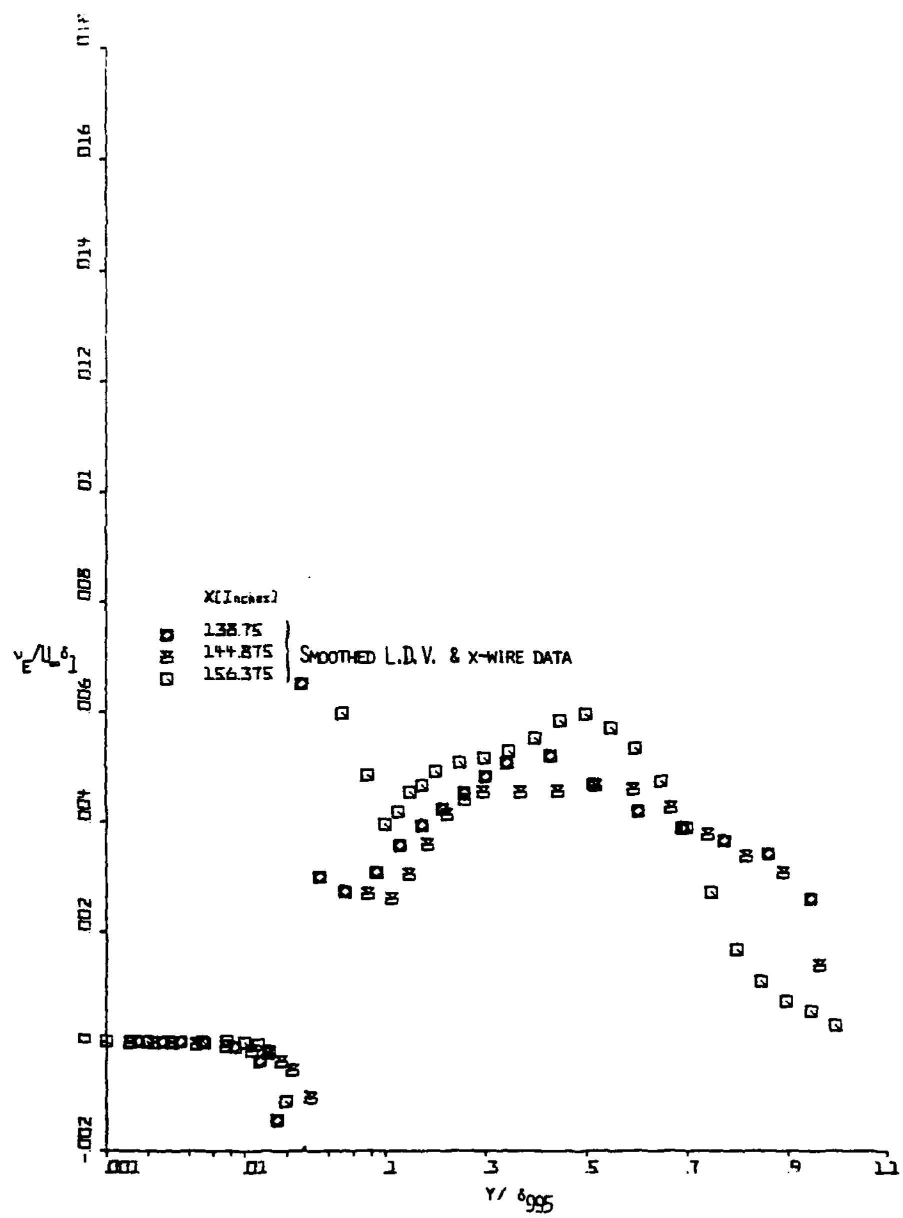

Figure 42(d). Eddy viscosity distributions, $\nu_e/U_\infty\delta_1$ vs. y/δ: downstream of separation.

Table 7: The ratio of $U_\tau \delta_{99}$ for successive locations

Streamwise location in inches	$U_\tau \delta_{99}$ ft.^{2}/sec.	Ratio of $U_\tau \delta_{99}$ for successive stations
86.5	0.255	
		1.066
105.3	0.272	
		1.058
112.4	0.288	
		0.909
118.5	0.262	

is in reasonable agreement with the inner layer data at 86.5 inches.

At first it is a little surprising that there is similarity in the inner layer mixing length distributions and similarity in the inner layer eddy viscosity distributions near separation when δ is used for scaling y. However, as shown in Table 7 the ratio of $U_\tau \delta$ at successive stations is near unity in this region, so $y^+/(y/\delta)$ is the same for successive stations and the profiles near the wall are similar with respect to y^+ as well. In the intermittent separation region, the inner layer similarity disappears and the eddy viscosity decreases with respect to x in the outer layer. In the separated region, ν_e can be defined everywhere except where $\partial U/\partial y = 0$. Eddy viscosity profiles also show some similarity in the outer layer as well as near the wall in the separated region.

For both mixing length and eddy viscosity, the data in the vicinity of separation indicate much lower values in the outer region than for attached boundary layers. As shown below in section V.5, normal stresses effects can be used to explain this behavior.

C. Skewness and flatness factor distributions

Some measurements of skewness and flatness factors of the u and v fluctuations have been done in zero pressure gradient boundary layers and in channel flows by Dumas (1966), Zaric (1972), Kreplin (1973), Antonia (1973) and Ueda and Hinze (1975). Only Sandborn (1959) is known to have made measurements of the flatness factor in an adverse pressure gradient boundary layer flow in the vicinity of separation.

Figures 43 (a) and 44 (a) show a comparison of the present laser anemometer data for F_u and F_v with the zero pressure gradient boundary layer data of Antonia (1973). The good agreement observed between the two sets of data in the logarithmic

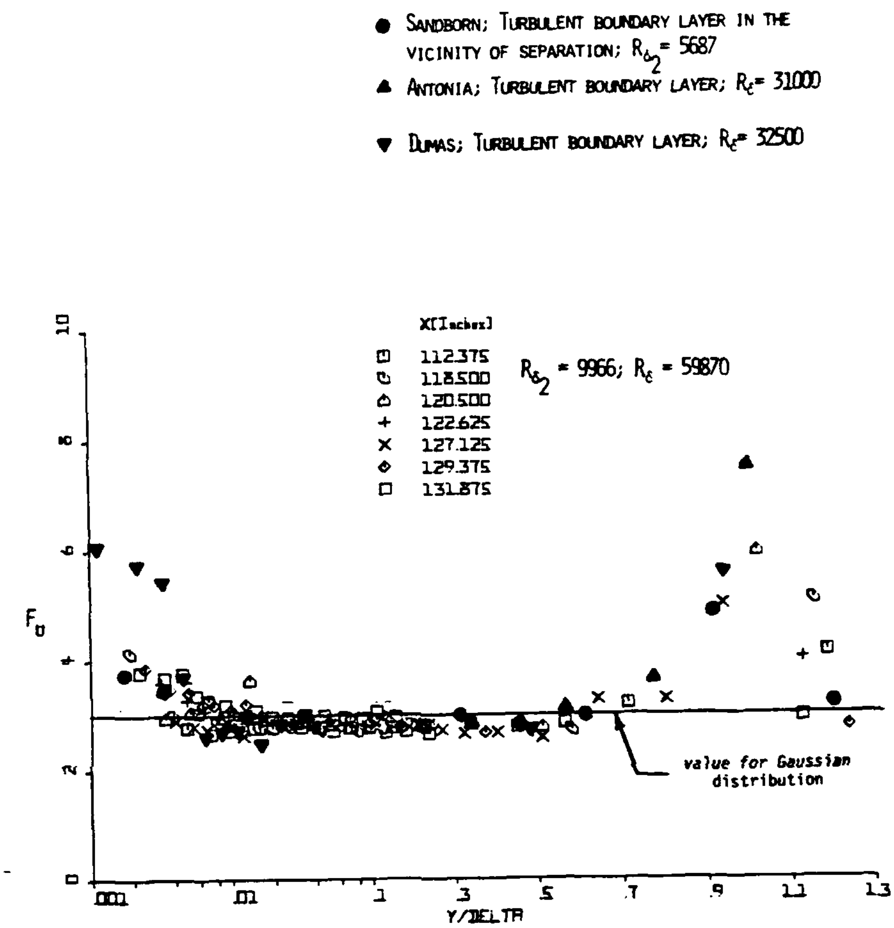

Figure 43(a). Flatness factor F_u profiles: upstream results.

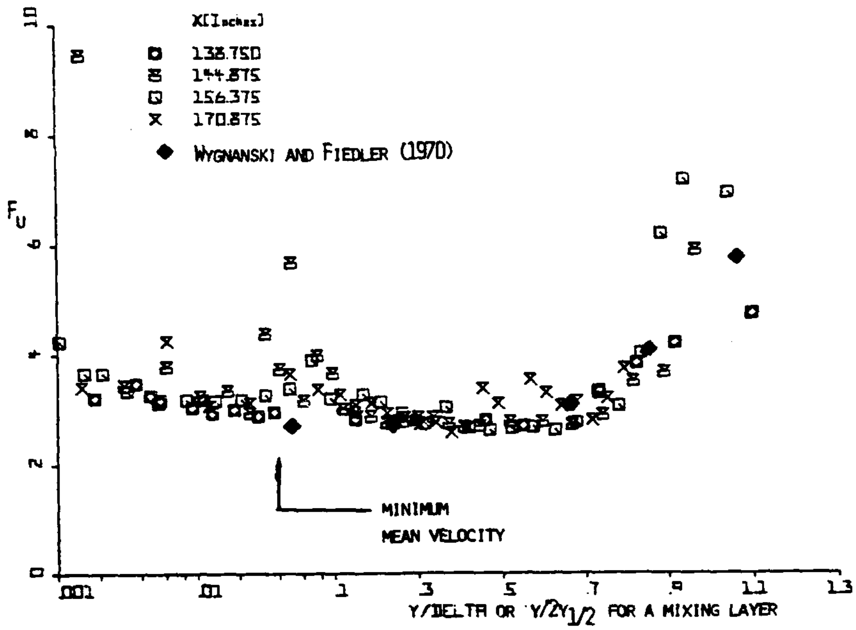

Figure 43(b). Flatness factor F_u profiles: downstream of separation.

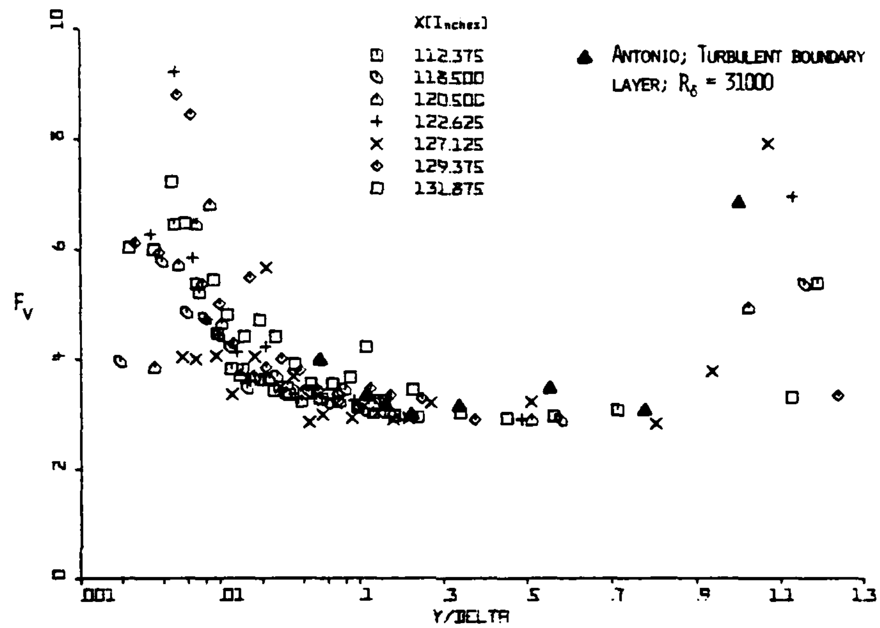

Figure 44(a). Flatness factor F_v profiles: upstream results.

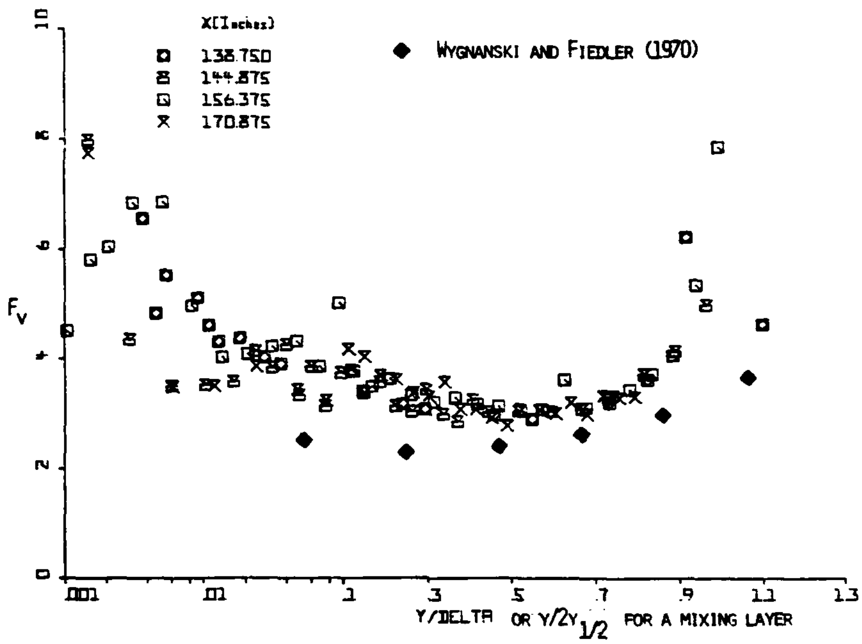

Figure 44(b). Flatness factor F_V profiles: downstream of separation.

region and the outer region indicates that the pressure gradient does not have much effect on F_u and F_v in those regions. Comparison with Figures 43 (b) and 44 (b) for the flow downstream of separation indicates that separation also does not have much effect on F_u and F_v over the shear layer.

However, when plotted against y^+ in Figure 45, the data for F_u upstream of separation indicate an apparent effect of pressure gradient in the region close to the wall, mainly in the buffer layer. In the viscous sublayer for both zero and adverse pressure gradient flows, the flatness factor attains values much higher than the value for a gaussian probability distribution, which is equal to 3. This is possible because the inrush phase of the bursting cycle which brings in high velocity fluid from the outer region results in large amplitude positive u fluctuations and consequently produces a large skirt in the velocity probability distribution. Similarly, near the outer edge of the boundary layer, intermittent large amplitude negative u fluctuations occur as a result of the large eddies driving the fluid from the low velocity regions outwards, which tends to increase the flatness factor. In the buffer layer near a y^+ of 13, the zero pressure gradient flows of Ueda and Hinze, Zaric, and Kreplin all show a dip in the F_u flatness factor distributions and a change in sign in the skewness factor S_u distributions for u as shown in Figure 46. Ueda and Hinze have remarked that this location is where u' attains the maximum value. The present data neither show any such predominant dip in F_u nor sign change of S_u in the buffer layer. Sandborn's (1959) data for F_u in an adverse pressure gradient boundary layer flow show a behavior similar to the present data. The present data for F_u and S_u also show reasonable agreement with those of Dumas (1966), but the significance of this is clouded since the pressure-gradient-flow conditions were not mentioned in his paper.

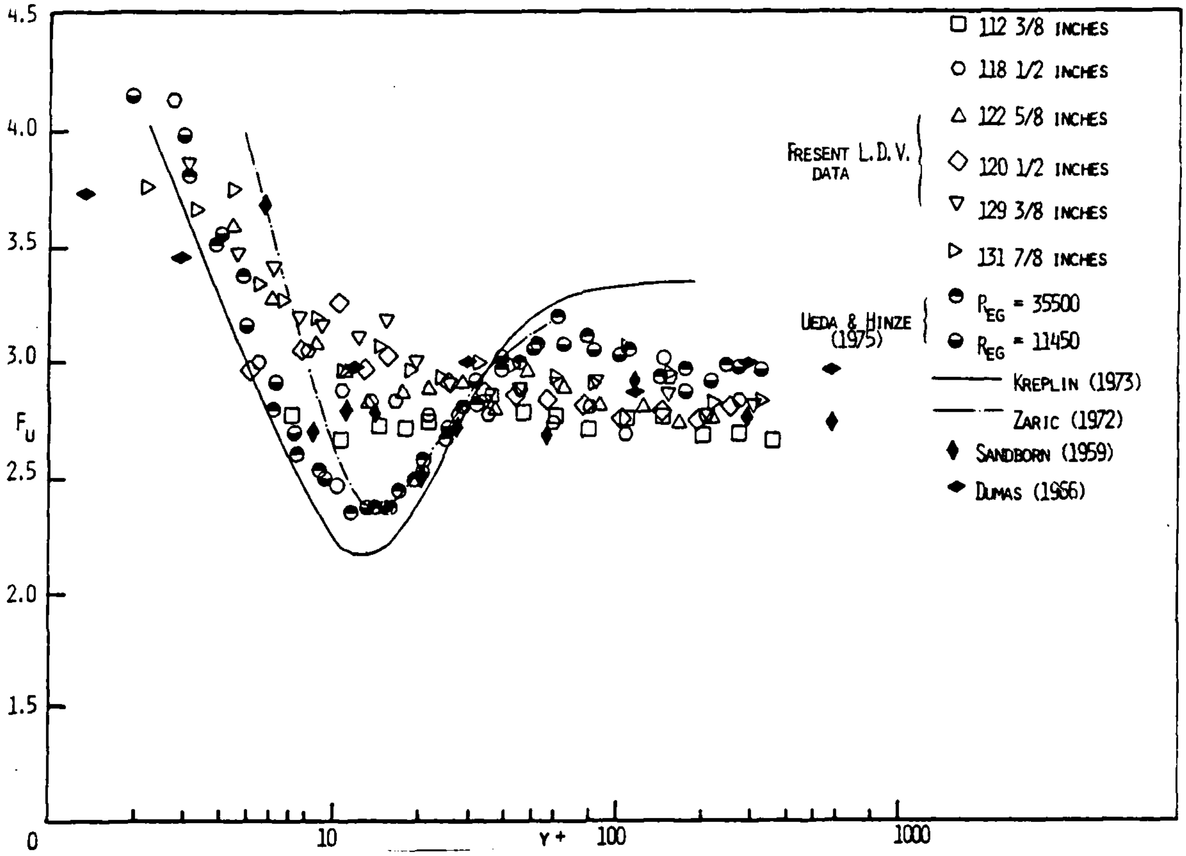

FIGURE 45. F_U VS. Y^+ UPSTREAM OF SEPARATION.

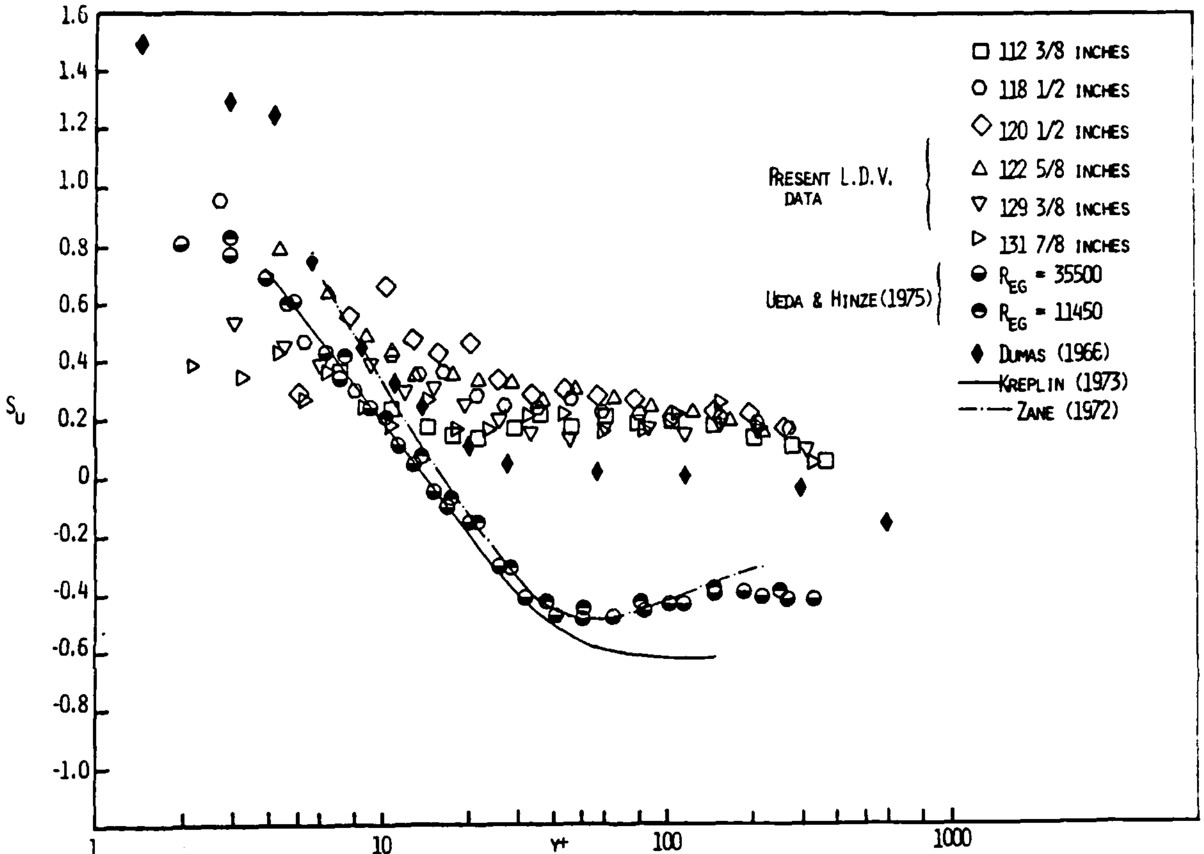

FIGURE 46. SKEWNESS FACTOR S_u VS. Y^+ UPSTREAM OF SEPARATION.

The present data for S_u as shown in Figure 47 (a) indicate a change in sign at a location farther away from the wall ($y/\delta \simeq 0.4$). This location corresponds to the region where the Reynolds shear stress and the turbulent intensities reach their maximum values. The intense momentum exchange in this region results in the lack of occasionally very high or very low fluctuations and as a consequence the probability distribution does not have much skewness. As one moves closer to the wall, the intermittent large amplitude positive u fluctuations tend to make the probability distributions more positively skewed (Eckelmann, 1974) and vice-versa when one moves away from the wall.

The location corresponding to zero skewness for u occurs very close to the wall in zero-pressure-gradient flows because the Reynolds shear stress attains a maximum value in that region. Furthermore, the intense mixing in that region surpresses large amplitude u fluctuations, thus removing the skirt in the positively skewed velocity probability distribution and changing it to a more nearly top-hat shape with a low flatness factor. The same does not happen in adverse pressure gradient flows in the region of maximum shear because the probability distribution in that region is more nearly gaussian with only a slight skewness and with no significant large amplitude fluctuations to be suppressed.

Downstream of separation the skewness S_u is reduced to negative values in the backflow region as shown in Figure 47 (b). A maximum is observed in the vicinity of the minimum mean velocity. As shown in Figure 43 (b), F_u also has a local maximum near this location. The second zero-skewness point is slightly closer to the wall than the location of the maximum shear stress.

The flatness factor distributions for v in Figures 44 (a) and (b) show a

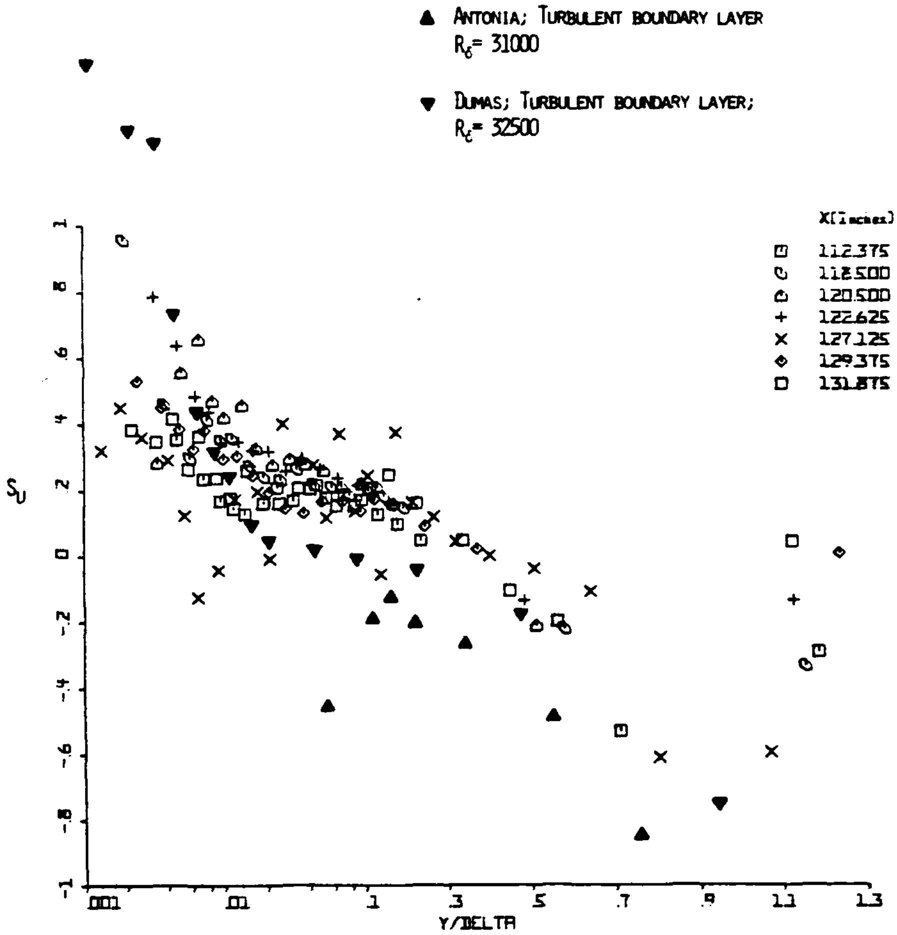

Figure 47(a). Skewness factor S_u vs. y/δ profiles, laser anemometer data: upstream results.

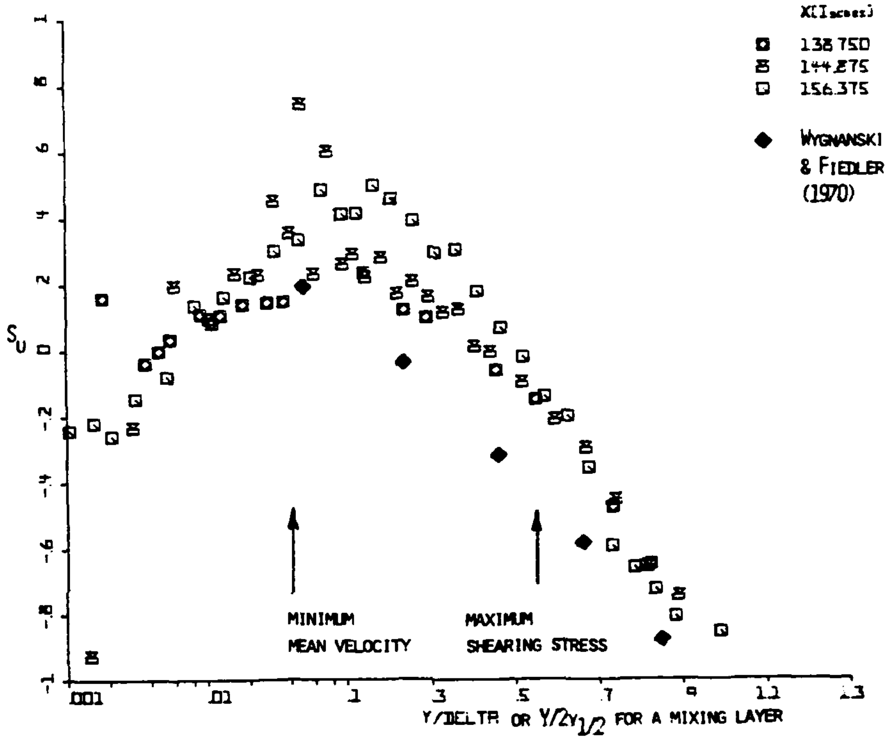

Figure 47(b). Skewness factor S_u vs. y/δ profiles laser anemometer data: results downstream of separation.

trend similar to that of u, the only difference being the reduced width of the flat region. Figures 48 and 49 show that there is a significant variation of S_v along the flow. Only downstream of 112 inches is there profile similarity in the outer region. S_v shown in Figure 49 exhibit a shape approximately opposite in sign to that of S_u, with a large positive skewness factor near the outer edge of the boundary layer, gradually decreasing to negative values towards the wall. This results in the appearance of two zero-skewness points in the distributions of S_v both upstream and downstream of separation. The zero-skewness point which is farther from the wall occurs in the region of maximum shear both upstream and downstream of separation, which indicates that the backflow has no influence on the location of this point as in the case of S_u. Downstream of separation the flatness and skewness factors away from the wall are in qualitative agreement with those of Wygnanski and Fiedler (1970) for a plane mixing layer. This is not surprising since the mean velocity profiles resemble those in mixing layers.

D. Diffusion of turbulence kinetic energy

The diffusion term $\partial/\partial y\ (\overline{pv}/\rho + 1/2\ \overline{q^2 v})$ of the turbulence kinetic energy equation is known to become more important as a turbulent boundary layer approaches separation (Bradshaw, 1967b; Simpson and Collins, 1978). The term $\overline{pv}/\rho$ which represents the diffusion flux due to pressure forces cannot be measured directly using available techniques. Normally, it is estimated by the difference of other measureable terms in the turbulence kinetic energy equation, although experimental uncertainties make the results quite uncertain. Here the turbulence kinetic energy diffusion flux

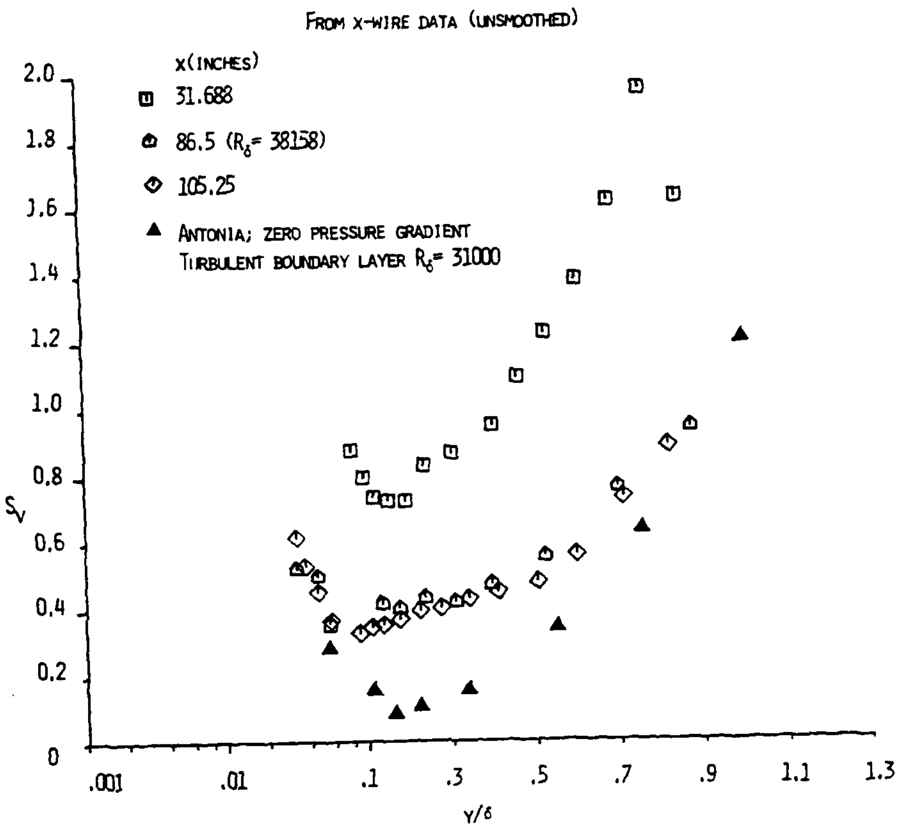

Figure 48. Skewness factor S_v vs. y/δ profiles from cross hot-wire anemometer data.

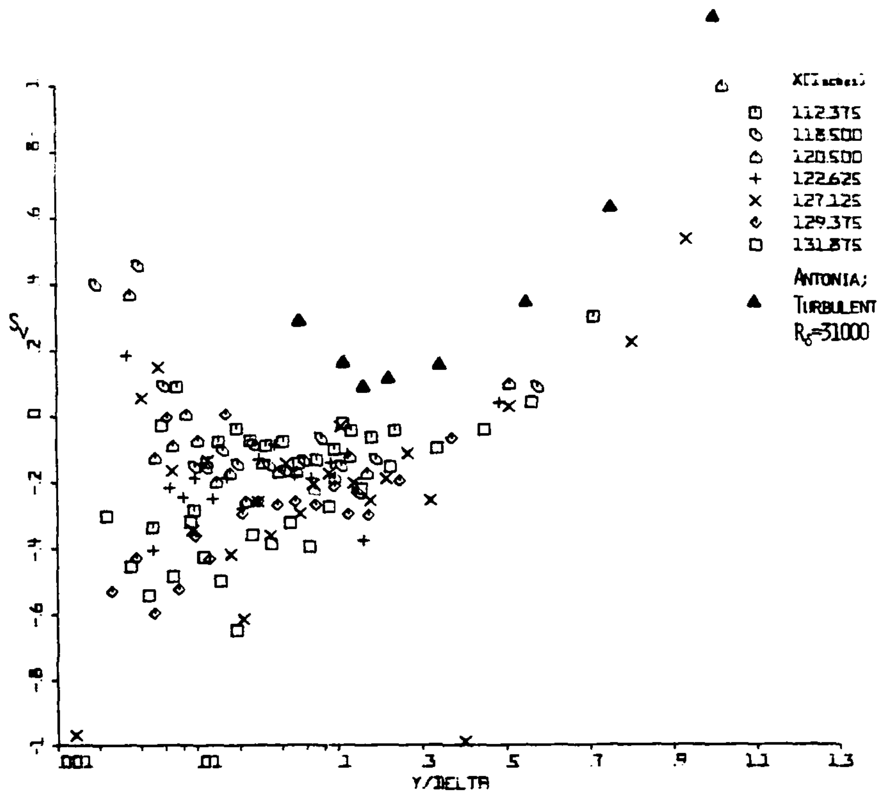

Figure 49(a). Skewness factor S_v vs. y/δ from laser anemometer data: upstream results.

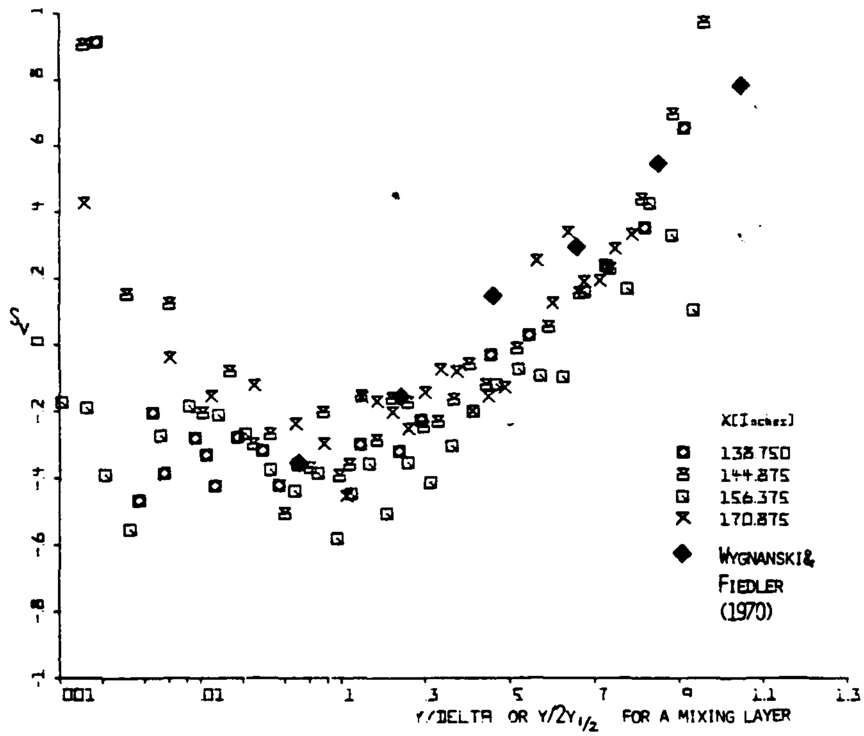

Figure 49(b). Skewness factor S_v vs. y/δ from laser anemometer data: results downstream of separation.

$$1/2\ \overline{q^2 v} = 1/2\ (\overline{u^2 v} + \overline{v^3} + \overline{w^2 v}) \tag{24}$$

was estimated using $\overline{u^2 v}$ and $\overline{v^3}$ cross-wire anemometer measurements and the approximation proposed by Bradshaw (1967b), $\overline{w^2 v} = (\overline{u^2 v} + \overline{v^3})/2$.

Figures 50 (a) and (b) show the present results. The flux of turbulence kinetic energy is positive in the regions where data have been plotted, indicating that the flux is directed away from the wall. For locations downstream of 117.6 inches the data are limited only to the region near the outer edge of the boundary layer. Nearer the wall at these locations the flux is expected to be negative, since most of the turbulence energy production is in the middle of the boundary layer and previous strong adverse pressure gradient data (East and Sawyer, 1979) have this behavior.

East and Sawyer proposed a gradient model based on a mixing length formulation

$$\overline{q^2 v} = 0.4\ \ell \frac{d}{dy} (\overline{q^2})^{3/2} \tag{25}$$

They obtained experimental data for seven equilibrium turbulent boundary layers with $U \sim x^R$ and R approximately equal to 0.4, 0.2, 0, -0.2, -0.4, -0.6, and -0.8. The above model agreed with those data satisfactorily in the outer half of the boundary layer in all cases. Agreement in the inner regions improved for increasingly adverse pressure gradients. Using the mixing length and turbulence kinetic energy distributions obtained from the present equilibrium experiments, the results from this model are shown in Figures 50. Agreement in the outer region is within the uncertainty of the measurements. In the inner region only the general shape of the predictions agree with measurements.

It can be observed from Figures 51 (a) and (b) that the diffusion is small at the upstream stations, becoming appreciable downstream from 117 inches. Farther

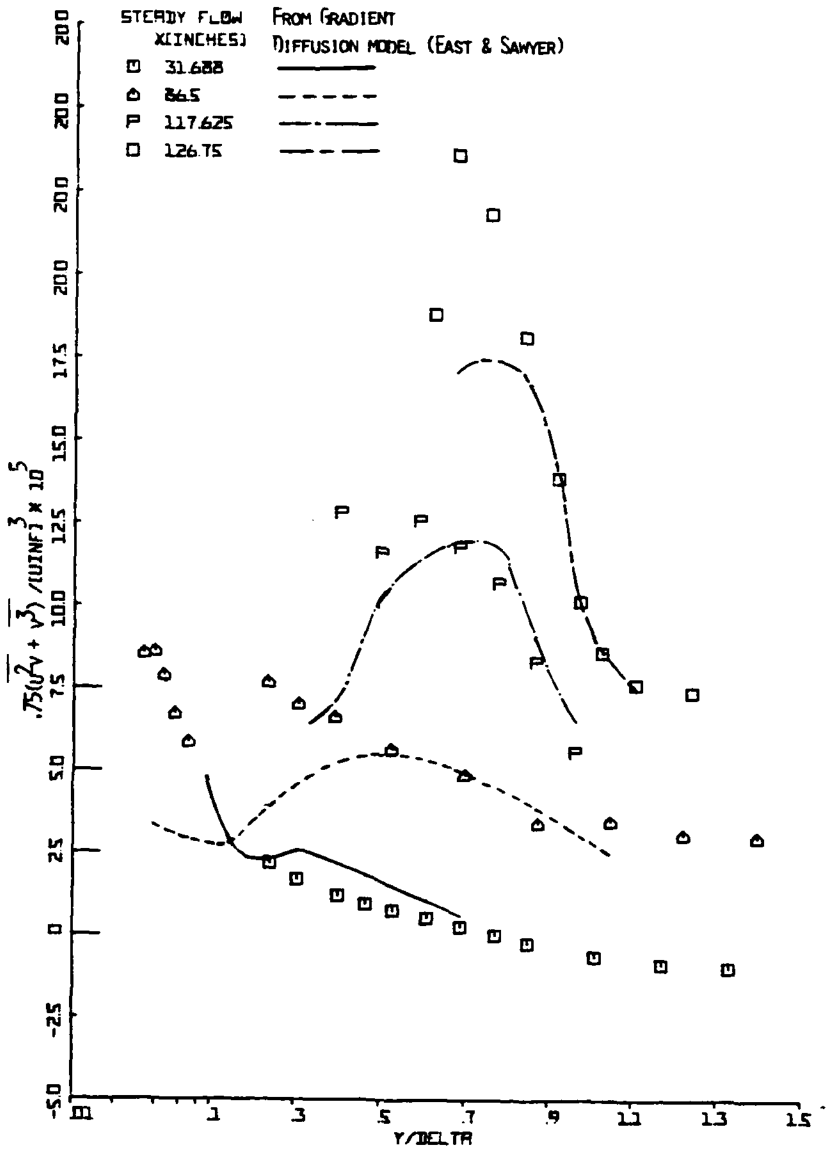

Figure 50(a). Turbulent kinetic energy diffusion flux vs. y/δ - hot-wire anemometer results compared to East and Sawyer's gradient diffusion model: upstream of separation.

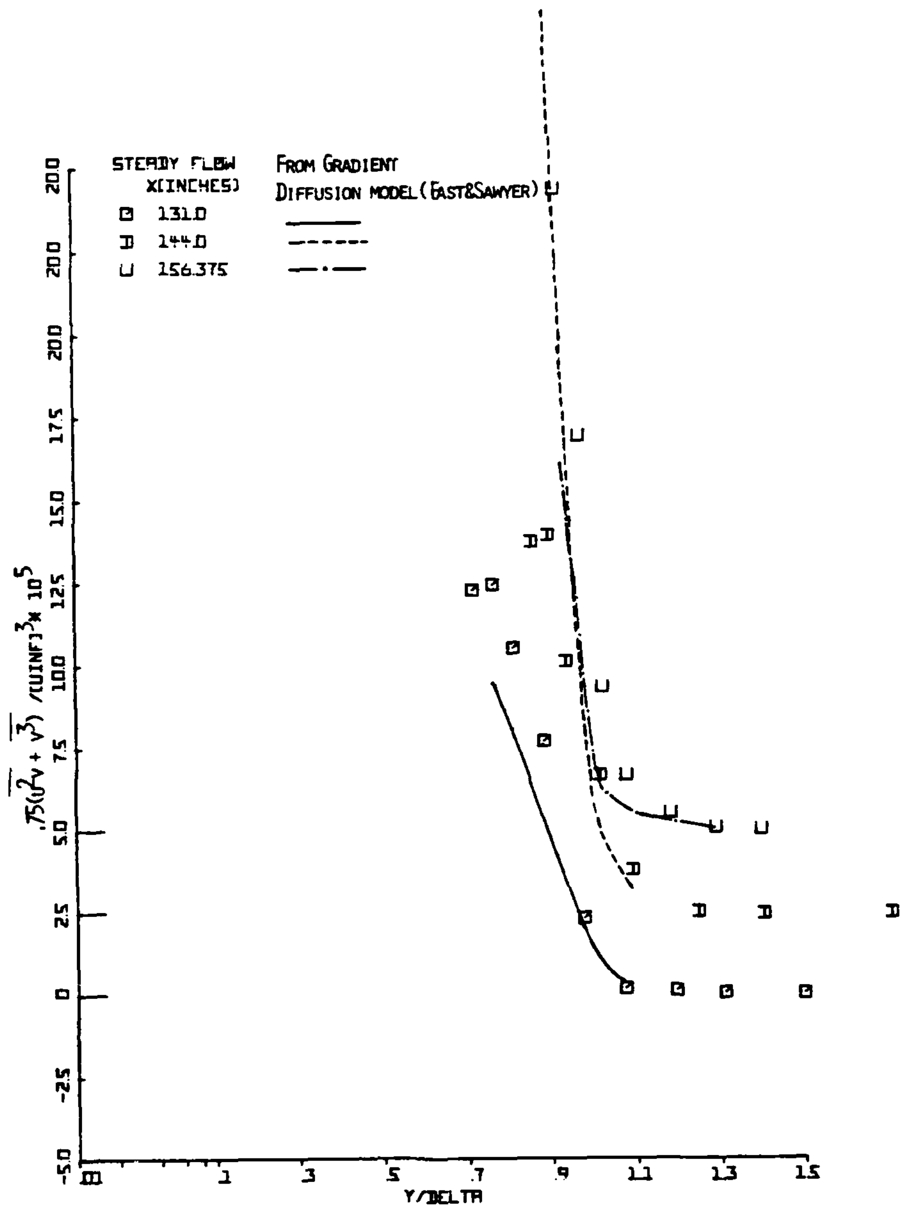

Figure 50(b). Turbulent kinetic energy diffusion flux vs. y/δ - hot-wire anemometer results compared to East and Sawyer's gradient diffusion model: downstream of separation.

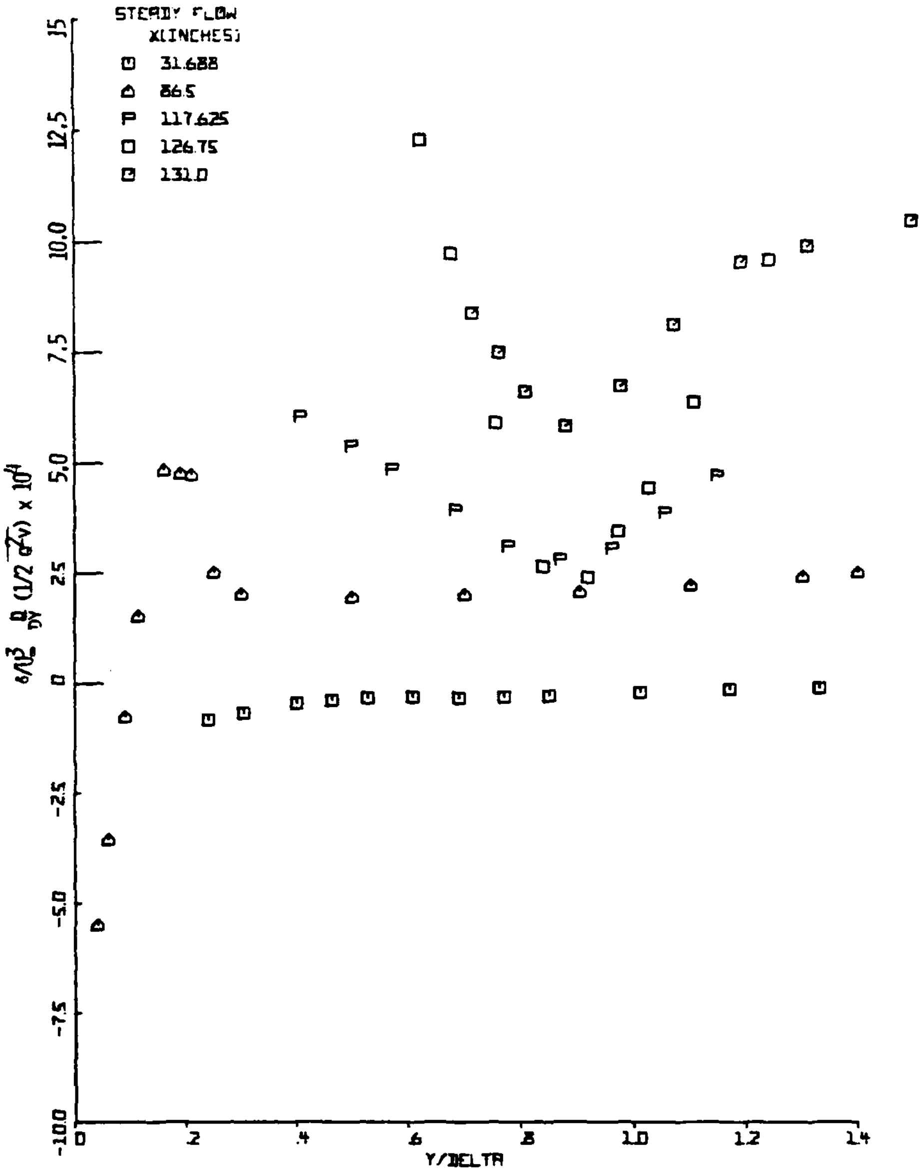

Figure 51(a). Turbulent kinetic energy diffusion vs. y/δ downstream of separation.

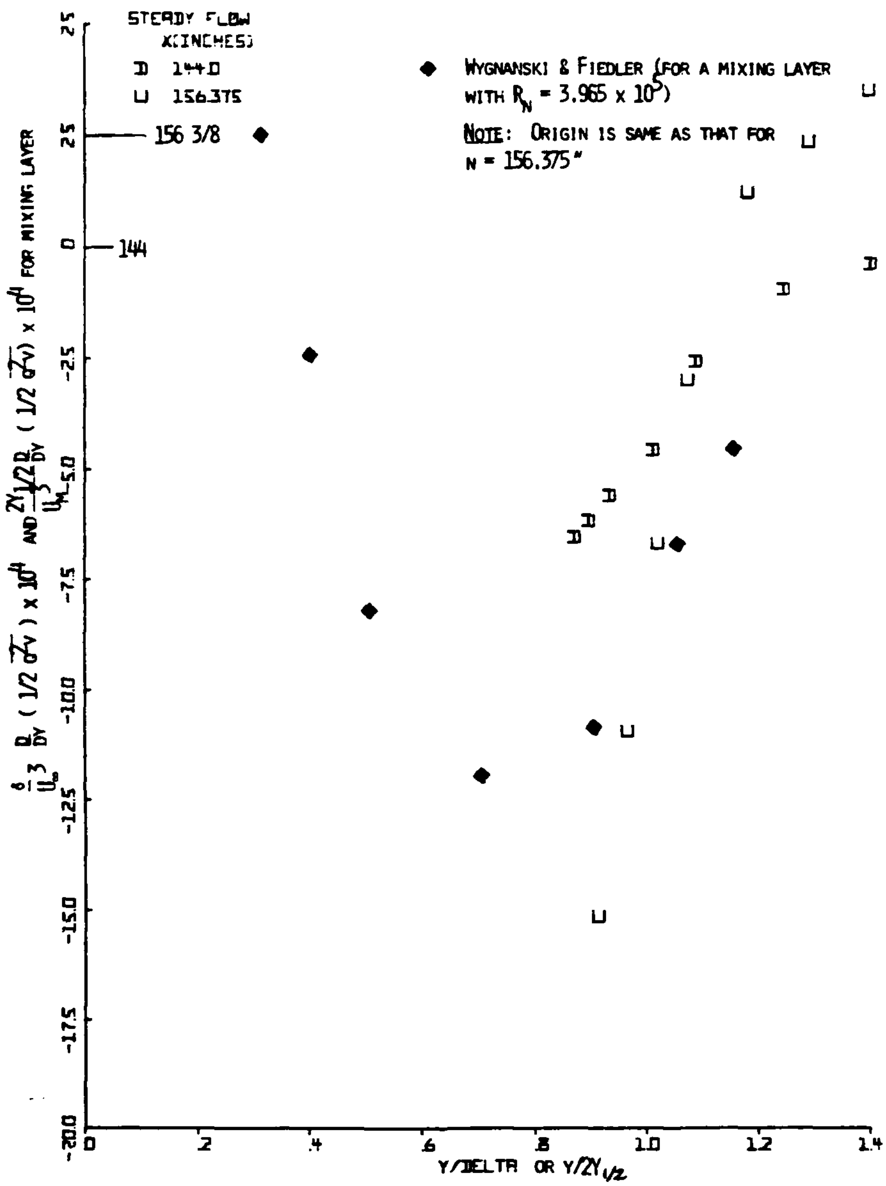

Figure 51(b). Turbulent kinetic energy diffusion vs. y/δ: downstream of separation.

downstream as separation is approached, the diffusion increases continuously. It is interesting to note that such large negative diffusion rates occur on the low velocity side of mixing layers also. This can be seen in Fig. 51 (b) which has the data of Wygnanski and Fiedler (1970) plotted for comparison with the present data at x = 156 3/8 inches. The maximum velocity in the mixing layer U_m and the total shear layer thickness $2y_{1/2}$ were used for nondimensionalizing those data. This similarity in behavior with the mixing layer suggests that the diffusion, which is responsible for the lateral spread of mixing layers, is also responsible for the rapid growth of separated boundary layers. The large gain of energy by diffusion in the outer region and the associated increase in entrainment of the nonturbulent fluid seems to be responsible for the maintenance of the large eddies and the large growth rates of separated boundary layers.

The increase in entrainment rate of free-stream fluid as separation is approached is demonstrated in Figure 52 in terms of the entrainment velocity, V_p, obtained from mean velocity measurements using the relationship

$$V_p = \frac{d}{dx}\left[U_\infty \, (\delta_{0.995} - \delta^*)\right] \tag{26}$$

Upstream of separation these results are in good agreement with Bradshaw's (1967) correlation

$$\frac{V_p}{U_\infty} = 10 \, \frac{\tau_{max}}{\rho U_\infty^2} \tag{27}$$

for boundary layer and mixing layers. Downstream of separation there is poor agreement, in contrast to the good agreement obtained by Simpson et al. (1977) for their separating flow. This might be because of some three-dimensionality which seems to exist in that region.

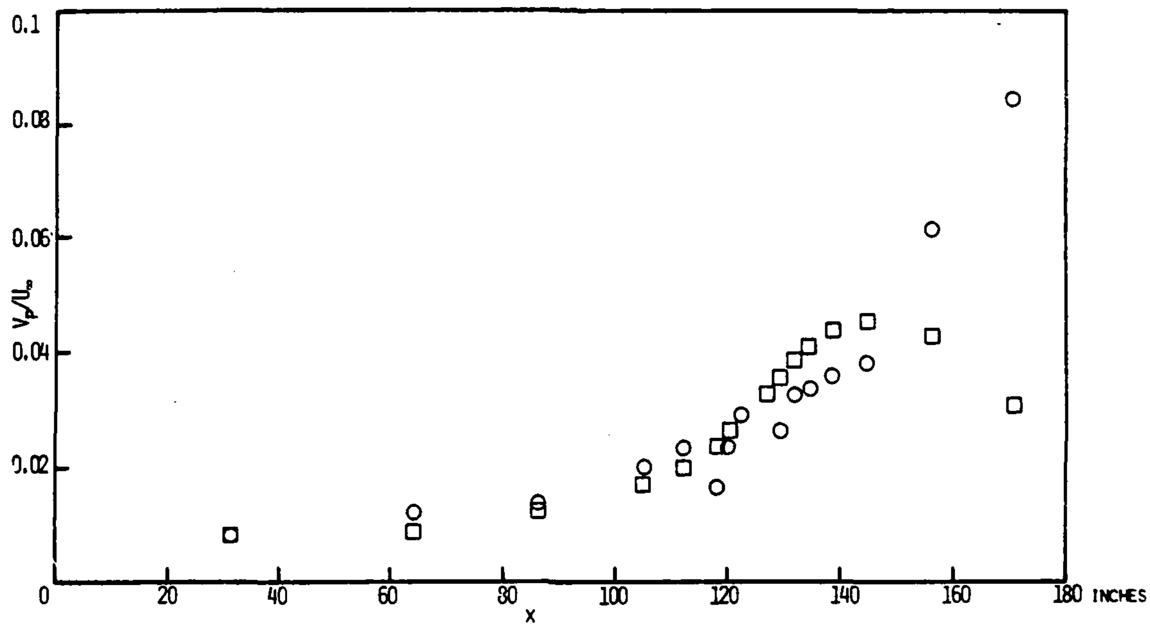

Figure 52. Entrainment velocity V_p/U_∞ vs. X: □ from equation (26); ○ from equation (27).

Figure 53 shows the distribution of the diffusion function $G/(\tau_{max}/\rho)^{\frac{1}{2}}$, which was defined by Bradshaw (1967a) to relate the turbulence kinetic energy diffusion to the turbulent shear stress.

$$G = \frac{(\overline{pv}/\rho + \frac{1}{2}\overline{q^2v})}{(\tau/\rho)(\tau_{max}/\rho)^{\frac{1}{2}}} \qquad (28)$$

The diffusion function used by Bradshaw and that computed from the data of East and Sawyer (1979) are also shown. Although there are large differences up to half of the boundary layer thickness, the present data blend in with their data in the outer region. When compared with Bradshaw's diffusion function, the differences are larger and there is no region of agreement of all. The diffusion function given by Bradshaw was derived from the zero pressure gradient boundary layer data of Klebanoff (1955). These results indicate that the diffusion function is dependent upon pressure gradient conditions.

V.4 Momentum and Turbulence Energy Balances

In order to further understand the effect of separation on the transport of momentum and turbulence kinetic energy, terms of the governing equations were obtained using the measured quantities described above. The x-direction and y-direction momentum equations are, respectively

$$U\frac{\partial U}{\partial x} + V\frac{\partial U}{\partial y} = \frac{-1}{\rho}\frac{\partial p}{\partial x} + \frac{\partial(-\overline{uv})}{\partial y} - \frac{\partial\overline{u^2}}{\partial x} \qquad (29)$$

$$U\frac{\partial V}{\partial x} + V\frac{\partial V}{\partial y} = \frac{-1}{\rho}\frac{\partial p}{\partial y} + \frac{\partial(-\overline{uv})}{\partial x} - \frac{\partial\overline{v^2}}{\partial y} \qquad (30)$$

For each equation the terms on the left side are inertia or convective terms while the terms on the right side describe the pressure gradient, the shearing stress gradient, and the normal stress gradient, respectively. The turbulence energy

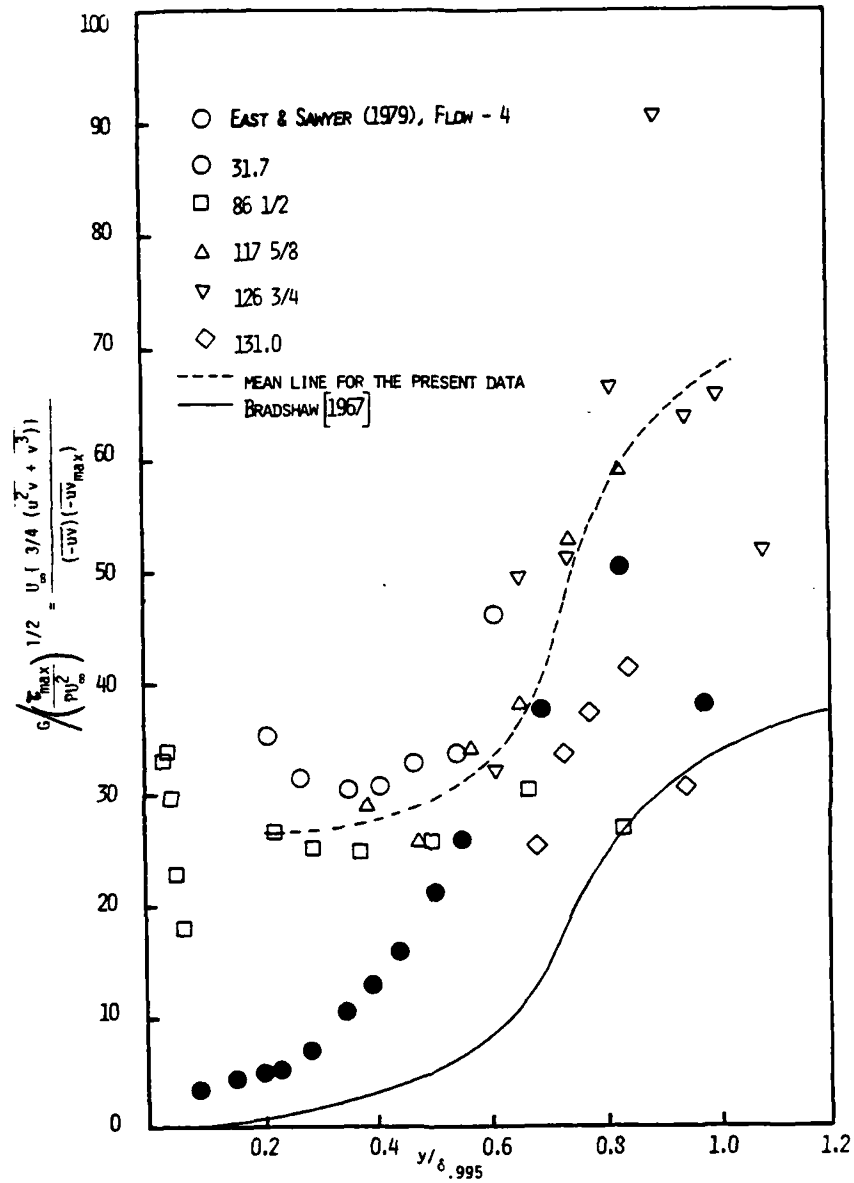

Figure 53. Bradshaw's (1967) diffusion parameter vs. $y/\delta_{.995}$ for several sets of data.

equation is

$$\frac{U}{2}\frac{\partial \overline{q^2}}{\partial x} + \frac{V}{2}\frac{\partial \overline{q^2}}{\partial y} = \frac{-\partial}{\partial y}\left(\overline{v\left(\frac{p}{\rho} + \frac{q^2}{2}\right)}\right) - \overline{uv}\,\frac{\partial U}{\partial y} - (\overline{u^2} - \overline{v^2})\,\frac{\partial U}{\partial x} + \varepsilon \qquad (31)$$

The terms on the left side are advection terms while the terms on the right side describe turbulent diffusion, turbulent shear stress production, normal stresses production, and dissipation, respectively. Dissipation was not measured. In all three equations the viscous terms have been neglected since they are much smaller than the other terms.

An estimate of uncertainties of all the significant terms for a few typical points across the boundary layer are given in Table 8 for 118.5 inches and 131.875 inches. Very near the wall the uncertainties are high, but beyond $y/\delta \simeq 0.02$, the uncertainties of most of the dominant terms are less than 30% - 40% at many points. In general, the terms involving derivatives with respect to y have less uncertainty as compared to those involving derivatives with respect to x, since the latter terms are much smaller and were computed from data acquired on different days. Hence each data point used to determine x derivatives corresponded to slightly different experimental conditions.

An exception to this is the inertia terms of the x-direction momentum equation. In this case the two-dimensional continuity equation can be used to obtain a single term involving only a y derivative of a given velocity profile.

$$U\,\frac{\partial U}{\partial x} + V\,\frac{\partial U}{\partial y} = -U^2\,\frac{\partial (V/U)}{\partial y}$$

This expression was used only when U was much larger than V, since the uncertainty in V/U becomes large as U approaches zero. The relative uncertainty in this term is large in the outer region because y-direction gradients are small.

Estimate of Uncertainties for the terms of the Momentum and Energy equations.

Table 8a. Terms involving derivatives with respect to x at x = 118.5 inches.

y/δ	0.00385		0.0192		0.192		0.962	
	Uncertainty ($\pm$)	Absolute Value	Uncertainty ($\pm$)	Absolute Value	Uncertainty ($\pm$)	Absolute Value	Uncertainty	Absolute Value
$-10^2 x \frac{\delta}{U_\infty^2} \frac{\partial u'^2}{\partial x}$	0.02	0.149	0.05	0.075	0.02	0.024	0	-0.138
$-10^2 x \frac{\delta}{U_\infty^2} \frac{1}{\rho} \frac{\partial P}{\partial x}$	30.36	-5.04	3.2	-5.66	1.7	-2.14	4.68	-3.73
$-10^2 x \frac{\delta}{U_\infty^2} \frac{\partial (u'^2 - v'^2)}{\partial x}$	0	0.148	0	0.057	0.01	0.012	0	-0.084
$-10^2 x \frac{1}{\rho} \frac{\partial (P_\infty - \rho v'^2)}{\partial x}$	0	-1.86	0	-1.87	0.02	-1.87	0	-1.8
$10^2 x \frac{\delta}{U_\infty^2} U^2 \frac{\partial (V/U)}{\partial x}$	0.007	0.002	0.013	-0.004	0.35	0.035	0.57	0.968
$-10^2 x \frac{\delta}{U_\infty^2} \frac{1}{\rho} \frac{\partial P}{\partial y}$	4.9	6.42	1.01	4.28	0.28	0.55	0.08	-1.42
$10^3 x \frac{\delta}{U_\infty^3} \frac{U}{2} \frac{\partial (u'^2 + v'^2)}{\partial x}$	0.034	-0.073	0.112	-0.109	0.045	-0.071	0.855	0.937
$10^3 x \frac{\delta}{U_\infty^3} (u'^2 - v'^2) \frac{\partial U}{\partial x}$	0.01	-0.041	0	-0.276	0.01	-0.426	0.03	-0.044

Estimate of Uncertainties for the terms of the Momentum and Energy equations.

Table 8b. Terms involving derivatives with respect to y at x= 118.5 inches.

y/δ	0.0038		0.02		0.2		0.8	
	Uncertainty ($\pm$)	Absolute Value	Uncertainty ($\pm$)	Absolute Value	Uncertainty ($\pm$)	Absolute Value	Uncertainty	Absolute Value
$10^2 x \frac{\delta}{U_\infty^2} \frac{\partial(\overline{-uv})}{\partial y}$	1.261	6.28	0.276	0.77	0.118	0.32	0.26	-0.34
$10^2 x \frac{\delta}{U_\infty^2} U^2 \frac{\partial(V/U)}{\partial y}$	26.445	0.52	3.685	4.95	1.746	1.76	3.5	3.98
$10^2 x \frac{\delta}{U_\infty^2} \nu \frac{\partial^2 U}{\partial y^2}$	2.914	-2.15	0.031	-0.32	0.001	0	0.001	0
$10^2 x \frac{\delta}{U_\infty^2} \nu \frac{\partial^2 V}{\partial y^2}$	0.375	0	0	0	0.001	0.02	0	0
$-10^2 x \frac{\delta}{U_\infty^2} \frac{\partial v'^2}{\partial y}$	2.205	-6.42	1.041	-4.18	0.29	-0.56	0.13	0.52
$-10^3 x \frac{\delta}{U_\infty^3} \left(\overline{-uv} \frac{\partial U}{\partial y}\right)$	3.597	-5.1	0.302	-2.42	0.464	-1.29	0.51	-0.42
$10^3 x \frac{\delta}{U_\infty^3} \frac{V}{2} \frac{\partial(u'^2+v'^2)}{\partial y}$	2.495	0.43	0.072	0.19	0.08	0.2	0.455	-1.33

Estimate of Uncertainties for the terms of the Momentum and Energy equations.

Table 8c. Terms involving derivatives with respect to x at x = 131.875 inches.

y/δ	0.0022		0.019		0.112		0.562	
	Uncertainty	Absolute Value	Uncertainty (±)	Absolute Value	Uncertainty (±)	Absolute Value	Uncertainty	Absolute Value
$-10^2 x \frac{\delta}{U_\infty^2} \frac{\partial u'^2}{\partial x}$	0.2[illegible]	-0.061	0.038	0	0.15	0.06	0.09	-0.599
$-10^2 x \frac{\delta}{U_\infty^2} \frac{1}{\rho} \frac{\partial P}{\partial x}$	1.23	5.71	0	-3.02	0.34	-1.75	8.84	1.06
$-10^2 x \frac{\delta}{U_\infty^2} \frac{\partial (u'^2 - v'^2)}{\partial x}$	0.2	-0.059	0.02	0.01	0.19	0.056	0	-0.451
$-10^2 x \frac{1}{\rho} \frac{\partial (P_\infty - \rho v'^2)}{\partial x}$	0.02	-1.98	0.01	-1.98	0.04	-1.98	0.09	-1.83
$10^2 x \frac{\delta}{U_\infty^2} U^2 \frac{\partial (V/U)}{\partial x}$	0	0	0.004	0	0.3	-0.172	0.26	0.671
$-10^2 x \frac{\delta}{U_\infty^2} \frac{1}{\rho} \frac{\partial P}{\partial y}$	0.53	4.05	0.77	4.62	0.61	2.0	0.07	-1.42
$10^3 x \frac{\delta}{U_\infty^3} \frac{U}{2} \frac{\partial (u'^2 + v'^2)}{\partial x}$	0.003	0.003	0.013	0.05	0.035	-0.04	0.55	2.29
$10^3 x \frac{\delta}{U_\infty^3} (u'^2 - v'^2) \frac{\partial U}{\partial x}$	0.045	-0.039	0.09	-0.32	0.05	-0.652	0.1	-1.9

Estimate of Uncertainties for the terms of the Momentum and Energy equations.

Table 8d. Terms involving derivatives with respect to y at x = 131.875 inches.

y/δ	0.0022		0.02		0.2		0.8	
	Uncertainty	Absolute Value	Uncertainty	Absolute Value	Uncertainty	Absolute Value	Uncertainty	Absolute Value
$10^2 \times \frac{\delta}{U_\infty^2} \frac{\partial(\overline{-uv})}{\partial y}$	5.598	-4.62	0.434	2.54	0.039	0.69	0.015	-0.52
$10^2 \times \frac{\delta}{U_\infty^2} U^2 \frac{\partial(V/U)}{\partial y}$	1.158	0	0.108	0.44	0.119	0.08	0.35	0.7
$10^2 \times \frac{\delta}{U_\infty^2} \nu \frac{\partial^2 U}{\partial y^2}$	2.843	-1.07	0.066	-0.05	0.001	0	0.002	0
$10^2 \times \frac{\delta}{U_\infty^2} \nu \frac{\partial^2 V}{\partial y^2}$	0.706	0	0.003	0	0	0	0	0.3
$-10^2 \times \frac{\delta}{U_\infty^2} \frac{\partial \overline{v'^2}}{\partial y}$	1.218	-4.05	0.841	-4.4	-0.208	-1.22	0.363	1.2
$-10^3 \times \frac{\delta}{U_\infty^3} \left(\overline{-uv} \frac{\partial U}{\partial y}\right)$	1.66	-2.38	0.184	-0.54	0.854	-2.38	0.68	-0.71
$10^3 \times \frac{\delta}{U_\infty^3} \frac{\nu}{2} \frac{\partial(\overline{u'^2}+\overline{v'^2})}{\partial y}$	1.675	0	0.091	0.05	0.09	0.66	0.62	-3.02

On the whole, even though the uncertainties are large it is still possible to arrive at certain conclusions regarding the relative importance of the various terms in the momentum and turbulence energy equations as the boundary layer passes through separation.

Although the momentum and energy balances were examined at a number of stations, the results are presented here for three representative stations only. They correspond to a location upstream of separation (118.5 inches), a location in the intermittent separation region (131 7/8 inches), and one in the fully-separated region (156 3/8 inches). Figures 54 and 55 show the distributions of the various non-dimensional terms of the momentum equations and Figure 57 represent the terms of the energy equation. The locations of the maximum shear stress $-\overline{uv}$ and the maximum $(u'^2 + v'^2)$ are shown on all the plots.

Figure 55 indicates that the only important terms in the equation for momentum transport in the y-direction are the pressure gradient and the normal stress terms. This is true both upstream and downstream of separation and leads to the following simplification of eqn. (30):

$$\frac{-1}{\rho}\frac{\partial P}{\partial y} = \frac{\partial v'^2}{\partial y}$$

Upon integration it becomes $P(x,y) = P_\infty - \rho v'^2$. Differentiating this equation with respect to x produces

$$\frac{-1}{\rho}\frac{\partial P}{\partial x} = \frac{-1}{\rho}\frac{\partial P_\infty}{\partial x} + \frac{\partial v'^2}{\partial y} \qquad (32)$$

The pressure gradient $\frac{\partial P}{\partial x}$ evaluated using eqn. (32) is also plotted in Figure 54. A first look at Figure 54 indicates large discrepancies between $\frac{\partial P}{\partial x}$ computed using eqns. (29) and (32). However, in view of the uncertainties of $\partial P/\partial x$ derived from

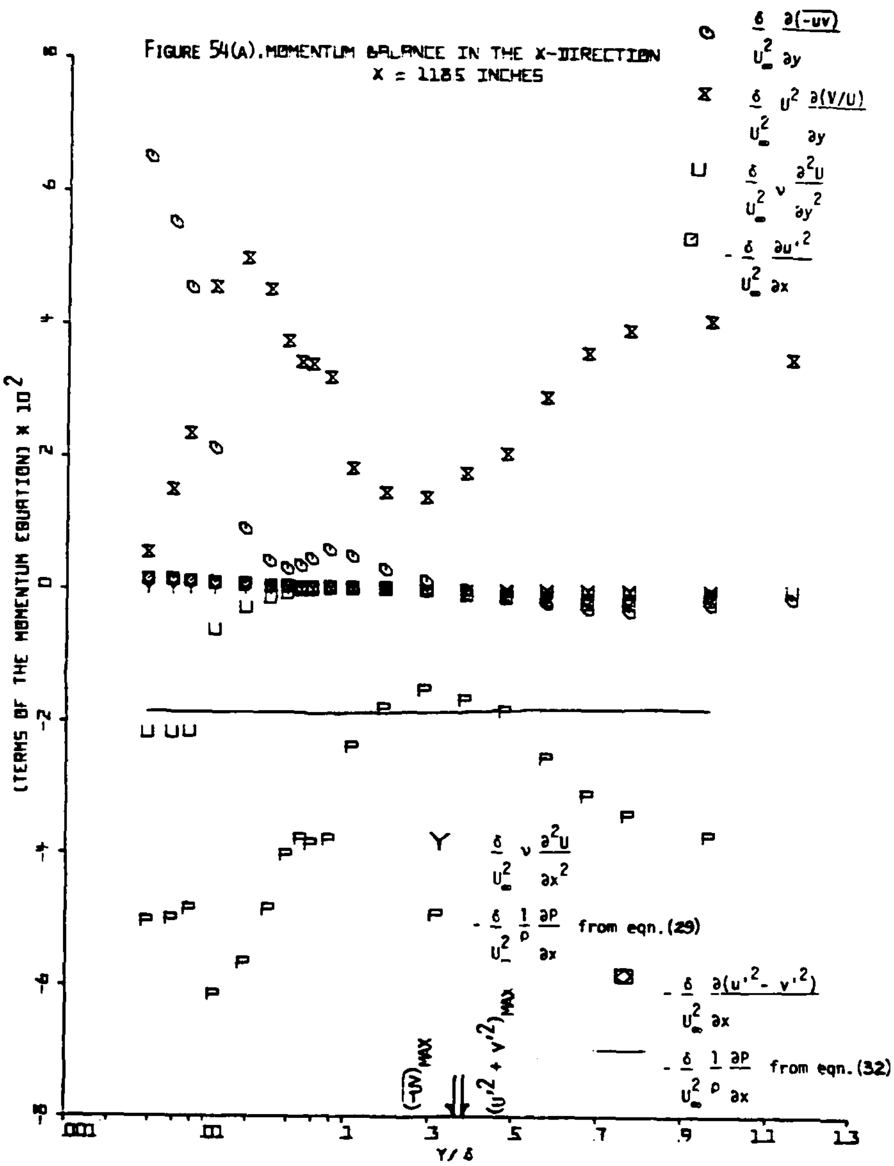
FIGURE 54(A). MOMENTUM BALANCE IN THE X-DIRECTION
X = 1185 INCHES
(TERMS OF THE MOMENTUM EQUATION) X 10^2
Y/δ
from eqn.(29)
from eqn.(32)

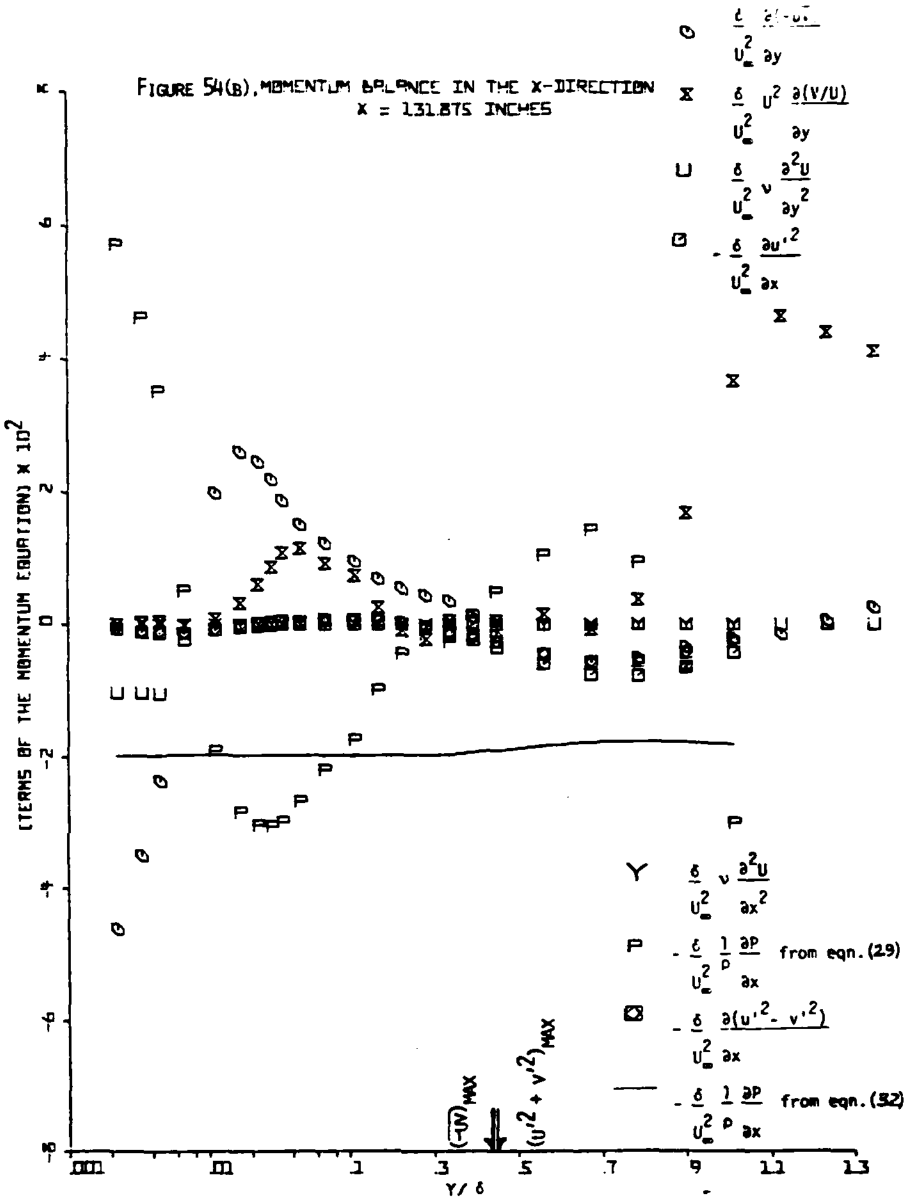

FIGURE 54(B). MOMENTUM BALANCE IN THE X-DIRECTION
X = 131.875 INCHES
(TERMS OF THE MOMENTUM EQUATION) × 10²
Y/δ
from eqn. (29)
from eqn. (52)

FIGURE 54(c) MOMENTUM BALANCE IN THE X-DIRECTION
X = 156.375 INCHES

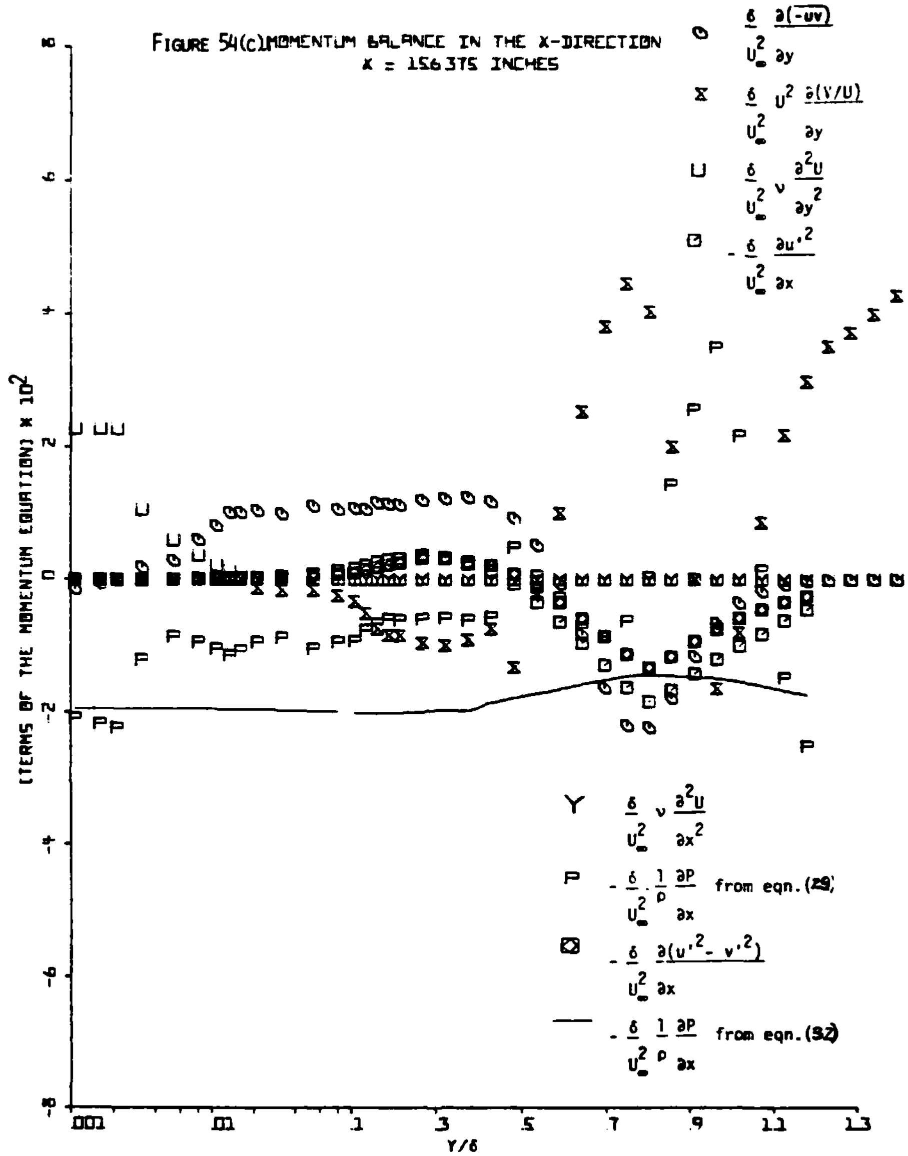

FIGURE 55(A). MOMENTUM BALANCE IN THE Y-DIRECTION
X = 118.5 INCHES

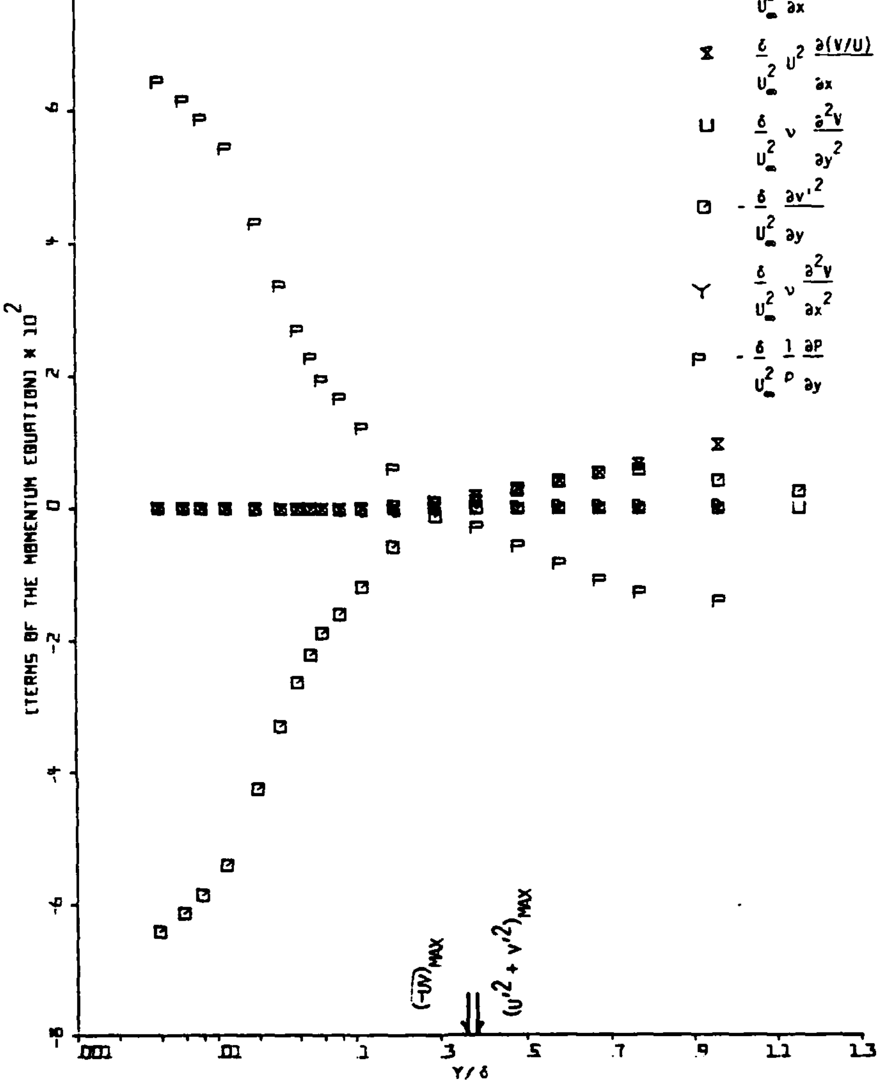

FIGURE 55(B).

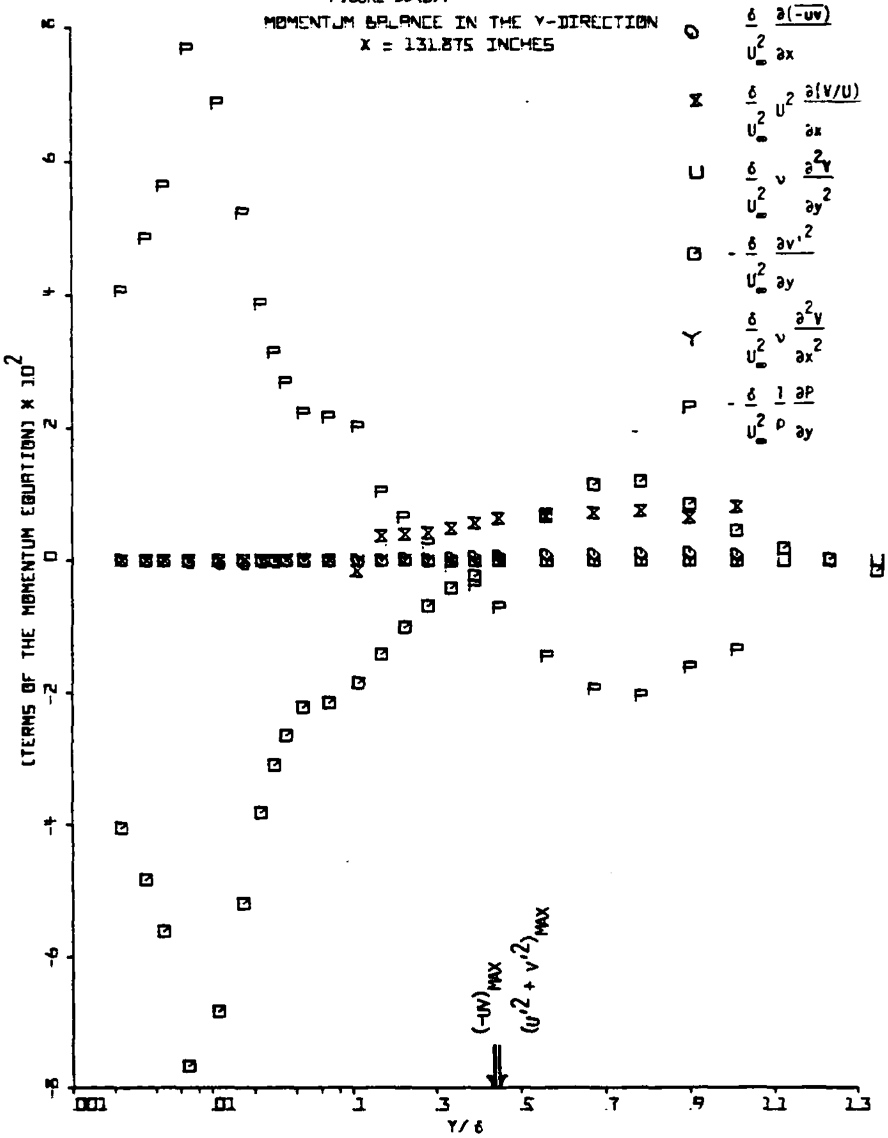
MOMENTUM BALANCE IN THE Y-DIRECTION
X = 131.875 INCHES
$\frac{\delta}{U_\infty^2}\frac{\partial(\overline{-uv})}{\partial x}$
$\frac{\delta}{U_\infty^2}U^2\frac{\partial(V/U)}{\partial x}$
$\frac{\delta}{U_\infty^2}\nu\frac{\partial^2 V}{\partial y^2}$
$-\frac{\delta}{U_\infty^2}\frac{\partial \overline{v'^2}}{\partial y}$
$\frac{\delta}{U_\infty^2}\nu\frac{\partial^2 V}{\partial x^2}$
$-\frac{\delta}{U_\infty^2}\frac{1}{\rho}\frac{\partial P}{\partial y}$
(TERMS OF THE MOMENTUM EQUATION) X 10^2
Y/ δ
$(\overline{-uv})_{MAX}$
$(\overline{u'^2}+\overline{v'^2})_{MAX}$

FIGURE 55(c).

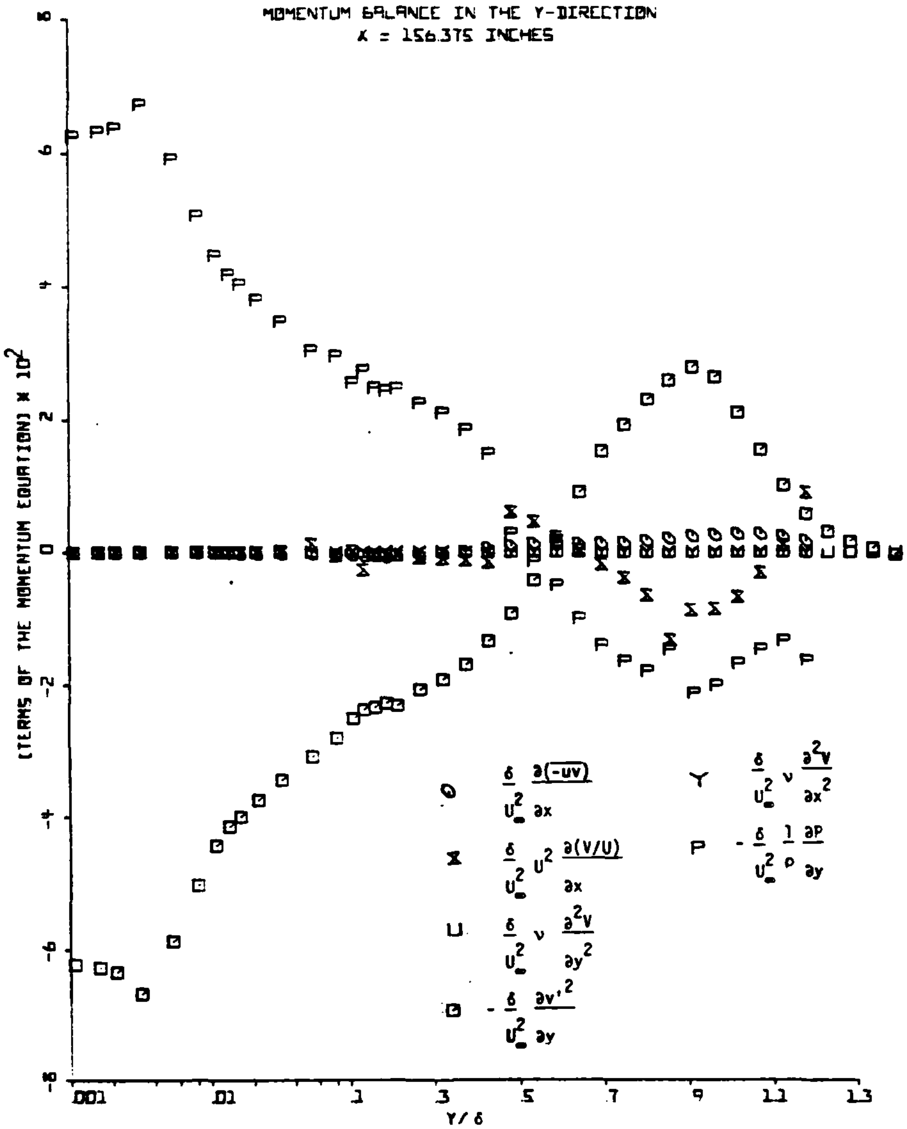

MOMENTUM BALANCE IN THE Y-DIRECTION
X = 156.375 INCHES
(TERMS OF THE MOMENTUM EQUATION) X 10^2
8
6
4
2
0
-2
-4
-6
-8
.001
.01
.1
.3
.5
.7
.9
1.1
1.3
Y/δ
$\frac{\delta}{U_\infty^2}\frac{\partial(-uv)}{\partial x}$
$\frac{\delta}{U_\infty^2}U^2\frac{\partial(V/U)}{\partial x}$
$\frac{\delta}{U_\infty^2}\nu\frac{\partial^2 V}{\partial y^2}$
$-\frac{\delta}{U_\infty^2}\frac{\partial v'^2}{\partial y}$
$\frac{\delta}{U_\infty^2}\nu\frac{\partial^2 V}{\partial x^2}$
$-\frac{\delta}{U_\infty^2}\frac{1}{\rho}\frac{\partial P}{\partial y}$

eqn. (29), the results are in agreements within these uncertainties.

A comparison of Figure 54 indicates that in the separated region the convective terms become unimportant in the inner layer. The momentum transfer due to shear mainly balances the x-direction pressure gradient. In the outer region in addition to the important convective terms, the normal stresses term becomes important as separation is approached, as has already been shown by Simpson et al. (1977). The normal stresses play an important role in the vicinity of the maximum shear stress. At 118 inches, the normal stresses term is still quite small. The momentum balance at 112 inches shows that the normal stresses term is more important. Its importance increases progressively downstream as can be seem from Figures 54 (b) and (c), which show that this term contributes up to half of the momentum transport in the outer region. This is shown more clearly in Figures 56 (a) and (b) by the distributions of the ratio of the normal stresses term to the shear stress term. However, due to uncertainties in the gradients the uncertainty of these results in the outer region is large, as shown in Table 5. Thus the inner layer in the separated region could be modeled by neglecting the convective terms while in the outer layer the additional effect of the normal stresses must be included.

Figures 57 show the importance of the normal stresses turbulence energy production from just upstream of intermittent separation to far downstream. The results for the Bradshaw (1967) flow are in qualitative agreement with the data shown in Figure 57 (a). Figures 58 (a) and (b) show the ratio of the normal stresses production to the shear production for the several locations in the vicinity of separation. As indicated by the present data and the data of Simpson et al. (1977) and Schubauer and Klebanoff (1950), the normal stresses

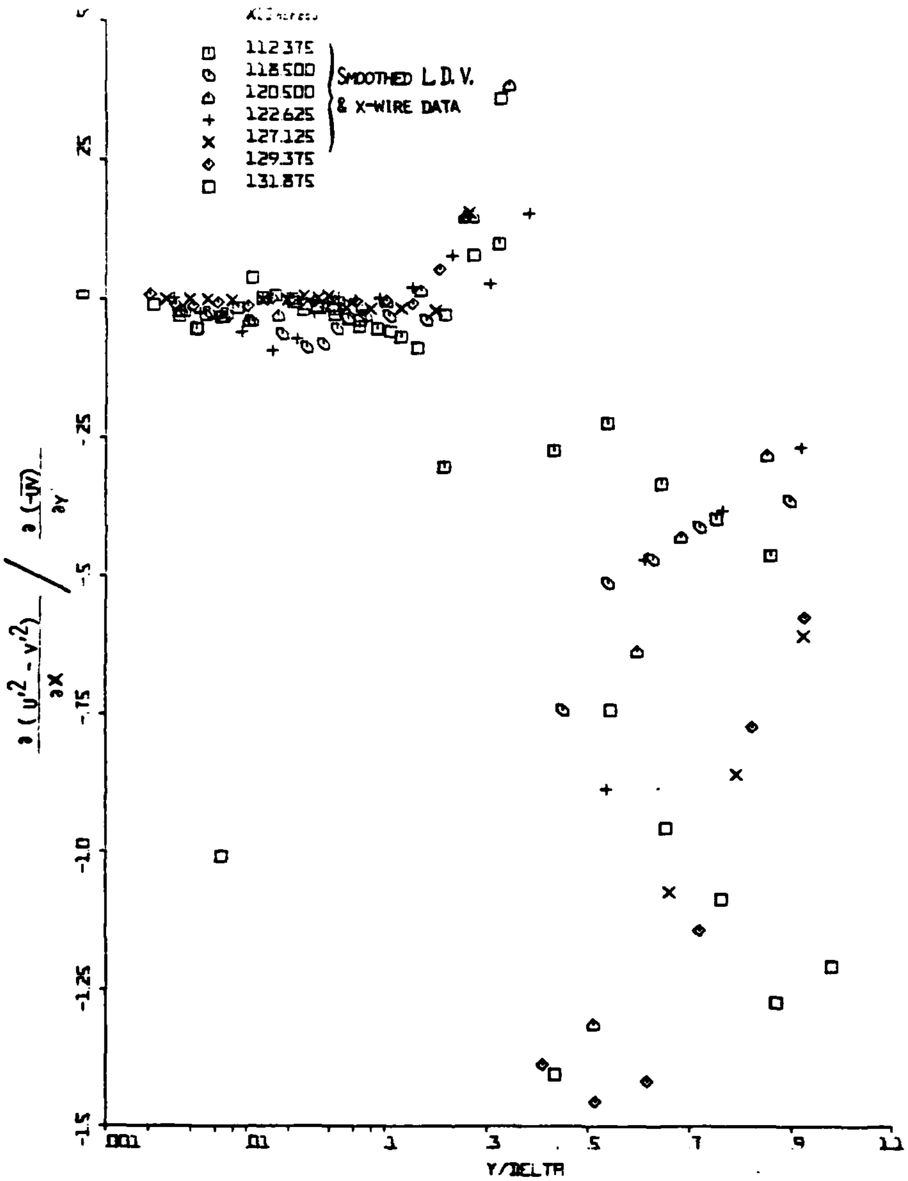

Figure 56(a). Ratio of normal stresses to shear stress terms in the momentum equation: upstream of separation.

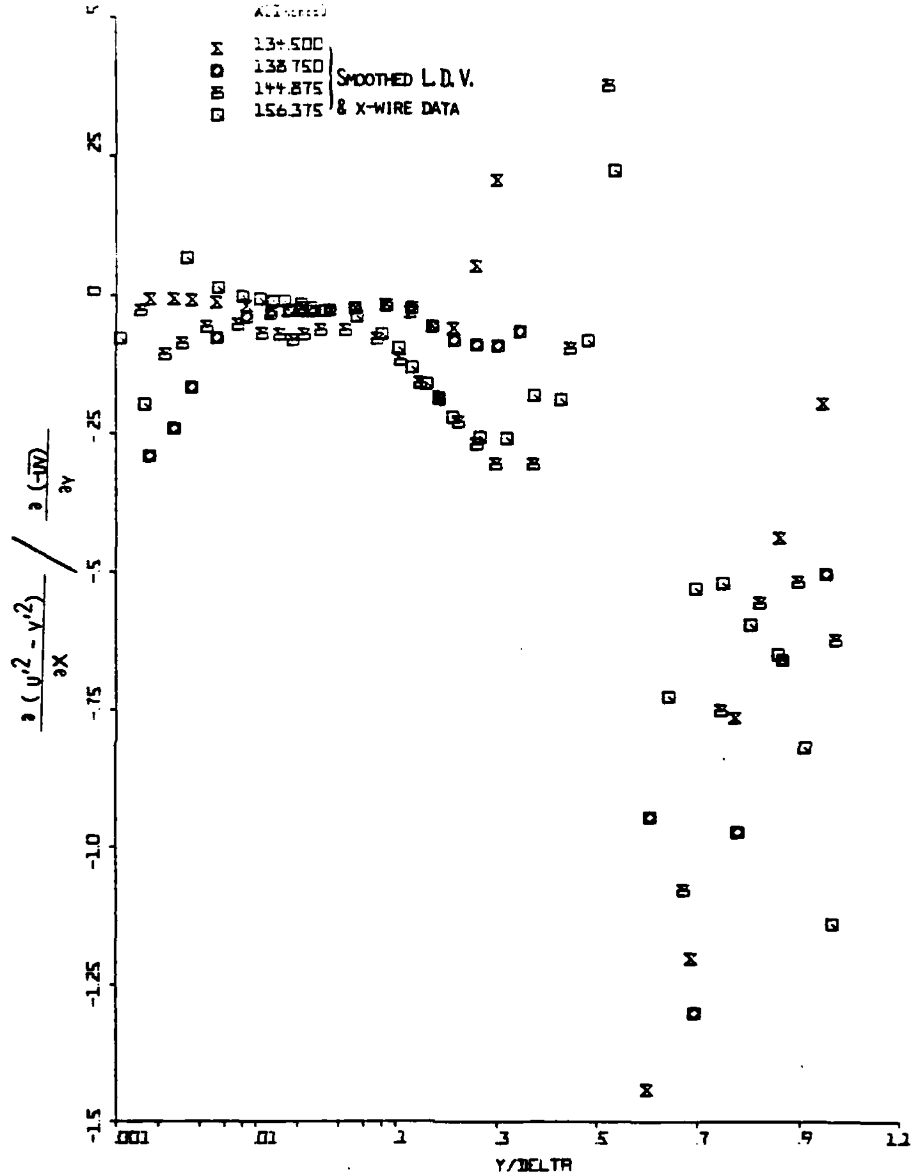

Figure 56(b). Ratio of normal stresses to shear stress terms in the momentum equation: downstream of separation.

FIGURE 57(A).
ENERGY BALANCE
X = 1185 INCHES

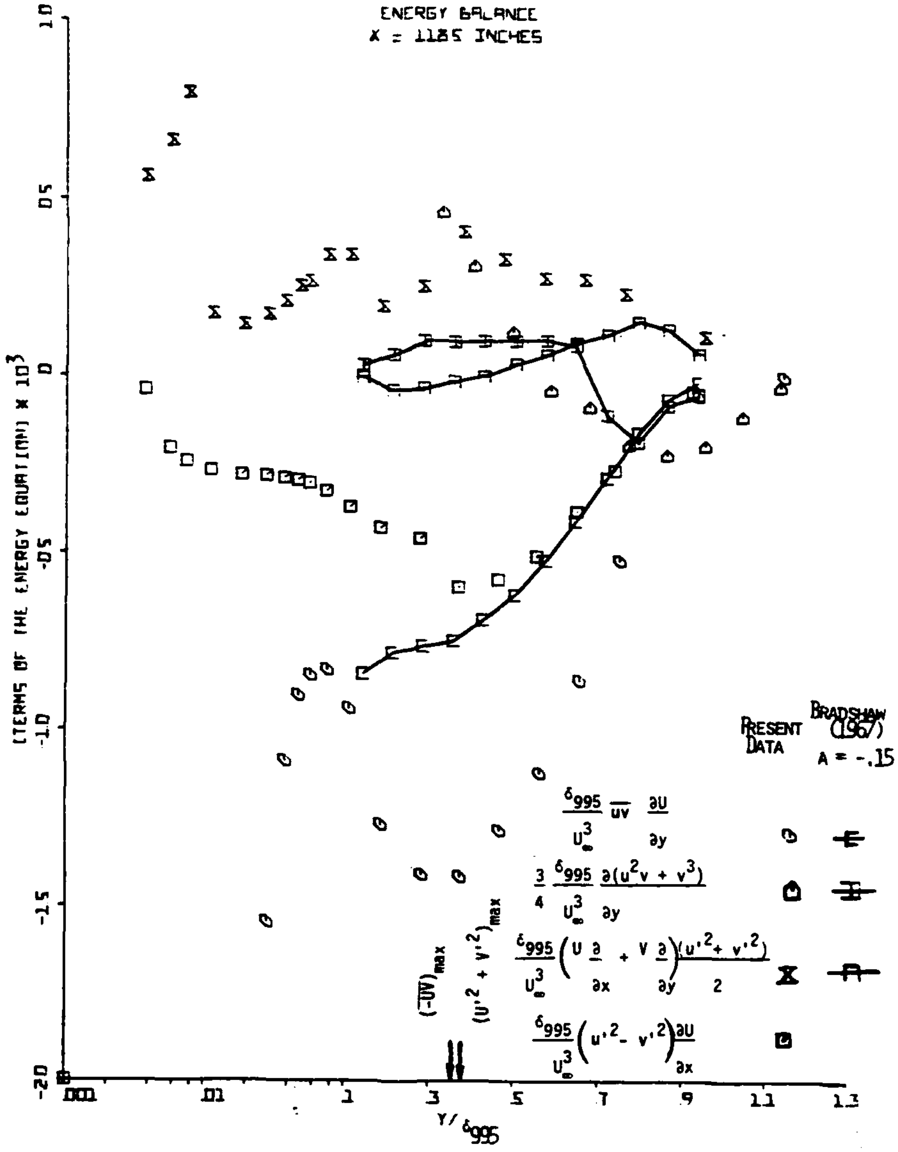

FIGURE 57(B).
ENERGY BALANCE
X = 131.875 INCHES

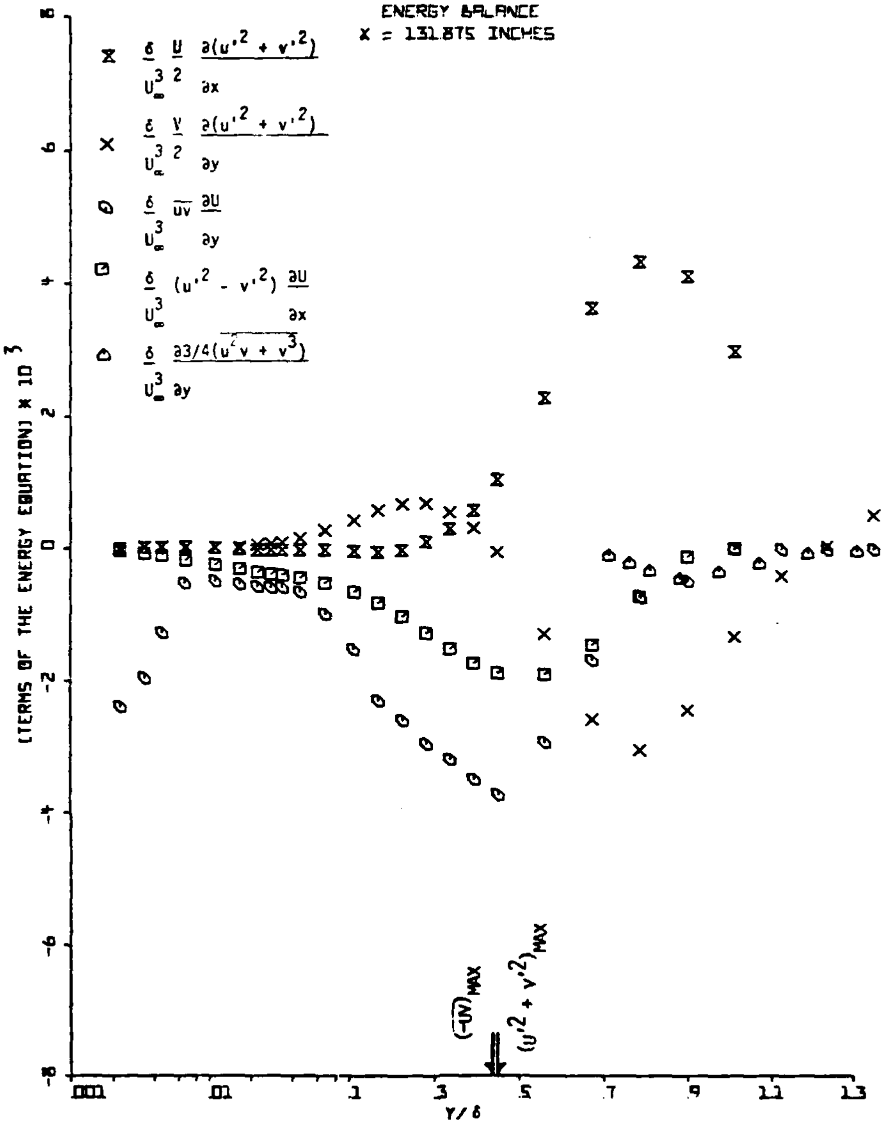

Figure 57(c). Energy balance at 156 3/8 inches.

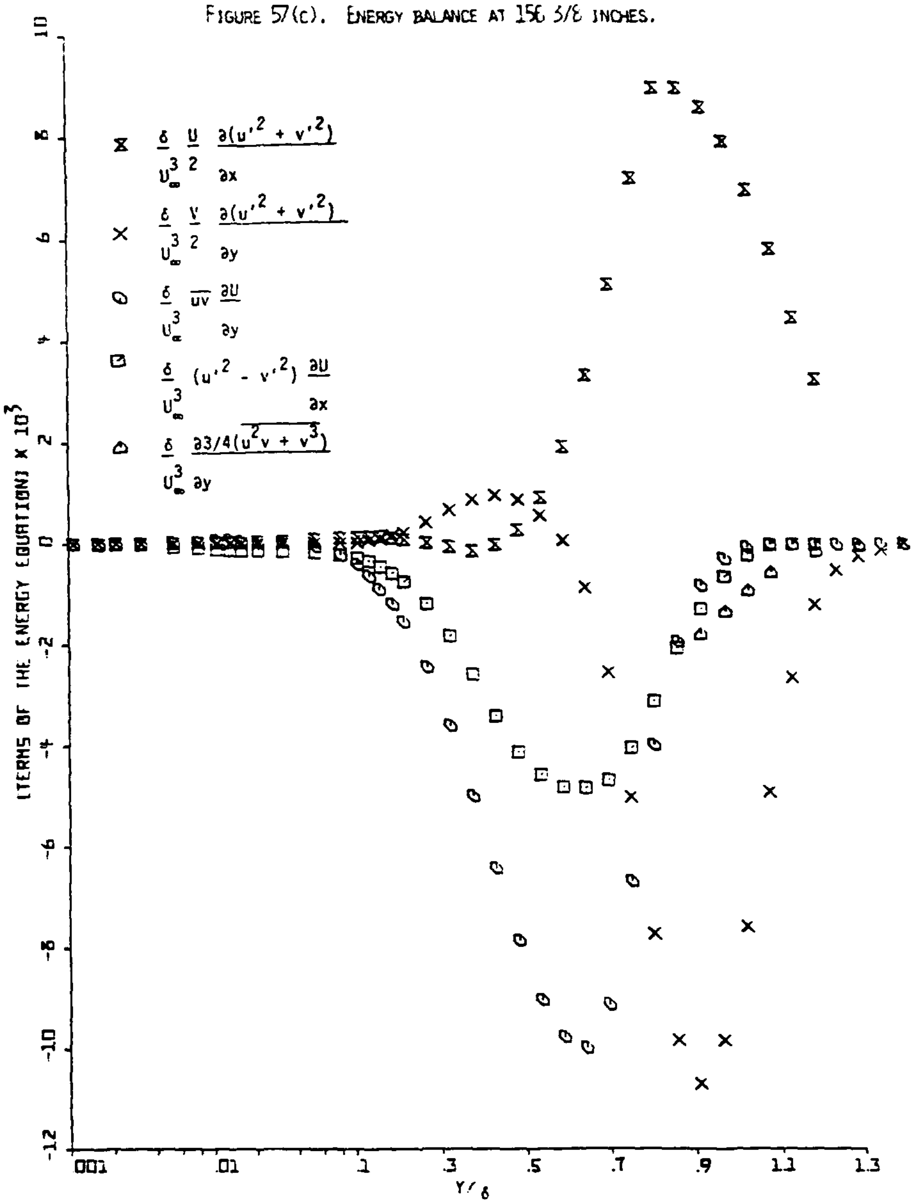

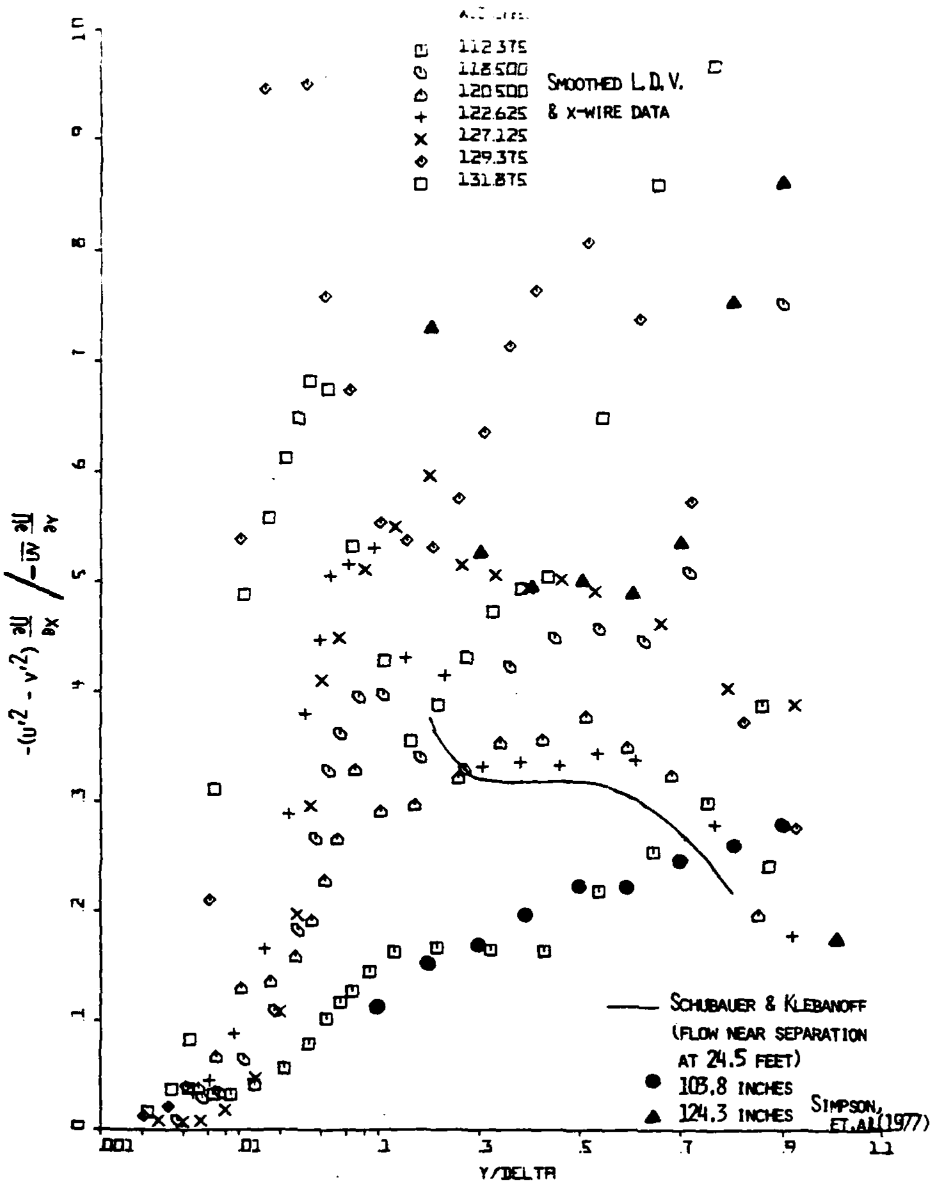

Figure 58(a). Ratio of normal stresses production to shear stress production upstream of separation.

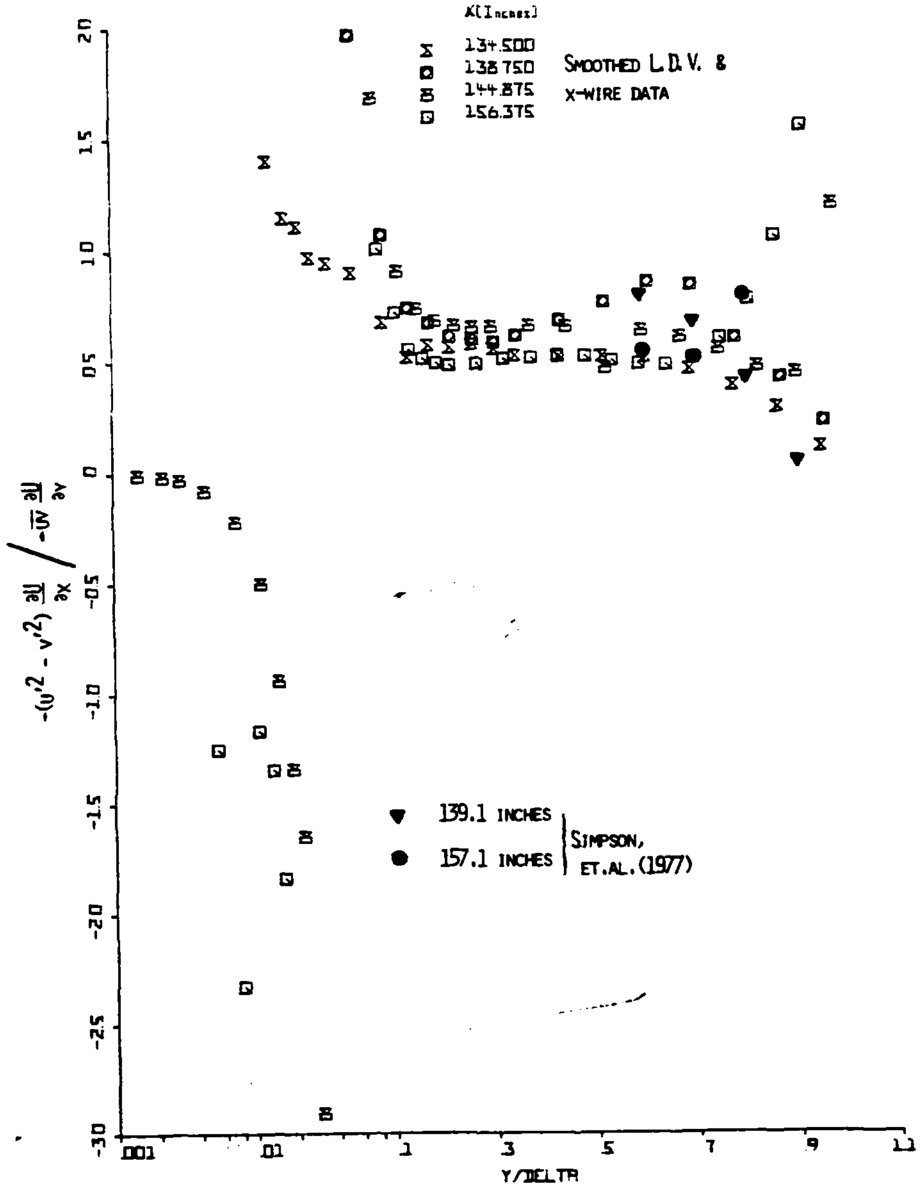

Figure 58(b). Ratio of normal stresses production to shear stress production downstream of separation.

effect becomes increasingly important as separation is approached. In fact both sets of SMU data show good agreement in the corresponding regions of development, with a near doubling of the ratio in the intermittent separation region. The present data in that region indicate the presence of a hump in the distributions near y/δ of 0.05 to 0.1, which becomes more significant as separation is approached. This is a result of the mean velocity profiles becoming inflexional in nature, which produces a reduced $\partial U/\partial y$ in that region. In fact these humps increase rapidly along the flow until $\partial U/\partial y$ attains a zero value for each profile in the backflow region where the velocity reaches a minimum value. The earlier data of Simpson et al. (1977) at 124.3 inches also suggest the presence of a hump. In the backflow region the two types of production oppose each other as shown in Figure 58 (b), but they aid one another in the forward flow region. The distributions in the outer layer tend toward similarity and the ratio seems to be almost a constant of 0.6 for $0.2 \leq y/\delta \leq 0.7$.

As far as shear production alone is concerned, the present data in the region upstream of separation is in agreement with those of Spangenberg et al. (1967) and others who observed two peaks in distributions for boundary layers subjected to large adverse pressure gradients. The present data indicate that as separation is approached, the peak near the wall becomes weaker until it vanishes in the region of fully-developed separation. In the backflow zone of the separated region there is no shear production as indicated by Figure 57 (c) and advection is also insignificant. Hence the only mode by which turbulence energy can reach the backflow zone is by turbulent diffusion. This conclusion is consistent with the results discussed in section IV.3.D above: diffusion plays a major role in transporting the turbulent kinetic energy in separated flows from the middle part of the layer, where it is mainly produced, to the outer region and the region near the wall. The absence of production near the wall in separated flow also leads one to conclude that the backflow near the wall is controlled by the large-scaled outer region flow, rather than by some wall-shear-stress-related "law of the wall".

V.5 Effects of Normal Stresses on Turbulence Correlations

As noted above in section V.4 and in the earlier work of Simpson *et al*. (1977), the normal stresses turbulence energy production terms are important in separating flows. Simpson *et al*. defined a nondimensional factor F as the ratio of total turbulence energy production to the shear-stress-related turbulence energy production

$$F = 1 - \frac{(\overline{u'^2} - \overline{v'^2})\partial U/\partial x}{-\overline{uv}\ \partial U/\partial y} \tag{33}$$

Figures 58 show F-1. Following Collins and Simpson (1976), the turbulence parameters in the expression for F can be inter-related so that F can be expressed as a function of the rate of strain ratio. The F factor can then be incorporated into some of the turbulence models and correlations to account for normal stresses effects.

Collins and Simpson expressed

$$(\overline{u'^2} - \overline{v'^2}) = C_1\overline{q^2} \tag{34}$$

However, the present data available at a number of streamwise locations indicate that at the location of the maximum shearing stress a better expression is

$$(\overline{u'^2} - \overline{v'^2}) = \frac{C_2\overline{q^2}}{F^{1/3}} \tag{35}$$

This reduces to equation (34) for flat plate flow with F = 1. Collins and Simpson found C_1 to be a constant equal to 0.32 for Klebanoff's (1954) zero

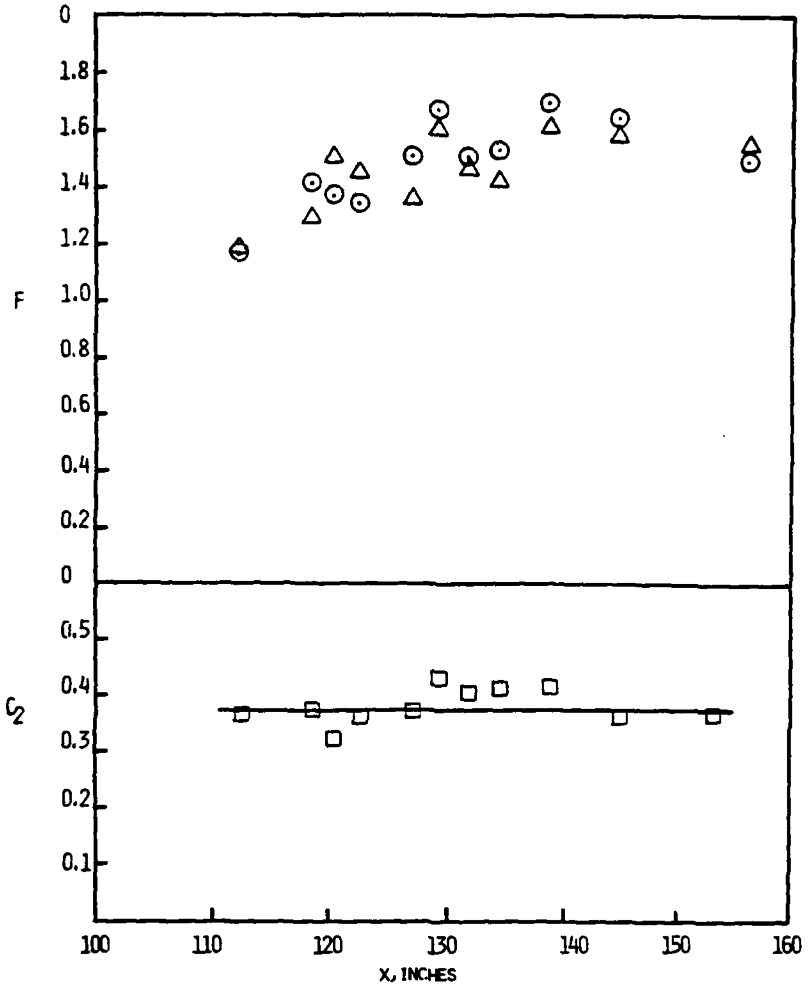

FIGURE 59 (A). NORMAL STRESSES PRODUCTION FACTOR F GIVEN BY ⊙, FROM EQUATION (33) AND △, FROM EQUATION (37). (B) □ CONSTANT C_2 FROM EQUATION (35). SOLID LINE IS AVERAGE VALUE.

Figure 59 (c). □, $-\overline{uv}/q^2$; ■, A_2 given by equation (36); solid line for flat plate boundary layer with $F = 1$. (d) ◇, c_2/A_2 from equation (37) at the maximum shear stress location; solid line is average value.

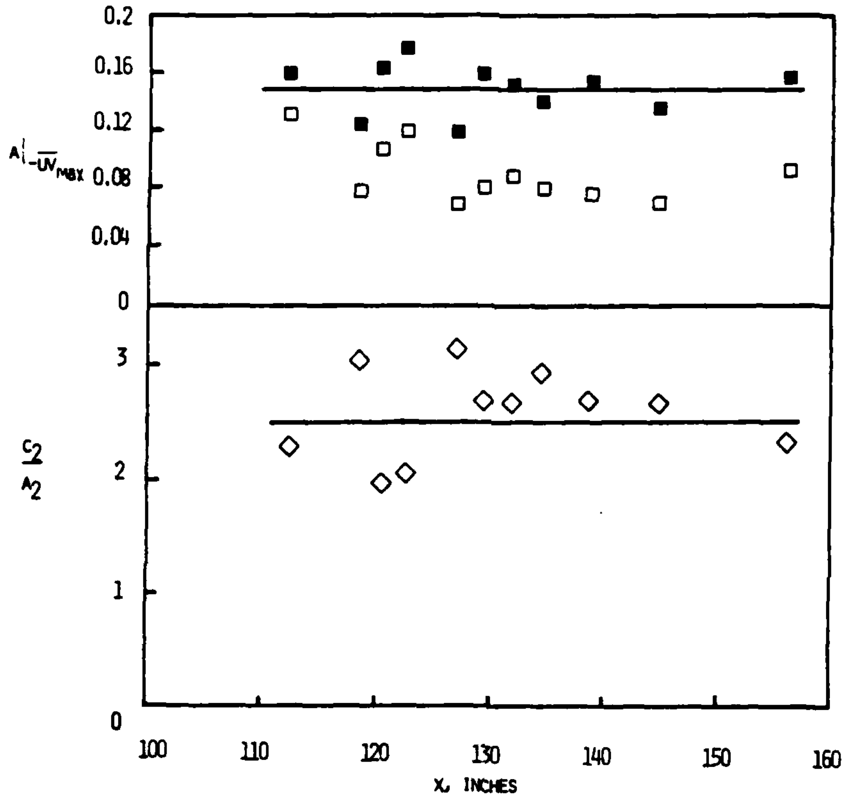

pressure gradient flow and 0.28 and 0.23 for Bradshaw's (1967) adverse pressure gradient flow. In view of the definition for C_2 in equation (35) the separating flow of Simpson et al. (1977) yields values for C_2 of 0.33 at 88 inches where F = 1 and 0.44 at 103.8 and 124.3 inches. The distribution of C_2 for present data is shown in Fig. 59 (b) and an average value of 0.375, which lies within the experimental uncertainty of 26%, was chosen for further analysis.

The Reynolds shearing stress can also be related to F and $\overline{q^2}$ by a modification to Bradshaw's correlation

$$-\overline{uv} = a_2\overline{q^2}/F^{4/3} \tag{36}$$

Figure 59 (c) shows that this is a good fit to the present data at the location of the maximum shearing stress with $a_2 = 0.15$. Equations (33), (35), and (36) can be combined into the form

$$F = \frac{1}{1 + \frac{C_2}{a_2} \frac{\partial U/\partial x}{\partial U/\partial y}} \tag{37}$$

at the location of the maximum shearing stress. As shown in Figure 59 (d), C_2/a_2 is nearly a constant within the experimental uncertainty of $\pm$ 17% with an average value of 2.5, which is close to the value of 2.0 used by Collins and Simpson in the prediction model for separating flows. Figure 59 (a) shows that equation (37) agrees with equation (33) within the experimental uncertainty of $\pm$ 14%.

A two term binomial expansion of equation (37) is similar to Bradshaw's (1973) F factor used to account for the effect of extra strain rates in complex turbulence flows. However, unlike the case with Bradshaw's factor the constant C_2/a_2 is derived directly from the turbulence structure and is not just an empirical constant derived from tuning a prediction method.

As shown in Figures 41 and 42, the mixing length and eddy viscosity distributions in the outer region decrease in magnitude in the downstream direction. This syems to be consistent with Gartshore's (1967) suggestion of decreased Reynolds stress in flows with an extra strain rate $\partial V/\partial y$, as in his own experiments on retarded wakes. Figures 60 (a) and (b) show these parameters at the maximum shearing stress for each location. F was fit to these data with the following results.

$$\frac{\ell}{\delta} = \left(\frac{1}{F^{1.25}}\right) \frac{\ell}{\delta}\bigg|_{F = 1} \tag{38}$$

and

$$\frac{\nu_e}{U_\infty \delta_1} = \left(\frac{1}{F^{1.5}}\right) \frac{\nu_e}{U_\infty \delta_1}\bigg|_{F = 1} \tag{39}$$

These fits were obtained in the following manner. The normally accepted value of 0.08 was used for ℓ/δ at F = 1. Using this, an average value for ℓ/δ in the outer region, and the value of F at the location of the maximum shearing stress, the exponenet on F in equation (38) was determined at each streamwise location. This exponent was within 12% of 1.25 and the modified correlation $F^{1.25}$ ℓ/δ agrees within the limits of experimental uncertainty of 21% with the normally accepted value of 0.08.

For evaluating the exponent in equation (39), all values were taken at the location of the maximum shearing stress; 105.3 inches was considered the location where F = 1. Equation (39) agrees with the data within the uncertainty of 26%.

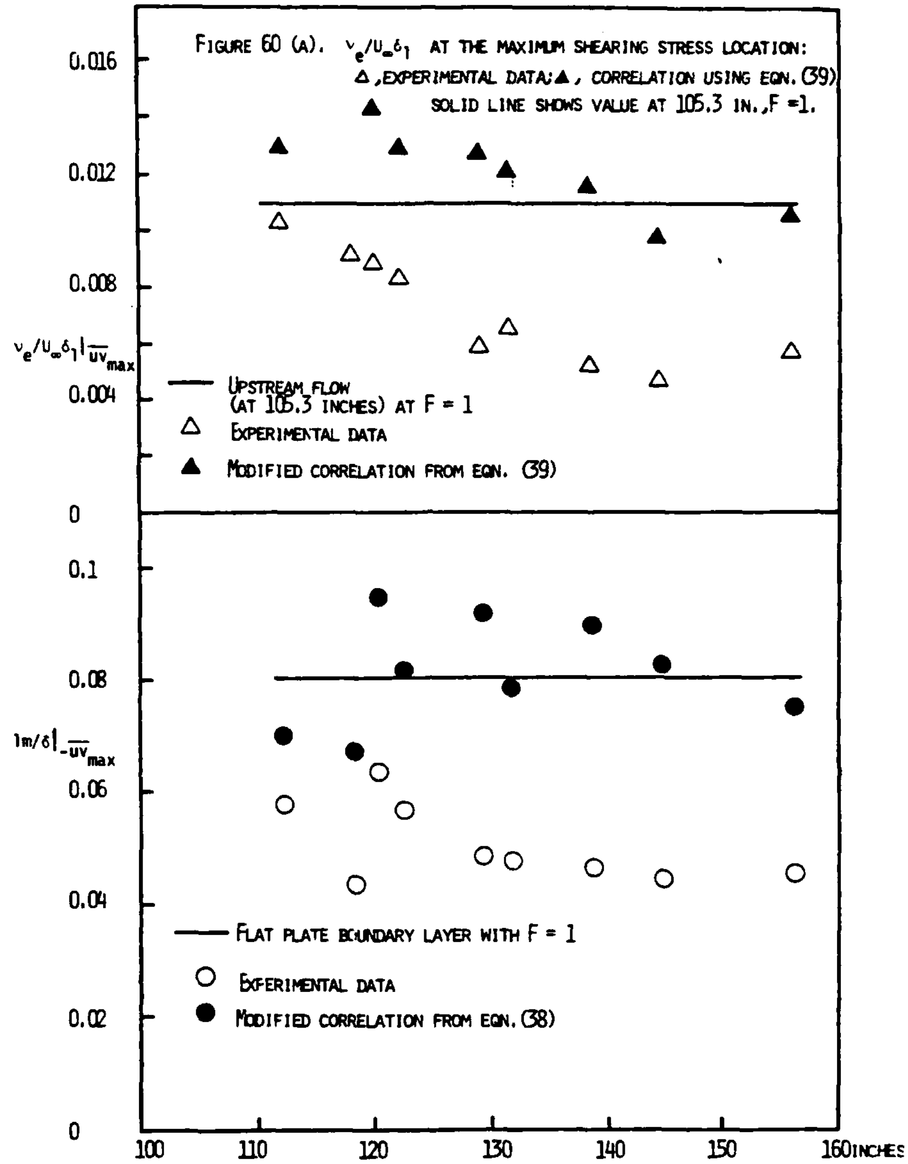

FIGURE 60 (A). $\nu_e/U_\infty\delta_1$ AT THE MAXIMUM SHEARING STRESS LOCATION: △, EXPERIMENTAL DATA; ▲, CORRELATION USING EQN. (39) SOLID LINE SHOWS VALUE AT 105.3 IN., F = 1.

FIGURE 60 (B) ℓ/δ AT THE MAXIMUM SHEARING STRESS LOCATION: O, EXPERIMENTAL DATA; O, CORRELATION USING EQUATION (38); SOLID LINE FOR FLAT PLATE BOUNDARY LAYER WITH F = 1.

V.6 Characteristic Frequencies from Spectra in Separated Flow

Strickland and Simpson (1975) showed that the characteristic bursting frequency could be determined by the peak in the first moment of the spectra $nF(n)$ of the wall shearing stress. These characteristic frequencies for the Simpson et al. (1977) separating flow correlated with the outer flow velocity and length scales, U_∞ and δ, as do the bursting frequencies for the zero-pressure-gradient case. However, $U_\infty/\delta n_b$ was between 11.7 and 8.35 for that separating flow, whereas values of about 5 are reported for the zero-pressure-gradient case. The basic conclusion of these earlier results is that the characteristic frequency of the most energetic turbulent fluctuations scale on the large-scale structure of the shear flow.

In the earlier work of Simpson et al. (1977) no spectral measurements in the separated flow were made. In the present flow spectral data for u were obtained from the laser anemometer velocity signals. Since the LDA signal data rate was under 400 signals per second and signal dropout was present, the spectra are only reliable under 100Hz. The first moment of each spectral distribution $nF(n)$ was obtained and the frequency of the peak was selected as the characteristic frequency n_b. In many cases the $nF(n)$ peak was constant over a frequency range, which is represented in Figures 61 as a line over the range of $U_\infty/\delta n_b$ values for a spectrum at a given y/δ.

Figure 61a shows that upstream of intermittent separation $U_\infty/\delta n_b$ is essentially constant throughout the inner flow region with a value of about 10 ± 3. At successive downstream locations the range of $U_\infty/\delta n_b$ for a given $nF(n)$ peak becomes progressively larger near the wall as shown in Figure 61 (b-f). In most cases a single frequency characterises the $nF(n)$ peak in the outer region. $U_\infty/\delta n_b$

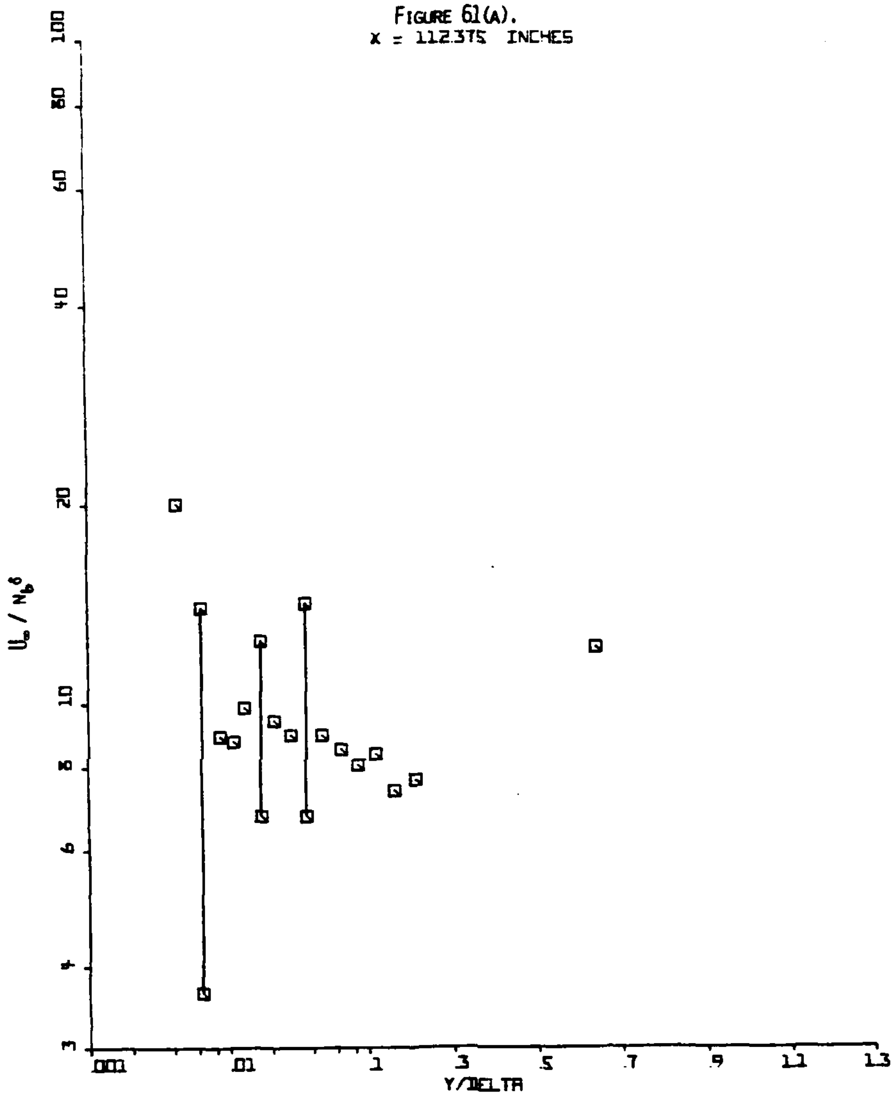

Figure 61(a). Characteristic frequency parameter U_∞ / $_b\delta$ vs. y/δ.

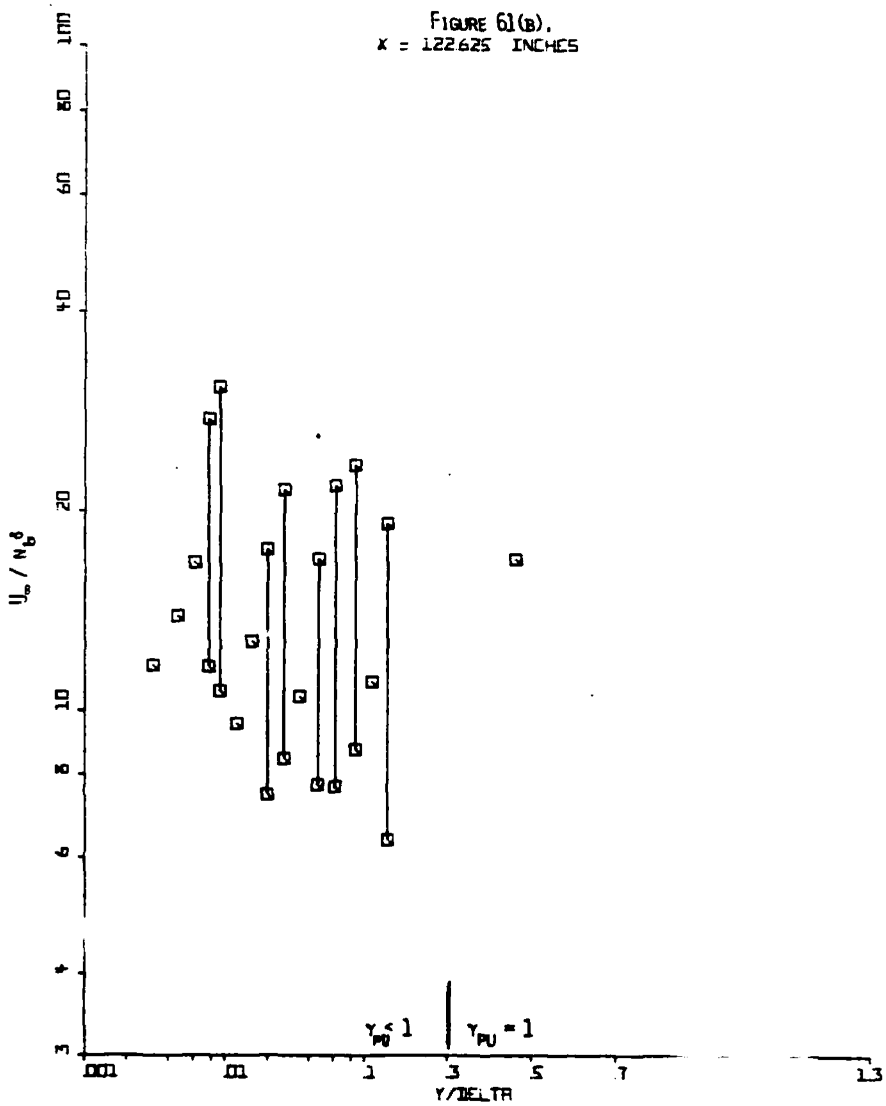

Figure 61(b). Characteristic frequency paramete /$n_b\delta$ vs. y/δ.

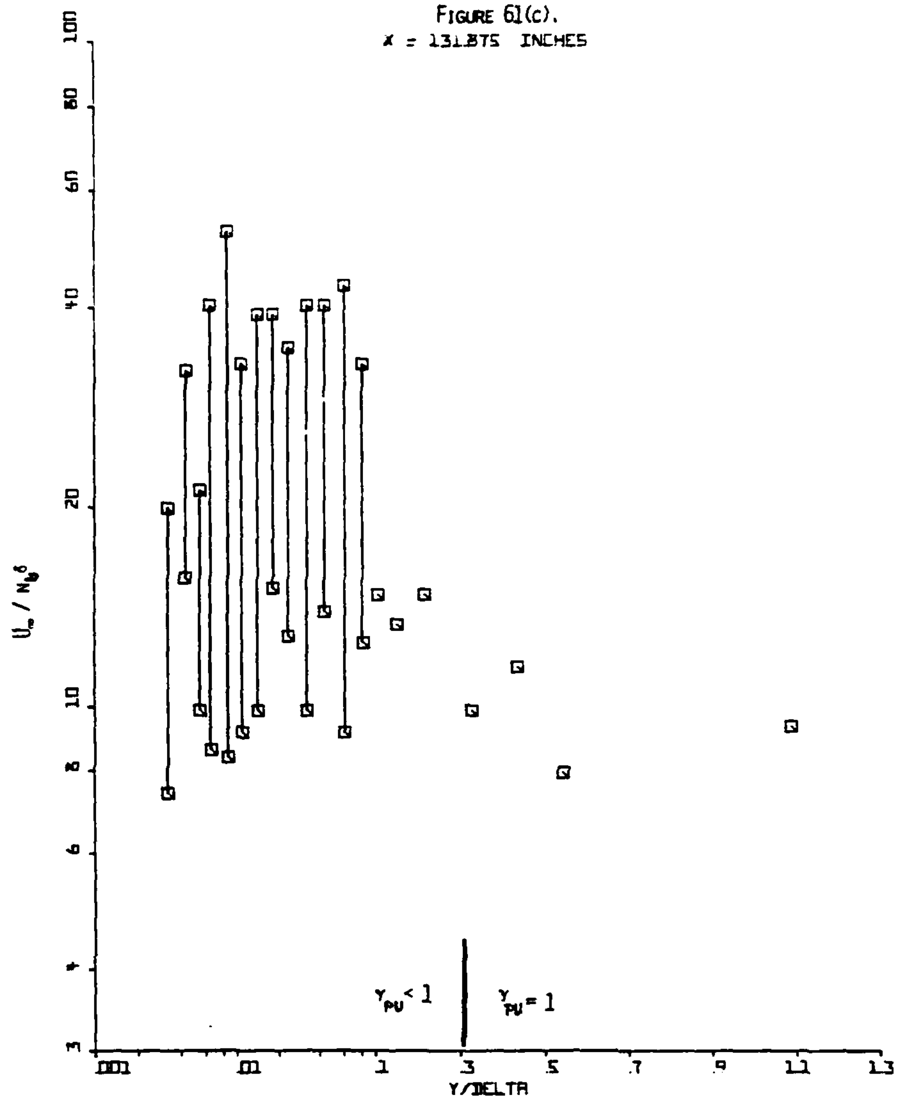

Figure 61(c). Characteristic frequency parameter $U_\infty / n_b \delta$ vs. y/δ.

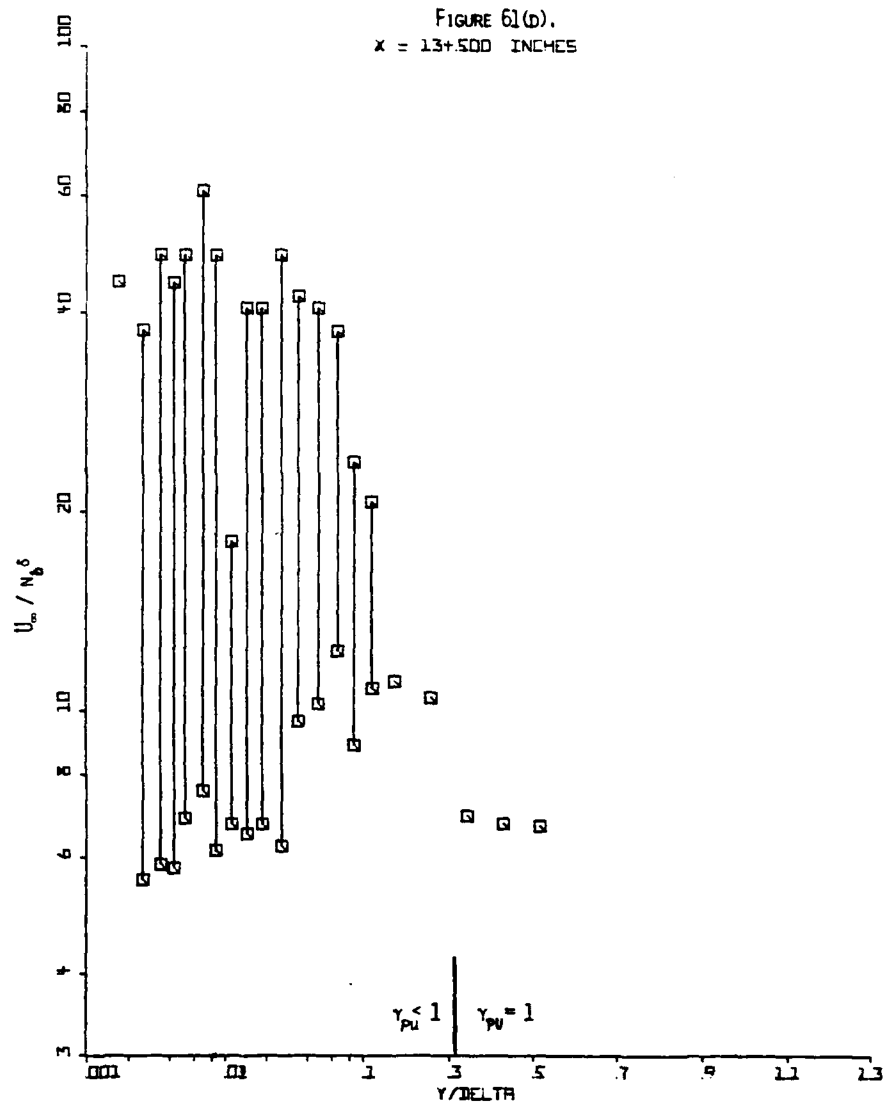

Figure 61(d). Characteristic frequency parameter $U_\infty / n_b\delta$ vs. y/δ.

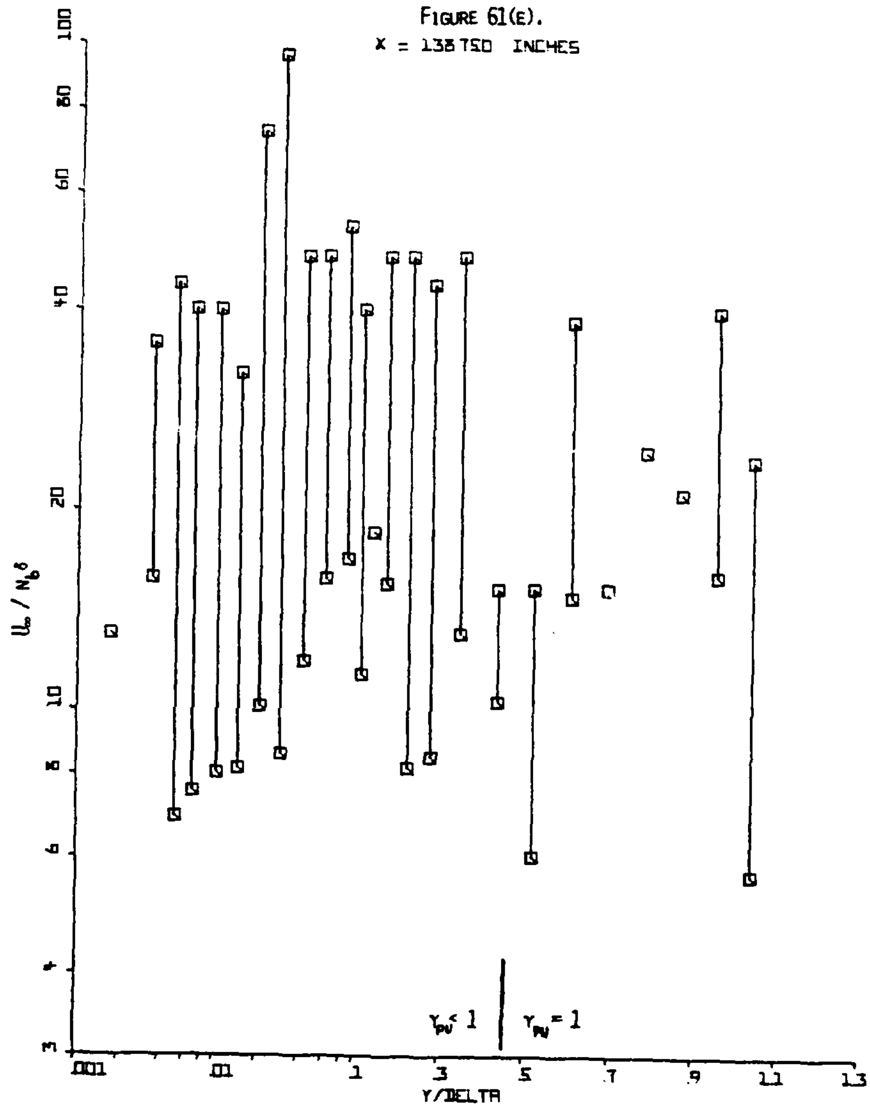

Figure 61(e). Characteristic frequency parameter $U_\infty / n_b \delta$ vs. y/δ.

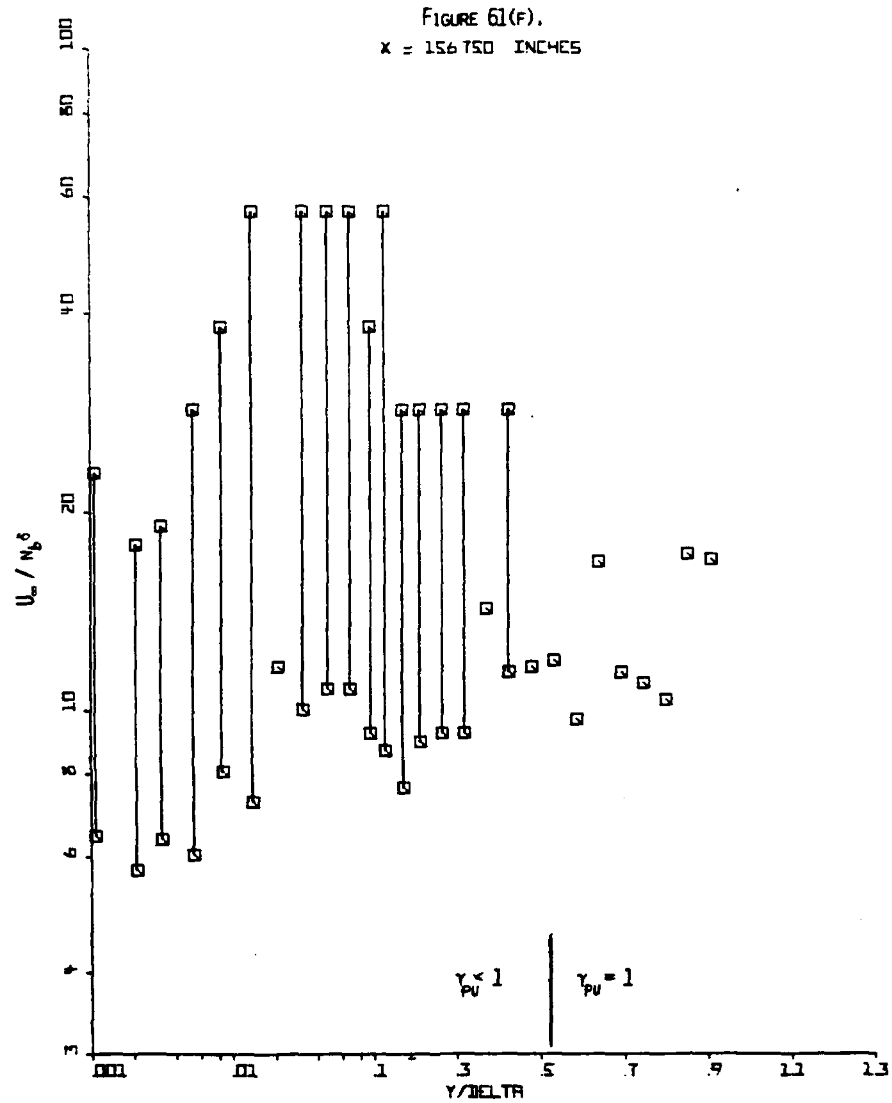

Figure 61(f). Characteristic frequency parameter $U_\infty / n_b\delta$ vs. y/δ.

is about 10 $\pm$ 3 at the lower end of the $U_\infty/\delta n_b$ bands. The upper values of $U_\infty/\delta n_b$ are about 40 or so in the inner region.

These results indicate that the characteristic frequency of the outer region correlate with U_∞ and δ along the flow, with an approximately constant value of $U_\infty/\delta n_b$ of about 10 $\pm$ 5. This is consistent with the earlier work of Simpson et al. (1977). Nearer the wall the frequency range of the energetic turbulent motions descends to frequencies one-fourth as large.

For attached boundary layers the spectra for the near wall flow have a range of frequencies over which the peak of each nF(n) distribution is constant (Rotta, 1962). This is a consequence of the logarithmic law-of-the-wall velocity profile. For a separated flow the law-of-the-wall is not valid, so a different explanation of the nF(n) distribution near the wall is needed. The upper frequency end of the nF(n) peak is at approximately the same frequency as the outer region peak frequency. Note from Figs. 61 (b-f) that the wide frequency spectral peaks seem to occur at locations near the wall where $\gamma_u < 1$.

One simple speculation is that the celerity or speed of the eddies in the backflow region is much lower than that in the outer region. Fig. 17 of Simpson et al. (1977) supports this idea. Thus, as large scale structures pass through the outer flow at a frequency of about $U_\infty/10\delta$, these same structures move at a much lower average celerity in the backflow region, producing a much lower frequency spectrum.

VI. CONCLUSIONS - The Nature of a Separating Turbulent Boundary Layer

These experiments confirm the conclusions of Simpson et al. (1977) regarding a separating airfoil type turbulent boundary layer. The mean flow upstream of the beginning of intermittent separation obeys the law-of-the-wall and the Perry and Schofield (1973) velocity profile correlation for the outer region.

Sandborn's correlations for the locations of intermittent separation (γ_u = 0.8) and fully-developed separation hold. Pressure gradient relaxation begins upstream of intermittent separation near the wall jet control in this flow and continues until the location of fully-developed separation. The upstream-downstream intermittency γ_u, u', and v', and $-\overline{uv}$ profiles each approach similarity profiles downstream of separation. The frequency of passage of the outer region large scale eddies n_b scales on the free-stream velocity U_∞ and the boundary layer thickness δ. Normal stresses effects contribute significantly to the momentum and turbulence energy equations.

Much new information about the separated region has been gathered and leads to significant conclusions about the nature of the separated flow. For reference the most important results are summarized below.

1. The backflow mean velocity profile scales on the maximum negative mean velocity U_N and its distance from the wall N. A U^+ vs. y^+ law-of-the-wall velocity profile is not consistent with this correlation since both U_N and N increase with streamwise distance, while the law-of-the-wall length scale ν/U_τ varies inversely with the velocity scale U_τ. It does not appear possible to describe the separated flow mean velocity profiles by a universal "backflow function" that is added to a universal "wake function".

2. High turbulence levels exist in the backflow. u' and v' are of the same order as $|U|$. Since the free-stream velocity in the separated region is rather steady, this means that the near wall fluctuations are not mainly due to a flapping of the entire shear layer, but are due to turbulence within the separated shear layer.

3. Low levels of Reynolds shearing stress occur in the backflow. $-uv/u'v'$ and $-\overline{uv}/(u'^2 + v'^2)$ correlations are low in the backflow, but are comparable with those for mixing layers in the outer region.

4. Mixing length and eddy viscosity models are adequate upstream of separation and in the outer region, but are physically meaningless in the backflow. Normal stresses effects appear to account for the lower mixing length and eddy viscosity values observed in the outer region of the separated flow.

5. In the separated flow between the wall and the locations of the minimum mean velocity, the skewness factor for u, S_u, is negative. Between this point and the locations of the maximum shearing stress, S_u is positive. The flatness factor F_u reaches a local maximum of about 4 at the minimum mean velocity location. S_v has a profile shape and magnitudes that are approximately the mirror image or negative of S_u.

6. Negligible turbulence energy production occurs in the backflow. Normal and shear stresses production in the outer region supply turbulence energy to the backflow by turbulent diffusion. These results are consistent with the absence of a logarithmic mean velocity profile in the backflow, since classical turbulence energy production arguments indicate that the rate of production must equal the rate of dissipation in such a region.

These turbulence energy results lead to the conclusion that the backflow is controlled by the large-scale outer region flow. Movies of laser-illuminated smoke also have clearly revealed that the large eddy structure supplies most of near wall backflow. The small mean backflow does not come from far downstream as suggested in Figure 62(a), but appears to be supplied intermittently by large-scale structures as they pass through the separated flow as suggested by Figure 62(b).

A simple qualitative experiment was performed to determine qualitatively the influence of the downstream near wall conditions on the separation behavior. A deflection plate was located at the end of the second section (200 inches) as shown in Figure 63. For heights of this deflection plate up to 7 inches, no appreciable change in the separation zone location (122-140 inches) and behavior were noted. This result also seems to support the flow model suggested in Figure 62(b) where the backflow is supplied locally by outer region large-scale structures. Only after the deflection plate was high enough to begin to change the free-stream pressure gradient did the location of the separation zone change.

Of course, this mechanism for supplying the backflow may be dominant only when the thickness of the backflow region is small as compared with the turbulent shear layer thickness, as in the present case. Experiments (Fox and Kline, 1962) on separation in wide-angle diffusers indicate that the mean backflow can come from far downstream when the thickness of the backflow region is comparable to the thickness of the forward flow.

Downstream of fully-developed separation in these experiments, the mean backflow region appears to be divided into three layers: a viscous layer nearest the wall that is dominated by the turbulent flow unsteadiness but with little Reynolds shearing stress effects; a rather flat intermediate layer that seems to act as an overlap region between the viscous wall and outer regions; and the outer backflow region that is really part of the large-scaled outer region flow.

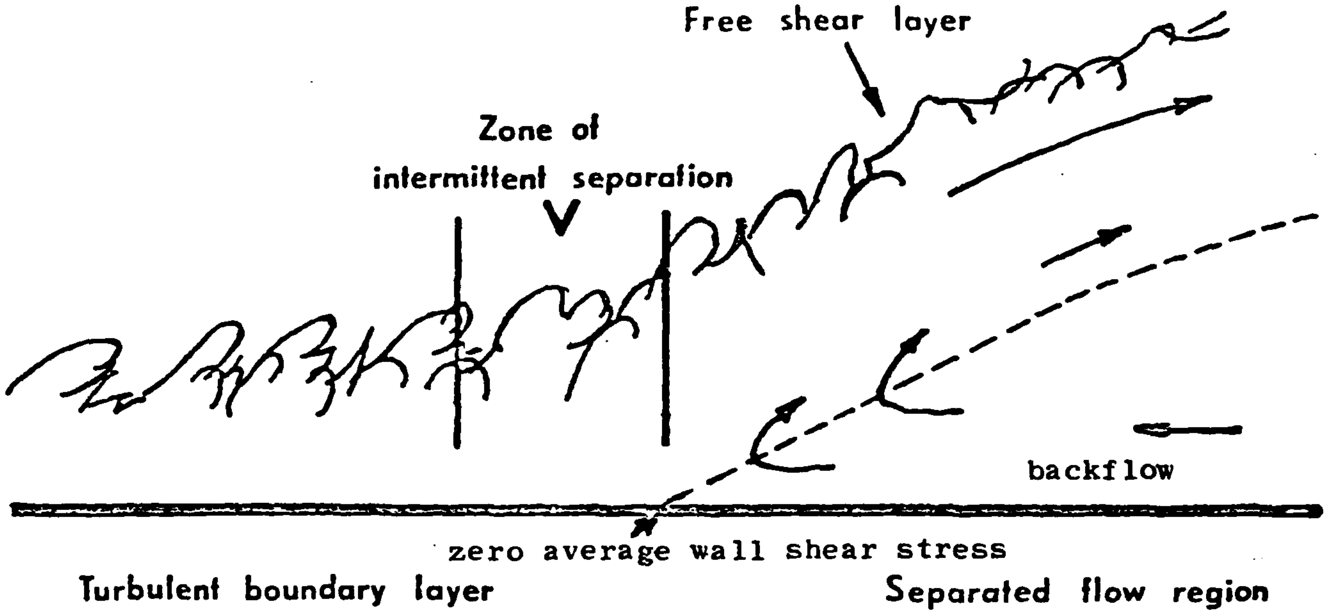

FIGURE 62 (A). TRADITIONAL VIEW OF TURBULENT BOUNDARY LAYER SEPARATION WITH THE MEAN BACKFLOW COMING FROM FAR DOWNSTREAM.

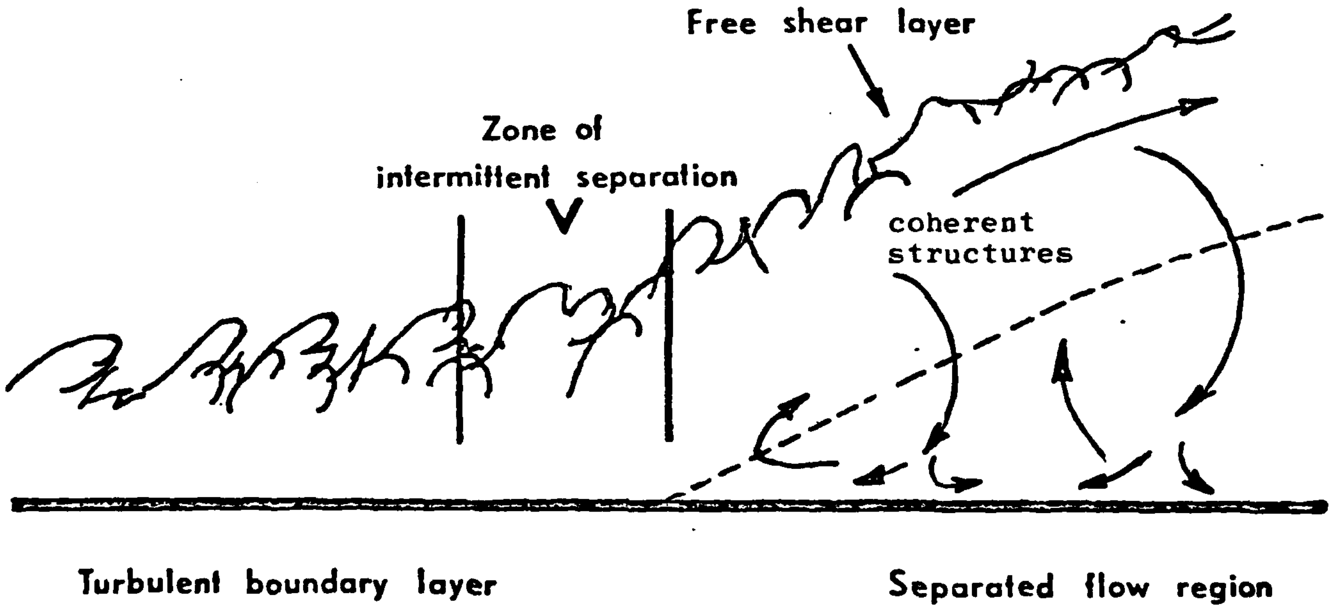

FIGURE 62 (B). A POSSIBLE FLOW MODEL WITH THE COHERENT STRUCTURES SUPPLYING THE SMALL MEAN BACKFLOW.

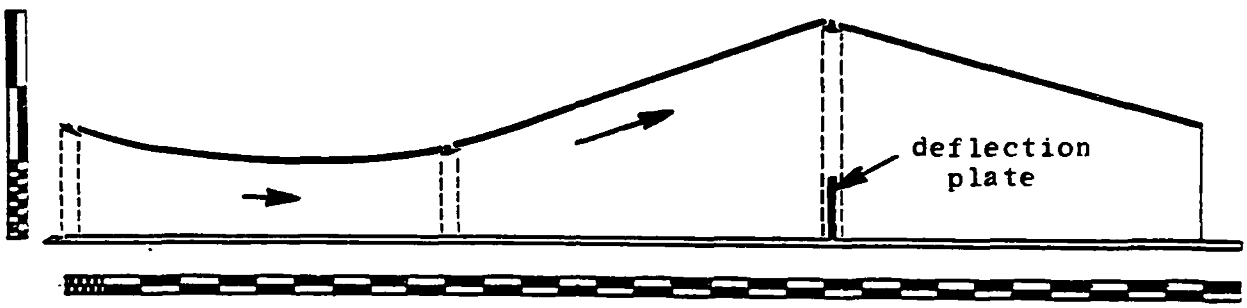

FIGURE 63. SIDEVIEW SCHEMATIC OF THE TEST SECTION FOR QUALITATIVE EXPERIMENT; SAME AS FIGURE 1 EXCEPT FOR THE DEFLECTION PLATE.

The Reynolds shearing stresses in this region must be modeled by relating them to the turbulence structure and not to local mean velocity gradients. The mean velocity profiles in the backflow are a result of time-averaging the large turbulent fluctuations and are not related to the cause of the turbulence. In contrast, in flows for which the eddy viscosity and mixing length models appear to be useful, the instantaneous velocity gradients are not extremely different from the local mean velocity gradient and significant local turbulence energy production occurs, i.e., the Reynolds shearing stresses is physically related to the mean velocity gradient.

VII. FUTURE WORK

Currently measurements of w' and S_w are being made in the separated flow to completely document this flow. During the 1980-81 period a scanning laser anemometer system will be developed to obtain almost instantaneous velocity profiles. These instantaneous profiles should prove useful in relating the instantaneous backflow to the outer region flow.

REFERENCES

Antonia, R.A. 1973 "Some Small Scale Properties of Boundary Layer Turbulence", Physics of Fluids, 16, pp. 1198-1206.

Bowles, E.B. 1977 "Design, Construction, and Testing of Wall Jet-Wall Suction Boundary Layer Control System , "Dept. of Civil/Mechanical Engrg. Internal Report WT-5, Southern Methodist University.

Bradshaw, P., Ferriss, D.H. and Atwell, N.P. 1967a "Calculation of Boundary Layer Development using the Turbulent Energy Equation," J. Fluid Mech., 28, pp. 593-616.

Bradshaw, P. 1967b "The Turbulence Structure of Equilibrium Boundary Layers, J. Fluid Mech., 29, pp. 625-645.

Bradshaw, P. 1973 "Effects of Streamline Curvature on Turbulent flow", AGARDograph No. 169.

Bragg, G.M. 1974 Principles of Experimentation and Measurement, Prentice-Hall, Englewood Cliffs, N.J.

Cebeci, T. and Smith, A.M.O. 1974 Momentum Transfer in Boundary Layers, Hemisphere Publishing Corporation, Washington.

Coles, D. and Hirst, E. 1969 Computation of Turbulent Boundary Layers - 1968 AFOSR - IFP Stanford Conference, Vol. II, Data Compilation, Dept. Mechanical Engineering, Stanford University.

Collins, M.A. and Simpson, R.L. 1978 "Flowfield Prediction for Separating Turbulent Shear Layers," AIAA J., 16, pp. 291-292.

Dumas, R. and Marcillat, J. 1966 "Répartition en amplitudes de la vitesse dans une couche limite turbulente", C.R. Acad. Sc. Paris, Série A, 262, pp. 700-703.

Durão, D.F.G. and Whitelaw, J.H. 1975 "The Influence of Sampling Procedures on Velocity Bias in Turbulent Flows," Proceedings of LDA Symposium Copenhagen, pp. 138-149, P.O. Box 70, DK - 2740 Skovlunde, Denmark.

East, L.F. and Sawyer, W.G. 1979 "An Investigation of the Structure of Equilibrium Turbulent Boundary Layers", Proc. of the NATO-AGARD Symposium.

Eckelmann, H. 1974 "The Structure of the Viscous Sublayer and the Adjacent Wall Region in a Turbulent Channel Flow," J. Fluid Mech., 65, p. 439.

Fox, R.W. and Kline, S.J. 1962 "Flow Regimes for Curved Subsonic Diffusers," J. Basic Engrg., TASME, 84, pp. 303-312.

Gartshore, I.S. 1967 "Two-dimensional Turbulent Wakes", J. Fluid Mech. 30, pp. 547-560.

Halleen, R.M. 1964 "A Literature Review on Subsonic Free Turbulent Shear Flow," Report MD-11, Thermosciences Div., Dept. of Mech. Engrg., Stanford Univ.

Higuchi, H. and Peake, D.J. 1978 "Bi-directional, Buried-wire Skin Friction Gage," NASA-TM 78531.

Klebanoff, P. 1954 "Characteristics of Turbulence in a Boundary Layer with Zero Pressure Gradient," NACA Report 1247.

Kline, S.J. and McClintock, F.A. 1953 "Describing Uncertainties in Single-Sample Experiments," Mechanical Engineering, 75, pp. 3-8

Kreplin, H-P. 1973, M. Sc. Thesis, Max-Planck-Institut für Strömungsforchung. (referenced from Ueda and Hinze, 1975).

McLaughlin, K.D. and Tiederman, W.G. 1973 "Biasing Correction for Individual Realization of Laser Anemometer Measurements in Turbulent Flow," Physics of Fluids, 16, pp. 2082-2088.

Miller, J.A. 1976 "Simple Linearized Hot-Wire Anemometer," J. Fluids Engineering, 98, pp. 550-557.

Murthy, V.W. and Rose, W.C. 1978 "Wall Shear Stress Measurements in a Shock-wave Boundary-layer Interaction," AIAA Journal, 16, pp. 667-672.

Oka, S. and Kostić, Z. 1972 "Influence of Wall Proximity on Hot-Wire Velocity Measurements," DISA Information, no. 13, pp. 29-33.

Perry, A.E. and Schofield, W.H. 1973 "Mean Velocity and Shear Stress Distributions in Turbulent Boundary Layers," Physics Fluids, 16, pp. 2068-2074.

Rao, K.N., Narasimha, R., Badri Narayanan, M.A. 1971 "The 'Bursting' Phenomenon in a Turbulent Boundary Layer," J. Fluid Mech., 48, pp. 339-352.

Rotta, J.C. 1962 "Turbulent Boundary Layers in Incompressible Flow," Progress in Aeronautical Sciences, 2, Pergamon Press.

Rubesin, M.W., Okuno, A.F., Mateer, G.G., and Brosh, A. 1975 "A Hot-Wire Surface Gage for Skin Friction and Separation Detection Measurements," NASA TM X-62, 465.

Sandborn, V.A. 1959 "Measurements of Intermittency of Turbulent Motion in a Boundary Layer," J. Fluid Mech, 6, pp. 221-240.

Sandborn, V. A. and Kline, S. J. 1961 "Flow Models in Boundary-Layer Stall Inception," J. Basic Engineering, TASME, 83, pp. 317-327.

Sandborn, V. A. and Liu, C. Y. 1968 "On Turbulent Boundary Layer Separation," J. Fluid Mech., 32, pp. 293-304.

Sandborn, V. A. and Slogar, R. J. 1955 "Study of the Momentum Distribution of Turbulent Boundary Layers in Adverse Pressure Gradients," NACA TN 3264.

Saripalli, K. R. and Simpson, R. L. 1979 "Investigation of Blown Boundary Layers with an Improved Wall Jet System," Final Technical Report-NASA Langley Research Center.

Schubauer, G. B. and Klebanoff, P. S. 1951 "Investigation of Separation of the Turbulent Boundary Layer," NACA Report 1030.

Simpson, R. L. 1976 "Interpreting Laser and Hot-film Anemometer Signals in a Separating Boundary Layer," AIAA Journal, 14, pp. 124-126.

Simpson, R. L. 1979 "Summary of the Colloquium on Turbulent Flow Separation (January 1979)," Project SQUID Report SMU-3-PU.

Simpson, R. L. and Barr, P. W. 1975 "Laser Doppler Velocimeter Signal Processing Using Sampling Spectrum Analysis," Rev. Sci. Inst., 46, pp. 835-837.

Simpson, R. L. and Chew, Y.-T. 1979 "Measurements in Highly Turbulent Flows: Steady and Unsteady Separated Turbulent Boundary Layers," Proceedings of Third Int. Workshop on Laser Velocimetry, pp. 179-196, Hemisphere.

Simpson, R. L. and Collins, M. A. 1978 "Prediction of Turbulent Boundary Layers in the Vicinity of Separation," AIAA Journal, 16, pp. 289-290.

Simpson, R. L. and Shackleton, C. R. 1979 "Laminariscent Turbulent Boundary Layers: Experiments on Nozzle Flows," Project SQUID Report SMU-2-PU.

Simpson, R. L. and Wallace, D. B. 1975 "Laminariscent Turbulent Boundary Layers: Experiments on Sink Flows," Project SQUID Report SMU-1-PU.

Simpson, R. L. Chew, Y.-T., and Shivaprasad, B. G. 1980 "Measurements of Unsteady Turbulent Boundary Layers with Pressure Gradients," Southern Methodist University, Dept. of Civil and Mechanical Engineering Report WT-6.

Simpson, R. L., Heizer, K. W., and Nasburg, R. E., 1979 "Performance Characteristics of a Simple Linearized Hot-Wire Anemometer," J. Fluids Engineering, 101, pp. 381-382.

Simpson, R. L., Strickland, J. H., and Barr, P. W. 1974 "Laser and Hot-film Anemometer Measurements in a Separating Turbulent Boundary Layer," Report WT-3, Thermal and Fluid Sciences Center, SMU. AD -A001115.

Simpson, R. L., Strickland, J. H. and Barr, P. W. 1977 "Features of a Separating Turbulent Boundary Layer in the Vicinity of Separation," J. Fluid Mech., 79, pp. 553-594.

Spangenberg, W. G., Rowland, W. R., and Mease, N. E. 1967 "Measurements in a Turbulent Boundary Layer in a Nearly Separating Condition," Fluid Mechanics of Internal Flow, G. Scvran, editor, Elsevier Publishing Co., N. Y.,pp. 110-151.

Strickland, J. H. and Simpson, R. L. 1973 " The Separating Turbulent Boundary Layer: An Experimental Study of an Airfoil Type Flow," Thermal and Fluid Sciences Center, Southern Methodist University, Report WT-2; also AD-771170/8GA.

Strickland, J. H. and Simpson, R. L. 1975 "Bursting Frequencies Obtained from Wall Shear Stress Fluctuations in a Turbulent Boundary Layer," Physics Fluids, 18, pp. 306-308.

Ueda, H. and Hinze, J. O. 1975 "Fine-Structure Turbulence in the Wall Region of a Turbulent Boundary Layer," J. Fluid Mech. , 67, pp. 125-143.

Wood, N. B. 1975 "A Method for Determination and Control of the Frequency Response of the Constant-Temperature Hot-Wire Anemometer," J. Fluid Mech., 67, pp. 769-786.

Wygnanski, I. and Fiedler, H. E. 1970 "The Two-Dimensional Mixing Region," J. Fluid Mech., 41, pp. 327-361.

Zaric, Z. 1972, 4th All-Union Heat and Mass Transfer Conf. Minsk, U.S.S.R. (referenced by Ueda and Hinze, 1975).

APPENDIX

TABULATION OF LASER, CROSS HOT-WIRE AND SINGLE HOT-WIRE ANEMOMETER DATA

(Note that only first three digits in each number are valid.)

AD-A095 252 PURDUE UNIV LAFAYETTE IN PROJECT SQUID HEADQUARTERS F/G 20/4
MEASUREMENTS OF A SEPARATING TURBULENT BOUNDARY LAYER.(U)
APR 80 R L SIMPSON, Y CHEW, B G SHIVAPRASAD N00014-75-C-1143
UNCLASSIFIED SQUID-SMU-4-PU NL

3 OF 3

END
DATE
FILMED
3-81
DTIC

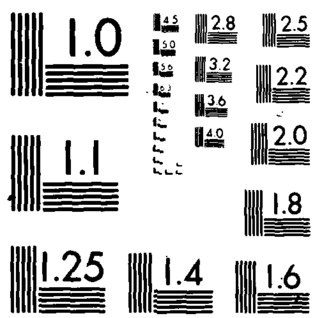

MICROCOPY RESOLUTION TEST CHART
NATIONAL BUREAU OF STANDARDS-1963-A

Y=112.375 INCHES

DATE: 4- 7-75
DS 112W

L.D.V. MEASUREMENTS

Y (INS.)	U (F.P.S.)	u'^2 (F.P.S.)^2	S_u	F_u	γ_u	
.01000	11.95000	21.94370	.35406	2.77096	1.00000	
.01500	13.48600	22.70751	.23337	2.56509	1.00000	
.02000	15.30500	22.51549	.16510	2.72763	1.00000	
.02500	16.07400	22.15098	.14428	2.72477	1.00000	
.03000	16.78800	21.84142	.12810	2.75458	1.00000	
.04000	17.55700	21.57759	.15934	2.78176	1.00000	
.05000	18.58000	21.54157	.20763	2.34562	1.00000	
.06500	19.96000	21.72912	.16491	2.79376	1.00000	
.08500	19.94400	21.49528	.20306	2.77496	1.00000	
.11000	20.75700	22.04575	.17754	2.70641	1.00000	
.15000	22.01900	23.06584	.18533	2.76498	1.00000	
.20000	23.17600	23.55529	.17045	2.76777	1.00000	
.25000	24.94600	25.33595	.12687	2.67902	1.00000	
.35000	26.87100	27.17016	.09782	2.59182	1.00000	
.50000	29.09500	26.93491	.04668	2.66371	1.00000	
1.50000	46.63000	15.12390	-.53236	3.20990	1.00000	
2.50000	54.59200	.74911	-.29490	4.14666	1.00000	(F.S.)

Y (INS.)	V (F.P.S.)	v'^2 (F.P.S.)^2	S_v	F_v	γ_v	
.01000	.10200	.49735	N.A.	6.46840	.62021	
.01500	N.A.	.77539	.06839	5.19506	.65195	
.02000	N.A.	1.60329	N.A.	4.45116	.64567	
.02500	-.04000	2.00715	-.13859	3.32442	.46303	
.03000	.02500	2.49817	-.07698	3.80561	.48725	
.04000	-.05400	3.21596	-.03630	3.62061	.50859	
.05000	-.01200	3.85993	-.07193	3.42187	.47937	
.06500	-.00600	4.28505	-.09081	3.33124	.47975	
.08500	.05900	5.03459	-.07642	3.36641	.51765	
.11000	.07400	5.65132	-.14433	3.27096	.57503	
.15000	.61900	6.34159	-.13300	3.21252	.57916	
.20000	.50400	7.50050	-.09841	3.12960	.56532	
.25000	.71900	8.47133	-.04704	3.17695	.56617	
.35000	.74900	8.73493	-.06381	2.96190	.58052	
.50000	1.10400	9.65525	-.04163	2.93787	.65880	
1.50000	2.60500	5.12008	.30200	3.09020	.83918	
2.50000	3.00800	.85596	.96568	5.38553	1.00000	(F.S.)

Y (INS.)	U-V (F.P.S.)	$-\overline{uv}$ (F.P.S.)^2	S_{u-v}	F_{u-v}	γ_{u-v}	
.01000	12.77305	2.93440	.17147	3.26557	.99321	
.01500	12.23253	2.50250	.32267	2.66254	1.00000	
.02000	14.65785	2.66450	.17663	2.75635	1.00000	
.02500	15.66954	2.57560	.13270	2.54201	.99940	
.03000	16.35239	3.14590	.06645	2.71378	1.00000	
.04000	17.47325	3.23940	.10775	[illegible]	.99965	
.05000	18.21359	3.57840	.12237	2.46035	1.00000	
.06500	18.50622	3.47930	.15352	1.94472	1.00000	
.08500	19.5982[illegible]	4.15070	.15526	2.51018	1.00000	
.11000	20.14932	[illegible]	.05959	3.00051	.99934	
.15000	21.44735	4.62410	.17356	2.56425	.99949	
.20000	22.46174	4.68110	.04984	3.07570	1.00000	
.25000	24.20444	5.71120	.07548	3.03142	1.00000	
.35000	25.23462	6.62510	.02544	2.66394	1.00000	
.50000	29.87963	7.49370	-.04450	2.77751	1.00000	
1.50000	43.88545	3.22707	-.48376	3.12650	1.00000	
2.50000	51.32415	-.23914	-.30892	4.32420	1.00000	(F.S.)

X=116.500 INCHES

DATE: 3-17-76
DS 11F.

L.D.V. MEASUREMENTS

Y (INS.)	U (F.P.S.)	$\overline{u'^2}$ (F.P.S.)^2	S_u	F_u	∂_u	
.00500	2.04500	1.03564	.95547	4.14150	.99923	
.01000	4.28500	2.95466	.44135	2.99507	1.00000	
.01500	7.0[illegible]	13.35707	.29711	3.05001	1.00000	
.02000	8.14900	16.04003	.41349	2.87594	.99331	
.02500	10.10100	16.79213	.35029	2.52674	.99960	
.03000	9.75900	15.43792	.35632	2.52537	.99958	
.04000	11.65700	17.18509	.27289	2.76315	1.00000	
.05000	12.03800	17.20640	.23950	2.76341	1.00000	
.06500	12.89700	16.94393	.22893	2.77073	1.00000	
.08500	13.42500	17.33136	.26329	2.58206	1.00000	
.11000	14.13700	18.75440	.21792	2.74020	1.00000	
.15000	15.07900	19.47122	.20933	2.90510	1.00000	
.20000	16.12900	20.30377	.18587	2.70053	1.00000	
.28000	17.41300	22.71947	.20055	2.92608	.99981	
.38000	18.91700	24.17473	.17890	2.76364	1.00000	
.50000	20.60000	25.51432	.14855	2.62719	1.00000	
1.50000	36.97600	24.23977	-.22393	2.72255	1.00000	
3.00000	51.17300	.76615	-.33653	5.08845	1.00000	(F.S.)

Y (INS.)	V (F.P.S.)	$\overline{v'^2}$ (F.P.S.)^2	S_v	F_v	∂_v	
.00500	.27900	.02291	.39996	N.A.	.98195	
.01000	.75100	.06356	N.A.	5.78263	.88250	
.01500	.17400	.43815	.09230	4.55006	.62517	
.02000	-.04400	.83435	-.26539	4.74966	N.A.	
.02500	.17000	1.23505	-.15183	4.42980	.60512	
.03000	.14700	1.03193	-.15717	4.19062	.56474	
.04000	.22000	1.85039	-.10376	3.45158	.55446	
.05000	.29400	2.55479	-.14557	3.61496	.63171	
.06500	.35700	2.91235	-.05643	3.67269	.59769	
.08500	.40400	3.59387	-.14990	3.44937	.65732	
.11000	.48400	4.35346	-.16729	3.40459	.62079	
.15000	.56500	4.91267	-.13607	3.19555	.62198	
.20000	.66700	5.56776	-.06542	3.44441	.61423	
.28000	1.04100	6.77496	-.14937	3.05196	.62524	
.38000	1.22400	6.06094	-.23170	3.24160	.69615	
.50000	1.41100	5.95201	-.12839	2.98998	.71463	
1.50000	3.31600	2.59932	.09017	2.69582	.66550	
3.00000	4.93100	1.01744	.98558	5.35647	1.00000	(F.S.)

Y (INS.)	U-V (F.P.S.)	$-\overline{uv}$ (F.P.S.)^2	S_{u-v}	F_{u-v}	∂_{u-v}	
.00500	2.02513	.02459	N.A.	3.39162	.99839	
.01000	7.23755	.67530	.08174	2.76588	1.00000	
.01500	7.37930	.17550	N.A.	3.17733	.99765	
.02000	8.90997	1.30870	.39412	2.85068	.99293	
.02500	9.79416	1.49270	.34277	2.74600	.99753	
.03000	9.90223	1.58820	.34637	2.91925	.99696	
.04000	10.43905	1.74531	.21517	2.83301	.99719	
.05000	11.98393	1.63890	.22628	2.50790	.99842	
.06500	12.03701	1.88300	.12714	2.75432	.99715	
.08500	13.11571	1.91240	.16980	2.82060	.99957	
.11000	13.47914	1.71930	.15468	3.04447	.99833	
.15000	14.48424	2.06600	.23938	2.91810	.99965	
.20000	15.78670	2.39440	.18322	2.80477	1.00000	
.28000	16.77121	2.60922	.20911	2.82514	.99971	
.38000	18.04943	3.97930	.22474	2.84454	1.00000	
.50000	19.69192	4.64316	.11251	2.76253	1.00000	
1.50000	33.76544	N.A.	-.29935	2.76004	1.00000	
3.00000	44.20333	-.07266	-1.35006	7.82474	1.00000	(F.S.)

[illegible] DATE: 5-24-76
CS 120

L.D.V. MEASUREMENTS

Y (INS.)	U (F.P.S.)	$\overline{u'^2}$ (F.P.S.)^2	S_u	F_u	η_u	
.01000	N.A.	4.22479	N.A.	2.96855	.99952	
.01500	4.98400	6.14976	.55478	3.06259	.99113	
.02000	N.A.	10.26479	.55534	3.27161	.99115	
.02500	7.44100	13.75648	.46567	2.96947	.99436	
.03000	8.54800	15.41143	.42006	3.03393	.99703	
.04000	9.50500	15.67122	.45505	3.65679	.99954	
.05000	10.13300	16.57093	.32657	2.91207	.99950	
.06500	10.69900	16.93454	.27765	2.55246	.99953	
.08500	11.86500	17.61340	.29354	2.86059	1.00000	
.11000	12.49900	18.52209	.27710	2.53638	1.00000	
.15000	13.33700	19.45013	.25983	2.82195	1.00000	
.20000	14.10300	20.22931	.21114	2.75807	1.00000	
.28000	15.33700	22.32326	.22106	2.79010	1.00000	
.38000	16.66200	24.46757	.21056	2.75386	1.00000	
.50000	18.43700	26.29474	.15956	2.60829	1.00000	
1.50000	34.34600	27.03740	-.21217	2.78640	1.00000	
3.00000	50.17700	1.63612	-1.01956	5.94677	1.00000	(F.S.)

Y (INS.)	V (F.P.S.)	$\overline{v'^2}$ (F.P.S.)^2	S_v	F_v	η_v	
.01000	.10100	.21856	.37014	N.A.	.55053	
.01500	.21000	.59276	-.12819	5.71255	.63079	
.02000	.30500	.61260	-.09036	6.47046	.71233	
.02500	.29900	.80215	.00631	6.62627	.70254	
.03000	.43100	.85651	-.07200	4.54606	.70559	
.04000	.18500	1.47309	-.20028	3.70061	.57036	
.05000	.22900	1.85177	-.17527	3.56632	.60414	
.06500	.29300	2.54065	-.26110	3.54070	.63167	
.08500	.15700	3.54795	-.14315	3.39364	.57575	
.11000	.20000	4.15513	-.16873	3.22725	.56407	
.15000	.37900	4.91550	-.17103	3.28105	.56404	
.20000	.21200	5.65247	-.22396	3.36434	.55262	
.28000	.74300	7.15231	-.19578	3.10449	.65669	
.38000	1.04700	7.94614	-.12435	3.01432	.61770	
.50000	1.20500	8.85134	-.17359	3.03586	.66788	
1.50000	2.78200	9.91211	.10091	2.90363	.80057	
3.00000	4.57500	2.21391	.09886	4.92981	1.00000	(F.S.)

Y (INS.)	U-V (F.P.S.)	$-\overline{uv}$ (F.P.S.)^2	S_{u-v}	F_{u-v}	η_{u-v}	
.01000	N.A.	-.00039	N.A.	2.82225	1.00000	
.01500	4.41780	N.A.	.52821	3.10214	.97730	
.02000	5.67043	.74793	.74915	3.46903	.98439	
.02500	6.98332	N.A.	.50605	3.02450	.98357	
.03000	7.93503	.35730	.39462	2.79421	.98670	
.04000	9.14543	1.13360	.33962	3.02270	.99346	
.05000	9.93723	1.40420	.22159	2.65834	.99013	
.06500	10.77196	1.39530	.21970	2.95823	.99425	
.08500	11.73643	2.22710	.20151	2.85363	.99509	
.11000	12.75540	2.54270	.24439	2.47913	.99588	
.15000	12.95044	2.96120	.23083	2.33555	.99545	
.20000	13.73047	3.35530	.26122	2.35834	.99649	
.28000	14.59294	3.54220	.17986	2.77440	.99790	
.38000	15.97793	3.49330	.18814	2.74759	.99683	
.50000	17.56575	4.19750	.17232	2.75362	.99972	
1.50000	31.51762	5.93453	-.21482	2.76341	1.00000	
3.00000	45.27985	.30921	-1.25127	5.60459	1.00000	(F.S.)

X=122.625 INCHES

DATE: 3-24-76
IS 122.

L.D.V. MEASUREMENTS

Y (INS.)	U (F.P.S.)	$\overline{u'^2}$ (F.P.S.)^2	S_u	F_u	γ_u
.01000	3.94500	6.20227	.78556	3.60135	.99446
.01500	5.37000	11.00063	.63517	3.26765	.99025
.02000	6.70800	13.73579	.48305	3.07943	.99709
.02500	7.21700	15.03412	.43547	2.96314	.99656
.03000	7.74800	15.07940	.34461	2.83409	.99331
.04000	8.17400	15.89415	.34650	2.87015	.99075
.05000	8.77300	16.05403	.32073	2.89168	.99434
.06500	9.06500	16.47593	.31788	2.91472	.99556
.08500	9.62400	17.15451	.25707	2.80440	.99669
.11000	10.38000	17.67429	.29653	2.96757	.99922
.15000	11.06000	18.53526	.26415	2.89380	.99794
.20000	11.71800	20.06449	.23685	2.81057	.99935
.28000	12.89600	21.15095	.21477	2.80783	.99966
.38000	14.14000	23.10677	.19450	2.74268	1.00000
.50000	15.64600	25.15273	.15592	2.75630	1.00000
1.50000	30.34900	31.20742	-.13485	2.68172	1.00000
3.50000	49.64600	.65299	-.13621	4.02409	1.00000 (F.S.)

Y (INS.)	V (F.P.S.)	$\overline{v'^2}$ (F.P.S.)^2	S_v	F_v	γ_v
.01000	-.02200	.17557	.18735	6.29043	.47946
.01500	.13400	.50451	N.A.	N.A.	.61429
.02000	.11400	.75599	-.21440	5.54659	.56674
.02500	.00900	1.00162	-.24839	4.71315	.53291
.03000	.06800	1.32456	-.18513	4.43182	.51468
.04000	-.02200	1.64427	-.25105	4.11125	.45791
.05000	-.03900	2.12818	-.18606	3.60941	.50030
.06500	.04400	2.57715	-.28137	4.22460	.55605
.08500	.00600	3.06591	-.12980	3.42028	.49267
.11000	.00100	3.75845	-.08741	3.28717	.50911
.15000	.06900	4.35415	-.17853	3.50179	.54431
.20000	.18500	5.06733	-.19052	3.28679	.56665
.28000	.59900	6.65026	-.13938	3.23459	.59716
.38000	.89400	6.31055	-.11400	3.34482	.67060
.50000	1.07100	9.74020	N.A.	N.A.	.62768
1.50000	2.97400	10.52665	.04382	2.90634	.79860
3.50000	4.93000	.79171	1.08254	6.96020	1.00000 (F.S.)

Y (INS.)	U-V (F.P.S.)	$-\overline{uv}$ (F.P.S.)^2	$S_{u\text{-}v}$	$F_{u\text{-}v}$	$\gamma_{u\text{-}v}$
.01000	4.17755	.53919	.68671	3.29496	.94378
.01500	5.74731	.49559	.55754	3.34769	.97548
.02000	6.73866	.87400	.41890	3.05609	.97409
.02500	7.21283	1.06540	.43193	2.99165	.98105
.03000	7.65789	1.50000	.36612	2.95929	.97431
.04000	8.19470	1.36350	.31103	2.89773	.97421
.05000	9.00136	1.35790	.26346	2.86090	.97826
.06500	8.96515	1.02400	.27763	2.85764	.98331
.08500	9.64243	1.47020	.27522	2.91357	.98115
.11000	10.48205	1.56270	.24833	2.95691	.99231
.15000	10.93934	1.59920	.21739	2.95033	.95479
.20000	11.51017	2.32410	.22383	2.95679	.98829
.28000	12.44072	2.34610	.26806	2.90554	.99409
.38000	13.86765	2.67340	.21068	2.82584	.99544
.50000	15.17626	3.61613	.22370	2.53589	.99609
1.50000	27.76357	7.66727	-.21794	2.77763	1.00000
3.50000	44.96732	.39010	N.A.	N.A.	1.00000 (F.S.)

X=127.125 INCHES

DATE: 2- 3-73
AS 127

L.D.V. MEASUREMENTS

Y (INS.)	U (F.P.S.)	$\overline{u'^2}$ (F.P.S.)^2	S_u	F_u	η_u	
.00200	.64100	.42367	.53945	4.11623	.84640	
.00500	N.A.	N.A.	N.A.	N.A.	.97567	
.00700	1.05800	.65370	.44902	3.20946	.93004	
.01000	1.05100	.83909	.35969	2.95557	.90017	
.01500	1.72200	1.34054	.29146	2.86959	.93968	
.02000	2.69900	1.60653	.12175	2.60372	.98652	
.02500	2.97700	1.74754	N.A.	2.74669	.98552	
.03500	N.A.	2.95097	N.A.	2.65871	.99990	
.04500	3.87900	12.10149	.17435	2.61894	.85344	
.06500	N.A.	15.13063	.19809	3.30219	.94605	
.08000	5.18900	16.57130	N.A.	3.47524	.90143	
.10000	N.A.	15.57073	.39955	3.39314	.85959	
.12500	5.89900	15.14954	.28659	3.27115	.92065	
.16000	6.02200	18.30050	.27581	3.26783	.92497	
.20000	6.82700	19.19165	.11573	3.31016	.94449	
.25000	6.90100	21.55240	.37027	3.46044	.94315	
.32000	8.77900	19.47551	.13742	3.19901	.95553	
.40000	8.54700	21.65473	.24272	2.84291	.98211	
.52000	9.88700	23.13312	N.A.	2.96692	.98540	
.64000	10.55300	29.18517	.37234	3.50150	.93161	
.80000	12.81500	31.57013	.16250	2.80301	.99566	
1.00000	15.97900	32.63033	.11725	2.71467	1.00000	
1.20000	17.59700	30.15987	.04304	2.65290	1.00000	
1.50000	21.92100	33.89778	-.00026	2.67700	1.00000	
1.90000	27.64700	32.75057	-.04057	2.57229	1.00000	
2.40000	35.25900	24.04100	-.10857	3.27674	1.00000	
3.00000	43.83700	11.74453	N.A.	3.28774	1.00000	
3.50000	47.06300	4.35140	N.A.	4.99043	1.00000	
4.00000	48.43300	.71910	-.59780	12.47213	1.00000	(F.S.)

Y (INS.)	V (F.P.S.)	$\overline{v'^2}$ (F.P.S.)^2	S_v	F_v	η_v	
.00200	-.09400	.01021	N.A.	3.81442	N.A.	
.00500	.15700	.02915	N.A.	N.A.	N.A.	
.00700	.19300	.02403	N.A.	N.A.	N.A.	
.01000	.17500	.02443	N.A.	N.A.	N.A.	
.01500	-.11100	.01536	.05563	N.A.	N.A.	
.02000	-.14400	.04637	.14851	4.04021	N.A.	
.02500	-.10400	.16620	-.15791	3.99570	.39825	
.03500	N.A.	.52528	-.34794	4.06299	N.A.	
.04500	N.A.	.75315	-.13752	3.36490	.38350	
.06500	N.A.	1.56059	-.41967	4.04372	.37625	
.08000	N.A.	2.35539	N.A.	N.A.	.43545	
.10000	-.18700	2.54243	-.26139	3.48180	.47464	
.12500	-.20700	3.14001	-.36337	3.69723	.48023	
.16000	N.A.	N.A.	N.A.	N.A.	.23547	
.20000	-.13300	3.93550	-.29761	2.97879	.48747	
.32000	-.04900	5.00001	-.17339	2.91510	.49137	
.40000	-.03000	5.83159	-.02955	3.13646	.49023	
.52000	.22300	6.71929	-.20231	3.02266	.54349	
.64000	.38300	8.51467	-.25718	2.99751	.55395	
.80000	.55900	9.65277	-.18955	2.91612	.59542	
1.00000	1.08100	9.92504	-.11279	3.18805	.65853	
1.20000	1.86500	11.82590	-.25739	N.A.	.66044	
1.50000	1.97500	12.75604	N.A.	N.A.	.71063	
1.90000	2.56100	11.10209	.02919	3.21835	.76943	
2.40000	4.22000	10.73307	-.19050	N.A.	.91870	
3.00000	5.78400	5.20976	.22564	2.81544	.99576	
3.50000	6.57800	3.30971	.53594	3.78545	.99997	
4.00000	N.A.	.01493	N.A.	7.92031	.99875	(F.S.)

Y (INS.)	U-V (F.P.S.)	$-\overline{uv}$ (F.P.S.)^2	S_{u-v}	F_{u-v}	R_{u-v}	
.00200	N.A.	-.19142	.19587	3.11164	.97328	
.00500	N.A.	-.02009	.20852	2.57292	.99143	
.00700	1.26395	.13191	N.A.	N.A.	.92727	
.01000	N.A.	.31063	.09426	2.56710	.95457	
.01500	1.41754	-.13712	.20003	2.94205	.94798	
.02000	2.47525	-.15509	-.01077	2.83020	.95345	
.02500	3.29504	-.09503	-.05706	2.71386	.99749	
.03500	3.07589	N.A.	.27745	2.79406	N.A.	
.04500	4.93737	2.97212	N.A.	N.A.	.89529	
.06500	5.04162	3.45730	N.A.	N.A.	.85993	
.08000	5.36123	2.54010	N.A.	N.A.	.89476	
.10000	5.31[illegible]	2.91300	.09204	2.73954	.88730	
.12500	6.10935	2.62510	.38530	N.A.	.89610	
.16000	5.92257	2.31270	.12793	2.96222	.89205	
.20000	6.54153	2.40520	.34934	3.20792	.93214	
.25000	6.79139	2.44510	.37256	2.96522	.92697	
.32000	8.092[illegible]	2.52595	.47070	3.32001	.92349	
.40000	8.34375	2.77056	.32658	3.05519	.93543	
.50000	9.17535	3.16340	.26090	2.92546	.93647	
.64000	10.65553	3.47750	.27231	2.92561	.95994	
.80000	11.92974	3.47950	.12411	2.62154	.97300	
1.00000	14.11795	4.35190	.13757	2.68151	.97567	
1.20000	16.04975	4.56000	.09961	2.54173	.99199	
1.50000	22.90680	4.62950	-.09602	2.62961	1.00000	
1.70000	23.07267	4.52170	-.31357	3.17899	.95507	
2.40000	31.17150	3.90100	-.26522	3.06927	1.00000	
3.00000	36.39302	3.14210	-.54861	3.12281	1.00000	
3.50000	39.06566	2.79250	-1.44010	N.A.	1.00000	
4.00000	40.95331	1.00010	-1.01262	7.42363	1.00000	(F.S.)

X=129.375 INCHES

DATE: 3-27-79
DS 129W

L.D.V. MEASUREMENTS

Y (INS.)	U (F.P.S.)	$\overline{u'^2}$ (F.P.S.)^2	S_u	F_u	γ_u	
.01000	1.18000	5.55150	.53056	3.36841	.69013	
.01500	1.90300	7.53370	.44918	3.47703	.77793	
.02000	2.39700	9.34040	.38429	3.41922	.75154	
.02500	2.71000	10.31759	.32353	3.20329	.79956	
.03000	2.94900	11.30495	.39103	3.17139	.80841	
.04000	3.22900	13.40775	.29422	3.10570	.81691	
.05000	3.54500	14.59080	.30159	3.19075	.82513	
.06500	3.54900	15.61525	.24324	3.00463	.83945	
.08500	4.01100	15.90430	.19347	2.91337	.84294	
.11000	4.22000	16.57375	.14436	2.84109	.85052	
.15000	4.47500	17.71779	.12893	2.89058	.85842	
.20000	4.98700	19.15457	.16719	2.90594	.85973	
.28000	5.33300	20.67512	.16401	2.92053	.91230	
.38000	5.96600	21.31363	.13719	2.87090	.92716	
.50000	7.90500	23.36525	.17497	2.85627	.96028	
.70000	9.80700	26.95230	.18294	2.76204	.97963	
1.00000	13.20900	32.90904	.09072	2.51395	.99376	
1.50000	19.72500	36.55017	.02087	2.67801	1.00000	
5.00000	47.74300	.46301	.00795	2.77696	1.00000	(F.S.)

Y (INS.)	V (F.P.S.)	$\overline{v'^2}$ (F.P.S.)^2	S_v	F_v	γ_v	
.01000	-.18900	.13356	-.53147	6.11196	.24477	
.01500	-.12200	.27424	-.42994	5.93046	.37771	
.02000	-.06400	.70776	-.59742	N.A.	.45235	
.02500	.00900	.97929	N.A.	N.A.	.49483	
.03000	-.02400	.93583	-.52538	5.35625	.57170	
.04000	.02700	1.35973	-.36335	4.99320	.53956	
.05000	.03400	1.81324	-.43451	4.27456	.55568	
.06500	.05100	2.52159	N.A.	5.47691	.52255	
.08500	.07500	2.32437	-.29573	3.33783	.55315	
.11000	-.09300	2.88306	-.26042	3.99359	.51769	
.15000	.10100	3.45347	-.27047	3.79411	.55810	
.20000	.17100	4.10054	-.26165	3.42620	.56977	
.28000	.70700	5.51137	-.26896	3.21131	.60674	
.38000	.80700	6.44119	-.21401	3.14979	.67053	
.50000	.85000	7.46213	-.29529	3.45133	.63327	
.70000	1.15700	8.57436	-.29935	3.33623	.68815	
1.00000	1.42200	10.74573	-.19564	3.27234	.67649	
1.50000	2.37200	11.60717	-.06649	2.91053	.74174	
5.00000	5.86700	.40457	.21468	3.33285	1.00000	(F.S.)

Y (INS.)	U-V (F.P.S.)	$-\overline{uv}$ (F.P.S.)^2	S_{u-v}	F_{u-v}	γ_{u-v}	
.01000	1.34490	.76770	.48120	3.63317	.70638	
.01500	2.28575	1.23260	.39792	3.67541	.79045	
.02000	2.57925	.95750	.43756	3.28727	.77363	
.02500	2.88951	1.13950	.38571	3.37769	.76071	
.03000	2.92032	.52329	.33241	3.09811	.80799	
.04000	3.23003	.43430	.25050	3.00637	.77239	
.05000	3.51641	.39310	.26245	3.21472	.80260	
.06500	3.46903	.72170	.25903	3.13937	.79124	
.08500	3.79512	1.03340	.17434	3.30310	.82774	
.11000	3.95037	1.31450	.19955	3.11233	.81237	
.15000	4.55747	1.55744	.20593	3.00573	.81334	
.20000	4.95477	1.67820	.26028	3.00348	.83451	
.28000	6.24995	1.87220	.21223	2.95488	.87920	
.38000	4.57544	2.44320	.29970	2.79300	.89995	
.50000	7.49507	2.93550	.19490	2.88665	.89911	
.70000	9.01411	N.A.	-.02328	N.A.	.90135	
1.00000	12.10414	3.55814	.11861	2.77633	.95936	
1.50000	17.11455	5.30543	.02449	2.74032	.99225	
5.00000	40.80341	-.12351	-.12959	3.00975	1.00000	(F.S.)

Y=131.875 INCHES

DATE: 3-29-79
DS 131W

L.D.V. MEASUREMENTS

Y (INS.)	U (F.P.S.)	$\overline{u'^2}$ (F.P.S.)^2	S_u	F_u	γ_u	
.01000	.21000	4.95512	.38198	3.77343	.53375	
.01500	1.19300	6.35051	.34745	3.67149	.64007	
.02000	1.44900	8.75593	.41719	3.75046	.64942	
.02500	1.42100	9.23145	.26332	3.35451	.64964	
.03000	1.70900	10.45591	.36219	3.26622	.70994	
.04000	1.97000	11.86593	.23515	3.18735	.73205	
.05000	1.95100	13.39955	.17532	2.95986	.69317	
.06500	2.25900	14.64738	.25883	3.07493	.69647	
.08500	2.37700	16.42819	.16008	2.96287	.71239	
.11000	2.59900	16.02759	.15838	2.93293	.71693	
.15000	3.21400	17.61125	.20807	2.99309	.78056	
.20000	3.19400	18.37185	.21502	2.99443	.74859	
.28000	3.90300	19.62472	.15253	2.94142	.60532	
.38000	4.70500	22.30749	.15443	2.90749	.85403	
.50000	5.79800	23.31027	.20751	3.06856	.88274	
.70000	7.49900	26.34532	.24572	2.95214	.92897	
1.00000	10.16200	24.80765	.16079	2.91979	.96943	
1.50000	15.95300	37.63649	.04544	2.32968	.99537	
2.00000	21.64700	40.33360	-.10539	2.77192	1.00000	
2.50000	28.70200	39.21452	-.20073	2.85409	1.00000	
5.00000	46.79900	.54237	.04208	2.96491	1.00000	(F.S.)

Y (INS.)	V (F.P.S.)	$\overline{v'^2}$ (F.P.S.)^2	S_v	F_v	γ_v	
.01000	-.17300	.11677	-.30372	6.03226	.24920	
.01500	-.08900	.19355	-.45611	5.99691	.41035	
.02000	.03000	.32774	-.54311	7.24324	.59799	
.02500	.08600	.45465	N.A.	6.48745	.62410	
.03000	.05100	.55675	-.48579	5.36349	.56345	
.04000	.04700	1.14659	-.32116	5.43868	.52905	
.05000	-.01600	1.53972	-.42634	4.80436	.55679	
.06500	-.03600	1.96171	-.49866	4.39563	.51705	
.08500	-.02400	2.41812	N.A.	4.70917	.52156	
.11000	.05600	2.50775	-.36048	4.39327	.56624	
.15000	.12300	3.43187	-.38901	3.90837	.57164	
.20000	-.01000	3.70220	-.22318	3.53616	.54069	
.28000	.10400	4.62508	-.39673	3.54246	.54339	
.38000	.66900	5.68007	-.27367	3.66957	.63008	
.50000	.81600	7.56325	N.A.	4.22609	.65360	
.70000	.99000	8.71135	-.22048	3.24136	.64632	
1.00000	1.80300	10.09469	-.15206	3.43124	.71647	
1.50000	2.15700	11.45543	-.09517	3.02029	.75271	
2.00000	2.71300	12.44319	-.04090	2.91797	.80453	
2.50000	2.97900	12.15747	.04343	2.95891	.87063	
5.00000	6.26300	.53337	.27551	3.29304	1.00000	(F.S.)

Y (INS.)	U-V (F.P.S.)	$-\overline{uv}$ (F.P.S.)^2	$S_{u\text{-}v}$	$F_{u\text{-}v}$	$\gamma_{u\text{-}v}$	
.01000	.57134	.59556	.25314	3.65532	.56952	
.01500	1.73743	.60477	.35045	3.76060	.67841	
.02000	1.40229	.45490	.43100	4.02233	.69392	
.02500	1.67517	.40780	.31039	3.67770	.70728	
.03000	1.71957	.48290	.27762	3.51237	.65999	
.04000	1.84977	.44071	.30047	3.16559	.67278	
.05000	2.1693[illegible]	.62510	.18305	3.426[illegible]	.67321	
.06500	2.44796	.84430	.30456	3.19215	.68674	
.08500	2.55797	.97120	.20707	2.98345	.71323	
.11000	2.59940	1.35340	.23719	3.05935	.70958	
.15000	3.09943	1.75430	.27515	3.00835	.71819	
.20000	3.37711	2.38850	.27184	3.00003	.75409	
.28000	3.49307	2.72400	.22114	3.07240	.74010	
.38000	4.52544	2.93440	.21355	2.97574	.75957	
.50000	5.50124	3.11570	.33427	3.13017	.81517	
.70000	7.35523	4.07860	.20427	3.17414	.88576	
1.00000	9.44610	5.09370	.18993	2.86787	.93151	
1.50000	14.22984	5.50401	.02130	2.74539	.96717	
2.00000	19.16837	5.95456	-.07715	2.44042	.99386	
2.50000	24.40934	5.54237	-.20473	2.49655	.99874	
5.00000	40.08837	-.03349	N.A.	4.59145	1.00000	(F.S.)

X=134.500 INCHES

DATE: 3-31-78
DS 134W

L.D.V. MEASUREMENTS

Y (INS.)	U (F.P.S.)	$\overline{u'^2}$ (F.P.S.)^2	S_u	F_u	η_u	
.01000	.33900	3.47099	.24184	3.15824	.81260	
.01500	.41000	7.84930	.21034	3.43660	.53791	
.02000	.55500	8.93747	.21894	3.43970	.54916	
.02500	.51300	9.68310	.20759	3.26640	.56294	
.03000	.37900	10.81772	.26780	3.23090	.53907	
.04000	.40900	12.27073	.19478	3.12903	.53243	
.05000	.49900	13.07459	.29788	3.17101	.51202	
.06500	.29500	13.48182	.20914	3.09034	.51733	
.08500	.65300	14.99580	.13563	3.00533	.56030	
.11000	.94300	15.59363	.15657	2.90602	.60437	
.15000	.78800	17.64907	.16898	3.06947	.56576	
.20000	1.10200	19.45530	.20457	2.95707	.57391	
.28000	1.69300	20.06458	.23411	3.00783	.65500	
.38000	2.24500	21.21800	.24213	2.96619	.65899	
.50000	2.76900	25.04572	.16656	2.87303	.70554	
.70000	4.22500	26.66710	.15056	2.79474	.77025	
1.00000	6.48000	32.61872	.17075	2.95400	.89313	
1.50000	11.40000	39.34902	.10329	2.71173	.97567	
2.00000	17.12800	45.85567	-.00179	2.90113	.99227	
2.50000	22.92400	46.04303	-.11832	2.58839	1.00000	
3.00000	29.01900	44.23753	-.32813	3.16629	.99939	
4.00000	46.82400	.52634	-.09223	3.01351	1.00000	(F.S.)

Y (INS.)	V (F.P.S.)	$\overline{v'^2}$ (F.P.S.)^2	S_v	F_v	η_v	
.01000	.24400	.09280	.38233	4.92660	.79967	
.01500	.08700	.28511	-.41647	5.54992	.63126	
.02000	.05300	.43743	-.27589	5.46025	.59831	
.02500	.04700	.49303	-.25961	5.42490	.55136	
.03000	.07800	.67483	-.24252	4.95882	.54564	
.04000	.03700	1.00192	N.A.	4.92931	.58270	
.05000	.04300	1.10774	-.28044	3.86877	.54169	
.06500	.07300	1.42299	-.28879	4.02676	.52159	
.08500	.01700	1.95035	-.29446	4.06406	.50992	
.11000	.10900	2.51470	-.34843	4.05561	.53506	
.15000	.05100	2.88514	-.34921	4.17885	.51952	
.20000	.11800	3.47334	-.43192	4.10289	.52703	
.28000	.17700	4.47319	-.36717	3.90705	.55269	
.38000	.56300	6.05312	-.30036	3.64063	.59540	
.50000	.60700	6.79348	-.40978	3.59738	.65269	
.70000	.85800	7.85216	-.25574	3.30762	.60711	
1.00000	.94700	10.26222	-.23711	3.37784	.64009	
1.50000	1.62100	12.90946	-.21428	3.15069	.71602	
2.00000	2.52100	13.55359	-.02707	3.10857	.75892	
2.50000	3.72800	14.22097	-.08034	2.97514	.79751	
3.00000	4.33100	13.47917	.20198	3.05343	.89280	
4.00000	6.72400	.50000	N.A.	2.79465	1.00000	(F.S.)

Y (INS.)	U-V (F.P.S.)	$-\overline{uv}$ (F.P.S.)^2	$S_{u\text{-}v}$	$F_{u\text{-}v}$	$\eta_{u\text{-}v}$	
.01000	.08768	1.23321	.31159	3.88743	.47686	
.01500	.53174	.26620	.26238	3.60876	.55684	
.02000	.36345	.36470	.17934	3.51075	.54659	
.02500	.38466	.44130	.16324	3.46380	.53650	
.03000	.45820	.53750	.08626	3.44939	.52093	
.04000	.47800	.73550	.15567	3.51765	.56222	
.05000	.32244	.91910	.24849	3.38086	.49230	
.06500	.61235	1.04810	.16444	3.12684	.57313	
.08500	.68730	1.24570	.21373	3.28938	.57216	
.11000	1.09752	1.39640	.23463	N.A.	.57871	
.15000	.99415	1.67280	.21063	3.51713	.54572	
.20000	.93471	1.93440	.26915	3.24147	.55533	
.28000	1.17520	2.25510	.27393	3.16943	.57253	
.38000	1.98124	2.24530	.26279	3.10233	.61758	
.50000	2.53940	N.A.	.30552	3.11525	.63895	
.70000	3.81025	3.95360	.23773	3.13253	.70162	
1.00000	6.73747	N.A.	.24817	2.97674	.82666	
1.50000	9.71414	5.94427	.03833	3.10381	.87929	
2.00000	14.71172	7.09141	.02131	2.87285	.95039	
2.50000	19.43575	7.46279	-.11941	2.76013	.98589	
3.00000	24.36384	7.03492	-.28309	2.82955	.99657	
4.00000	39.57425	-.11593	-.15823	3.34267	1.00000	(F.S.)

X=138.750 INCHES

DATE: 3- 3-78
DS 138

L.D.V. MEASUREMENTS

Y (INS.)	U (F.P.S.)	$\overline{u'^2}$ (F.P.S.)^2	S_u	F_u	γ_u
.01000	-.79300	3.01766	-.14094	3.97369	.30476
.01500	-.85500	5.23673	-.04006	3.50813	.34828
.02000	-1.16100	7.39405	-.02055	3.35462	.31531
.03000	N.A.	9.33804	.03129	3.24254	.45544
.04000	-1.43500	10.65415	.06161	3.13007	.33547
.06000	-1.39300	12.31329	.13471	3.24062	.34677
.08500	-1.74400	12.90550	.19365	3.08570	.30863
.12000	-1.47600	14.74941	.15847	2.92504	.32971
.17000	-1.51800	15.15380	.17770	3.01326	.32344
.25000	-1.32700	17.17066	.24987	2.93569	.35544
.35000	-1.08900	17.54349	.22294	2.86651	.38400
.50000	-.38800	20.23523	.17735	2.86272	.45210
.65000	.37900	21.91777	.24508	2.85786	.43252
1.00000	2.39100	29.03302	.20017	2.60207	.65529
2.00000	10.38700	45.03349	.09473	2.77415	.95530
3.50000	27.06200	49.81226	-.25147	3.16067	.99956
5.50000	44.47300	9.76269	-1.38128	10.83774	1.00000

Y (INS.)	V (F.P.S.)	$\overline{v'^2}$ (F.P.S.)^2	S_v	F_v	γ_v
.01000	-.14400	.15915	-.45587	5.73408	.33218
.01500	-.10200	.25982	-.39277	5.67716	.38538
.02000	-.03000	.37440	-.37516	5.07588	.47315
.03000	-.11300	.60923	-.23035	4.90009	.47598
.04000	-.04500	.79943	-.39068	5.13536	.50394
.06000	.11600	1.14354	-.31097	4.42056	.60131
.08500	.02900	1.63050	-.22319	4.19740	.50407
.12000	-.02800	2.05536	-.18311	4.09810	.49623
.17000	.09800	2.95737	-.34543	3.84225	.53412
.25000	.09000	3.45287	-.39322	3.72892	.57050
.35000	.14500	4.54755	-.40806	3.67768	.57554
.50000	.45900	5.67726	-.49524	3.71336	.64019
.65000	.33100	6.89950	-.34071	3.36018	.61095
1.00000	.63100	9.28516	-.23699	3.18935	.57696
2.00000	1.68800	14.10971	-.16252	2.93608	.69200
3.50000	4.33500	14.55575	.11790	3.04685	.69039
5.50000	8.45300	4.97575	1.09771	5.20886	1.00000

Y (INS.)	U-V (F.P.S.)	$-\overline{uv}$ (F.P.S.)^2	$S_{u\text{-}v}$	$F_{u\text{-}v}$	$\gamma_{u\text{-}v}$
.01000	-1.04792	.24253	.07257	4.15682	.24786
.01500	-1.01115	.42315	-.02444	4.12702	.32396
.02000	-1.32086	.05179	-.05452	3.27493	.32415
.03000	-1.08469	.47434	-.04909	3.27307	.35721
.04000	-1.15540	.09932	.05563	3.27923	.32965
.06000	-1.16572	.06972	.05857	3.27380	.38347
.08500	-1.19076	.55554	.13047	3.18244	.28532
.12000	-1.19641	-.09800	.19276	3.04497	.36815
.17000	-1.37177	.84946	.24246	3.13959	.37030
.25000	-1.30531	.80359	.24540	3.05455	.39816
.35000	-.87165	1.36070	.29251	3.06533	.39002
.50000	-.45962	2.29020	.33618	3.09698	.44104
.65000	.52991	2.60140	.33566	2.97966	.49746
1.00000	2.49849	4.11215	.32258	2.93101	.60571
2.00000	9.69293	6.57900	.16998	2.83399	.89997
3.50000	22.60316	6.15350	-.25251	2.32521	.99350
5.50000	36.77465	1.50200	-1.57787	6.57157	1.00000

Y=138.750 INCHES

DATE: 3- 9-78
DS 138W

L.D.V. MEASUREMENTS

Y (INS.)	U (F.P.S.)	u'^2 (F.P.S.)^2	S_u	F_u	γ_u
.01000	N.A.	2.55360	N.A.	3.21165	.65040
.02000	-.95100	7.75477	-.03907	3.48590	.36086
.02500	-1.18500	8.88927	-.00415	3.26037	.32000
.03000	-1.28400	9.66319	.03288	3.17653	.30682
.05000	-1.22700	11.57775	.11191	3.04180	.36942
.06000	-1.14900	12.75233	.09344	3.17640	.33654
.07000	-1.39400	13.34777	.10622	2.93561	.31335
.10000	-1.28100	13.60592	.13959	3.00361	.34518
.15000	-1.44700	15.93734	.14495	2.56343	.34755
.20000	-1.47300	17.13207	.15014	2.95570	.36749
.80000	1.41700	25.51595	.23676	2.81428	.59016
1.30000	4.95300	33.55038	.12366	2.79339	.78433
1.60000	9.09800	39.25915	.10096	2.79210	.91763
2.50000	14.44000	48.55025	-.05995	2.80490	.99063
3.00000	21.64000	51.50545	-.14935	2.68866	.99897
4.00000	33.00200	41.22513	-.47534	3.34529	1.00000
4.50000	37.74400	31.69403	-.65104	3.33419	1.00000
5.00000	41.49300	16.59655	-1.01656	4.20475	1.00000
6.00000	45.76000	1.03514	.20037	4.73606	1.00000 (F.S.)

Y (INS.)	V (F.P.S.)	v'^2 (F.P.S.)^2	S_v	F_v	γ_v
.01000	.07200	.07491	.91492	11.20118	.65753
.02000	.01700	.29343	N.A.	6.55218	.55539
.02500	.14400	.36443	-.20629	4.62397	.66979
.03000	.13000	.51151	-.39103	5.52327	.62751
.05000	.09700	.90234	-.28372	5.09837	.59456
.06000	.10200	1.09424	-.33341	4.59853	.56094
.07000	-.02200	1.32751	-.42769	4.30615	.45415
.10000	-.07500	2.01319	-.29050	4.36160	.53690
.15000	.01100	2.52575	-.31839	4.01913	.50500
.20000	.10500	3.14544	-.42399	3.29653	.58439
.80000	.79400	7.95173	-.29989	3.42480	.62827
1.30000	.99900	11.20395	-.37055	3.17979	.62425
1.60000	1.22000	12.72941	-.22715	3.06562	.63976
2.50000	2.42200	15.45355	-.03115	2.97473	.73966
3.00000	3.29600	15.92752	.02912	2.89500	.79717
4.00000	5.25200	12.17570	.23457	3.19029	.93833
4.50000	6.45700	9.70584	.35185	3.63099	.99696
5.00000	7.29200	7.33424	.65317	6.22700	.99627
6.00000	7.03400	1.25421	.71720	N.A.	1.00000 (F.S.)

Y (INS.)	U-V (F.P.S.)	$-\overline{uv}$ (F.P.S.)^2	$S_{u\text{-}v}$	$F_{u\text{-}v}$	$\gamma_{u\text{-}v}$
.01000	.75367	.11690	.18980	3.03908	.65298
.02000	-1.06205	.19410	.07965	3.47520	.34803
.02500	-.75235	.28690	.07810	3.36909	.41669
.03000	-.78347	.35350	.06942	3.35349	.42959
.05000	-.95034	.39550	.11622	3.27106	.39921
.06000	-1.33359	.35630	.15523	3.25158	.35585
.07000	N.A.	.35380	.17020	3.11047	.41969
.10000	-1.43117	.22910	.16320	3.25529	.36465
.15000	-1.26429	-.25620	.21278	3.25436	.35592
.20000	-1.04509	.98770	.29308	3.06979	.37902
.80000	1.28975	3.06780	.31728	2.94709	.53499
1.30000	4.47043	5.03540	.28194	2.90745	.71952
1.60000	6.63543	5.91760	.16772	2.75058	.77371
2.50000	13.97035	7.40830	.02442	2.72742	.94355
3.00000	19.52602	7.03430	-.13411	2.71778	.97056
4.00000	27.54275	5.55140	-.58172	3.47776	.99903
4.50000	30.71540	N.A.	-.89414	N.A.	.99735
5.00000	34.16565	N.A.	-1.00547	4.35735	1.00000
6.00000	38.71090	-.05551	-1.16366	7.27312	1.00000 (F.S.)

X=144.875 INCHES

DATE: 2-22-78
AS 144

L.D.V. MEASUREMENTS

Y (INS.)	U (F.P.S.)	u'^2 (F.P.S.)^2	S_u	F_u	γ_u
.01000	-.77000	1.04500	-.92655	9.45245	N.A.
.02000	-1.05400	4.99964	-.23408	3.43131	.29065
.04000	-2.34300	9.40152	.19773	3.76782	.23340
.07000	-3.38200	11.84638	.09734	3.23725	.15969
.11000	-3.17300	13.60271	.23386	3.32680	.18830
.16000	-3.29900	15.11701	.22932	2.93502	.19702
.21000	-3.71000	15.31055	.45449	4.36378	.14877
.27000	-3.50900	15.71485	.35564	3.74737	.16619
.33000	-3.27800	N.A.	N.A.	N.A.	.21133
.40000	-3.64400	15.00245	.23409	3.15267	.17397
.50000	-3.29000	20.49554	N.A.	3.97982	.21765
.65000	-2.67800	19.40773	.26500	3.65964	.28049
.80000	-1.96900	25.59273	.29664	3.02316	.34504
1.00000	-.98000	25.68599	.22418	2.95127	.39965
1.25000	.52500	30.27729	.28311	2.87581	.50794
1.50000	1.34700	36.88121	.17257	2.75157	.57785
1.75000	3.23000	36.71167	.20868	2.78126	.70249
2.00000	4.48300	43.28850	.16556	2.85592	.74779
2.25000	7.04700	46.66960	.11642	2.84813	.84546
2.50000	8.95300	51.48694	.12746	2.73159	.89966
2.75000	10.13600	54.47518	.01202	2.66246	.90605
3.00000	13.03000	54.21315	-.00448	2.69935	.95905
3.50000	17.50100	59.10719	-.09715	2.77363	.98859
4.00000	22.69300	58.55081	-.20873	2.77380	.99826
4.50000	27.02000	52.31079	-.29486	2.72914	1.00000
5.00000	31.96300	43.58746	-.45196	2.89629	1.00000
5.50000	37.77200	36.55085	-.65730	3.52120	1.00000
6.00000	41.50800	19.44695	-.74697	3.68516	1.00000
6.50000	43.83000	12.56454	-1.30237	5.89676	1.00000

Y (INS.)	V (F.P.S.)	v'^2 (F.P.S.)^2	S_v	F_v	γ_v
.01000	.04300	.02075	.90802	7.98595	.58961
.02000	.03100	.38950	.15208	4.33164	.53914
.04000	.15900	.64399	.12324	3.50741	.57634
.07000	.29200	1.02526	-.20736	3.52256	.64594
.11000	.03900	1.53195	-.07871	3.57592	.55803
.16000	.17900	2.43232	-.30086	4.13189	.56484
.21000	.18100	2.57964	-.27176	3.64656	.59112
.27000	.09400	3.28077	-.50655	4.25705	.57789
.33000	.38200	3.27656	-.36060	3.34359	.59921
.40000	.07800	4.47086	-.35865	3.96202	.53399
.50000	.30700	4.39070	-.20326	3.13062	.59598
.65000	-.02400	7.15573	-.39506	3.74863	.54371
.80000	.33000	9.73276	-.36096	3.79622	.56999
1.00000	.79000	11.03263	-.15245	3.35836	.62670
1.25000	.49000	12.50553	-.28666	3.56727	.56997
1.50000	.77300	13.44916	-.15935	3.14646	.59448
1.75000	.98700	14.23984	-.17438	3.03292	.63630
2.00000	1.21600	17.74827	-.24534	3.44763	.61653
2.25000	1.40400	17.59794	-.22977	3.00117	.63336
2.50000	1.74900	18.15237	-.16251	2.94993	.69209
2.75000	1.92500	22.43033	-.05816	3.25307	.68297
3.00000	1.74500	21.11972	-.12009	3.03453	.65615
3.50000	2.32000	20.43055	-.01113	3.03133	.68757
4.00000	3.16600	20.87074	.05576	3.05096	.74819
4.50000	3.98100	19.23631	.15993	3.07503	.80308
5.00000	4.85200	17.37064	.22845	3.32302	.90098
5.50000	6.69500	15.26357	.44123	3.72407	.96957
6.00000	7.42500	N.A.	N.A.	N.A.	.99346
6.50000	7.87200	N.A.	N.A.	N.A.	.99976

Y (INS.)	U-V (F.P.S.)	$-\overline{uv}$ (F.P.S.)^2	S_{u-v}	F_{u-v}	γ_{u-v}
.01000	-.22759	-.05542	-.00419	8.23711	.45706
.02000	-1.59754	.71176	-.09530	3.62731	.26202
.04000	-2.16655	.33753	.11766	3.79844	.20766
.07000	-3.19751	.44996	.04255	3.58952	.18992
.11000	-2.99810	1.13630	.21770	3.92421	.21311
.16000	-3.57734	.45570	.14940	3.26764	.19566
.21000	-3.61137	-.15370	.15412	3.10045	.19901
.27000	-2.89355	.73830	.30294	3.34410	.25654
.33000	-3.23145	.36370	.37275	3.21585	.23142
.40000	-3.56651	.30460	.40173	3.16986	.21304
.50000	N.A.	.85290	.45956	3.22622	.31980
.65000	-2.60213	1.56740	.57504	3.92339	.27716
.80000	-2.13403	2.02630	.35693	2.93795	.35822
1.00000	-1.43256	2.65330	.36817	2.96586	.39947
1.25000	-.34365	3.55030	.34407	2.92495	.45993
1.50000	1.35763	4.69840	.23054	2.73458	.53618
1.75000	2.30373	5.06000	.30849	3.31619	.59364
2.00000	3.30074	5.59410	-.05315	3.05254	.61204
2.25000	5.28204	6.57590	.09971	2.76590	.73259
2.50000	5.60730	6.75370	-.26227	3.36339	.73992
2.75000	7.96477	7.07050	-.15959	2.97290	.78736
3.00000	10.56973	7.37550	-.07685	2.90053	.85391
3.50000	14.39575	8.07240	-.13193	2.78067	.93202
4.00000	18.49349	8.28320	-.21251	2.88545	.96649
4.50000	22.09829	7.85240	-.32753	2.91433	.98247
5.00000	25.95057	6.75630	-.47848	3.06471	.99566
5.50000	29.10565	5.44540	-.84979	4.12810	.99750
[illegible].00000	32.14613	3.66090	-.83956	3.91698	1.00000
6.[illegible]0000	34.75538	.50620	-1.00311	4.47264	1.00000

X=144.875 INCHES

DATE: 3- 1-79
DS 144X

L.D.V. MEASUREMENTS

Y (INS.)	U (F.P.S.)	$\overline{u'^2}$ (F.P.S.)^2	S_u	F_u	η_u
.01000	-.03600	3.37090	.02182	3.13640	.46065
.01500	N.A.	2.83348	-.00816	2.97163	.65335
.02500	N.A.	3.27190	.24279	3.22209	.53455
.03000	N.A.	4.36534	.15008	2.97566	.43787
.03500	-2.57600	8.67196	-.06410	3.13702	.17259
.05000	-1.81400	10.51399	.02238	3.20293	.26083
.06000	-2.66200	11.10369	.10583	3.14280	.20502
.07000	-2.91900	12.45568	.09625	3.11380	.17840
.08500	-3.43400	13.02559	.16205	3.01422	.18390
.10000	-3.39800	12.42422	.11697	3.02239	.19185
.12000	-3.37300	13.11453	.09904	2.98245	.17481
.14000	-3.64400	13.33411	.19057	2.86703	.15297
.17000	-3.51400	13.49519	.18599	2.93854	.16693
.20000	-3.64400	14.75639	.12070	2.99379	.18355
.24000	-3.24900	14.91226	.15823	2.70933	.21576
.30000	-3.81100	14.93900	.30797	2.71256	.18405
.37000	-3.78300	16.64420	.27795	2.93627	.17127
.45000	-3.57700	17.15037	.33021	2.94199	.18361
.55000	-3.03300	18.10111	.26240	2.91974	.24208
.70000	-3.94400	19.35525	.32089	2.86456	.22997

Y (INS.)	V (F.P.S.)	$\overline{v'^2}$ (F.P.S.)^2	S_v	F_v	η_v
.01000	-.09300	.12006	-.00591	6.97596	.35292
.01500	-.00600	.13503	N.A.	6.12675	.49234
.02500	.41100	.26811	.08971	3.99874	N.A.
.03000	.24900	.25194	.16942	3.62107	N.A.
.03500	.00200	.40385	.14252	N.A.	.53257
.05000	-.04300	.60553	-.08095	4.59082	.45483
.06000	.19000	.79698	-.23775	4.55844	.61357
.07000	.04700	1.02085	-.37643	4.94397	.53339
.08500	N.A.	1.32009	-.26428	3.93843	.36357
.10000	-.13800	1.60271	-.27849	4.10075	.47612
.12000	.35900	1.80803	-.33579	4.01040	.61315
.14000	-.03400	1.97698	-.23552	3.96218	.52545
.17000	N.A.	2.30587	-.31054	3.83101	.53054
.20000	-.07500	2.60777	-.25965	4.13706	.51546
.24000	.03100	2.95541	-.28928	4.24429	.54569
.30000	.04900	3.34956	-.28454	3.87417	.50994
.37000	-.06700	3.93983	-.37717	3.92660	.51222
.45000	-.11900	4.47505	-.33687	3.69621	.49088
.55000	.12800	5.41730	-.47672	3.79968	.57630
.70000	.20900	6.41097	-.44745	3.63593	.58324

Y (INS.)	U-V (F.P.S.)	$-\overline{uv}$ (F.P.S.)^2	$S_{u\text{-}v}$	$F_{u\text{-}v}$	$\eta_{u\text{-}v}$
.01000	-.22062	N.A.	.06654	N.A.	.44556
.01500	N.A.	.09743	N.A.	3.42736	.45761
.02500	N.A.	.09533	.23379	3.17088	.45874
.03000	1.65461	N.A.	N.A.	2.89412	N.A.
.03500	-1.83846	-.13937	-.06679	3.25508	.25292
.05000	-2.41121	.15024	-.01903	3.16925	.24611
.06000	-2.90052	.43179	.03771	3.04161	.19476
.07000	-2.61703	.07241	.10834	3.24916	.24143
.08500	-3.22579	-.11993	.13174	3.28145	.17769
.10000	-3.25407	.20798	.20596	3.07523	.17238
.12000	-3.83409	.97557	.09997	3.26631	.18262
.14000	-3.41671	.60455	.16715	3.37900	.19634
.17000	-3.37394	.31130	.16417	3.15028	.21129
.20000	-3.57227	.46040	.26701	3.36557	.19111
.24000	-3.52843	.41750	.22741	3.10019	.19430
.30000	-3.52777	.49510	.30291	3.21482	.20229
.37000	-3.41529	.50450	.34532	3.30933	.21443
.45000	-3.34317	.83020	.39556	3.11391	.22307
.55000	-2.92457	1.16350	.45006	3.26098	.27655
.70000	-2.85244	1.21430	.47224	3.18752	.29820

X=156.[illegible] INCHES

DATE: 3-20-78
DS 156

L.D.V. MEASUREMENTS

Y (INS.)	U (F.P.S.)	u'^2 (F.P.S.)^2	S_u	F_u	γ_u
.01000	[illegible]	4.05737	-.24446	4.23194	.12152
.01500	-1.[illegible]	5.54232	-.21969	3.66954	.20314
.02000	-2.76700	7.60309	-.25922	3.66764	.17137
.03000	-3.77500	9.[illegible]76	-.14635	3.34261	.15467
.05000	-3.72900	11.27529	-.06033	3.12743	.12929
.08000	-4.20300	13.16993	.13798	3.17639	.13075
.13000	-4.89100	12.65551	.16407	3.15150	.07604
.20000	-4.87200	13.74704	.22212	3.17859	.08865
.30000	-4.97000	13.64977	.30352	3.25407	.09620
.45000	-4.70700	16.47051	.33625	3.37264	.13501
.65000	-4.89700	17.30539	.45749	3.59359	.12656
.90000	-4.39100	17.73522	.41474	3.19060	.16374
1.20000	-3.95300	19.75020	.41528	3.02918	.19412
1.60000	-3.00800	25.04142	.49835	3.28384	.24134
2.00000	-1.77300	29.45981	.45896	3.14839	.34273
2.50000	.58300	35.69023	.39270	2.94055	.47880
3.00000	2.95800	46.37065	.29639	2.75304	.62439
3.50000	5.46700	53.19777	.30593	3.03368	.73747
4.00000	8.59400	56.71159	.17848	2.65590	.85658
4.50000	11.93100	63.32610	.06997	2.51383	.93029
5.00000	15.11000	67.57399	-.02025	2.55376	.96811
5.50000	18.97600	66.40245	-.14110	2.58580	.98739
6.00000	22.82600	67.81424	-.19871	2.62891	.99507
6.50000	27.14800	65.17850	-.35750	2.76259	1.00000
7.00000	31.25400	60.95518	-.59465	3.30149	1.00000
7.50000	34.95600	51.06100	-.65869	3.06443	1.00000
8.00000	37.98700	46.26095	-.72764	4.01059	1.00000
8.50000	41.33300	41.89106	-.81133	6.20931	1.00000
9.00000	43.07900	15.22459	-1.08861	7.15491	1.00000
9.50000	44.12300	9.61825	-.95558	10.34807	1.00000
10.00000	44.68400	1.97439	.33140	6.94157	1.00000

Y (INS.)	V (F.P.S.)	v'^2 (F.P.S.)^2	S_v	F_v	γ_v
.01000	-.08200	.05692	-.17452	N.A.	.34305
.01500	-.11400	.13692	-.19189	5.80300	.37596
.02000	-.05500	.21862	N.A.	6.04753	.47629
.03000	-.00100	.34913	N.A.	6.83412	.47549
.05000	.22300	.69427	-.27481	6.86094	.67429
.08000	.14400	1.15892	-.18750	4.96732	.57568
.13000	.11800	1.42879	-.21506	4.02856	.56186
.20000	.01300	2.06523	-.26834	4.07776	.48349
.30000	.00800	2.96415	-.37514	4.21650	.51255
.45000	.09800	4.00040	-.44132	4.31268	.55055
.65000	.07500	5.05207	-.38843	3.86086	.52233
.90000	.63600	6.73252	-.58457	N.A.	.63015
1.20000	.50800	8.44536	-.44834	3.78006	.57300
1.60000	.85200	10.14425	-.35564	3.49814	.62635
2.00000	.64300	12.21475	-.50653	3.62714	.60840
2.50000	.89300	14.37523	-.35252	3.32937	.64444
3.00000	1.24800	17.32974	-.41159	3.21998	.65361
3.50000	1.52700	19.95016	-.30249	3.29645	.64628
4.00000	1.95300	19.90445	-.19839	3.17304	.69693
4.50000	2.44700	22.52015	-.11954	3.13017	.69544
5.00000	2.72900	23.07939	-.07214	3.07866	.70131
5.50000	3.53700	23.17652	-.09294	3.07167	.75196
6.00000	4.31000	23.07435	-.09792	3.62464	.79095
6.50000	5.20400	20.85337	.15850	3.09936	.88749
7.00000	6.07300	18.75574	.24030	3.27339	.92094
7.50000	6.68100	16.33073	.16997	3.44497	.95767
8.00000	7.94100	15.37539	.42623	3.72794	.99113
8.50000	8.43900	12.52027	.33085	4.06594	.99923
9.00000	8.45900	11.25790	N.A.	5.34215	.99078
9.50000	8.89500	N.A.	N.A.	N.A.	.99787
10.00000	N.A.	3.16365	2.35971	12.93537	1.00000

Y (INS.)	U-V (F.P.S.)	$-\overline{uv}$ (F.P.S.)^2	$S_{u\text{-}v}$	$F_{u\text{-}v}$	$\gamma_{u\text{-}v}$
.01000	-2.07603	.39410	N.A.	4.48435	.14192
.01500	-1.98271	.19590	-.09554	4.02840	.21161
.02000	-2.41910	.06370	-.08374	3.52518	.13360
.03000	-2.83971	-.10600	-.12035	3.35340	.15819
.05000	-3.63732	-.16610	-.09513	3.25481	.16566
.08000	-4.05451	-.03610	-.02562	3.15626	.17593
.12000	-4.41513	.13940	.13748	3.29815	.10800
.20000	-4.35950	.34620	.32923	N.A.	.09697
.30000	-4.53317	.37010	.30165	3.24996	.16031
.45000	-4.72707	.45370	.41702	3.75831	.14144
.65000	-4.81252	1.03130	.46343	3.73140	.15909
.90000	-4.78141	1.51420	.54401	3.43627	.15813
1.20000	-4.30643	2.51340	.56496	3.47395	.22351
1.60000	-2.88840	3.74640	.53295	3.13777	.29772
2.00000	-1.35621	4.34300	.52834	3.33060	.39200
2.50000	-.26370	5.44120	.49019	3.16813	.43767
3.00000	2.19623	6.21490	.34083	2.88047	.59084
3.50000	4.40857	7.91330	.29846	2.79199	.65067
4.00000	7.23503	9.70130	.17918	2.57082	.74216
4.50000	9.91354	10.83490	.09981	2.71026	.81071
5.00000	12.70659	11.97700	-.00332	2.66679	.85103
5.50000	15.94203	12.06210	-.12845	2.72487	.93015
6.00000	19.24565	12.02110	-.25929	2.81097	.96139
6.50000	22.42921	10.60170	-.39241	2.93242	.97887
7.00000	25.53904	9.31150	-.54020	3.10105	.98779
7.50000	28.04304	5.53360	-.59808	3.16831	.99622
8.00000	30.92431	2.04400	-.85025	3.59920	.99938
8.50000	32.84752	.63590	-1.21532	4.57862	.99655
9.00000	34.34385	1.56100	-1.34234	5.42854	1.00000
9.50000	36.03099	.40610	-1.96223	9.38707	1.00000
10.00000	36.64755	-.37360	N.A.	N.A.	1.00000

X=156.375 INCHES

DATE: 3-15-78
DS 156d

L.D.V. MEASUREMENTS

Y (INS.)	U (F.P.S.)	u'^2 (F.P.S.)^2	S_u	F_u	γ_u
.01000	-1.59200	2.53023	-.35407	4.01074	.13761
.01500	-1.97300	4.14770	-.36456	3.85285	.15891
.02000	-2.52000	5.70947	-.34521	3.61187	.12425
.02500	-2.74100	7.08356	-.14489	3.49910	.13882
.04000	-3.23600	10.43529	-.10748	3.35927	.13221
.06500	-3.95800	12.54739	.11314	3.16713	.13231
.10000	-4.07900	13.81929	.16421	3.01987	.12646
.17000	-4.65200	13.14947	.11657	3.02987	.09733
.25000	-4.44200	14.46266	.22912	2.90726	.11452
.40000	-5.09300	14.58423	.21997	2.97264	.10955
.55000	-4.60800	16.37505	.29980	3.01753	.12632

Y (INS.)	V (F.P.S.)	v'^2 (F.P.S.)^2	S_v	F_v	γ_v
.01000	-.19300	.05477	-.17005	6.48295	N.A.
.01500	-.04500	.08173	N.A.	N.A.	.48632
.02000	-.15200	.14490	N.A.	5.54024	.29034
.02500	.06800	.20434	N.A.	5.29766	.55712
.04000	-.00500	.37821	-.12749	4.87853	.50634
.06500	.10200	.78393	-.03754	N.A.	.55505
.10000	.06000	1.43784	-.13527	4.08780	.53012
.17000	.02700	2.06545	-.26715	4.08702	.48858
.25000	.09200	2.60951	-.23195	4.09902	.56615
.40000	.10900	3.50790	-.28789	3.82019	.52156
.55000	.09200	4.74303	-.47357	4.02660	.53486

Y (INS.)	U-V (F.P.S.)	$-\overline{uv}$ (F.P.S.)^2	S_{u-v}	F_{u-v}	γ_{u-v}
.01000	-1.70128	.39170	N.A.	5.61944	.12235
.01500	-2.05625	.19590	-.37003	4.03401	.14422
.02000	-2.22737	.06370	-.41267	4.37825	.17247
.02500	-2.58799	-.07560	-.22596	3.71280	.13574
.04000	-3.25125	-.19000	.00446	3.44881	.16329
.06500	-3.74753	-.16190	.06819	3.37321	.17259
.10000	-4.36139	.04230	.09431	3.60285	.12206
.17000	-4.47736	.35550	.13535	3.35841	.12774
.25000	-4.97374	.45710	.25261	3.24665	.11217
.40000	-4.72908	.72540	.37036	3.35909	.14412
.55000	-5.41073	1.00920	.39153	3.33892	.13045

X=170.[illegible] INCHES

DATE: 2-20-78
AS 170A

L.D.V. MEASUREMENTS

Y (INS.)	U (F.P.S.)	u'^2 (F.P.S.)^2	η_u
.02000	-2.24000	5.73124	.26781
.08000	-4.46200	16.16040	.10441
.16000	-5.[illegible]1100	19.03577	.06794
.32000	-6.23900	20.55623	.05265
.64000	-6.27500	22.43917	.07407
1.00000	-6.[illegible]3[illegible]00	23.40524	.06888
1.50000	-5.00100	26.41960	.13116
2.00000	-5.00300	30.41523	.15082
2.50000	-3.94900	37.69960	.19853
3.00000	-2.54100	45.52201	.30144
3.50000	-1.09400	53.50923	.39649
4.00000	.40600	61.74816	.49873
4.50000	2.53100	70.81223	.62793
5.00000	4.76000	80.60212	.73049
5.50000	7.19500	88.92490	.80392
6.00000	10.75300	97.15016	.88942
6.50000	12.46800	100.20010	.90848
7.00000	16.65900	101.40490	.95096
7.50000	19.36500	102.01000	.96784
8.00000	22.02700	101.60640	.99237
8.50000	24.25200	99.38096	.99657
9.00000	26.97400	94.01242	.99638
9.50000	31.15600	85.00840	1.00000
10.00000	31.67000	74.21823	1.00000
10.50000	36.75900	[illegible].59110	1.00000

Y (INS.)	V (F.P.S.)	v'^2 (F.P.S.)^2	η_v
.02000	.39600	.13772	.85769
.08000	.11100	.60114	.58972
.16000	-.07800	1.72757	.52283
.32000	.06900	2.50817	.52560
.64000	-.17500	3.83118	.49299
1.00000	.33300	5.53299	.60465
1.50000	.43000	8.34745	.55369
2.00000	.57400	11.33339	.58270
2.50000	.64600	11.68402	.61914
3.00000	.93200	13.61517	.62865
3.50000	1.08000	15.62924	.60717
4.00000	.98400	20.32747	.60640
4.50000	1.36000	24.11783	.61336
5.00000	1.72000	27.04385	.65337
5.50000	1.41600	27.77290	.61280
6.00000	1.92800	29.70250	.65954
6.50000	1.72900	31.24810	.62[illegible]
7.00000	2.41200	32.60410	.6523[illegible]
7.50000	3.20500	34.80670	.70264
8.00000	3.25700	32.41059	.69524
8.50000	3.75700	31.21200	.74007
9.00000	4.27300	27.04729	.79272
9.50000	4.77700	24.49319	.84695
10.00000	5.39900	22.93129	.87420
10.50000	6.26300	19.69395	.94125

Y (INS.)	U-V (F.P.S.)	$\eta_{u \cdot v}$
.03000	-3.20589	.05549
.08000	-4.99495	.09470
.14000	-5.64895	.09257
.32000	-5.85035	.07337
.56000	-5.47855	.07008
1.00000	-4.70127	.09204
1.50000	-5.73175	.13497
2.00000	-5.14203	.18879
2.50000	-4.37553	.22940
3.00000	-3.17455	.31398
3.50000	-1.47764	.39049
4.00000	.24407	.46071
4.50000	1.52305	.50724
5.00000	3.57635	.62888
5.50000	5.76592	.67435
6.00000	7.20111	.72365
6.50000	9.47730	.79717
7.00000	11.34613	.83936
7.50000	12.64573	.83022
8.00000	14.65535	.87549
8.50000	15.95500	.87324
9.00000	21.75534	.97233
9.10000	N.A.	.97362
10.00000	26.31955	.98211
10.50000	N.A.	.98223

X= 31.688 INCHES DATE: 7- 6-78

HOT-WIRE (X-WIRE) MEASUREMENTS

Y (INS.)	U (F.P.S.)	V (F.P.S.)	u'^2 (F.P.S.)^2	v'^2 (F.P.S.)^2	$-\overline{uv}$ (F.P.S.)^2	$\overline{u^2 v}$ (F.P.S.)^3	S_v	
.05000	44.11500	N.A.	23.09764	6.98016	4.86200	N.A.	N.A.	
.06200	44.81700	N.A.	20.80272	5.34997	4.83200	4.77100	N.A.	
.07500	46.46200	N.A.	19.44810	5.01312	4.60300	3.24600	N.A.	
.09500	47.91900	N.A.	18.09652	4.63110	4.46800	2.43500	N.A.	
.12000	49.07100	1.73800	16.44627	4.19881	4.20100	1.47400	.71970	
.15000	51.28300	1.93300	15.00013	3.92040	3.10400	.71610	.82820	
.19000	53.36400	1.97500	12.98492	3.45216	2.66700	-.04730	.86360	
.25000	55.43400	2.04540	9.87216	2.79693	1.92700	-.58020	.94630	
.29000	57.04400	2.14200	8.17395	2.35009	1.50400	-.91490	1.09170	
.33000	58.15100	2.17200	6.83300	1.88235	1.16100	-.67640	1.22410	
.38000	59.12000	2.15500	5.12117	1.43042	.75640	-.68950	1.38840	
.43000	59.63800	2.04300	3.56454	.97532	.29140	-.72250	1.62420	
.48100	60.50800	2.03900	2.49440	.59195	-.00519	-.87760	1.95280	
.53000	61.00200	2.04500	1.52029	.25231	-.22530	-.98900	1.63460	
.63000	61.78300	2.04900	.68459	.09333	.11210	-1.36900	N.A.	
.73000	62.18300	2.01900	.39665	.03063	.00430	-1.53500	N.A.	(F.S.)

X= 54.188 INCHES DATE: 6-31-78

HOT-WIRE (X-WIRE) MEASUREMENTS

Y (INS.)	U (F.P.S.)	u'^2 (F.P.S.)^2	v'^2 (F.P.S.)^2	$-\overline{uv}$ (F.P.S.)^2	
.04500	43.96800	30.27200	7.00661	8.19200	
.05200	44.78500	32.00165	7.59003	7.35000	
.06300	46.36900	31.78704	7.30621	7.56200	
.07600	47.67700	31.23692	7.34952	7.36700	
.10100	50.04500	30.70269	7.43653	7.29100	
.12600	51.81400	29.46319	7.35494	7.20200	
.15000	53.44400	29.09524	7.54601	6.94000	
.20000	56.16000	26.47103	7.20923	6.57400	
.27000	59.22700	23.45465	6.56897	5.49000	
.35000	62.19400	19.87376	5.57432	4.59400	
.45000	65.40400	15.17103	4.15752	3.44500	
.52500	67.17900	11.47177	2.75692	2.59400	
.70000	70.54500	5.04668	.98206	1.09200	
.80400	71.32400	3.66340	.17556	.51000	
.90000	72.19100	2.40250	.07840	.20000	
1.00000	72.39000	1.88236	.06250	.00500	(F.S.)

X= 86.500 INCHES DATE: 7-11-78

HOT-WIRE (X-WIRE) MEASUREMENTS

Y (INS.)	U (F.P.S.)	V (F.P.S.)	u'^2 (F.P.S.)^2	v'^2 (F.P.S.)^2	$-\overline{uv}$ (F.P.S.)^2	$\overline{u^2 v}$ (F.P.S.)^3	S_v	
.03700	34.68000	1.02500	30.12912	7.15028	5.91100	13.90500	.57760	
.04450	35.92000	1.15400	25.91213	6.91690	5.82100	14.53100	.53670	
.05250	36.35000	1.25500	28.70672	6.79124	5.47000	12.47500	.50280	
.06250	36.06000	1.33100	26.72960	6.80166	5.99500	10.50900	.35050	
.07750	39.11000	1.39800	28.17486	7.14493	6.08600	9.10600	.22250	
.09750	40.61000	1.45900	27.35476	7.21997	6.24300	9.03200	.14690	
.12300	42.07000	1.53100	27.17537	7.50212	6.32600	N.A.	.14820	
.15300	43.65000	1.59000	27.25884	7.68398	6.43300	N.A.	.41610	
.20200	45.71000	1.65900	26.24513	7.52423	6.18800	N.A.	.40310	
.27200	48.31000	1.77800	24.53029	7.87364	6.29800	10.95300	.43530	
.35400	50.87000	1.85200	22.87709	7.62321	5.79400	8.61100	.42490	
.45200	53.69000	2.01700	20.26800	7.20386	5.34200	7.14500	.47520	
.60200	57.44000	2.22800	16.01600	5.86548	4.04100	4.54900	.55760	
.80200	61.76000	2.49000	9.97296	3.87696	2.50100	3.53200	.76170	
1.00200	64.05000	2.72300	4.23125	1.72134	1.06700	1.40700	.93950	
1.20200	66.47000	2.92400	.86806	.93702	.02260	1.55200	N.A.	
1.40200	56.71000	3.09200	.57973	.59444	.24350	1.07000	N.A.	(F.S.)

X=105.250 INCHES DATE: 7- 8-78

HOT-WIRE (X-WIRE) MEASUREMENTS

Y (INS.)	U (F.P.S.)	u'^2 (F.P.S.)^2	v'^2 (F.P.S.)^2	$-\overline{uv}$ (F.P.S.)^2	S_v	
.05900	22.54900	24.29504	4.23943	4.28000	.61300	
.06900	23.36100	24.29504	4.43945	4.38900	.52700	
.08300	24.53500	24.53221	4.78297	4.37300	.45070	
.10100	25.49700	24.25548	5.30842	4.69500	.36250	
.12600	26.70500	24.43137	5.81292	5.12600	.34530	
.15100	27.59700	25.33109	6.57410	5.62300	.32180	
.20100	29.42800	25.84705	7.24146	5.83800	.34190	
.25100	31.15100	26.69789	7.74509	6.09800	.34930	
.32100	33.14300	26.46074	8.30016	6.55600	.36800	
.40100	34.15100	27.51003	8.65535	6.35000	.39370	
.50200	36.37800	25.97941	8.60010	6.29200	.40000	
.62100	39.97400	25.63397	8.45646	6.42400	.42650	
.75100	42.71600	23.12649	8.03156	5.89200	.44670	
.90100	45.55000	19.26332	7.06496	5.04900	.47640	
1.10100	48.65400	15.95204	5.84189	4.32500	.55330	
1.30100	51.44200	11.62126	4.26010	2.94000	.72840	
1.50100	54.04100	7.03310	2.30228	1.67300	.88200	
1.70100	56.34900	3.10112	1.56250	.72740	1.28390	
1.90100	57.30500	.76580	.66374	.19240	N.A.	
2.10100	57.55700	.19862	.21650	.02580	1.56070	(F.S.)

X=111.250 INCHES DATE: 9-16-78

HOT-WIRE (X-WIRE) MEASUREMENTS

Y (INS.)	U (F.P.S.)	V (F.P.S.)	u'^2 (F.P.S.)^2	v'^2 (F.P.S.)^2	$-\overline{uv}$ (F.P.S.)^2	
.07500	20.24900	.15700	19.74914	3.83376	3.06200	
.09500	21.29400	.22510	21.22445	4.56250	3.01200	
.12000	22.06700	.24910	20.46658	5.09405	3.46000	
.15000	22.66500	.04440	22.74336	5.63113	3.54200	
.20000	23.93200	.03300	23.01121	6.37563	4.53800	
.27000	25.73100	.08150	24.81036	7.24635	5.26000	
.35000	27.33100	.07490	24.26548	7.85120	5.33800	
.45000	29.58800	.18720	25.84706	8.36366	5.77800	
.60000	32.38900	.35170	25.86740	8.86253	6.04800	
.80000	36.26100	.60590	24.71084	8.75568	5.73700	
1.00000	40.04900	.91950	21.30746	8.16816	5.48300	
1.20000	43.56200	1.20300	19.76692	7.14493	4.34700	
1.40000	46.92700	1.59100	15.50794	5.55013	3.62800	
1.60000	49.83100	1.96300	11.50566	4.25597	2.35300	
1.80000	52.29000	2.33100	6.58949	2.86964	1.39500	
2.10000	54.50800	2.73900	1.65123	1.14276	.24050	
2.40000	55.13800	3.03600	.25194	.30349	.03400	(F.S.)

X=117.625 INCHES DATE: 7-24-78

HOT-WIRE (X-WIRE) MEASUREMENTS

Y (INS.)	U (F.P.S.)	V (F.P.S.)	u'^2 (F.P.S.)^2	v'^2 (F.P.S.)^2	$-\overline{uv}$ (F.P.S.)^2	$\overline{u^2v}$ (F.P.S.)^3	S_v	
.90100	29.14100	2.02000	29.48490	8.97003	4.07600	N.A.	N.A.	
1.10100	31.52700	2.42800	27.94180	8.94010	4.36000	11.48500	.11303	
1.35000	35.41500	2.96900	26.13254	8.53772	4.11300	9.56900	.10290	
1.60000	39.82600	3.53700	22.17469	7.54601	3.57500	10.61000	.16650	
1.85000	43.14900	4.02000	19.14760	5.92436	2.85800	9.09400	.24230	
2.10200	46.47100	4.49700	12.25000	4.36810	1.72900	7.61200	.31810	
2.35000	49.33000	5.04500	6.36553	2.81233	.89770	4.39300	.36520	
2.60100	51.07900	5.39800	2.40970	1.41848	.27550	N.A.	.14770	
2.85000	51.71200	5.62000	.52984	.62442	.05389	N.A.	N.A.	
3.10100	51.85700	5.74200	.17148	.22555	-.01690	N.A.	N.A.	(F.S.)

X=126.750 INCHES DATE: 7-22-78

HOT-WIRE (X-WIRE) MEASUREMENTS

Y (INS.)	U (F.P.S.)	V (F.P.S.)	$\overline{u'^2}$ (F.P.S.)^2	$\overline{v'^2}$ (F.P.S.)^2	$-\overline{uv}$ (F.P.S.)^2	$\overline{u^2v}$ (F.P.S.)^3	S_v	
2.37000	34.90700	3.92000	29.31140	9.35136	4.02200	12.71900	.17320	
2.52000	36.94500	4.37000	26.33742	8.30366	3.70500	16.59800	.35510	
2.82000	40.79500	5.04400	19.99878	6.36048	3.19400	14.70200	.47670	
3.12000	44.23800	5.69700	13.63096	4.57960	1.81400	11.75800	.49310	
3.42000	46.91100	6.21900	6.25000	2.77869	.79730	6.41600	.76280	
3.62000	48.01100	6.49200	2.91385	1.74504	.45810	2.20600	.82550	
3.82000	48.84900	6.70400	1.02010	1.07744	.18930	.60200	.99360	
4.12000	48.94300	6.78100	.31697	.44769	.02529	.02900	.50540	(F.S.)

X=131.000 INCHES DATE: 7-27-78

HOT-WIRE (X-WIRE) MEASUREMENTS

Y (INS.)	U (F.P.S.)	V (F.P.S.)	$\overline{u'^2}$ (F.P.S.)^2	$\overline{v'^2}$ (F.P.S.)^2	$-\overline{uv}$ (F.P.S.)^2	$\overline{u^2v}$ (F.P.S.)^3	S_v	
3.00000	37.19400	4.59000	25.08006	7.86803	3.43800	13.37800	.21240	
3.20000	39.53000	5.19900	21.78089	6.55872	2.62600	13.36200	.26490	
3.40000	41.63100	5.68000	16.98264	5.59323	2.00000	10.78600	.35110	
3.70000	44.09000	6.25700	12.20904	3.73649	1.32700	7.90600	.47600	
4.10000	47.31700	7.22700	2.63738	1.85777	.54070	1.74400	.65730	
4.50000	47.96600	7.51400	.53319	.68096	.07710	.09090	N.A.	
5.00000	47.42500	7.54200	.19740	.25817	.00078	.04090	.72610	
5.50000	47.33600	7.60500	.11560	.14394	-.00191	.00668	.28630	
6.30000	46.98200	7.30500	.06625	.07464	-.00722	.00297	.29840	(F.S.)

X=139.000 INCHES DATE: 7-20-78

HOT-WIRE (X-WIRE) MEASUREMENTS

Y (INS.)	U (F.P.S.)	V (F.P.S.)	$\overline{u'^2}$ (F.P.S.)^2	$\overline{v'^2}$ (F.P.S.)^2	$-\overline{uv}$ (F.P.S.)^2	
4.00000	35.19000	4.92700	34.40996	10.51056	N.A.	
4.12000	36.29000	5.24400	32.46720	9.59141	N.A.	
4.37000	38.18000	5.77200	26.41960	8.80902	3.17700	
4.62000	40.81000	6.40600	20.46659	6.56897	1.46300	
4.87000	42.94000	6.91400	17.18932	5.56960	1.68000	
5.12000	45.04000	7.52300	7.79526	3.74810	1.30200	
5.62000	46.51000	8.02200	1.80634	1.71349	.11220	
6.12000	46.82000	8.20000	.57199	.69369	.03350	
6.62000	46.85000	8.26200	.33617	.35294	.00262	
7.12000	46.78000	8.35200	.20921	.22648	.02760	(F.S.)

X=144.000 INCHES DATE: 7-26-78

HOT-WIRE (X-WIRE) MEASUREMENTS

Y (INS.)	U (F.P.S.)	V (F.P.S.)	$\overline{u'^2}$ (F.P.S.)^2	$\overline{v'^2}$ (F.P.S.)^2	$-\overline{uv}$ (F.P.S.)^2	$\overline{u^2v}$ (F.P.S.)^3	S_v	
5.50000	42.00900	8.90400	25.05003	7.77852	N.A.	11.23800	.20180	
5.75000	43.76000	9.67200	19.11354	6.25500	N.A.	9.67100	.39630	
6.00000	45.34300	10.17900	10.91542	4.54969	.64070	6.44900	.42510	
6.50000	46.90500	10.75000	2.97906	2.29825	.27940	2.67400	.89980	
7.00000	47.06400	10.97710	.89170	1.12148	-.00372	.49770	1.04500	
8.00000	46.64300	10.95400	.30008	.37626	-.04610	-.00954	.07610	
9.00000	45.74600	11.39200	.16794	.20258	-.03670	-.03953	-.47610	
11.00000	46.40000	11.35000	.07706	.06724	-.02530	-.05738	N.A.	(F.S.)

X=156.375 INCHES DATE: 7-21-78

HOT-WIRE (X-WIRE) MEASUREMENTS

Y (INS.)	U (F.P.S.)	V (F.P.S.)	$\overline{u'^2}$ $(F.P.S.)^2$	$\overline{v'^2}$ $(F.P.S.)^2$	$-\overline{uv}$ $(F.P.S.)^2$	$\overline{u^2 v}$ $(F.P.S.)^3$	S_v
8.50100	43.54800	7.63400	15.26465	5.56488	1.96900	14.26800	.74210
9.00000	44.46000	8.19500	5.05350	4.38065	.78090	6.96500	.85060
9.50000	44.99300	8.37700	1.86050	2.12576	.07730	1.21900	1.34700
10.00000	45.30300	8.59200	1.24546	1.50063	-.03206	.53600	.82980
11.00000	45.24300	8.60200	.60762	.68558	-.04032	.21970	.73080
12.00000	45.32500	8.82500	.38254	.34129	-.05164	.02300	.34260
13.00000	45.13600	8.97000	.25462	.21326	-.05720	-.00196	.11140 (F.S.)

X=169.750 INCHES DATE: 7-25-78

HOT-WIRE (X-WIRE) MEASUREMENTS

Y (INS.)	U (F.P.S.)	V (F.P.S.)	$\overline{u'^2}$ $(F.P.S.)^2$	$\overline{v'^2}$ $(F.P.S.)^2$	
11.50000	42.03700	10.67000	36.39502	8.63184	
12.50000	44.05400	11.45700	14.50086	4.72629	
13.50000	44.26800	11.77900	3.75748	2.82240	
15.50000	44.16900	12.04200	.66912	.92795	
17.50000	44.16900	12.25000	.32036	.42942	(F.S.)

X = 11.375 INCHES DATE: 10-11-77

HOT-WIRE (SINGLE WIRE) MEASUREMENTS

Y (INS.)	U (F.P.S.)	u'^2 (F.P.S.)^2
.00200	6.51700	.94535
.00250	7.95300	1.73479
.00300	8.39300	3.21336
.00350	9.72400	4.37500
.00400	11.30100	7.02560
.00450	12.92900	9.13403
.00500	14.22500	11.15051
.00600	16.48800	14.13803
.00800	20.70000	18.67758
.01000	24.17400	21.83566
.01200	26.85800	22.65940
.01500	29.02300	22.71146
.01800	32.14500	21.17563
.02100	33.60600	20.32919
.02500	34.19300	18.49957
.03000	35.65200	16.40018
.03700	37.08300	13.97412
.04500	38.20400	12.61940
.05500	39.44100	11.22362
.07000	40.71600	10.01312
.09000	42.12400	9.16709
.11500	43.62700	8.80567
.14500	45.09900	8.46529
.19500	47.23400	8.01441
.26500	49.61900	6.62604
.34500	51.93300	4.35852
.44500	53.79000	1.32977
.59500	54.52900	.05523
.79500	54.65200	.00765 (F.S.)

X = 21.750 INCHES DATE: 10-13-77

HOT-WIRE (SINGLE WIRE) MEASUREMENTS

Y (INS.)	U (F.P.S.)	u'^2 (F.P.S.)^2
.00150	4.45400	2.32905
.00200	5.25600	5.40411
.00250	7.52200	9.53410
.00300	8.82200	11.60671
.00350	10.32700	11.77050
.00400	13.29200	15.39034
.00450	13.80800	15.69493
.00500	15.61000	17.48951
.00550	17.03100	19.36800
.00600	17.68400	19.94494
.00650	18.27600	19.78675
.00700	20.23300	20.63770
.00800	22.69500	18.65025
.01000	26.78300	20.53035
.01200	29.35500	21.12423
.01400	31.06000	20.63770
.01700	33.44400	19.52451
.02000	35.64300	16.99626
.02300	36.85900	16.27450
.02700	37.69800	14.33174
.03200	38.56500	12.97697
.03900	39.84200	11.97431
.04700	41.31800	11.59256
.05700	42.42700	11.16955
.07200	43.90100	11.20913
.09200	45.45400	11.29448
.11700	46.79300	10.81654
.14700	48.47800	10.35468
.19700	51.69300	9.20918
.26700	53.95500	6.31949
.34700	55.74100	3.95019
.44700	57.57100	1.72443
.59700	58.97600	.19160
.79700	59.09600	.00895
.99700	59.15200	.02943 (F.S.)

X = 31.250 INCHES DATE: 1-26-78

HOT-WIRE (SINGLE WIRE) MEASUREMENTS

Y (INS.)	U (F.P.S.)	u'^2 (F.P.S.)^2
.00350	14.65100	17.97343
.00400	17.09300	22.61858
.00450	19.12000	26.40327
.00500	20.91400	28.95160
.00550	22.79500	30.76232
.00600	24.85300	33.06745
.00650	26.56500	34.55011
.00700	27.30400	35.37944
.00750	29.37600	35.37944
.00800	29.65300	35.15229
.00850	30.35900	35.53128
.00900	30.89400	35.53125
.01000	32.11300	35.27673
.01200	34.04500	33.21425
.01400	35.75300	32.26584
.01600	36.75200	30.53358
.01900	38.24100	29.15778
.02200	39.53400	26.36338
.02500	40.92100	25.55942
.02900	42.10300	23.47550
.03400	43.04400	21.36307
.04100	44.36200	19.97210
.04900	45.42500	18.90412
.05900	46.72800	17.85548
.07400	47.90700	16.29527
.09400	49.43200	15.72419
.11900	51.61800	13.95670
.14900	53.35600	12.65482
.19900	55.37100	9.95859
.26900	57.61900	7.10134
.34900	59.89600	4.30955
.44900	61.89900	2.49972
.59900	63.76800	.45667
.79900	63.75200	.06162 (F.S.)

X = 44.000 INCHES DATE: 1-24-78

HOT-WIRE (SINGLE WIRE) MEASUREMENTS

Y (INS.)	U (F.P.S.)	u'^2 (F.P.S.)^2
.00300	12.46800	17.55060
.00350	14.15900	23.43846
.00400	16.70000	30.25273
.00450	18.21500	33.14167
.00500	19.07300	35.59075
.00600	20.97700	39.75081
.00650	22.53900	42.50831
.00750	25.45100	46.29736
.00950	30.82600	50.34652
.01150	34.99100	49.65937
.01350	36.93300	47.24605
.01650	39.29600	44.33542
.01950	40.93600	40.45357
.02250	42.18500	38.19210
.02650	43.15500	36.41302
.03150	44.80700	33.70304
.03850	46.10300	31.40304
.04650	47.73300	29.72099
.05650	49.44400	28.22771
.07150	50.68500	26.77293
.09150	52.43200	25.26632
.11650	54.17800	23.17059
.14650	55.09100	21.27460
.19650	58.27400	17.66702
.26650	60.89200	13.97268
.34650	63.13200	10.13546
.44650	65.71800	6.55045
.59650	67.91300	2.34937
.79650	68.04000	.71604
.99650	69.10100	.50052
1.19650	69.25500	.48109
1.39650	69.36000	.47151 (F.S.)

X= 52.500 INCHES DATE: 1-31-78

HOT-WIRE (SINGLE WIRE) MEASUREMENTS

Y (INS.)	U (F.P.S.)	$\overline{u'^2}$ (F.P.S.)^2	
.00300	14.49000	21.33115	
.00350	17.19000	29.24354	
.00400	19.17200	29.24354	
.00450	20.56800	34.19560	
.00500	22.43900	35.69272	
.00550	24.38700	36.87502	
.00600	26.39200	39.99374	
.00650	28.27500	40.85126	
.00700	29.39200	41.71276	
.00750	30.76000	42.00195	
.00800	32.20300	42.58328	
.00850	32.81000	41.90545	
.00900	33.71600	42.34906	
.00950	34.65500	42.48512	
.01000	36.75800	41.13744	
.01100	37.19700	39.90457	
.01300	38.61700	38.41294	
.01500	39.97300	37.76929	
.01700	41.58000	36.22378	
.02000	43.56900	33.41599	
.02300	44.49100	31.63187	
.02600	45.49000	30.38745	
.03000	46.62200	28.28964	
.03500	47.74400	27.19111	
.04200	49.22400	26.20684	
.05000	50.57100	25.13347	
.06000	52.24300	24.53998	
.07500	53.63500	23.08609	
.09500	55.46800	21.74601	
.12000	57.43900	20.31149	
.15000	59.35800	18.92590	
.20000	62.50400	16.24147	
.27000	65.78200	12.41519	
.35000	66.94200	8.83439	
.45000	70.66300	5.06110	
.60000	72.93400	1.62264	
.80000	74.01400	.12253	
1.00000	75.20000	.02936	
1.20000	74.49300	.01798	(F.S.)

X= 64.250 INCHES DATE: 8-11-77

HOT-WIRE (SINGLE WIRE) MEASUREMENTS

Y (INS.)	U (F.P.S.)	$\overline{u'^2}$ (F.P.S.)^2	
.00400	15.23000	15.47741	
.00450	16.74000	16.79595	
.00500	18.33000	21.89577	
.00550	19.98000	25.23421	
.00600	21.17000	29.04416	
.00650	22.52000	29.97370	
.00700	23.77000	31.80556	
.00750	24.71000	33.77500	
.00800	25.85000	35.20581	
.00850	27.03000	35.68940	
.00900	28.23000	37.36385	
.01000	29.93000	38.42252	
.01100	31.62000	39.31604	
.01300	34.16000	38.65949	
.01500	35.96000	38.15647	
.01700	37.40000	37.10150	
.02000	39.03000	36.49293	
.02300	40.38000	35.12092	
.02600	41.20000	34.02534	
.03000	42.35000	33.44265	
.03500	43.49000	32.96500	
.04200	45.06000	32.61397	
.05000	46.42000	32.21098	
.06000	47.69000	31.80556	
.07500	49.41000	30.76349	
.09500	51.23000	29.89528	
.12000	53.17000	28.27232	
.15000	55.19000	25.66302	
.20000	57.75000	21.96368	
.27000	60.67000	17.51376	
.35000	63.38000	13.30421	
.45000	66.07000	9.10160	
.60000	68.90000	4.74571	
.80000	71.17000	1.24959	
1.00000	71.67000	.31242	
1.20000	71.65000	.22359	(F.S.)

X= 74.250 INCHES DATE: 1-26-78

HOT-WIRE (SINGLE WIRE) MEASUREMENTS

Y (INS.)	U (F.P.S.)	$\overline{u'^2}$ (F.P.S.)^2	
.00350	12.47300	17.01244	
.00400	14.45100	20.73197	
.00450	15.99900	24.33126	
.00500	17.33500	26.60006	
.00550	19.16500	29.57324	
.00600	20.05600	30.96997	
.00650	21.35600	32.79485	
.00700	22.29500	33.60457	
.00750	23.27700	34.67197	
.00800	24.01500	36.09293	
.00850	24.72800	35.09393	
.00900	25.46700	36.51635	
.00950	26.13300	37.11322	
.01000	26.72200	37.45646	
.01050	27.21400	36.68539	
.01150	28.42600	37.02766	
.01350	30.31800	37.19388	
.01550	32.49300	36.00860	
.01750	33.86900	35.08695	
.02050	35.48700	32.31376	
.02350	36.90000	30.34748	
.03050	38.76700	27.99500	
.03550	40.05000	27.18306	
.04250	41.15000	25.45302	
.05050	42.56400	24.95914	
.06050	43.53800	23.91712	
.07550	45.15300	23.71139	
.09550	47.04800	23.23479	
.12050	48.39300	22.42902	
.15050	50.13800	21.57215	
.20050	52.72200	19.65845	
.35050	58.49900	12.09765	
.45050	61.97600	11.47056	
.60050	65.21100	6.86923	
.80050	68.56400	2.34641	
1.00050	70.08700	.30039	
1.20050	70.26500	.06759	(F.S.)

X= 87.500 INCHES DATE: 12-21-77

HOT-WIRE (SINGLE WIRE) MEASUREMENTS

Y (INS.)	U (F.P.S.)	$\overline{u'^2}$ (F.P.S.)^2	
.00350	9.48500	6.10453	
.00400	10.74700	8.63357	
.00450	12.76900	12.41097	
.00500	13.53300	13.73623	
.00550	14.61400	15.98459	
.00600	15.94700	18.22939	
.00650	17.10800	20.56003	
.00700	19.02800	23.95198	
.00750	19.67700	24.62100	
.00800	20.19200	25.50450	
.00900	21.62000	27.74561	
.01100	25.04900	30.00569	
.01300	27.09800	30.93122	
.01500	28.41300	29.63600	
.01800	30.25200	29.34112	
.02100	31.80100	28.39293	
.02400	32.71100	26.96459	
.02800	33.69900	25.64180	
.03300	34.91900	24.62100	
.04000	36.14500	23.69695	
.04800	37.25500	22.40072	
.05800	38.28400	22.51258	
.07300	39.35700	22.06394	
.09300	40.93300	22.12775	
.11800	42.16300	21.93659	
.14800	43.65200	22.25566	
.19800	46.20600	21.61982	
.25800	48.81200	20.96397	
.34800	51.15000	18.75479	
.44800	53.66900	16.53197	
.59800	57.94200	13.08957	
.79800	62.11700	7.59717	
.99800	65.42300	3.39364	
1.19800	66.97100	.47002	
1.39800	67.77700	.02480	
1.77100	67.87900 *	0.00000	(F.S.)

X=104.310 INCHES DATE: 8-10-77

HOT-WIRE (SINGLE WIRE) MEASUREMENTS

Y (INS.)	U (F.P.S.)	u'^2 (F.P.S.)^2	
.00450	9.80000	12.44162	
.00700	10.44000	13.49443	
.00750	11.02000	14.90457	
.00800	11.96000	17.06001	
.00850	12.47000	17.97787	
.00950	13.44000	19.61501	
.01150	15.39000	22.00398	
.01350	16.79000	22.36953	
.01550	17.90000	23.33814	
.01950	19.38000	23.15139	
.02150	20.06000	23.27931	
.02550	20.98000	23.22056	
.03050	22.06000	22.52136	
.03750	23.11200	22.00398	
.04550	24.04000	21.54913	
.05550	24.84000	21.37979	
.06750	25.70000	21.71914	
.08250	26.50000	22.06117	
.10050	27.40000	22.40527	
.12550	28.18000	23.27931	
.16050	29.51000	23.69263	
.20050	30.77000	24.33234	
.25050	31.99000	25.62842	
.32050	33.79000	26.37394	
.40050	35.74000	26.49923	
.50050	37.89000	26.63772	
.62050	40.67000	26.94009	
.75050	43.45000	26.75070	
.92050	47.25000	25.13735	
1.10050	51.00000	20.59835	
1.30050	54.52000	14.72994	
1.50050	57.48000	6.94711	
1.70050	59.62000	3.99271	
1.90050	60.65000	1.18912	
2.10050	60.75000	.45725	
2.30050	60.92000	.31412	(F.S.)

X=118.500 INCHES DATE: 8-10-77

HOT-WIRE (SINGLE WIRE) MEASUREMENTS

Y (INS.)	U (F.P.S.)	u'^2 (F.P.S.)^2	
.00800	4.35000	4.81950	
.01000	5.01000	6.56835	
.01200	5.97000	9.53633	
.01400	6.59000	10.29750	
.01600	7.38000	11.94266	
.01900	8.73000	13.70969	
.02200	9.40000	14.49858	
.02500	9.70000	15.02319	
.03000	10.42000	15.47437	
.03700	11.23000	15.64010	
.04500	11.86000	16.05826	
.05500	12.58000	16.55734	
.07000	13.34000	16.10038	
.09000	13.86000	16.48194	
.11500	14.55000	18.14225	
.14500	15.16000	18.36564	
.18000	15.94000	19.55571	
.22000	16.45000	20.40076	
.28000	17.48000	21.40924	
.36000	18.88000	23.60114	
.45000	20.50000	25.26232	
.58000	22.22000	26.55304	
.73000	24.78000	28.31053	
.90000	27.49000	30.00659	
1.10000	31.03000	29.83432	
1.35000	35.29000	28.08224	
1.60000	39.73000	25.42095	
1.85000	43.33000	21.50655	
2.10000	47.04000	16.78180	
2.35000	50.25000	9.69971	
2.60000	52.15000	3.87393	
2.85000	52.30000	N.A.	
3.10000	52.52000	N.A.	(F.S.)

X=122.625 INCHES DATE: 2-16-78

HOT-WIRE (SINGLE WIRE) MEASUREMENTS

Y (INS.)	U (F.P.S.)	u'^2 (F.P.S.)^2	
.47000	18.47260	17.65445	
.60000	20.14990	20.05039	
.80000	22.92110	22.83270	
1.10000	27.47300	23.78344	
1.40000	31.30980	22.69435	
1.90000	37.77400	18.41434	
2.00000	40.49960	15.92491	
2.20000	43.33470	12.33326	
2.40000	45.81340	9.79872	
2.60000	48.07070	6.25599	
3.20000	51.56870	.29612	
3.70000	51.92600	.05200	
4.50000	51.93770	.00688	(F.S.)

X=127.130 INCHES DATE: 8-10-77

HOT-WIRE (SINGLE WIRE) MEASUREMENTS

Y (INS.)	U (F.P.S.)	u'^2 (F.P.S.)^2	
1.12000	17.46000	28.62572	
1.42000	21.50000	31.62515	
1.82000	27.40000	32.10619	
2.32000	34.37000	27.77262	
3.12000	45.29000	12.82370	
3.62000	48.86000	2.60719	
3.82000	49.25000	1.02093	
4.12000	49.44000	.54464	
4.62000	49.53000	.34740	(F.S.)

X=131.975 INCHES DATE: 2-16-78

HOT-WIRE (SINGLE WIRE) MEASUREMENTS

Y (INS.)	U (F.P.S.)	u'^2 (F.P.S.)^2	
2.00000	24.59640	29.05754	
2.20000	26.69180	29.75335	
2.40000	29.51790	25.79004	
2.60000	32.01960	25.84053	
3.20000	39.16420	17.54710	
3.70000	44.75740	6.82954	
4.50000	49.34420	.41049	
5.80000	49.69070	.01422	
6.30000	49.67130	.00464	(F.S.)

X=139.750 INCHES DATE: 2-16-78

HOT-WIRE (SINGLE WIRE) MEASUREMENTS

Y (INS.)	U (F.P.S.)	u'^2 (F.P.S.)^2	
4.12000	38.05040	21.48387	
4.62000	43.47530	11.24385	
5.12000	47.01220	3.40576	
5.62000	48.75210	.56094	
6.12000	48.95160	.15509	
6.62000	48.86100	.07249	
7.12000	48.95040	.03106	
7.62000	49.00060	.01380	(F.S.)

X=144.875 INCHES DATE: 2- 7-78

HOT-WIRE (SINGLE WIRE) MEASUREMENTS

Y (INS.)	U (F.P.S.)	u'^2 $(F.P.S.)^2$
4.50000	27.06490	48.43735
5.00000	33.27940	38.67601
5.50000	39.69250	23.51593
6.00000	42.92390	9.97559
6.50000	45.63270	2.56801
7.00000	46.58430	.92090
7.50000	46.55720	.45258
8.00000	46.57250	.35001
8.50000	46.69130	.23925
9.00000	46.55900	.16805
9.50000	46.70320	.12534
10.00000	46.63380	.09742
10.50000	46.20050	.08613
11.00000	46.91670	.07554
11.50000	46.61550	.06096
12.00000	46.42900	.05858
12.50000	46.01510	.05644
13.00000	46.48530	.05425
13.50000	46.91790	.04794
14.00000	46.94180	0.00000 (F.S.)

X=151.000 INCHES DATE: 2-14-78

HOT-WIRE (SINGLE WIRE) MEASUREMENTS

Y (INS.)	U (F.P.S.)	u'^2 $(F.P.S.)^2$
5.00000	24.31000	65.55569
5.50000	27.03330	58.90092
6.00000	36.14450	47.34486
6.50000	46.66790	17.14713
7.00000	49.28720	6.41247
7.50000	50.56810	1.68293
8.00000	51.72900	.75096
8.50000	51.89110	.42073
9.00000	51.83360	.16382
9.50000	51.68420	.12820
10.00000	51.57360	.05444
10.50000	51.28100	.03383
11.00000	51.67770	.02265
11.50000	51.55060	.01077
12.00000	51.84450	.00455
12.50000	51.94990	.00455
13.00000	51.95380	0.00000
13.50000	51.98980	0.00000
14.00000	52.05310	0.00000 (F.S.)

X=156.375 INCHES DATE: 2- 7-78

HOT-WIRE (SINGLE WIRE) MEASUREMENTS

Y (INS.)	U (F.P.S.)	u'^2 $(F.P.S.)^2$
6.50000	27.98630	54.91307
7.00000	33.71560	47.25773
7.50000	37.35250	37.30191
8.00000	41.78960	17.24989
8.50000	43.73260	7.32930
9.00000	44.14250	3.11454
9.50000	45.05240	1.20499
10.00000	46.04430	.73840
10.50000	46.19910	.51278
11.00000	45.69390	.34969
11.50000	45.44350	.23952
12.00000	46.05370	.15421
12.50000	45.84250	.11065
13.00000	46.06430	.08742
13.50000	45.92630	.05771
14.00000	45.59970	.04715
14.50000	45.94490	.03588
15.00000	45.90560	.02467
15.50000	46.00910	.02051 (F.S.)

X=163.250 INCHES DATE: 2- 9-78

HOT-WIRE (SINGLE WIRE) MEASUREMENTS

Y (INS.)	U (F.P.S.)	u'^2 $(F.P.S.)^2$
8.00000	27.74400	57.44721
8.50000	31.10000	45.72009
9.00000	34.31700	33.00815
9.50000	38.03600	28.15846
10.00000	41.41100	11.37065
10.50000	42.25400	5.84682
11.00000	43.72900	2.04156
11.50000	43.96400	1.47236
12.00000	43.56100	.95258
12.50000	43.59900	.57131
13.00000	44.16200	.37384
13.50000	44.47900	.34190
14.00000	44.25000	.24650
14.50000	43.29200	.20505
15.00000	42.49900	.13965
15.50000	44.45300	.12063
16.00000	44.12400	.09471
16.50000	45.57500	.08419
17.00000	44.05100	.07671
17.50000	43.77900	.04832 (F.S.)

X=170.875 INCHES DATE: 2- 2-78

HOT-WIRE (SINGLE WIRE) MEASUREMENTS

Y (INS.)	U (F.P.S.)	u'^2 $(F.P.S.)^2$
9.50000	29.03900	53.20794
10.50000	35.03600	40.65521
11.50000	39.60300	16.61597
12.50000	41.81000	3.14035
13.50000	42.55100	1.52709
14.50000	42.79300	.72910
15.50000	42.90800	.37649
16.50000	42.89300	.18045
17.50000	43.47900	.14593
18.50000	43.92100	.05774 (F.S.)

LMED

8